Acid Gas Removal from Natural Gas with Alkanolamines: A Modeling and Experimental Study

Negar Sadegh
Ph.D. Thesis
March 2013

DTU Chemical Engineering
Department of Chemical and Biochemical Engineering

Acid Gas Removal from Natural Gas with Alkanolamines: A Modeling and Experimental Study

Negar Sadegh

Ph.D. Thesis

Center for Energy Resources Engineering

Department of Chemical and Biochemical Engineering

Technical University of Denmark

DK-2800 Lyngby, Denmark

Front cover: Asgard B Platform, Statoil Acid gas (CO_2 and H_2S) Removal Plant

Address: Center for Energy Resources Engineering
Department of Chemical and
Biochemical Engineering
Technical University of Denmark
Søltofts Plads, Building 229
DK-2800 Kgs. Lyngby
Denmark
Phone: +45 4525 2800
Fax: +45 4525 4588
Web: www.cere.dtu.dk

Print: J&R Frydenberg A/S
København
December 2013

ISBN: 978-87-93054-13-4

Acknowledgments

This thesis is submitted as partial fulfillment of the requirement for the PhD degree at Technical University of Denmark (DTU). The work has been carried out at the department of Chemical and Biochemical Engineering of DTU and department of Gas Processing and LNG of Statoil research and development center from April 2009 to July 2012. The work has been done under supervision of associate professor Kaj Thomsen and Professor Erling Stenby from DTU. The experimental part of the project was done under the guidance of Doctor Eivind Johannessen and Doctor Even Solbraa from Statoil. The project was funded by Statoil ASA.

First and foremost, I would like to say my deepest thanks from all my heart to my parents, my father, Mohammad Reza Sadegh, and my mother, Soraya Payandeh, who have been a constant force in my life. Their understanding and their eternal love without any regret or complaint encouraged me to move forward during all my life. No words can explain how much I am thankful to them. I am always proud to be their daughter. I would like to say my sincerest gratitude to my brothers, Pirooz Sadegh and Parsa Sadegh, for always supporting me and being there with me. I owe them all the moments of my happy childhood.

Most of all, I would like to express my deepest thanks to my endless love, my husband, Misagh (Hossein) Alimadadi, for his love that encouraged me to work hard during my Ph.D. studies. His paitience and faithful support specialy during the final stages of this PhD is so appreciated. I was far from my family and my beloved country, Iran, during my Ph.D. studies, his presence and his love never let me to feel far away from my beloved ones. I owe my achievements to him for making this hard period, happy and sweet for me. No words can express my eternal love to him.

I wish to express my sincere gratitude to associate professor Kaj Thomsen for his guidance and supervision throughout this work. I have benefited a lot from the data bank and programs. He always allowed me to solve problems with my own approach and at my own time. His attitude towards advising me allowed me to make many of my own mistakes and have many of my own successes. I am really thankful to him for his kind supervision during these years. It was always inspiring to work with him.

I would also like to give a special thanks to Professor Erling Stenby, my supervisor and the head of CERE and Chemistry department of DTU, for giving me the opportunity to join CERE, for his very

kind leader ship. He is a great leader with brilliant innovative ideas that makes CERE such a pleasant place to study.

I have also been fortune enough to have been given the opportunity to travel to Norway to continue my research work in the Statoil research and development center under the supervision of Doctor Even Solbraa and Doctor Eivind Johannessen. I would like to thanks them for their kindness, encouragement and hospitality. I especially thank them for great supervising the experimental part of my project. I have learned a lot from them. Before I move to Statoil I had no experience to work in laboratory and it was their exceptional guidance that makes it possible to do this extensive experimental work. I would like to specifically thank Doctor Eivind Johannessen for his patience to many of my rising questions. I would also like to thank to Doctor Lars Henrik Gjertsen and Doctor Cecilie Gotaas Johnsen, the heads of the department and group for providing me such opportunity. My special thanks to Gunn Iren Rudolfsen and Ole Johan Berg, two expert technicians, that without them it was not possible to perform high pressure measurements. I thank to Doctor Maria G. Lioliou to teach me how to do measurements with low pressure cell.

I would like to say me deep gratitude to Professor Dominique Richon for generously reviewing the experimental part of the PhD dissertation. He was always very generous to answer my questions about any experimental topic.

I would like to thank Patricia Wagner and Anne Louise Biede for their great work in CERE administration. Special thanks to Patricia Wagner for always be kind to me. She made me feel like I am at home. Many thanks my colleagues in CERE, Chemical engineering department of DTU and Statoil, Gas Process and LNG department for making such a nice atmosphere which makes me always enjoy being part of them.

And finally, financial support from the Statoil Company is greatly appreciated.

Negar Sadegh

Lyngby, Denmark

March 2013

Dedicated

to my eternal loves, meanings of my life

My father, Mohammad Reza Sadegh

and

My mother, Soraya Payandeh

Summary

Some 40 % of the world's remaining gas reserves are sour or acid, containing large quantities of CO_2 and H_2S and other sulfur compounds. Many large oil and gas fields have more than 10 mole % CO_2 and H_2S content. In the gas processing industry absorption with chemical solvents has been used commercially for the removal of acid gas impurities from natural gas. Alkanolamines are the most commonly used category of chemical solvents for acid gas capture. This Ph.D. project is about thermodynamics of natural gas cleaning process with alkanolamines as solvent. It covers both modeling and experimental study of alkanolamine-water-acid gas systems. The project is collaboration between DTU and Statoil. Thermodynamic modeling is being done at DTU and experiments were performed at Statoil laboratories. In modeling part of the project, thermodynamic models were developed for CO_2-MDEA-H_2O, CO_2-MEA-H_2O, CO_2-MDEA-MEA-H_2O, H_2S-MDEA-H_2O, H_2S-CH_4-MDEA-H_2O systems and the constituent binary subsystems of the mentioned mixtures. The experimental part of the project includes vapor-liquid equilibrium measurements for CO_2-MDEA-H_2O and CO_2-MDEA-PZ-H_2O at atmospheric pressure, high pressure vapor-liquid equilibrium experiments for H_2S-CH_4-MDEA-H_2O, density measurements for aqueous MDEA and aqueous activated MDEA and piperazine solubility measurements in aqueous MDEA. The developed Extended UNIQUAC model was used to validate the measured data points. The effect of total pressure on acid gas solubility was also quantitatively investigated through both experimental and modeling approaches.

Resume på dansk

Ca. 40 % af verdens resterende gasreserver indeholder store mængder af de sure gasser CO_2 og H_2S og andre svovlforbindelser. Mange store olie og gasfelter har mere end 10 mol % CO_2 og H_2S indhold. De sure gasser fjernes industrielt ved absorption med kemiske opløsningsmidler. Vandige alkanolaminer, simple kombinationer af alkoholer og ammoniak, er den mest almindeligt anvendte gruppe af kemiske opløsningsmidler for absorption af sur gas. Dette ph.d.-projekt handler om termodynamisk modellering og eksperimentelle målinger vedrørende naturgas rensningsprocesser med anvendelse af alkanolaminer som opløsningsmiddel. Projektet er et samarbejde mellem DTU og Statoil. Den termodynamiske modellering blev udført på DTU og eksperimenter blev udført på Statoils laboratorier. I modelleringsdelen af projektet blev termodynamiske modeller tilpasset CO_2-MDEA-H_2O, CO_2-MEA-H_2O, CO_2-MDEA-MEA-H_2O, H_2S-MDEA-H_2O, H_2S-CH_4-MDEA-H_2O-systemer. Den eksperimentelle del af projektet omfatter damp-væske ligevægt målinger for CO_2-MDEA-H_2O og CO_2-MDEA-PZ-H_2O ved atmosfærisk tryk samt højtryks målinger af damp-væske ligevægt for H_2S-CH_4-MDEA-H_2O systemet. Desuden blev der udført densitet målinger for vandig MDEA og vandig MDEA tilsat piperazin. Piperazins opløselighed i vandig MDEA blev også bestemt eksperimentelt. Den ”Extended UNIQUAC” model blev benyttet til simulering af de eksperimentelle datapunkter. Virkningen af totaltryk på sur gas opløselighed blev også undersøgt kvantitativt med både eksperimentelle og modelbaserede metoder.

Nomenclature

List of Abbreviations:

VLE: Vapor-Liquid Equilibrium

SLE: Solid-Liquid Equilibrium

AARD: Average Absolute Relative Deviation

AAD: Average Absolute Deviation

MEA: Monoethanolamine

MDEA: Methyldiethanolamine

PZ: Piperazine

CO_2: Carbon dioxide

H_2S: Hydrogen sulfide

S^{2-}: Sulfide ion

H^+: Hydrogen ion

OH^-: Hydroxide ion

$MDEAH^+$: MDEA protonated ion

H_2CO_3: Carbonic acid

HCO_3^-: Bicarbonate ion

CO_3^{2-}: Carbonate ion

$MEACOO^-$: MEA carbonate ion

CH_4: Methane

$AgNO_3$: Silver Nitrate

NaOH: Sodium Hydroxide

Ag: Silver

Ag_2S: Silver sulfide

HCl: Hydrochloric acid

Na_2S: Sodium Sulfide

NRTL: Non-Random Two Liquid thermodynamic model

UNIQUAC: UNIversal QUAsi Chemical thermodynamic model

MSA: Mean Spherical Approximation

SRK: Soave-Redlich-Kwong thermodynamic model

e-NRTL: Electrolyte NRTL thermodynamic model

N: Number of data points

ppm: part per million

wt%: Weight percent

rpm: Round per minute

LNG: liquefied natural gas

pH: A measure of the activity of the (solvated) hydrogen ion

R: Gas constant

m : Molality (mole of solute per kg of solvent)

M: Molarity (mole of solute per liter of solution)

SI: Saturation Index

List of symbols:

H^E: Excess Enthalpy

G^E: Excess Gibbs Energy

C_p: Heat Capacity

H^{abs}: Heat of Absorption

C_p^0: Standard state heat capacity

H_f^0: Standard state enthalpy of formation

G_f^0: Standard state Gibbs free energy of formation

μ_i: Chemical potential

ρ : Density

α: Loading , mole acid gas per mole amine

$\acute{\alpha}$: Loading, mole acid gas/kg rich solvent

P_{cr}: Critical pressure

T_{cr}: Critical temperature

ω : Acentric factor

V_i^{∞} : Partial molar volume of component "i" at infinite dilution

γ_i : Activity coefficient of component "i"

$H_{i,w}$: Henry's constant of solute "i" in water

R^2: Coefficient of Determination

$M_{ø}$: Apparent molar property

List of Contents

List of Tables

List of Figures

Chapter 1

Motivation and Scope of the Work

Chapter 1

Motivation and Scope of the Work

1 Motivation and Scope of the Work

1.1 Background

A large portion of the world's natural gas resources comprise high amount of CO_2 and H_2S (acid gases). Removal of CO_2 from the natural gas is of high importance because of the transport requirements and sale gas specifications. Similarly H_2S has to be removed to meet the toxicity limit. Acid gas removal is best accomplished by chemical absorption (Prausnitz et al. 1999) and aqueous alkanolamine solutions are the most widely used solvent in industry for this purpose. In order to properly design the absorption equipment, information on vapor-liquid equilibria, thermal effects and kinetics of mass transfer and of chemical reactions is required (Prausnitz et al. 1999). This research addresses thermodynamics of acid gas removal from natural gas by aqueous alkanolamine solutions. The aim of this work is to understand the thermodynamics of the process by developing consistent thermodynamic models and providing required acid gas solubility data.

1.1.1 Knowledge Gap

A large number of different thermodynamic models have been developed for the calculation of acid gas solubility in alkanolamines. "Because of chemical reactions and strong deviation from ideality in the liquid phase, it is not simple to model the thermodynamic behaviour of aqueous mixtures containing alkanolamines and sour gases (Prausnitz et al. 1999)". However it is well known that many of the most widely used models may bring about large errors when extrapolated to high pressures, high amine concentrations, mixed solvents and mixed CO_2 and H_2S gases. Also most of the available thermodynamic models have difficulties to represent heat of the reaction which is one of the key parameters to calculate the energy cost of the plant. Regarding the experimental data, there are very few VLE data at high pressures. In addition there is no data for MDEA [1] concentrations higher than 75 wt%. Likewise, the data for MDEA/PZ[2] solvent with high MDEA concentration is very scarce.

[1] MDEA : Methyldiethanolamine
[2] PZ: Piperazine

1.1.2 Objective of This Work

- To develop a thermodynamic model that can describe thermodynamic and thermal properties of the acid gas-alkanolamine mixtures over large range of pressure, temperature and amine concentration.
- To investigate the effect of total pressure on acid gas solubility.
- To obtain experimental data at conditions (mentioned above) that there is a gap in open literature.

1.2 Collaborative Research Organizations

This work has been a collaborative effort between Technical University of Denmark (DTU) at Lyngby, Denmark and Statoil ASA Research and Development center (department of gas processing and LNG) in Trondheim, Norway. The modelling part of the work was carried out at the center for energy resources engineering (CERE) at DTU Chemical Engineering and the experimental data were obtained at the department of Gas Processing and LNG, Statoil ASA Research and development laboratories.

1.3 Outline of the Dissertation

This dissertation is divided into 10 chapters. It begins with outlining the scope and motivation of the work. Chapters 2 and 3 address background for natural gas treatment process and chemical aqueous phase thermodynamics as well as describing information on the structure of the developed thermodynamic model. Chapter 4 describes improvements that were implied in the modeling work of this study compared to previous studied model. Chapter 5 discusses the developed thermodynamic models for CO_2-MDEA-H_2O, CO_2-MEA-H_2O, CO_2-MDEA-MEA-H_2O systems and the constituent subsystems as well as presenting the results of the modeling. Chapter 6 shows the developed thermodynamic model for H_2S-MDEA-H_2O, acid gas-CH_4-MDEA-H_2O systems and the constituent subsystems as well as modeling the effect of total pressure on acid gas solubility. Chapter 7 addresses the experimental challenges of obtaining VLE data for CO_2-MDEA-H_2O and density data for MDEA-H_2O systems. In chapter 8, the effect of PZ is studied by acquiring VLE data for CO_2-MDEA-PZ-H_2O at two concentrations of PZ; the experimental results of measured density data for MDEA-PZ-H_2O are also provided. Chapter 9 presents the high pressure VLE data measured for H_2S-CH_4-MDEA-H_2O systems. Chapter 10 attempts to summarize the work presented throughout this dissertation and to suggest recommendation for future continuation of this study. It

is noted that appendix presents preliminary results for piperazine solubility measurements in aqueous MDEA.

Chapter 2

Introduction to Natural Gas Treating Process,

Acid Gas Removal from Natural Gas

Chapter 2

Introduction to Natural Gas Treating Process, Acid Gas Removal from Natural Gas

2 Introduction to Natural Gas Treating Process, Acid Gas Removal from Natural Gas

2.1 Chapter Overview

The share of natural gas in the world energy panorama has been appreciably growing for the last years. This increase is expected to continue in the next few decades with the progressive replacement of fuel oil and coal by this relatively environment-friendly source of energy. However, this development depends on the progress of gas processing technologies to give access to reserves that are not exploitable (Barreau et al. 2006). Many of the available gas fields are acid, containing large quantities of CO_2 , H_2S and other sulfur compounds. Gas that contains sulfur compounds impurities is called sour gas. Natural gas is usually considered sour if the hydrogen sulfide content is more than 5.7 milligrams per cubic meter of natural gas (4 ppm[3] by volume) (Kirk Othmer 2005). Processes that remove hydrogen sulfide and/or mercaptans (generally acid gases) are referred as sweetening processes because they result in products that no longer have acid gases. This chapter gives an introduction on the process of acid gas removal from natural gas. The chapter addresses different issues of the process including the reasons for acid gas removal, different common technologies and amine treating process which is the mostly applied technology in industry.

2.2 Reasons for Acid Gas Removal

Natural gas extracted from some wells can contain significant amounts of sulfur containing compounds and carbon dioxide. The composition of acid gases in natural gas varies widely depending on the gas field. Acid gas impurities, i.e. CO_2 and H_2S are detrimental to natural gas properties.

[3]ppm: part per million

For instance, in cryogenic conversion of natural gas to LNG[4], CO_2 transforms to solid state, hence, hinders the transportation of liquid in the pipes or the corrosive H_2S reduces the service time of the transportation pipes. In addition H_2S is hazardous for human beings and CO_2 has no heating value. As a result the concentration of acid gas impurities in natural gas must be reduced to a specified level before further processing (NREL 2009), (Bishnoi 2000), (Cadours et al. 2007).

2.3 Acid gas Removal Technologies

The conventional acid gas removal technologies can be classified as (NREL 2009):

- Chemical Absorption: In chemical absorption process, acid gases components react chemically with a solvent and form dissolved chemical compounds. The solvent is regenerated in a stripper column by application of heat. Heat breaks the chemical bounds between acid gases and solvent and drives out the acid gases from the solution. The most common solvent for chemical absorption process is alkanolamine (amine process).
- Physical Absorption: In physical absorption process, acid gases absorb in an organic solvent physically and without chemical reaction. Acid gases are absorbed in the solvent due to their high solubility. Since solubility rises with increasing pressure and decreasing temperature, physical absorption is mostly effective at high pressures and low temperatures. Therefore, compared to amine process, usually physical absorption capital investment and operating costs are higher due to high pressure equipment and refrigerating units required to achieve operating conditions (process operates at high pressure and low temperature). In addition, physical solvent is used for bulk removal of acid gases whereas application of chemical solvent is to achieve very low acid gas concentrations. It should be noted that hence sometimes a physical solvent has lower operating and capital costs the choice between a physical and an amine based solvent is case dependent. However chemical absorption with amines dominates the market nowadays.
- Hybrid Process: In a hybrid process a physical and chemical solvent are applied simultaneously to benefit from the advantages of both processes.
- Membrane Separation Process: Membrane separation systems are mainly used for bulk removal of CO_2. This process is commonly applied at conditions with large flows or high CO_2 concentrations.

[4]LNG: Liquefied Natural Gas

2.4 Amine Process

In the gas processing industry absorption with chemical solvents has been used commercially for the removal of acid gas impurities from natural gas. The currently preferred chemical solvent technology for acid gas removal is chemical absorption of acid gases by amine-based absorbents. Alkanolamines[5], are the most commonly used category of amine chemical solvents used for acid gas removal. Chemical absorption of CO_2 with alkanolamines as solvent has been used in a large variety of industries over years. Natural gas treating, production of hydrogen and ammonia from synthesis gas and CO_2 capture from combustion gases are among the biggest industries that are utilized chemical absorption of CO_2 with alkanolamines (Bishnoi 2000). Removal of acid gas from process gas with alkanolamines has been developed in 1930's (Bishnoi 2000) and nowadays, aqueous solutions of MEA and MDEA are the most commonly used solvents for gas sweetening. The use of blend amines is also increasing, since it reduces the operating costs and improves products quality (Kim et al. 2008). It is notable that MDEA is advantageous over other amines due to selective removal of H_2S from its mixture with CO_2. The selectivity of absorption is due to the higher rate of the reaction of MDEA with H_2S than the reaction of MDEA with CO_2 (Anufrikov et al. 2007). H_2S has H^+ that can give directly to MDEA; the proton transfer reaction is always fast and spontaneous. Moreover, comparing to other amines, MDEA is more stable, less volatile and less corrosive, it has lower heat of reaction and higher absorption capacity (Anufrikov et al. 2007).

Design, operation, simulation and optimization of acid gas removal from natural gas process and CO_2 capture from combustion gas plants, require accurate prediction of phase and chemical equilibrium, as well as thermal properties of the system (Zhang and Chen 2011).

2.4.1 Amine Type

Four types of amine are used commercially to remove acid gases: primary amines such as MEA[6], secondary amines such as DEA[7], tertiary amines such as MDEA[8] and cyclic amines such as PZ[9]. Figure 2-1 and Figure 2-2 shows chemical structure of the mentioned types of amines (Bishnoi 2000).

[5] Alkanolamines: Alkanolamines are organic chemical compounds which their chemical structure comprise an alcohol (-OH) and one of the amino (-NH_2, -NHR, -NR_2) functional groups attached to an alkane chain (Kirk Othmer 2005).
[6] MEA: Monoethanolamine (RNH_2: R is the alkyl group, $R = CH_2 - CH_2 - OH$)
[7] Diethanolamine (R_2NH: R is the alkyl group, $R = CH_2 - CH_2 - OH$)
[8] Methyldiethanolamine (R_2NCH_3: R is the alkyl group, $R = CH_2 - CH_2 - OH$)
[9] Piperazine ($C_4H_{10}N_2$: PZ is a saturated heterocyclic compound with two heteroatoms., $R_2N_2H_2$, R is the alkyl group, R= $CH_2 - CH_2$)

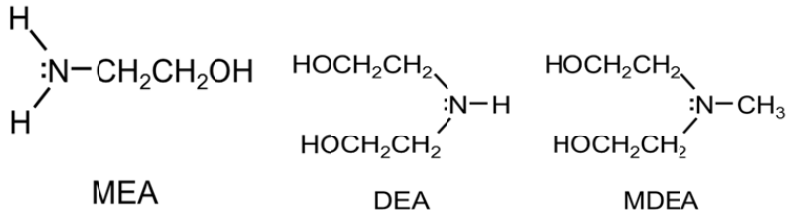

Figure 2-1. Chemical structure of primary, secondary and tertiary amines (Lecomte et al. 2009)

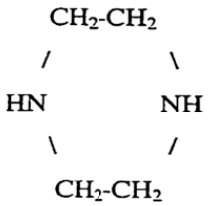

Figure 2-2. Chemical structure of PZ which is a cyclic amine (Lecomte et al. 2009)

The reaction between H_2S and amines is almost instantaneous and happens due to the fast proton transfer between amine and hydrogen sulfide:

$$H_2S + Amine \leftrightarrow [Amine]H^+ + HS^- \quad (2\text{-}1)$$

Primary and secondary amines react with CO_2 and create carbamate, for example the reaction for MEA (RNH_2) which is a primary amine can be written as:

$$CO_2 + H_2O + \mathrm{RNH_2} \leftrightarrow [\mathrm{RNH}]COO^- + H^+ + H_2O \quad (2\text{-}2)$$

Since three alkyl groups are connected to the nitrogen atom in MDEA chemical structure, the direct reaction between CO_2 and MDEA is hindered. Accordingly, CO_2 dissolves in water first, and form carbonic acid (H_2CO_3), and then carbonic acid reacts with the basic amine. The reaction between CO_2 and MDEA can be shown as:

$$CO_2 + H_2O + MDEA \leftrightarrow MDEAH^+ + HCO_3^- \quad (2\text{-}3)$$

The acid-base reaction between MDEA (more generally, the tertiary amines) and CO_2 is slower than MDEA reaction with H_2S. Hence, MDEA selectively removes H_2S. Unlike tertiary amines, in most cases primary and secondary amines react simultaneously with H_2S and CO_2, and that impedes

selective removal of the acid gases. To overcome slow rate of reaction of MDEA with CO_2, usually small amount of primary or secondary amines are mixed with MDEA. Reactions between amines and acid gases are exothermic (heat produced during the reaction). Based on the Le Chatelier's principle, by increasing acid gases concentration (increasing acid gas partial pressure) and/or decreasing temperature, the above reactions proceed to the right side. It is noted that the selection of proper amine solution for optimized acid gas removal process depends on process conditions, acid gas partial pressures and purity of treated gases (NREL 2009). In recent years, aqueous solutions of MEA are only applied for treatment of gases containing low concentrations of CO_2 and H_2S, particularly when maximum removal of these impurities is intended (Anufrikov et al. 2007). The major advantages of MEA are: High reactivity, low cost, and low capacity for absorption of hydrocarbons (Anufrikov et al. 2007). The main disadvantages of MEA are: High corrosiveness of MEA which enhances by temperature, high heat of reaction with CO_2 and H_2S which results in high energy requirements for solvent regeneration and consequently the total cost of the process increases, relatively high vapor pressure which brings about notable amine losses via vaporization.

Even though MDEA is more expensive than MEA and it has lower rate of reaction with CO_2 compared to primary and secondary amines, the following advantages makes it the most widely used amine in natural gas treatment industry: selective absorption of H_2S from its mixture with CO_2; low heat of reaction of acid gases with MDEA which results in notably lower regeneration energy compared to MEA; significantly lower vapor pressure which reduces amine loss by evaporation; higher absorption capacity; very low corrosion rate; high thermal and chemical stability. Lower corrosion rate and lower vapor pressure allow using higher concentration of MDEA in the absorber column which results in lower circulation energy and consequently smaller plant size and lower plant cost. In addition, the low miscibility of MDEA with hydrocarbons results in negligible loss of the hydrocarbons (Posey 1997), (Jou et al. 1994).

Due to the mentioned advantages when only removal of H_2S is intended MDEA is solely used as the absorbent. For simultaneous removal of H_2S and CO_2 certain additives are used in MDEA based solution.

It is notable that since removal of CO_2 with MDEA is slow, additives such as piperazine are used to enhance the rate of reaction between CO_2 and MDEA. Addition of optimized amount of faster reacting amines, enhances rate of reaction without compromising advantages that MDEA offers.

2.4.2 Flow Scheme

Figure 2-3 shows a typical amine process.

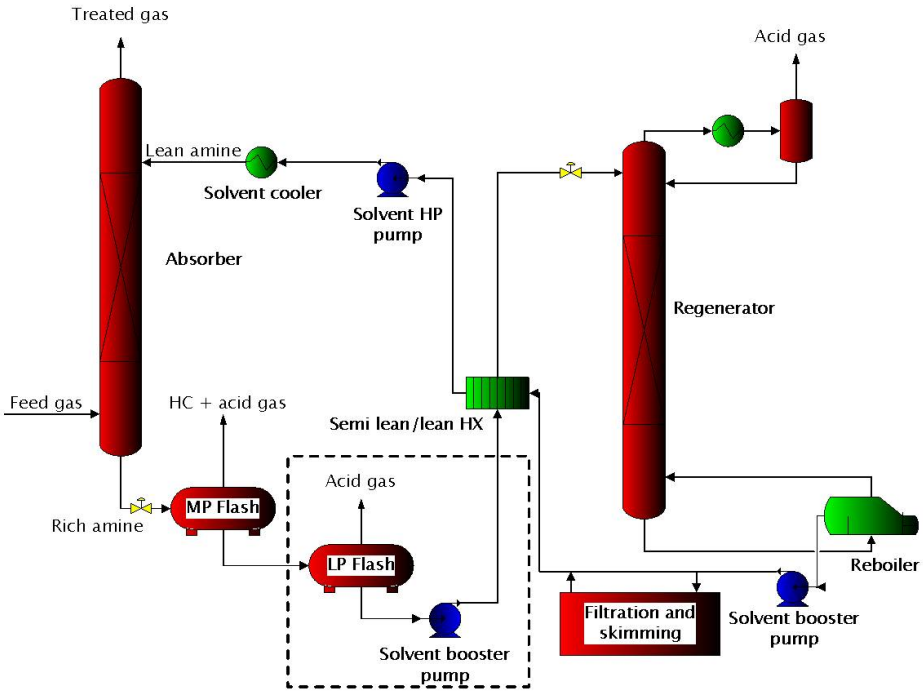

Figure 2-3. Typical Amine Flow Diagram

The inlet sour gas may contain CO_2, H_2S, mercaptans and other acid gases. The concentration of the acid gases is widely dependent on the reservoir of natural gas. Typically concentrations of CO_2 and/or H_2S in natural gas are between 0 to 50 % (molar basis). After the acid gas removal, the concentration of H_2S should be lower than about 4 ppm by volume and that of CO_2 is depending on the application. For sale purpose, the CO_2 content should be reduced down to 2.5 mole percent and for producing LNG that should be lowered down to 50 ppm (Bishnoi 2000; Posey 1997). As shown in Figure 2-3 feed gas (natural gas) enters at the bottom of the absorber column while lean amine solution[10] (solvent) enters the column at the top. In the absorber, the lean amine solution is contacted counter currently with the gas stream. As the amine solution flows down the absorber column, it contacted with gas stream and acid gases react with the amine, hence, amine solution

[10]Lean Amine: Unloaded aqueous amine solution

becomes loaded with acid gases and leaves the bottom of the absorber as the rich amine[11]. The sweetened gas [12]stream exists at the top of the absorber where it goes for further processing. The rich amine solution leaves the bottom of the absorber and enters one or two flush drums where dissolved hydrocarbons are removed. The recovered hydrocarbons are usually used as plant fuel. The rich amine solution is heated by exchanging heat with lean solvent stream in the heat exchanger and then fed to the top of the stripper column. As the rich amine solution flows down the stripper column to the reboiler, acid gases are driven out of the solution and the solution is regenerated. The reboiler at the bottom of the stripper column provides the heat required to strip acid gases from the solution. The lean amine solution which exits from the bottom of the stripper (reboiler) enters the filtering and skimming[13] unit to remove particles and heavy liquid hydrocarbons, then exchanges heat with the rich amine stream in the heat exchanger and is further cooled by the cooler before entering at the top of the absorber column. The stripped gas stream is cooled to recover the water and then is sent for further processing such as sulfur recovery units like Claus sulfur plant[14] (Bishnoi 2000; Posey 1997).

The absorber typically is a packed or a tray column. Absorption capacity, process kinetics and the ability to cool the lean amine stream using cooling water usually determine absorber temperature (Bishnoi 2000). In natural gas treatment process, absorber typically operates at 40 °C. Decrease in absorption capacity at higher temperatures and very slow rate of reaction at lower temperatures, makes the absorption unfeasible at temperatures far from 40 °C (Anufrikov et al. 2007). The absorber operating pressure is dependent on the studied process. In natural gas treatment process the absorber typically operate at about 70 bar (7000 kPa) or higher pressures (Bishnoi 2000). For the flue gas, the absorber pressure is around atmospheric pressure. Typical operating temperature of the stripper is around 120 °C. Increasing temperature of solvent inside the stripper removes acid gases from the solvent; recall that reaction between acid gases and aqueous amine is exothermic therefore increasing temperature moves the reaction to the reactant side and leads to produce molecular reactants (acid gases and amine in the molecular form). At higher temperatures there is a possibility of amine degradation and consequent equipment corrosion. The stripper pressure is around 1, 2 bar (100, 200 kPa). Notice that the mentioned numbers are typical operating conditions and the actual operating conditions may deviate a lot from these values.

[11]Rich Amine: Aqueous amine solution loaded with acid gases
[12]Sweetened Gas: Gas that does not contain significant amounts of H_2S (generally acid gases)
[13] Skimming: Heavy hydrocarbons in the solvent create a liquid phase on top of the solvent. Removing the top layer of liquid is called skimming.
[14]Claus Process: Gas desulfurizing process; recover elemental sulfur from the hydrogen sulfide gas.

In natural gas treatment process, typical amine concentration in the absorbent aqueous solution depends on the amine type and acid gases, for removal of both H_2S and CO_2, the MEA concentration is between 20 to 30 mass% which is equivalent to 6 to 11 mole % (for aqueous MEA solvent) and MDEA concentration is in the range of 30 to 50 mass% which is equivalent to 6 to 13 mole % (for aqueous MDEA solvent) (NREL 2009). Hence, in mole percent scale typical MDEA and MEA concentration is similar.

Amine process economy is mainly dependent on the energy requirements for the solvent regeneration which is a function of the heat of reaction between acid gases and amine solution. It also depends on the solution circulation rate which depends on solution capacity and concentration (NREL 2009). Generally increasing solution concentration, leads to decrease circulation rate and consequently the plant costs reduce. However, in order to prevent equipment corrosion, solution concentration should be complied with the limits recommended for each solvent type (NREL 2009).

2.5 Role of Thermodynamics

The physical and chemical phenomena are both involved in acid gas treating, however absorption of acid gases into the aqueous alkanolamine solutions is governed by the mechanism of mass transfer with chemical reaction (Posey 1997). Equilibrium solubility is required to calculate the driving force for mass transfer. Therefore a thermodynamic model for predicting equilibrium solubility at all applicable conditions of temperature, amine concentration and acid gas loading[15] is highly demanded (Posey 1997). Thermodynamics is also needed for calculation of the free amine concentration (Bishnoi 2000). Chemical equilibrium calculations for all the species present in the liquid phase determine the amount of free amine for a specified overall acid gas concentration (Bishnoi 2000). The more available free amine, leads to faster rate of reaction between amine and acid gases (Bishnoi 2000). A consistent thermodynamic model not only quantifies the amine solution speciation and partial pressure of molecular species in the gas phase, it also describes volatility and enthalpic behavior of the solvent.

It is worth noting that thermodynamics defines the equilibrium state of the system and how fast the equilibrium state is reached is discussed in the context of kinetics. Hence in acid gas removal process, thermodynamics determines maximum absorption capacity of the solvent, whereas kinetic defines how fast the absorption/desorption occurs. Accordingly, higher absorption capacity (equilibrium solubility defined by thermodynamics) brings about utilizing less solvent in the

[15]Loading = mole of absorbed acid gas per mole of amine.

absorber column, hence, higher cost efficiency can be achieved. Similarly, slow kinetic necessitates a larger absorber column, hence, larger plant size. If the kinetic is very slow, in an industrially applicable time the system state is far from equilibrium. In such a case the actual solubility deviates significantly from solubility calculated by equilibrium thermodynamic models. Having mentioned the importance of kinetics on actual process it is out of scope of this study, and equilibrium thermodynamic aspect of amine based acid gas removal is addressed only.

Chapter 3

Background Thermodynamics,

Modeling Structure

Chapter 3

Background Thermodynamics, Modeling Structure

3 Background Thermodynamics, Modeling Structure

3.1 Chapter Overview

Acid gas removal from natural gas is typically performed by physical and chemical absorption into aqueous alkanolamine solutions. Thermodynamics has important role in the design of acid gas treating plants. Thermodynamic modeling of the behavior of these systems includes consideration of both phase and chemical equilibria. Thermodynamics quantifies the driving force for mass transfer, equilibrium compositions and thus outlet concentrations. A consistent thermodynamic model also quantifies amine volatility and thermal properties of the system. Since the steam cost is over half of the total plant costs (Carson et al. 2000), prediction of heat of absorption is of great importance to increase cost efficiency.

This chapter addresses literature review over acid gas thermodynamic models, equilibrium thermodynamic of acid gas treatment process, and the relation between different types of regressed data and model parameters. Equilibrium thermodynamics is broken into two parts in this chapter. The first part covers physical vapor-liquid equilibria (VLE) of molecular species. The second part addresses the chemical reactions occur in acid gas-alkanolamine-water systems.

3.2 Literature Review of Published Models

Though different thermodynamic models for acid gas absorption processes have been studied for many years, thermodynamic modeling of these multi component systems remained as a hot topic. This owes to the fact that the reactions taking place in the solution give rise to a number of new ions and molecules in the system, which made modeling of the system complex.

Most of the available models can predict the CO_2 partial pressure above these solutions. However some important properties such as amine partial pressure, speciation, and heat of absorption are predicted with less accuracy. Thermodynamic models proposed for acid gas absorption process can be categorized in two groups: simple and complex models.

3.2.1 Simple Models

Simple models are the simplest ones and this family of models is usually called "Kent and Eisenberg" models. They have following characteristics: (i) they use simple mathematical relations for describing phase equilibrium and in most of them apparent equilibrium constants related to component concentrations instead of component activities. (ii) Activity coefficients for all species are set to one. (iii) Apparent equilibrium constants are defined as function of ionic strength. Apparent equilibrium constants are fitted to experimental data. Even though simple models based on the apparent equilibrium assumption, provide a simple way for prediction of acid gas partial pressure, they suffer from two major disadvantages. First, the model shows inefficiency when extrapolated to conditions other than those equilibrium constants were tuned for. Second, using apparent equilibrium constant gives only an approximation of the species composition. Using this method, (Van Krevelen et al. 1949) suggested a method for calculating the partial pressures of CO_2, H_2S, and NH_3 into aqueous solutions. Later (Danckwer and McNeil 1967) used the procedure of (Van Krevelen et al. 1949) for representing the phase behavior of amine-CO_2-water mixtures. The model of (Danckwer and McNeil 1967) used Henry law for acid gas partial pressure calculation and assumes apparent equilibrium constants are a function of ionic strength for speciation calculation. (Kent and Eisenberg 1976) modified (Danckwer and McNeil 1967) model for calculating CO_2 and H_2S partial pressure in MEA and DEA aqueous solutions. This model, though being simple, can well represent the CO_2 partial pressure. Hence, the model can be used in commercial simulators like HYSYS. Even though this model shows good results for CO_2 partial pressure, it has two main shortcomings. First it is only valid in concentration range used for fitting equilibrium constant. Second it cannot predict the composition of species precisely. Accurate prediction of the composition requires precise values for activity coefficients. (Gabrielsen et al. 2005) presented a correlation for describing the solubility of CO_2 in H_2O-MDEA solutions. Their model is based on Henry's law and apparent equilibrium constants that were tuned to experimental data.

3.2.2 Complex Models

This category can be divided into two subgroups: excess Gibbs energy or activity coefficient models and equation of state models. In general, these models are comprised of two terms: a term for short range interactions (non-electrolyte activity coefficient models or equation of state), and a term for long range interactions (based on the electrostatic theories). Combining a classic, short range interaction model, with an electrostatic term makes the model capable of representing the behavior of electrolyte systems.

Excess Gibbs Energy or Activity Coefficient Models

These models provide activity coefficients based on expressions for excess Gibbs energy of the liquid phase. The speciation in the liquid phase is calculated from the activity coefficients. An equation of state is often used for determination of fugacity coefficients of the vapor phase. (Deshmukh and Mather 1981) proposed a method based on the Guggenheim theory (Guggenheim and Turgeon 1955) for the H_2S/CO_2-MEA-H_2O system. In this model it is assumed that water behaves ideally and all the interaction parameters for water in the model are set to zero. Even though the model is simple, it shows good results for the CO_2 solubility. The model has problems with describing the phase behavior of the binary MEA-H_2O system. In 1975 (Edwards et al. 1975) presented a molecular thermodynamic model for calculating vapor-liquid equilibria for dilute solutions of weak electrolytes. They used a Guggenheim-type equation for representation of activity coefficients. The model of Edwards is applicable to weak electrolytes, in dilute solutions; at concentrations below 2 molal[16]. In 1978, (Edwards et al. 1978) modified their original model by replacing the Guggenheim term with the Pitzer model. This model is valid at concentrations up to 20 m. (Li and Mather 1994) used the Pitzer and Simonson model (Pitzer and Simonson 1986), which is an extension of the Pitzer model, for modeling the CO_2-MEA-MDEA-H_2O system. (Kuranov et al. 1996) used Pitzer model for representing the behavior of CO_2-MDEA-H_2O and H_2S-MDEA-H_2O systems. (Kamps et al. 2001) and (Ermatchkov et al. 2006) used the Pitzer model for the MDEA-CO_2-H_2O mixture. (Arcis et al. 2009) applied the Pitzer model for representing VLE data and heat of absorption for the MDEA-CO_2-H_2O system.

Several authors applied a type of excess Gibbs energy model that are local composition models. The Electrolyte NRTL model (e-NRTL) presented by (Chen et al. 1982) and the Extended UNIQUAC model presented by (Thomsen and Rasmussen 1999) are the most commonly used local

[16] molal: refers to molality which is defined as mole of solute per kg of solvent.

composition models applied for electrolyte systems. The e-NRTL model has been applied for modeling many alkanolamine-acid gas-water systems. (Austgen 1989), (Posey and Rochelle 1997), (Hilliard 2008), (le Bouhelec et al. 2007), (Bishnoi 2000) applied the e-NRTL model for their work. (Hessen et al. 2010) used the refined e-NRTL model for the CO_2-H_2O-MEA/MDEA system. (Zhang and Chen 2011) applied e-NRTL (e-NRTL in ASPEN PLUS) for modeling VLE, heat capacity and heat of absorption of CO_2-MDEA-H_2O system. (Addicks 2002) applied both Extended UNIQUAC and e-NRTL for VLE calculations in the CO_2-CH_4-MDEA-H_2O system. (Faramarzi et al. 2009) used the Extended UNIQUAC for modeling VLE of the CO_2-H_2O-MDEA/MEA system.

Equations of State

In the equation of state approach, an equation of state is used both for the liquid and the vapor phase. The model of (Furst and Renon 1993) is the most well-known electrolyte equation of state. The (Furst and Renon 1993) model is comprised of the SR (Schwartzentruber and Renon (1989)) EoS[17] and a simplified MSA[18] term. Several authors have applied the model of (Furst and Renon 1993) for acid gases-alkanolamine-H_2O systems. (Vallee et al. 1999) used this model for the CO_2/H_2S-DEA-H_2O system. (Li and Furst 2000) applied it for CO_2/H_2S-MDEA-H_2O mixtures. (Solbraa 2002) implemented the (Furst and Renon 1993) model for the MDEA-CO_2-H_2O system. (Huttenhuis et al. 2008) modified the (Solbraa 2002) model for the CO_2.CH_4-MDEA-H_2O system. (Derks et al. 2010) used the (Furst and Renon 1993) model for the CO_2–PZ–MDEA–H_2O system. (Button and Gubbins 1999) applied the SAFT[19] model for the CO_2-MEA/DEA-H_2O system.

3.3 Acid Gas Thermodynamics

As it was mentioned in section 2.5, thermodynamics plays an important role in acid gas treating. This section introduces two phenomena that are involved in thermodynamics of acid gas treating; furthermore the typical problem in acid gas thermodynamics is described.

3.3.1 Physical and Chemical Equilibria

Acid gas absorption or desorption can be simplified in two steps. In the first step gas phase species are dissolved into the aqueous phase, this step creates vapor-liquid equilibria. In the second step, chemical reactions occur in the aqueous phase and those convert aqueous gas species into ions. This step accounts for chemical equilibria. Acid gas thermodynamics involve both physical and chemical

[17] EoS: Equation of State
[18] MSA: Mean Spherical Approximation
[19] SAFT: Statistical Associating Fluid Theory

equilibria. Acid gases and alkanolamines partially dissociate in the aqueous phase and form a complex mixture of nonvolatile or moderately volatile solvent species, highly volatile acid gas (molecular) species, and nonvolatile ionic species.

3.3.2 Acid Gas Thermodynamics Problem

Acid gas thermodynamics is usually used to solve for the liquid phase speciation and partial pressure of each component present in the gas phase. In typical acid gas thermodynamics problem, system temperature, loading[20] and total amine concentration in the liquid phase are knows. The purpose of the calculations is to quantitatively obtain values for mole fraction of all species present in the liquid phase along with total pressure and composition of the gas phase (the partial pressure of each species in the gas phase). The solution of the problem is in essence analogous to bubble point pressure (Bubble P) calculations where temperature and composition of liquid phase is known and the calculations are performed in order to obtain bubble point pressure and composition of the vapor phase (Smith et al. 2005). In acid gas thermodynamics case, liquid phase is specified (T, total amount of acid gas, total amount of amine, and total amount of water) and the model will calculate liquid phase speciation (amount of all created species in the liquid phase), bubble pressure and gas phase composition (partial pressure of gas phase components). The calculated bubble pressure is then compared with the experimental value in the sum of squared residuals (objective function, see equation (5-1) in chapter 5). It is reminded that in addition to total pressure data other types of data (partial pressure, heat capacity, heat of absorption, excess enthalpy and freezing point) were used to fit model parameters. The calculated results for different properties are then compared with the measured values in the sum of squared residuals. The goal of the calculations is to minimize the sum of squared residuals.

Table 3-1 shows a list of known and unknowns in the typical acid gas thermodynamics problem.

Table 3-1. Typical acid gas thermodynamics problem

Known	Unknown
System temperature	Mole fraction of all species present in the liquid phase
Total amine concentration in the liquid phase	Bubble Pressure
Loading (Total acid gas concentration in the liquid phase)	Mole fraction of molecular species present in the gas phase (Partial pressure of gas phase species)

[20] Loading :moles of total acid gas (reacted + not reacted)/moles of amine

As an example, CO_2 removal by aqueous MDEA is discussed in details. Equation (2-3) ($CO_2 + H_2O + MDEA \leftrightarrow MDEAH^+ + HCO_3^-$) is the reaction between CO_2 and MDEA. The typical problem is to calculate pressure (P), mole fraction of species present in the liquid phase (x_i) along with mole fraction of each component in the vapor phase (y_i) while system temperature (T), loading (α_{CO_2}) (total CO_2 mole numbers) and total MDEA mole numbers (n_{MDEA}) are known. Nine equations consisting of physical and chemical equilibrium, mass balance and charge balance, completely describe the system. By solving these equations simultaneously all the system unknowns can be obtained. For simplification and since the example is introduced for illustrative purpose only, both vapor and liquid are assumed to be ideal. Known, unknowns and equations that are required to solve the above example are listed in Table 3-2.

Table 3-2. Example problem illustration

Known	Unknowns	Equations
T	x_{CO_2}	Physical Equilibrium condition (VLE):
$n_{MDEA,Total}$ ($x_{MDEA,Total}$)	x_{MDEA}	Raoult's Law:
	x_{H_2O}	$P_{H_2O} = y_{H_2O}P = x_{H_2O}P_{H_2O}^{Sat}$ [21]
	x_{MDEAH^+}	$P_{MDEA} = y_{MDEA}P = x_{MDEA}P_{MDEA}^{Sat}$ [22]
$n_{CO_2,Total}$ ($x_{CO_2,Total}$)	$x_{HCO_3^-}$	Physical Equilibrium condition (VLE):
$n_{H_2O,Total}$ ($x_{H_2O,Total}$)	y_{CO_2}	Henry's Law:
	y_{MDEA}	$P_{CO_2} = y_{CO_2}P = x_{CO_2}H_{CO_2,water}$ [23]
	y_{H_2O}	
	P	Chemical Equilibrium Condition:
		$K_{equilibrium}$ [24] $= \frac{x_{MDEAH^+}x_{HCO_3^-}}{x_{CO_2}x_{MDEA}x_{H_2O}}$
		Material Balance:
		$x_{CO_2,Total} = x_{CO_2} + x_{HCO_3^-}$
		$x_{MDEA,Total} = x_{MDEA} + x_{MDEAH^+}$
		$x_{H_2O,Total} = x_{H_2O} + 0.5\,x_{HCO_3^-} + 0.5\,x_{MDEAH^+}$
		Charge Balance:
		$x_{MDEAH^+} = x_{HCO_3^-}$
		Partial pressures sum:
		$P = P_{CO_2} + P_{H_2O} + P_{MDEA}$

[21] $P_{H_2O}^{Sat}$: Vapor pressure of pure water at system temperature
[22] P_{MDEA}^{Sat}: Vapor pressure of pure MDEA at system temperature
[23] $H_{CO_2,water}$: Henry's constant of CO_2 in pure water as solvent
[24] $K_{equilibrium}$: The equilibrium constant of equation (2-3)

Notice that the above example was presented to give better understanding of the acid gas thermodynamics problem, and the equations were presented based on ideality assumption for both phases. In reality ideal phase assumption is not valid and equations are more complex. Mixing amine and water releases considerable amount of heat and therefore mixture of amine and water cannot be assumed ideal. On the other hand, adding acid gas to mixture of amine and water, creates ionic species, columbic forces between the ions makes the solution even further from ideal state. At high pressures gas phase also deviates from ideal behavior. At real conditions (non-ideal phases) Raoult's and Henry's law (equations (3-1) and (3-2), respectively) are not valid anymore.

$$y_i \; P = x_i \; P_i^{Sat} \tag{3-1}$$

$$y_i \; P = x_i \; H_{i,solvent} \tag{3-2}$$

Where, y_i is mole fraction of component "i" in gas phase; P is system pressure; x_i is mole fraction of component "i" in liquid phase; P_i^{Sat} is the saturation pressure of component "i", and $H_{i,solvent}$ is the Henry's constant for component "i" in the solvent.

To treat these problems, thermodynamic models account for non-idealities of vapor and liquid phase are used for more rigorous calculations. The equations used in this work for thermodynamic modeling of acid gas treating will be presented in the remainder of this chapter.

3.4 Concentration Units

The experimental data available in literature are often presented in three concentration units: mole fractions, molarities and molalities. Most of the experimental data exist in the molality and loading (mole acid gas/mole amine) units, however thermodynamic models for electrolytes often use mole fraction unit. Molarity unit is also often used, but it is not a practical unit because it depends on temperature and to a certain extent also on pressure. Density of amine solution is required to convert experimental data in molarity units to molality units or mole fraction units. It is important to choose a concentration basis before start the modeling. In this work Extended UNIAQUAC model is developed based on mole fraction unit. Mole fraction unit is used for all equations.

3.5 Physical Equilibria, Vapor-Liquid Phase Equilibrium

In a closed system at constant temperature and pressure, physical equilibria determine the distribution of molecular component (including electrolytes) between the gas phase and the liquid

phase. Gas phase component dissolve in the liquid phase, and liquid phase component can evaporate.

3.5.1 Chemical Potential and Fugacity

Equilibrium between two phases, labeled α and β, is as follows:

$$\mu_i^{\alpha} = \mu_i^{\beta} \tag{3-3}$$

Where μ_i is the chemical potential of component "i".

The condition of phase equilibrium between the two phases is that the chemical potentials of each component in two phases are identical. The chemical potential does not have an intuitive equivalent physical meaning, thus it is of practical importance to express the chemical potential in terms of an auxiliary function that have more physical meaning. This useful auxiliary function is called fugacity (Prausnitz et al. 1999).

Equation (3-4) relates μ_i to fugacity. Fugacity has the same unit as pressure.

$$\mu_i - \mu_i^0 = RTln\frac{f_i}{f_i^0} \tag{3-4}$$

In the above equation, μ_i^0 and f_i^0 are standard state chemical potential and standard state fugacity of component "i", respectively. Standard states are reference points. The temperature of the standard state must be the same as the state of interest. However the composition and pressure of the two states need not be the same. It is reminded that in equation (3-4), the choice of standard state for either μ_i^0 or f_i^0 is arbitrary, but both may not be chosen independently; when one is chosen, the other one is fixed (Prausnitz et al. 1999). The ratio of f_i to f_i^0 is called activity:

$$a_i = \frac{f_i}{f_i^0} \tag{3-5}$$

By applying fugacity definition to equation (3-5), a new form of fundamental equation of phase equilibrium is obtained:

$$f_i^{\alpha} = f_i^{\beta} \tag{3-6}$$

3.5.2 Gas Phase Chemical Potential, Gas Phase Non-Idealities

The chemical potential of a component in an ideal gas mixture at T and P is determined by:

$$\mu_i^{ig}(T,P) = \mu_i^{0,\mathrm{ig}}(\mathrm{T},\mathrm{P}) + RTlny_i \tag{3-7}$$

Where y_i is the mole fraction of component "i" in the ideal gas mixture and $\mu_i^{0,\mathrm{ig}}$ is the standard state chemical potential at system temperature T and some arbitrary pressure P. Standard state chemical potential is defined as chemical potential of the pure ideal gas (superscript 0 stands for pure and superscript "ig" indicates ideal gas). Notice that ideal gas standard state chemical potential is usually given at 1 bar (pressure of 1 bar is represented by P_0, P_0 = 1 bar). The chemical potentials of gases are highly dependent on pressure. Standard state chemical potential at T and P is described by:

$$\mu_i^{0,ig}(T,P) = \mu_i^{0,\mathrm{ig}}(\mathrm{T},P_0) + RTln\frac{P}{P_0} \tag{3-8}$$

Replacing equation (3-8) in equation (3-7) yields to equation (3-9) for chemical potential of component "i" in an ideal gas mixture at pressure P:

$$\mu_i^{ig}(T,P) = \mu_i^{0,\mathrm{ig}}(\mathrm{T},P_0) + RTln\frac{Py_i}{P_0} \tag{3-9}$$

As it was mentioned earlier, in acid gas thermodynamics, gas phase is not ideal. The deviation of real mixture chemical potential from that of ideal gas mixture at T and P is described by the residual term ($\mathrm{RTln}\widehat{\varphi_i}$). Thus, the chemical potential of component "i" in a real gas mixture is defined by sum of the chemical potential of component "i" in an ideal gas mixture and the residual term:

$$\mu_i^{g}(\mathrm{T},\mathrm{P}) = \mu_i^{0,ig}(T,P) + \mathrm{RTln}\widehat{\varphi_i} = \mu_i^{0,\mathrm{ig}}(\mathrm{T},P_0) + RTln\frac{Py_i}{P_0} + \mathrm{RTln}\widehat{\varphi_i} \tag{3-10}$$

Where $\widehat{\varphi_i}$ is the fugacity coefficient of component "i" in the gas phase. Chemical potential of component "i" is related to the fugacity of component "i" in a gas phase by equation (3-4), thus for a gas phase equation (3-4) is written as:

$$\mu_i^{g} - \mu_i^{0,g} = RTln\frac{f_i^{g}}{f_i^{0,g}} \tag{3-11}$$

Where, $f_i^{0,g}$ is the standard state fugacity. $f_i^{0,g}$ is defined as the fugacity of pure ideal gas at system temperature and an arbitrary pressure. The arbitrary pressure called P_0 chosen to be 1 bar, and because fugacity of pure ideal gas is equal to pressure, thus standard state fugacity for component "i" in a gas phase ($f_i^{0,g}$) is set equal to 1 bar. Thus:

$$f_i^{0,g} = P_0 = 1\ bar \tag{3-12}$$

Substituting equation (3-10) in equation (3-11) yields to the equation for fugacity of component "i" in the vapor phase:

$$f_i^v = \widehat{\varphi_i} P y_i \tag{3-13}$$

In this study SRK[25] equation of state (Soave 1972) is used to calculate the fugacity coefficients in the gas phase (gas phase non-idealities)

.

3.5.3 Liquid Phase Chemical Potential, Liquid Phase Non-Idealities

The most difficult challenge in describing VLE in weak electrolyte systems is representing liquid phase behavior. Presence of ionic species in the liquid phase results in a highly non-ideal behavior. Liquid phase non-idealities (deviations from ideal phase) are usually expressed by activity coefficients.

The solution is defined as an ideal solution if the chemical potential of every component in the solution is described by:

$$\mu_i^{id}(T,P) = \mu_i^0(T,P) + \mathrm{RTln}x_i \tag{3-14}$$

Where R is the gas constant, T is the absolute temperature in Kelvin, and x_i is the mole fraction of component "i". μ_i^0 is known as the standard state or reference state chemical potential and is a function of temperature and pressure. For a real solution, the chemical potential is not a linear function of the logarithm of the mole fraction. The chemical potential of "i" in a real solution is defined based on the definition of the ideal solution and is calculated by the sum of two terms: an ideal term and an excess term ($\mu_i^{ex} = \mathrm{RTln}\gamma_i$). The excess term shows the deviation of chemical potential in a real mixture from chemical potential in an ideal mixture.

$$\mu_i^l(T,P) = \mu_i^{id}(T,P) + \mu_i^{ex}(T,P) = \mu_i^0(T,P) + \mathrm{RTln}x_i + \mathrm{RTln}\gamma_i = \mu_i^0(T,P) + \mathrm{RTln}(x_i\gamma_i) \tag{3-15}$$

Where activity coefficient of component "i" (γ_i) is a function of temperature, pressure, and composition of the solution. Standard state chemical potential is usually given at 1 bar (pressure of 1 bar is represented by P_0, P_0 = 1 bar). Standard state chemical potential at pressure P is related to

[25] SRK: Soave-Redlich-Kwong equation

standard state chemical potential at pressure P_0 by equation (3-17). The standard state chemical potential of a component at a certain pressure can be calculated by integration of equation (3-14) from P_0 to P. The pressure dependence of the chemical potential of component "i" is given by:

$$\left[\frac{\partial \mu_i}{\partial P}\right]_T = V_i \tag{3-16}$$

V_i is the partial molar volume of component "i". Assuming that the partial molar volume of the component is independent of pressure, integrating equation (3-14) results in:

$$\mu_i^{0,l}(T,P) = \mu_i^0(T,P_0) + V_i(P - P_0) \tag{3-17}$$

Replacing equation (3-17) in equation (3-15) yields to the following equation for chemical potential of component "i" in a real liquid mixture:

$$\mu_i^l(T,P) = \mu_i^0(T,P_0) + V_i\,(P - P_0) + RT\ln(x_i\gamma_i) \tag{3-18}$$

Chemical potential of component "i" in a liquid mixture is related to the fugacity of component "i" in a liquid phase by the general equation (3-4), thus for a liquid phase equation (3-4) is written as:

$$\mu_i^l - \mu_i^{0,l} = RT ln \frac{f_i^l}{f_i^{0,l}} \tag{3-19}$$

Where $f_i^{0,l}$ is the fugacity of "i" at some arbitrary condition known as the standard state.

If standard state chemical potential is defined at system pressure, then equation (3-14) in equation (3-19) results in the following equation for the fugacity of component "i" in the liquid phase:

$$\frac{f_i^l}{f_i^{0,l}} = x_i\gamma_i \rightarrow f_i^l = x_i\gamma_i f_i^{0,l} \tag{3-20.a}$$

If standard state chemical potential is defined at P_0 = 1 bar, then substituting equation (3-18) in equation (3-19) gives the following equation:

$$\frac{f_i^l}{f_i^{0,l}} = x_i\gamma_i \rightarrow f_i^l = x_i\gamma_i f_i^{0,l} exp\left(\frac{V_i\,(P-P_0)}{RT}\right) \tag{3-20.b}$$

Where $exp\left(\frac{V_i\,(P-P_0)}{RT}\right)$ is called Poynthing correction factor and is the term for correction of pressure.

definition of γ_i and $\mu_i^{0,l}\ (or\ f_i^{0,l})$ is incomplete unless a standard state (reference state) is specified. "At any composition, the activity coefficient depends on the choice of standard state. Because the choice of standard state is arbitrary, it is convenient to choose $\mu_i^{0,l}\ (or\ f_i^{0,l})$ such that γ_i assumes values close to unity and when, for a range of conditions, γ_i is exactly equal to unity, the solution is called ideal. "However, because of the intimate relation between the activity coefficient and the standard state fugacity, the definition of solution ideality ($\gamma_i = 1$) is not complete unless the choice of standard state is clearly indicated (Prausnitz et al. 1999)." To specify the conditions at which the activity coefficient of component "i" becomes equal to unity, frequently two choices are used. Either of two choices leads to an ideal solution definition. One leads to an ideal solution in the sense of Raoult's law and the other leads to an ideal solution in the sense of Henry's law. The process of identifying standard states at which the activity coefficients of all component in a solution become unity is called normalization. Next section will discuss standard states used in this modeling framework.

3.5.4 Standard States, Reference States

In this work water is considered as the solvent. The reference state for water is defined as the state of the pure component at the system temperature and pressure. Therefore, the chemical potential of water in an aqueous solution is calculated by the following equation:

$$\mu_w = \mu_w^0 + RTln(x_w\gamma_w) \tag{3-21}$$

In real mixture : $\gamma_w \rightarrow 1 \quad as \quad x_w \rightarrow 1$

μ_w^0 is the standard state chemical potential of water and equated to the molar Gibbs energy of pure liquid at system temperature and pressure. In the limit of $x_w \rightarrow 1$, γ_w becomes 1 and excess term vanishes. This standard state leads to the Raoult's law[26] definition for an ideal solution. Therefore, fugacity of water in aqueous solution is written as:

$$f_w(T,P) = f_{pure,w}(T,P)x_w\gamma_w \tag{3-22}$$

(If the standard state is considered at P_0 $then$: $f_w(T,P) = f_{pure,w}(T,P_0)x_w\gamma_w exp\left(\frac{V_w\,(P-P_0)}{RT}\right)$)

For a mixture of a nonvolatile solute dissolved in a solvent, equation (3-21) is used to define chemical potential of the solvent, here water, and the state of pure component is used as standard state for solvent. However, for a nonvolatile solute, for most cases, at normal temperatures and

[26]Raoult's law: At any T, P and x : $f_i(T,P,x) = f_{i,pure}\,(T,P,x)\,x_i \quad (x_i \rightarrow 1)$

pressures, a pure nonvolatile solute cannot exist as liquid, thus for a nonvolatile solute, pure liquid at system temperature and pressure is often not a suitable standard state (Prausnitz et al. 1999). Thus, the chemical potential of all the dissolved solutes, except water, is written as:

$$\mu_i = \mu_i^* + RTlna_i = \mu_i^* + RT\ ln(x_i\gamma_i^*) \quad (3\text{-}23)$$

In real mixture : $\gamma_i^* \rightarrow 1 \quad as \quad x_i \rightarrow 0$

Where μ_i^* is the standard state chemical potential of component "i", which is independent of composition, but is dependent on temperature, pressure and γ_i^* is the rational unsymmetrical activity coefficient. The standard state for the solute is defined by a hypothetical ideal solution of component "i" in the solvent, at system temperature and pressure and at unit concentration, $x_i = 1$ (Prausnitz et al. 1999). In this ideal solution, $\gamma_i = 1$. In the real solution, $\gamma_i^* \rightarrow 1$ as $x_i \rightarrow 0$ (Prausnitz et al. 1999). Keep in mind that it is very common to misunderstand the standard state for the solute as the solute at system temperature and pressure and at infinite dilution. That is not correct since at infinite dilution, the chemical potential of the solute is $-\infty$ (when $x_i = 0$ then $\ln(0) = -\infty$ and from equation (3-23) $\mu_i = -\infty$) (Prausnitz et al. 1999). As it was mentioned earlier, the standard state chemical potential for the solute "i" must define at some fixed (non-zero) concentration, this concentration is unit concentration. Unit concentration is used because its logarithm is zero, therefore from equation (3-23) at unit concentration, $\mu_i = \mu_i^*$ (Prausnitz et al. 1999).

This standard state definition leads to Henry's law[27] for an ideal solution. γ_i^* is the rational unsymmetrical activity coefficient and is defined by:

$$\gamma_i^* = \frac{\gamma_i}{\gamma_i^\infty} \quad (3\text{-}24)$$

(When $x_i \rightarrow 0$, then $\gamma_i \rightarrow \gamma_i^\infty$ therefore, $\gamma_i^* \rightarrow 1$)

Where γ_i^∞, is the infinite dilution activity coefficient of solute in water and it depends on temperature and pressure. According to this standard state definition, fugacity of the dissolved solute is defined by:

[27]Henry's law: At any T, P and x : $f_i(T,P,x) = H_{i,solvent}(T,P,solvent\ and\ solute\ nature)x_i \quad (x_i \rightarrow 0)$

$$f_i = H_{i,solvent} x_i \gamma_i^* \tag{3-25}$$

3.5.5 Vapor-Liquid Equilibria Condition

Equation (3-3) shows the condition for vapor-liquid equilibria. For the systems studied in this work, vapor-liquid equilibrium is considered for water, amine (MDEA, MEA), acid gases (CO_2 and H_2S) and methane. Equations for chemical potential are already explained in the previous sections. For water, the condition for vapor-liquid equilibria is formulated by combining equations (3-10) and (3-21) (note in equation (3-21) $\mu_w^{0,l}(T,P)$ is related to $\mu_w^0(T,P_0)$ according to equation (3-17): $\mu_w^{0,l}(T,P) = \mu_w^0(T,P_0) + V_w(P - P_0)$):

$$\frac{\mu_w^{0,l}(T,P_0) - \mu_w^{0,\mathrm{ig}}(T,P_0)}{RT} + \frac{V_w\,(P - P_0)}{RT} = \ln\left[\frac{P y_w \widehat{\varphi_w}}{x_w \gamma_w P_0}\right] \tag{3-26}$$

In this work, activity coefficients are calculated from the Extended UNIQUAC model and the SRK equation of state is used for calculating fugacity coefficients in the vapor phase.

For amines, MDEA and MEA, and also for H_2S the condition for vapor-liquid equilibria is obtained by combining equations (3-10) and (3-23), (note in equation (3-23) $\mu_{i,aq}^*(T,P)$ is related to $\mu_{i,aq}^*(T,P_0)$ according to equation (3-17): $\mu_{i,aq}^*(T,P) = \mu_{i,aq}^*(T,P_0) + V_i(P - P_0)$)

$$\frac{\mu_{i,aq}^*(T,P_0) - \mu_i^{0,\mathrm{ig}}(T,P_0)}{RT} + \frac{V_i\,(P - P_0)}{RT} = \ln\left[\frac{P y_i \widehat{\varphi_i}}{x_i \gamma_i^* P_0}\right] \tag{3-27}$$

Methane dissolves very little in the water. It is common to use Henry's constant for sparingly soluble gases in liquid. Carbon dioxide is supercritical at system temperature, and it does not exist at system temperature as pure component, hence pure component standard state properties are not available for it. In such cases, the first term in the right hand side of equation (3-27) is substituted by Henry's constant which leads to equation (3-28). Note that in this study Henry's constant is used to calculate standard state chemical potentials for CO_2 in order to calculate equilibrium constant for CO_2 in aqueous phase in equilibrium with CO_2 in the gas phase. Similar to CO_2, for CH_4 Henry's constant is used to calculate equilibrium constant for CH_4 in aqueous phase in equilibrium with CH_4 in gas phase.

$$\ln\left(\frac{H_i(T,P_{w,sat})}{P_0}\right) + \frac{V_i^{\infty}\,(P - P_{w,sat})}{RT} = \ln\left[\frac{P y_i \widehat{\varphi_i}}{x_i \gamma_i^* P_0}\right] \tag{3-28}$$

Equation (3-28) is known as Krichevski-Iliinskaya equation (Kritchevsky and Iliinskaya 1945) and is used at pressures above the boiling point pressure of the solvent. In this equation, P_0 is 1 bar, $P_{w,sat}$ is the vapor pressure of the solvent at the relevant temperature, P is the total pressure and V_i^{∞} is the partial molar volume of the solute at infinite dilution. In this study for both carbon dioxide and methane Henry's constant in pure water is used. For carbon dioxide a temperature dependent Henry's law correlation proposed by (Rumpf and Maurer 1993) is used.

$$\ln((H^*_{CO_2,w}\, M_w) = 192.876 - \frac{9624.4\ K}{T} + 1.441 \times 10^{-2} K^{-1} T - 28.749 \ln(T) \qquad (3\text{-}29)$$

$V^{\infty}_{CO_2}$ is calculated from the equation presented by Rumpf and Maurer (Rumpf and Maurer 1993). Henry's law correlation presented by Crovetto et al. (Crovetto et al. 1982) is used for methane. Notice that bubble point pressure of the studied electrolyte solutions can be found by simultaneously solving vapor-liquid equilibria equations. As explained earlier in this study SRK equation of state is used to calculate fugacity coefficients in the vapor phase (gas phase non-idealities). Classical mixing rule is utilized to calculate mixture properties. It is noted that all binary interaction parameters were fixed to zero i.e. there is no adjustable parameter. Pure component properties that are applied in this study are summarized in Table 3-3.

Table 3-3. Pure component properties used in SRK EoS

Component	P_{cr}*, bar	T_{cr}**, K	ω***
H_2O	220.64	647.096	0.344
CO_2	73.773	304.1282	0.225
H_2S	89.63	373.5	0.094
MDEA	41.6	741.9	0.6253
MEA	71.24	678.2	0.4467
CH_4	45.99	190.6	0.012

P_{cr} : Critical pressure

**T_{cr} : Critical pressure*

***ω : Acenric factor*

3.6 Chemical Equilibria, Speciation Equilibria

The term speciation describes what happens when electrolyte compounds are dissolved in water. Electrolytes dissociate partly or completely when dissolved in water. The composition of the created species in the solution at equilibrium is calculated by solving the equations for speciation equilibria. The condition for speciation equilibrium is that for each reaction the sum of the chemical potential of the reactants is equal to the sum of the chemical potentials of the products. Equations for

chemical potential of water and dissolved solutes were already illustrated in section 3.5. Reactions that occur in each system will be explained in next chapter. The condition for chemical equilibrium for each reaction is commonly shown by:

$$lnK = -\frac{\Delta G_j^0}{RT} = \sum_i v_{i,j} ln a_i \tag{3-30}$$

Where K is the equilibrium constant at the temperature T, ΔG_j^0 is the change of standard Gibbs energy of formation for the reaction "j". a_i is the activity of component "i" and $v_{i,j}$ is the stoichiometric coefficient of component "i" involved in reaction "j". Notice that in order to calculate the equilibrium composition of all the components present in the system, vapor-liquid equilibria equations and chemical equilibria equations have to be solved simultaneously.

3.7 Standard state properties

In this work, equilibrium constants are calculated from standard state chemical potentials (standard state chemical potential is equal to the molar Gibbs energy at standard state (G^0)). For most component, the values of standard state chemical potentials at 25 °C are listed in NIST[28] tables (NIST) and (DIPPR). Standard state chemical potentials at 25 °C that are not available in these tables are adjusted to all kinds of experimental data available in the developed regression data base. Standard state chemical potentials at interested temperature are calculated from their values at 25 °C by integrating the Gibbs-Helmholtz equation using standard state enthalpies and standard state heat capacities:

$$-\frac{dlnK}{dT} = \frac{d(\frac{\Delta G^0}{RT})}{dT} = -\frac{\Delta H^0}{RT^2} \quad \text{(at constant Pressure)} \tag{3-31}$$

Integrating equation (3-31) form 298.15 K (25 °C) to the temperature of interest gives:

$$\ln K_T - \ln K_{298.15} = \int_{298.15}^{T} \frac{\Delta H^0}{RT^2} dT \tag{3-32}$$

The change in standard state enthalpy of formation with temperature is calculated from the corresponding heat capacities:

$$\frac{d\Delta H^0}{dT} = \Delta C_P^0 \tag{3-33}$$

[28] NIST: National Institute of Standards and Technology

$C_{P,i}^{0}$ is the standard state heat capacity of component "i" and is correlated by the following equation for all solutes:

$$C_{P,i}^{0} = a_i + b_i T + \frac{c_i}{T - T_\Theta} \tag{3-34}$$

In the above equation, the term $T - T_\Theta$ provides for the steep change in $C_{P,i}^{0}$ below 25 °C. T_Θ is given the constant value of 200 K for all components.

Inserting equation (3-34) in equation (3-33) and then in equation (3-32) gives the equilibrium constant as a function of temperature:

$$R \ln K_T = R \ln K_{T_0} - \Delta H_{T_0}^{0} \left(\frac{1}{T} - \frac{1}{T_0} \right) + \Delta a \left(\ln \frac{T}{T_0} + \frac{T}{T_0} - 1 \right) + 0.5 \Delta b \left(\frac{(T - T_0)^2}{T} \right) +$$
$$\frac{\Delta c}{T_\Theta} \left(\frac{T - T_\Theta}{T} \ln \frac{T - T_\Theta}{T_0 - T_\Theta} - \ln \frac{T}{T_0} \right) \tag{3-35}$$

With the value of the equilibrium constant at the temperature T, the composition of the solution can be calculated at the temperature T if the activity coefficients are known at this temperature. It is noted that that in order to reproduce modeling predictions presented in this study it is of high importance to implement the developed model with the same fitted parameters and the same standard state properties presented in this work.

3.8 Extended UNIQUAC Model Structure

In this work, activity coefficients in the liquid phase are determined by the Extended UNIQUAC model, the version that was presented by (Thomsen and Rasmussen 1999). The vapor phase fugacities are calculated by SRK equation of state. The Extended UNIQUAC model was first developed by (Sander et al. 1986) in 1986, and is a combination of the original UNIQUAC model by (Abrams and Prausnitz 1975) and (Maurer and Prausnitz 1978) with an extended Debye-Huckel term. The Debye-Huckel term accounts for long range interactions and it allows the model to be used for electrolyte solutions. The Extended UNIQUAC model comprises three terms: a combinatorial (entropic) term, a residual (enthalpic) term and an electrostatic term. The combinatorial and residual terms are the same terms used in original UNIQUAC equation ((Abrams and Prausnitz 1975) and (Maurer and Prausnitz 1978)). The electrostatic term is the extended Debye-Huckel law.

$$\frac{G^E}{RT} = \left(\frac{G^E}{RT}\right)_{Combinatorial,UNIQUAC\ Entropic} + \left(\frac{G^E}{RT}\right)_{Residual,UNIQUAC\ Enthalpic} + \left(\frac{G^E}{RT}\right)_{Extended\ Debye-Huckel} \tag{3-36}$$

The combinatorial term is independent of temperature; it only depends on the relative size of the component:

$$\left(\frac{G^E}{RT}\right)_{Combinatorial,UNIQUAC\ Entropic} = \sum_i x_i\, ln\left(\frac{\varphi_i}{x_i}\right) - \frac{z}{2}\sum_i x_i q_i\, ln\left(\frac{\varphi_i}{\theta_i}\right) \tag{3-37}$$

Z=10 is the coordination number and x_i is the mole fraction of component "i". φ_i and θ_i are volume fraction and surface fraction of component "i", respectively:

$$\varphi_i = \frac{x_i r_i}{\sum_l x_l r_l} \tag{3-38}$$

$$\theta_i = \frac{x_i q_i}{\sum_l x_l q_l} \tag{3-39}$$

r_i and q_i are the volume and surface area parameters for component "i", respectively. Unlike the classical UNIQUAC model, in the Extended UNIQUAC model these parameters are considered as adjustable parameters and their values are determined by fitting to experimental data.

The residual term represent interaction between different pairs and is dependent of temperature:

$$\left(\frac{G^E}{RT}\right)_{Residual,UNIQUAC\ Enthalpic} = -\sum_i x_i\, q_i ln(\sum_k \theta_k\, \psi_{kl}) \tag{3-40}$$

where ψ_{kl} is

$$\psi_{kl} = \exp(-\frac{u_{kl}-u_{ll}}{T}) \tag{3-41}$$

u_{kl} and u_{ll} are energy interaction parameters between species. They are assumed symmetrical ($u_{kl} = u_{lk}$) and temperature dependent.

$$u_{kl} = u_{kl}^0 + u_{kl}^T(T - 289.15) \tag{3-42}$$

There are no adjustable parameters in SRK equation of state and Debye-Huckel term. All the adjustable parameters belong to UNIQUAC equation. Therefore, the model adjustable parameters are r_i, q_i for species i and u_{kl}^0 and u_{kl}^T for interaction energy between species k and l and some standard state properties and heat capacity parameters as will be described later. The model parameters are determined by fitting to experimental data.

Activity coefficient is derived from partial molar differentiation of the excess Gibbs energy expression:

$$ln\gamma_i = \left[\frac{\partial(\frac{nG^E}{RT})}{\partial n_i}\right]_{P,T,n_{j\neq i}} \tag{3-43}$$

Therefore combinatorial and residual parts of the rational, symmetrical activity coefficients are obtained by partial molar differentiation of combinatorial and residual UNIQUAC terms (equations (3-37) and (3-40)).

$$ln\gamma_i^C = ln\left(\frac{\emptyset_i}{x_i}\right) + 1 - \frac{\emptyset_i}{x_i} - \frac{z}{2}q_i\left[\ln\left(\frac{\emptyset_i}{\theta_i}\right) + 1 - \frac{\emptyset_i}{\theta_i}\right] \tag{3-44}$$

$$ln\gamma_i^R = q_i\left[1 - \ln(\textstyle\sum_k \theta_k\psi_{ki}) - \sum_k \frac{\theta_k\psi_{ik}}{\sum_l \theta_l\psi_{lk}}\right] \tag{3-45}$$

Setting $x_w = 1$ in equations (3-44) and (3-45), yield to infinite dilution activity coefficient equations:

$$ln\gamma_i^{C\infty} = ln\frac{r_i}{r_w} + 1 - \frac{r_i}{r_w} - \frac{Z}{2}q_i\left[ln\frac{r_i q_w}{r_w q_i} + 1 - \frac{r_i q_w}{r_w q_i}\right] \tag{3-46}$$

$$ln\gamma_i^{R\infty} = q_i[1 - ln\psi_{wi} - \psi_{iw}] \tag{3-47}$$

It is worth mentioning that the combinatorial and residual terms of the UNIQUAC excess Gibbs energy equation are based on the rational, symmetrical activity coefficient convention both for solvent (water) and solutes.

The expression for Extended Debye-Huckel law excess Gibbs energy function is

$$\left(\frac{G^E}{RT}\right)_{Extended\ Debye-Huckel} = -x_w M_w \frac{4A}{b^3}\left[\ln\left(1 + b\sqrt{I}\right) - b\sqrt{I} + \frac{b^2 I}{2}\right] \tag{3-48}$$

Where x_w is water mole fraction, M_w (kg/mol) is water molar mass, b is considered to be a constant equal to 1.50 $(kg/mol)^{1/2}$ and I is the ionic strength in (mol/(kg H_2O)) which is defined by:

$$I = \frac{1}{2}\sum_i m_i z_i^2 \tag{3-49}$$

Where m_i and z_i are the molality (mol/kg H_2O) and the charge number of ionic species "I", respectively.

In equation (3-48), A is the Debye-Huckel constant and is presented by:

$$A = \frac{F^3}{4\pi N_A}\left[\frac{d}{2(\varepsilon_0 DRT)^3}\right]^{\frac{1}{2}} \tag{3-50}$$

Where F ($C.mol^{-1}$) is the Faraday's constant, N_A (mol^{-1}) is Avogadro's number, ε_0 ($C^2J^{-1}m^{-1}$) is the vacuum permittivity, R ($Jmol^{-1}K^{-1}$) is the gas constant, T (K) is the temperature, d (kgm^{-3}) is the density of pure water and D is the dielectric constant (relative permittivity) of pure water. Notice the equation (3-50) represents a simplified function for Debye-Huckel constant. The assumptions used along with this equation are as follows: **1)** The mass and volume of ions are assumed to be zero. By this assumption, the density of solution becomes equal to density of pure water. **2)** The effect of ionic species in the dielectric constant is also neglected. By considering this approximation, D is considered as dielectric constant of pure water.

It is noted that d and D parameters are temperature dependent. Based on the d and D values, Debye-Huckel constant can be approximated by the following equation in the temperature range of $273.15\ K \leq T \leq 383.15\ K$.

$$A = \left[1.131 + 1.335\times10^{-3}\times(T-273.15) + 1.164\times10^{-5}\times(T-273.15)^2\right]\ (kg/mol)^{1/2} \tag{3-51}$$

It is reminded that there is no adjustable parameter in the Debye-Huckel term.

According to equation (3-43) activity coefficients are derived by partial molar differentiation of Debye-Huckel excess Gibbs energy term. Unlike UNIQUAC term, Debye-Huckel is described in terms of rational unsymmetrical convention for ions and rational symmetrical convention for water. The rational symmetrical activity coefficient of water derived from Debye-Huckel term is defined as:

$$ln\gamma_w^{DH} = \frac{2}{3}M_w A I^{\frac{3}{2}}\sigma(bI^{\frac{1}{2}}) \tag{3-52}$$

$$\sigma = \frac{3}{x^3}\left\{1 + x - \frac{1}{1+x} - 2\ln(1+x)\right\} \quad (3\text{-}53)$$

The rational unsymmetrical activity coefficient of ions derived from Debye-Huckel term is defined as:

$$\gamma_i^{*DH} = -Z_i^2 \frac{A\sqrt{I}}{1+b\sqrt{I}} \quad (3\text{-}54)$$

Activity coefficients of species are obtained by adding three contributions of Extended UNIQUAC model. It is noted that in Extended UNIQUAC model, activity coefficient of water is defined based on rational symmetrical convention and activity coefficient of ions is rational unsymmetrical convention. Therefore, the logarithm of the symmetrical activity coefficient of water in is the sum of the tree differentiations of the three terms of excess Gibbs energy terms of Extended UNIQUAC (sum of equations (3-44), (3-45), (3-52))

$$ln\gamma_w = ln\gamma_w^C + ln\gamma_w^R + ln\gamma_w^{DH} \quad (3\text{-}55)$$

The rational unsymmetrical activity coefficients of ions are obtained according to the definition of rational unsymmetrical activity coefficient (equation (3-24)) and by adding three contributions of Extended UNIQUAC:

$$ln\gamma_i^* = ln\gamma_i^{*,C} + ln\gamma_i^{*,R} + ln\gamma_i^{*,DH} = ln\frac{\gamma_i^C}{\gamma_i^{C\infty}} + ln\frac{\gamma_i^R}{\gamma_i^{R\infty}} + ln\gamma_i^{*DH} = ln\gamma_i^C - \ln\gamma_i^{C\infty} + \ln\gamma_i^R - ln\gamma_i^{R\infty} + ln\gamma_i^{*,DH} \quad (3\text{-}56)$$

In the Extended UNIQUAC model, Equations (3-55) and (3-56) are used to calculate activity coefficient of water (solvent) and dissolved solutes, respectively.

3.9 Types of Experimental Data

This section discusses how different types of experimental data are related to the model parameters.

3.9.1 Partial Pressure Data, Acid Gas Solubility Data

Data in the form of acid gas solubility (acid gas partial pressure over the mixture of aqueous amine), as a function of loading (mole acid gas/mole amine) and temperature have been used to model parameters. Equation (3-27) and (3-28) relate model parameters to partial pressure data of H_2S and partial pressure data of CO_2, respectively.

3.9.2 Total Pressure Data

Data in the form of total pressure of the solution as a function of temperature and concentration was used to adjust the activity coefficients by simultaneous optimization of the UNIQUAC model parameters. Total pressure is the sum of partial pressure of all vapor phase constituents, equation (3-57). By summation of all partial pressures, model parameters are related to total pressure data. Determination of activity coefficients from total pressure measurements was proposed by (Barker 1953). (Barker 1953) showed that the accuracy of activity coefficients derived from total pressure data is comparable with those derived from partial pressure measurements. That is beneficial especially at conditions where partial pressure data are scarce or not available.

$$P_{Total} = \sum_{i=1}^{n} P_{i,partial\ pressure} \tag{3-57}$$

In the above equation, P_{Total} is the total pressure. "n" is the number of components in the vapor phase and $P_{i,partial\ pressure}$ is the partial pressure of each component.

3.9.3 Pure Vapor Pressure Data

Pure vapor pressure data as a function of temperature were used to optmize model parameters. Pure vapor pressure data are related to infinite dilution activity coefficients. Using pure vapor pressure data for regression provides more accurate prediction of infinite dilution activity coefficients. The following equation shows the condition for vapor-liquid equilibria for a pure component.

$$-\frac{\Delta G^0}{RT} = ln\frac{y_i \varphi_i P_i^{Vapor}}{x_i \gamma_i^* P_0} \tag{3-58}$$

In the above equation P_0 is 1 bar, y_i and x_i are equal to 1 as both gas and liquid phases are pure. γ_i^* is the unsymmetrical activity coefficient for the dissolved solute and is defined by equation (3-24) ($\gamma_i^* = \frac{\gamma_i}{\gamma_i^\infty}$). According to the definitions for the standard state, for the pure solute (symmetrical activity convention):

$$\gamma_i \rightarrow 1 \qquad as \qquad x_i \rightarrow 1$$

Therefore above equation (3-48) is reduced to

$$-\frac{\Delta G^0}{RT} = ln\frac{\varphi_i \gamma_i^\infty P_i^{Vapor}}{1} \tag{3-59}$$

Where γ_i^{∞} is the infinite dilution activity coefficient (activity coefficient of component "i" in the mixture of component "i" and water when mixture is very dilute with respect to component "i") and is defined by:

$$ln\gamma_i^{\infty} = ln\gamma_i^{C\infty} + ln\gamma_i^{R\infty} \tag{3-60}$$

In this equation, C stands for the combinatorial term of the UNIQUAC equation and R indicates the enthalpy term of the UNIQUAC equation. $\gamma_i^{C\infty}$ and $\gamma_i^{R\infty}$ were already described by equations (3-46) and (3-47), respectively.

3.9.4 Heat Capacity Data

As stated by equation (3-33) the liquid phase heat capacity of a mixture is calculated by taking the derivative of the enthalpy of the liquid phase at constant pressure. Data in the form of the heat capacity of mixture as a function of temperature and concentration were used to adjust activity coefficients through simultaneous regression of the model parameters by taking the derivative of the UNIQUAC model. It is noted that heat capacity data are useful to determine heat capacity parameters in equation (3-34); also they are efficient for determining the value of the surface area parameter q, because the UNIQUAC contribution to the excess enthalpy and excess heat capacity is proportional to the parameter q. An important advantage of the Extended UNIQUAC model compared to models like the Pitzer is that temperature dependence is built into the model. This enables the model to describe thermodynamic properties that are temperature derivatives of the excess Gibbs function, such as heat of mixing and heat capacity

3.9.5 Excess Enthalpy Data

Excess enthalpy data is favorable for the modeling, since this type of data is directly related to the temperature dependence of excess Gibbs energy. Equation (3-61) describes the relationship between the temperature dependence of the activity coefficient, excess Gibbs energy and the excess enthalpy data.

$$\left(\frac{\partial(\frac{G^E}{RT})}{\partial T}\right)_{P,x} = -\frac{H^E}{RT^2} = x_w\left(\frac{\partial ln\gamma_w}{\partial T}\right)_{P,x} + x_{alkanolamine}\left(\frac{\partial ln\gamma_{alkanolamine}}{\partial T}\right)_{P,x} \tag{3-61}$$

Regressing excess enthalpy data improves model temperature dependency.

3.9.6 Freezing Point Depression Data

Freezing point data were also used in the parameter optmization process. This kind of data is useful to get a better prediction for water activity. In the temperature range considered, ice is the only solid phase that is formed. The solid – liquid equilibrium criterion is:

$$\mu_w^S = \mu_w^l \tag{3-62}$$

The solid phase is pure water; therefore the chemical potential of water in the solid phase is equal to its standard chemical potential in the solid phase.

$$\mu_w^S = \mu_w^{0,S} \tag{3-63}$$

The chemical potential of water in the liquid phase is shown by

$$\mu_w^l = \mu_w^{0,l} + RTlna_w \tag{3-64}$$

Combing equations (3-51) and (3-49) yields to:

$$-\frac{\Delta G^0}{RT} = lna_w \tag{3-65}$$

3.9.7 Heat of Absorption Data

Regressing heat of absorption data along with other types of data improve temperature dependency of the model. Heat of absorption is the heat involved when acid gas is absorbed in the liquid phase. Heat of absorption includes contributions of heat of all of the reactions and heat of physical absorption of gas molecules dissolving into the solution. When the solution becomes saturated (at high loadings), absorption of gas molecules into liquid only happened physically and the heat of absorption approaches physical heat of absorption (Posey 1997). In this work heat of absorption is calculated from the energy balance of the absorption process. The enthalpy balance for the absorption process thus is written as:

$$\Delta H_{abs} = \frac{n_{Final}H^L_{Final} - n_{Initial}H^L_{Initial} - \Delta n_{Acid\ Gas}H^g_{Acid\ Gas}}{\Delta n_{Acid\ Gas}} \tag{3-66}$$

In the above equation ΔH_{abs} is the heat of absorption which is usually given relative to the moles of acid gas absorbed, H^L_{Final} is the molar enthalpy of the final solution, $H^L_{Initial}$ is the molar enthalpy of the initial solution, $H^g_{Acid\ Gas}$ is the molar enthalpy of the gaseous acid gas absorbed in the liquid

solution, n_{Final} is the number of moles of the final solution, $n_{Initial}$ is the number of moles of the initial solution and $\Delta n_{Acid\ Gas}$ is the number of moles of acid gas absorbed.

Heats of absorption data reported in the literature are categorized into two types: I) integral heat of absorption, II) differential heat of absorption. The integral heat of absorption for a solution of amine-acid gas-water is the enthalpy change of the solution per mole of acid gas form loading zero to final acid gas loading. However, differential heat of absorption refers to the enthalpy change per mole of acid gas when very small amount of the acid gas is added to the loaded solution. H^L_{Final}, $H^L_{Initial}$ and $H^g_{Acid\ Gas}$ values are required to calculate both types of heat of absorption.

The total enthalpy of formation of an electrolyte solution at constant pressure and composition is calculated by:

$$nH = \widetilde{n_w} H_w + \sum_i \widetilde{n_i} H_i \tag{3-67}$$

Where H_w is the partial molar enthalpy of water and H_i is the partial molar enthalpy of solutes. $\widetilde{n_w}$ and $\widetilde{n_i}$ are the mole numbers of water and solutes at equilibrium, respectively. H_w and H_i are calculated from the derivatives of chemical potential with respect to temperature at constant pressure and composition.

Chemical potential of water is written by equation (3-21) ($\mu_w = \mu_w^0 + RTln(x_w\gamma_w)$), differentiation of equation (3-21) with respect to temperature at constant pressure and composition leads to:

$$\left[\frac{\partial\left(\frac{\mu_w}{RT}\right)}{\partial T}\right]_{P,x} = \left[\frac{\partial\left(\frac{\mu_w^0}{RT}\right)}{\partial T}\right]_{P,x} + \left[\frac{\partial ln\gamma_w}{\partial T}\right]_{P,x} \tag{3-68}$$

$$\frac{H_w}{RT^2} = \frac{H_w^0}{RT^2} + \frac{H_w^{ex}}{RT^2} \tag{3-69}$$

Thus:

$$H_w = H_w^0 + H_w^{ex} \tag{3-70}$$

Therefore, partial molar enthalpy of water (H_w) is calculated by the sum of water molar enthalpy of formation in the standard state (H_w^0) and partial molar excess enthalpy of water (H_w^{ex}).

Chemical potential of dissolved solute is described by equation (3-23) ($\mu_i = \mu_i^* + RTlna_i = \mu_i^* + RT\ ln(x_i\gamma_i^*)$), differentiation of equation (3-23) with respect to temperature at constant pressure and composition yields:

$$\left[\frac{\partial\left(\frac{\mu_i}{RT}\right)}{\partial T}\right]_{P,x} = \left[\frac{\partial\left(\frac{\mu_i^*}{RT}\right)}{\partial T}\right]_{P,x} + \left[\frac{\partial ln\gamma_i^*}{\partial T}\right]_{P,x} \tag{3-71}$$

$$\frac{H_i}{RT^2} = \frac{H_i^0}{RT^2} + \frac{H_i^{ex}}{RT^2} \tag{3-72}$$

Partial molar enthalpy of solutes (H_i) is calculated by the sum of molar enthalpy of formation of solutes in the standard state (H_i^0) and partial molar excess enthalpy of solutes (H_i^{ex}).

The molar enthalpy of absorbed acid gas is calculated by:

$$H_{Acid\ Gas}^{g} = H_{Acid\ Gas,T=298.15}^{0,g} + \int_{298.15}^{T} C_{P,AcidGas}^{0} dT \tag{3-73}$$

Where $H_{Acid\ Gas,T=298.15}^{0,g}$ is the molar enthalpy of formation of gaseous acid gas at 25 °C.

Chapter 4

Improving the Preexisting Model

Chapter 4
Improving the Preexisting Model

4 Improving the Preexisting Model

4.1 Chapter Overview

The Extended UNIQUAC model was previously used to represent thermodynamic properties of CO_2-MDEA-H_2O, CO_2-MEA-H_2O and CO_2-MDEA-MEA-H_2O systems by (Faramarzi et al. 2009). The reported results of (Faramarzi et al. 2009) model were not much satisfactory for high amine concentrations and heat of absorption. Moreover, (Faramarzi et al. 2009) model also showed unrealistic predictions of freezing point. Accordingly, a part of this study is to improve the performance of the Extended UNIQUAC model for CO_2-alkanolamine-H_2O systems.

4.2 Improvements in the Model

The preexisting model is improved in various aspects as described in the following.

4.2.1 Use Vapor-Liquid Equilibria (VLE) Data as Presented in the Article

Since the vapor pressure of amine is much smaller than that of the water, for mixtures of alkanolamine and water, it is very laborious to determine very low alkanolamine vapor pressure. Hence, in the literature, experimental VLE data for binary alkanolamine-H_2O mixtures are often presented as total pressure. However, for the loaded solutions (mixtures of acid gas-alkanolamine-H_2O) experimental VLE data are usually reported as acid gas partial pressures and occasionally as total pressure. In (Faramarzi et al. 2009) model, the calculated pressure which was compared to experimental data in the objective function (sum of squared residuals) was bubble point pressure (system total pressure). Accordingly, for cases that experimental VLE data were presented as acid gas partial pressure, experimental total pressure of the system was calculated by the following procedure: “The partial pressure of water was then taken as the saturation pressure of pure water and added to the reported partial pressures of non-water” (Thomsen and Rasmussen 1999). This means that in (Faramarzi et al. 2009) model, water activity coefficient was assumed to be very close to unity. This assumption is not so far from reality for dilute solutions, but at high amine concentrations, the system is far from ideality. Thus, the calculated total pressure based on this

assumption differs from the real value and that brings about inaccurate determination of activity coefficients. This can explain the large deviations of (Faramarzi et al. 2009) model at high amine concentrations. In addition, at high temperatures and for volatile amines like MEA, the deviation from ideality is significant. Hence, to improve the accuracy of the determination of activity coefficients in this study, the data are used as reported in the literature, i.e. both partial and total pressures were used in the objective function.

4.2.2 Density Correlations for Converting Volumetric Data

Many experimental data used for optimization of model parameters are presented in the volumetric concentration units. In order to convert them to weight concentration unit, density of aqueous amine solution is required. In the (Faramarzi et al. 2009) model, density of aqueous solution was assumed to be equal to pure water. This assumption brings about slight inaccuracy for data conversion from molarity to molality scale, since there is a small change in density upon addition of amines. In this study, the density at experimental conditions is calculated from the density correlations constructed for aqueous MDEA, aqueous MEA and aqueous MDEA-MEA at 25 °C. It is worth to clarify that usually the temperature at which the solvents are made, is not mentioned in the literature, however, it is most likely the ambient temperature, i.e. 25 °C.

In this study, density equations for MDEA/MEA-H_2O and MDEA-MEA-H_2O systems were correlated based on density data of (Hawrylak et al. 2000) and (Mandal et al. 2003), respectively. It is noted that high reliability and reproducibility of both sources were proven by comparison with other literature data. The developed density equations predict density of aqueous amine solutions at 25 °C and as a function of amine composition. Figure 4-1 and Figure 4-2 shows the experimental data points of (Hawrylak et al. 2000) for MDEA-H_2O and MEA-H_2O systems, respectively. The regression line fitted to the data is also

shown in the figures.

The developed correlation for the density of MDEA-H_2O and MEA-H_2O, are:

$$d_{MDEA} = -0.6491x^4 + 1.6104x^3 - 1.4096x^2 + 0.4832x + 0.9985 \quad (4\text{-}1)$$

$$d_{MEA} = -0.2452x^5 + 0.6034x^4 - 0.4067x^3 - 0.0717x^2 + 0.1351x + 0.9967 \quad (4\text{-}2)$$

Where, d is the solution density in $g.cm^{-3}$ and x is the MDEA or MEA mole fraction. The developed equations are valid for all amine concentrations ($0 \leq x \leq 1$). The equations are correlated with 99

% coefficient of determination[29], which indicates that the regression line fits the data well. The average absolute deviation[30] of Equation (4-1) and (4-2) are 0.11 and 0. 02 %, respectively.

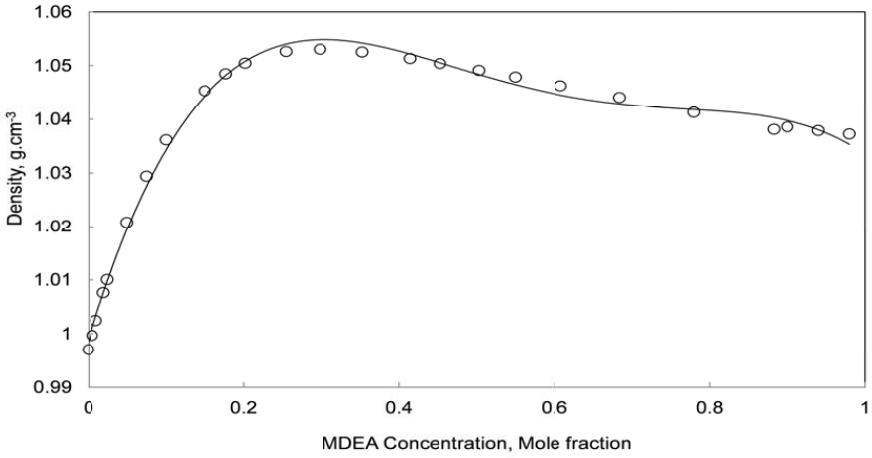

Figure 4-1. Density of aqueous MDEA at 25 °C. ○, Experimental data of (Hawrylak et al. 2000); Solid line, Regression line

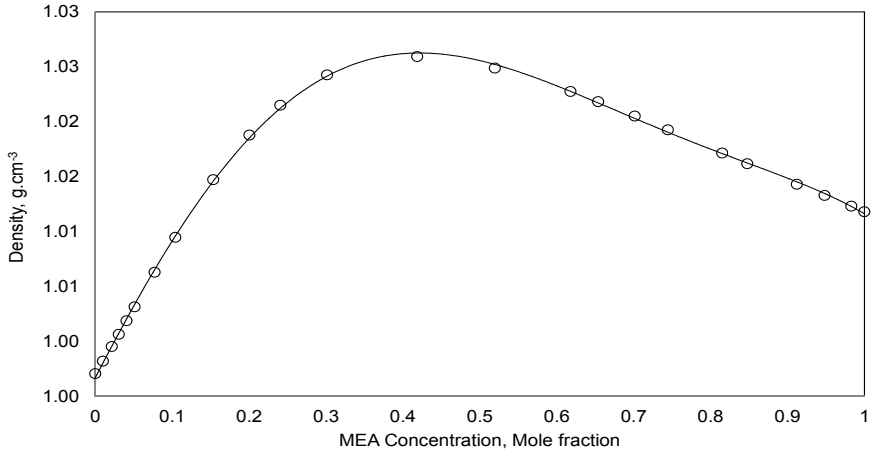

Figure 4-2. Density of aqueous MEA at 25 °C. ○, Experimental data of (Hawrylak et al. 2000); Solid line, Regression line

[29] R^2 (Coefficient of determination): A coefficient of determination describes how well a regression line fits a set of data. It is an overall measure of the accuracy of the regression. R^2 is mainly a number between 0 and 1. $R^2 = 1$ indicates that the correlated equation perfectly fits the data. The higher values of R^2 indicate the better goodness of fit.

[30] $AAD = \sum_{i=1}^{n} \frac{abs\,(d_{i,calc} - d_{i,exp})}{n}$

Figure 4-3 shows the experimental data points of MDEA-MEA-H_2O from (Mandal et al. 2003) and the regression line fitted to the data. The developed correlation for the density is:

$$d_{blend} = 0.0020512 \ln(x) + 1.0204 \quad (4\text{-}3)$$

Where d is density of the blend in $g.cm^{-3}$ and x is the ratio of MDEA mass percent to MEA mass percent. The developed equation is valid for $2 \leq x \leq 19$ and water mass% of 70. Equation (4-3) is correlated with 93 % coefficient of determination with AAD % of 0.19.

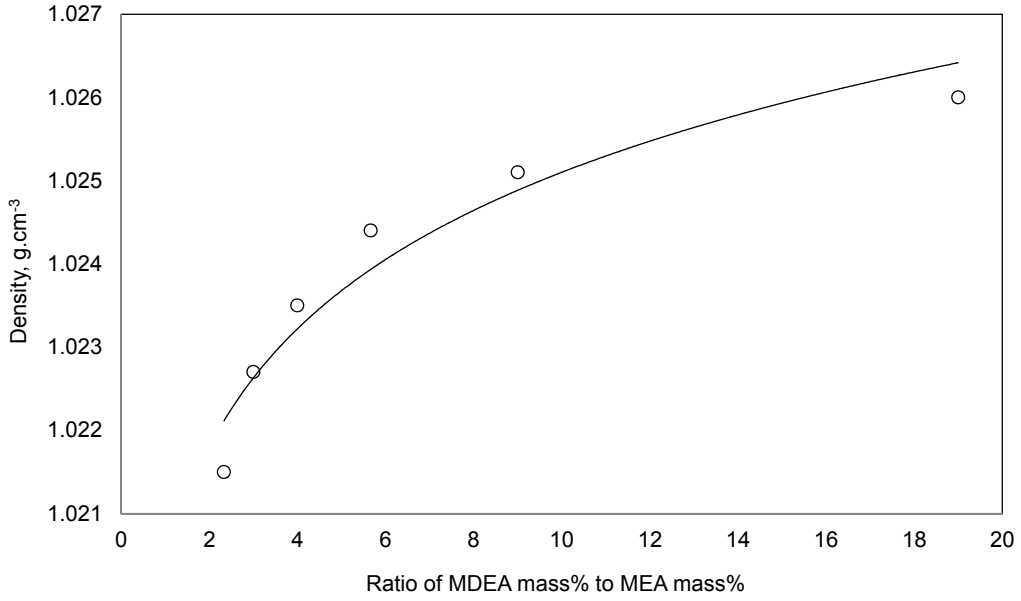

Figure 4-3. Density of aqueous blend of MDEA and MEA at 25 °C. ○, Experimental data of (Mandal et al. 2003); Solid line, Regression line

4.2.3 Addition of Heat of Absorption Data to Regression Data Base

Unlike (Faramarzi et al. 2009) model, in this study, heat of absorption data has been regressed along with other types of data (total pressure, partial pressure, heat capacity, excess enthalpy and freezing point). Including heat of absorption data for parameter optimization improves temperature dependence of the model. It also leads to more accurate predictions of heat of acid gas absorption into aqueous amine solutions. Having mentioned that, even in the absence of heat of absorption

data, a proper equilibrium data set should result in model parameters with the capability of predicting heat of absorption.

4.3 Summary

To improve the preexisting model from (Faramarzi et al. 2009), the following items are implemented. (i) Utilizing partial pressure data along with total pressure data for parameter regression, (ii) accurate conversion of molarity data to molality data and (iii) use of heat of absorption data for optimization of model parameters. In addition a more comprehensive data base is used in this study for fitting the model parameters which yields better results. The details of improved results in comparison with (Faramarzi et al. 2009) are shown in next chapter.

Chapter 5

Thermodynamic Modeling of

CO_2-Alkanolamine (MDEA/MEA/Blend)-H_2O

Systems

Chapter 5

Thermodynamic Modeling of CO_2-Alkanolamine (MDEA/MEA/Blend)-H_2O Systems

---

5 Thermodynamic Modeling of CO_2-Alkanolamine (MDEA/MEA/Blend)-H_2O Systems

5.1 Chapter Overview

Thermodynamic model that can predict the behavior of the gas sweetening process over the applicable conditions is a vital demand in industry. In this chapter, optimization of Extended UNIQUAC model parameters for CO_2-alkanolamines-H_2O systems (alkanolamines are MDEA, MEA and the blend of them) are discussed in the following manner. Firstly modeling of CO_2-MDEA-H_2O system and its sub systems are discussed, secondly modeling of CO_2-MEA-H_2O system and subsystems are presented and finally modeling of MDEA-MEA-H_2O and CO_2-MDEA-MEA-H_2O systems is investigated. The results of the developed models in this study are also compared with results of Extended UNIQUAC developed by (Faramarzi et al. 2009) and E-NRTL developed by (Hessen et al. 2010).

5.2 Evaluation of Parameters

This section addresses the procedure that was used for fitting the parameters, criteria for choosing the right parameters to fit and the final values of parameters.

5.2.1 Fitting Procedure

Large number of data available in open literature were first evaluated and then used to fit the Extended UNIQUAC model parameters. The type of data was as follows: VLE (total and partial pressure), SLE, heat capacity, excess enthalpy and heat of absorption. An advantage of local composition models such as the UNIQUAC equation is that binary parameters of a multicomponent system and of its constituent binary systems are the same and no higher-order parameters are required (Austgen 1989). Thus a model for a multicomponent system can be developed based on the parameters of its binary subsystems and by adjusting additional binary interaction parameters.

For instance, the model parameters of CO_2-alkanolamine-H_2O mixture contains parameters of alkanolamine-H_2O and CO_2-water systems and has additional interaction parameters, e.g. CO_2-amineH^+. The parameters of CO_2-alkanolamine-H_2O mixture are determined in a two-stage approach. In the first stage model parameters for binary alkanolamine-H_2O, r and q and binary interaction parameters, are determined by regressing pure alkanolamine vapor pressure and binary data (VLE (total pressure), Excess Enthalpy, freezing point and heat capacity). In the second stage, binary interaction parameters associated with the ternary system are fitted to ternary data (VLE, H_{abs}, C_p and SLE in case of MEA as an alkanolamine), while parameters for alkanolamine-H_2O system were fixed at the fitted values obtained in the stage 1 and parameters of CO_2-H_2O were retained at values determined by (Garcia et al. 2006). It is noted that the model parameters of CO_2-H_2O are adopted from (Garcia et al. 2006). Similarly, for the ternary system of MDEA-MEA-H_2O, model parameters of MDEA-H_2O and MEA-H_2O systems are combined and additional MDEA-MEA interaction parameter is adjusted to ternary data. For quaternary system of CO_2-MDEA-MEA-H_2O, model parameters of CO_2-MDEA-H_2O, CO_2-MEA-H_2O and MDEA-MEA-H_2O are combined and no more parameter is adjusted.

For optimization to be meaningful there must be an objective function that accounts for the deviation between calculated values by the model and the experimental data. The objective function is the function that the solvers try to minimize. In this work objective function is defined as follows which is the weighted sum of square of residuals (difference between calculated values by model and experimental values). Model parameters (volume, surface, and energy interaction), heat capacity parameters and standard state values are optimized by minimizing the following objective function named S:

$$S = \sum_{VLEdata}\left[\frac{P_{calc}-P_{exp}}{w_1\,(P_{exp}+(0.01\,bar))}\right]^2 + \sum_{P^{vap}data}\left[\frac{P_{cal}^{vap}-P_{exp}^{vap}}{w_2\,P_{exp}^{vap}}\right]^2 + \sum_{H^E data}\left[\frac{H_{calc}^{E}-H_{exp}^{E}}{w_3\,Rx}\right]^2 +$$
$$\sum_{H^{Abs}data}\left[\frac{H_{calc}^{Abs}-H_{exp}^{Abs}}{w_4\,y}\right]^2 + \sum_{C_P data}\left[\frac{C_{P,calc}-C_{P,exp}}{w_5\,R}\right]^2 + \sum_{C_P^{app}data}\left[\frac{C_{P,calc}^{app}-C_{P,exp}^{app}}{w_6\,R}\right]^2 +$$
$$+\sum_{SLEdata}\left[\frac{\Delta G^0 + RT\sum_i v_i ln a_i}{w_7\,RT}\right]^2 \qquad (5\text{-}1)$$

In the above equation "calc" and "exp" represent values calculated with the model and experimental data, respectively. w_1 to w_7 indicate the weight numbers used for each kind of data. Values of weight numbers are presented in Table 5-1. In equation (5-1), P is either the solution total pressure

(bar) or in most cases acid gas partial pressure (bar) , P^{Vap} is the alkanolamine pure vapor pressure (bar), H^E is the molar excess enthalpy ($J.mol^{-1}$), H^{Abs} is the heat of absorption CO_2 into aqueous alkanolamine solution (J), C_P is the molar heat capacity of ternary mixture (acid gas-H_2O-alkanolamine) ($J.mol^{-1}.K^{-1}$), C_P^{app} is the apparent[31] molar heat capacity of binary aqueous alkanolamine solution ($J.mol^{-1}.K^{-1}$), ΔG^0 is the change in molar standard chemical potential between solid and liquid phase ($J.mol^{-1}$), υ_i is the stochiometry coefficient of component "i", a_i is the activity of component "i" and R is the gas constant ($J.mol^{-1}.K^{-1}$). x = 1 K and y = 1 J are included to make the equation dimensionless. 0.01 bar is added to the denominator of the VLE term in order to not to give so much weight on the low pressure data.

Table 5-1 shows weighting factors that were used in optimization process for Vapor-liquid equilibrium (total pressure and partial pressure), pure amine vapor pressure, excess enthalpy, heat of absorption, heat capacity, apparent heat capacity and freezing point data. Choosing a correct number for the weights of different kinds of data helps the model to give satisfactory results for different properties. Weighting factors were chosen based on the quality and reliability of different kinds of data and also the experience achieved in the modeling. Different types of data were weighted corresponding to their estimated accuracy i.e. data of higher accuracy are weighted higher. The same weight is given to all data of the same type so that they contribute equally in the objective function. During the optimization process, slightly different weights in the range of data accuracy were tested. Based on the chosen weights different parameters had been obtained. Then with each set of parameters results have been calculated. Finally the weight numbers that gave the best calculated results were chosen as the final weights of the data.

[31] For electrolytes it is common to use apparent molar properties. Apparent molar properties are only used for binary solutions. An apparent molar property ($M_\emptyset$) of the molar property M for the salt S in an aqueous solution is defined by: $M_\emptyset = \frac{nM - n_w M_w^0}{n_S}$, where n_w is the water mole numbers, n_S is salt mole numbers, n is the total mole numbers and M_w^0 is the molar property of pure water.

Table 5-1. Weights for different kinds of data in the objective function

Data Type	Weight Number
VLE* (Amine**-H_2O and CO_2-Amine**-H_2O)	$W_1 = 0.05$
Pure amine** vapor pressure	$W_2 = 0.0075$
Excess enthalpy (Amine**- H_2O)	$W_3 = 120$
Heat of absorption (CO_2-Amine**-H_2O)	$W_4 = 0.02$
Ternary heat capacity (CO_2-Amine**-H_2O)	$W_5 = 10$
Apparent heat capacity (Amine**-H_2O)	$W_6 = 10$
Freezing point (amine-H_2O, CO_2-MEA-H_2O)	$W_7 = 0.01$

* *Total pressure and partial pressure.*

** *Amine indicates MDEA, MEA, blends of MDEA and MEA.*

The weighting factor for VLE data was selected so that for relatively high pressures, a difference of pressure of 5% between calculated and experimental values would give a squared residual of 1. As already stated the term of 0.01 in the denominator of the VLE term is added in order to avoid giving too much weight to very low pressure data. So that an experimental pressure of 0.01 bar would give a squared residual of 1 if the calculated pressure deviates from it by 10%. The pure alkanolamine vapor pressure data are weighted so that a 0.75% difference between the calculated and experimental pressures would lead to squared residual of 1. The weight factor for the excess enthalpy data was chosen so that an absolute difference of approximate 1000 J between the calculated and experimental values would give a squared residual of 1. The heat of absorption data are weighted so that an absolute difference of 0.02 J between calculated and experimental heat of absorption would result in a squared residual of 1. The weighting factor for heat capacity of ternary mixture is chosen so that an absolute difference of 80 $J.mol^{-1}.K^{-1}$ between calculated and experimental heat capacity of ternary mixture would result in a squared residual of 1. The apparent heat capacity data are weighted so that an absolute difference of 80 $J.mol^{-1}.K^{-1}$ between calculated and experimental heat capacity would result in a squared residual of 1. The SLE term is zero when the pertinent salt is at equilibrium. The weight of SLE data has been selected to be 0.01. The SLE data are weighted so that solubility indexes of 1.01 and 0.99 would give a squared residual of 1. Solubility index of a salt is defined by the ratio between the activity product and the solubility product of a salt ($SI = \frac{\prod_i a_i^{\vartheta_i}}{K}$). The saturation index is a measure of the degree of saturation of the salt. The saturation index of a salt is equal to unity at saturation. The saturation index is greater than one in supersaturated solutions and is less than one in unsaturated solutions. The number of

UNIQUAC parameters that are adjusted in this study for describing CO_2-MDEA-H_2O and CO_2-MEA-H_2O systems, is in total 16 (12 UNIQUAC parameters, 4 standard state properties) and 33 (24 UNIQUAC parameters, 6 standard state properties and 3 heat capacity parameter), respectively. Fitting this high number of parameters is not a trivial task. In order to obtain satisfactory set of parameters, lots of effort is required to create a reliable data base and to choose a proper fitting procedure. Assuming a reliable data base, optimization is performed using two different methods: a modified version of the Marquardt routine (Fletcher 1971) and a modified version of Nelder-Mead routine (StatLib). Marquardt is a nonlinear least square optimization method and is gradient based. Nelder-Mead is a simple optimization method for finding the minimum of a function of several variables. The program used for fitting parameters is called "estim" (Thomsen 1997). The estim program utilized optimization routines in this particular sequence: **1st:** Nelder-Mead. **2nd:** Marquardt. **3rd:** Nelder Mead. Experience showed that changing between two routines yields the best optimization results.

5.2.2 Determination of Effective Interaction Parameters, Selection of Interaction Parameters for Fitting

In the Alkanolamine-CO_2-water system where alkanolamine is MDEA, there are 3 molecular and 5 ionic species present in the liquid phase, primary amines like MEA form stable carbamates, thus there is one more component present in the liquid solution of CO_2-MEA-water. In each of the two cases a large number of binary interaction parameters including molecule-molecule, molecule-ion, and ion-ion, can be specified for the system. Nevertheless, since the concentration of many of these species present in the liquid phase is very low or negligible, parameters associated with them do not significantly affect representation of system behavior. Therefore, it is important to choose the effective parameters (parameters that modeling results are sensitive to them) and adjust them to the experimental data. Knowing the chemistry of the system and concentration calculations in an ideal solution helps to determine the effective parameters. Species concentration in ideal solution provides estimation of the component concentrations in the real mixture and chemistry of the system gives useful information about the possibility of coexistence of different species. It is noted that parameters have been determined for the species that according to the chemistry of the solution may exist in the solution. Pure component parameters (r and q) are only determined for species that are present at considerable concentration in the solution. Effective binary interaction parameters were primary selected based on two criteria's. The First criterion is the possibility of presence of pairs together in the system and the second one is the concentration of species. If both species

coexist with a very low concentration, their interaction parameter does not affect modeling results, hence is considered as ineffective parameter and excluded from fitting procedure. If both components exist together with high concentrations, the interaction parameter between them has influence in modeling results, thus is considered as effective parameter. If one species presents in low concentration, while the other component exists in high amount, the interaction parameter between them can have influence in the system behavior. In this case further analysis is required to determine whether or not this binary interaction parameter should be considered as effective parameter. The choice of effective parameters stem from experience with the model, sensitivity studies and from requirement for fitting the experimental data appropriately. Eventually, the following sets of effective parameters were chosen to adjust to the experimental data. It is noted that there are more effective parameters that were not determined in this work; values of these parameters were taken from other sources. Values of ineffective binary interaction parameters were assigned to $u^0 = 10^{10}$ and $u^T = 0$. These assigned values keep ineffective interaction parameters out of regression process.

- **MDEA-H_2O System**
  - ✓ MDEA-H_2O
  - ✓ $MDEAH^+$-H_2O
  - ✓ MDEA-MDEA

- **CO_2-MDEA-H_2O System**
  - ✓ $MDEAH^+$-CO_2

- **MEA-H_2O System**
  - ✓ MEA-H_2O
  - ✓ $MEAH^+$-H_2O
  - ✓ MEA-MEA
  - ✓ MEA-$MEAH^+$

- **CO_2-MEA-H_2O System**
  - ✓ $MEACOO^-$-H_2O
  - ✓ MEA-CO_2
  - ✓ $MEAH^+$-CO_2
  - ✓ MEA-HCO_3^-
  - ✓ $MEAH^+$-HCO_3^-

- **MDEA-MEA-H_2O System**
  - ✓ MDEA-MEA

The above parameters were fitted to the experimental data. Values of the adjusted parameters are presented in next sections.

5.2.3 Fitted Parameters

The parameters required by the UNIQUAC equation for the CO_2-alkanolamine-H_2O system include volume parameter, r, surface parameter, q, for the species and the binary interaction parameters representing energies of interaction between liquid phase species. Note that for some species heat capacity parameters and standard state properties (G_f^0, H_f^0) are also adjusted. In the following, values of the adjusted parameters for the studied systems are presented.

5.2.3.1 CO_2-MDEA-H_2O System

Carbon dioxide partially dissociates in an aqueous alkanolamine solution. This brings about formation of many ionic and molecular species in the solution and that give rise to complexity of the modeling. Accordingly, both physical and chemical equilibrium must be taken into consideration for modeling CO_2-alkanolamine-water mixtures.

Physical Equilibrium

In a closed system at constant pressure and temperature, distribution of molecular species between liquid and vapor phase is governed by physical equilibrium. CO_2 dissolves in the water, and water and MDEA present in the liquid phase have the possibility of vaporization. Note that ionic species do not vaporize and only exist in the liquid phase. Vapor-liquid equilibrium condition for the molecular species present in the system is written as follows. MDEA is shown as $R_2\acute{R}N$ where R: $CH_2 - CH_2 - OH$ and $\acute{R}$ is a methyl group (CH_3).

$$CO_2(aq) \leftrightarrow CO_2(g) \tag{5-2}$$

$$H_2O\ (l) \leftrightarrow H_2O\ (g) \tag{5-3}$$

$$R_2\acute{R}N\ (aq) \leftrightarrow R_2\acute{R}N\ (g) \tag{5-4}$$

Chemical Equilibrium

In the liquid phase CO_2 reacts with alkanolamine and water. A large number of reactions occur in the system and many ionic species are produced. The chemical reactions considered in this study for CO_2-MDEA-H_2O system are as follows:

Ionization of water: $H_2O\ (l) \leftrightarrow OH^-(aq) + H^+(aq)$ (5-5)

Dissociation of carbon dioxide: $CO_2(aq) + H_2O\ (l) \leftrightarrow HCO_3{}^-(aq) + H^+(aq)$ (5-6)

Dissociation of bicarbonate ion: $HCO_3{}^-(aq) \leftrightarrow CO_3{}^{2-}(aq) + H^+(aq)$ (5-7)

Protonation of alkanolamine: $R_2\acute{R}N\ (aq) + H^+(aq) \leftrightarrow R_2\acute{R}NH^+(aq)$ (5-8)

Table 5-2 to Table 5-7 show all the parameters that have been used for modeling the CO_2-MDEA-H_2O system, some of the parameters were fitted in this work and some were taken from literature. Table 5-2 shows volume parameter (r) and surface area parameter (q), values in bold were optimized in this work.

Table 5-2. UNIQUAC volume parameter (r) and surface area parameter (q). Bold parameters are obtained in this work.

Species	r	q
MDEA	**0.13445**	**0.54315**
$MDEAH^+$	**2.3931**	**1.0749**
H_2O	0.9200[a]	1.4000[a]
OH^-	9.3973[a]	8.8171[a]
H^+	0.13779[a]	10^{-15}[a]
$HCO_3{}^-$	8.0756[c]	8.6806[c]
$CO_3{}^{2-}$	10.828[c]	10.769[c]
CO_2	0.75[b]	2.45[b]

[a] (Thomsen et al. 1996)

[b] (Garcia et al. 2006)

[c] (Thomsen and Rasmussen 1999)

Table 5-3 and Table 5-4 list u_{ij}^0 and u_{ij}^T parameters (u_{ij}=u_{ji}) required for calculating UNIQUAC binary interaction energy parameters for the named pairs, respectively. As it was mentioned earlier, UNIQUAC binary interaction parameters are calculated in this way $u_{ij} = u_{ij}^0 + u_{ij}^T (T - 298.15)$. Parameters that are shown in bold are determined in this work. It should be mentioned that in the

original model (Thomsen et al. 1996) water-water and the like cation interaction energy parameters have been fixed at zero (Thomsen et al. 1996). Setting these parameters to zero, only has an influence on numerical value of the parameters and it does not affect value of binary interactions; binary interactions are calculated from differences in interaction energy parameters (Thomsen et al. 1996). As in the original model, H^+ is treated as a reference point for thermal properties and single ion activities (Thomsen et al. 1996). Therefore all the parameters for the hydrogen ion are fixed at chosen values (Thomsen et al. 1996). Hydrogen ion parameters are chosen on the basis of making hydrogen ion activity coefficients and other properties at all concentrations and all temperatures mostly determined by the Debye-Huckel term (Thomsen et al. 1996). For the pairs that are less probable to coexist in the mixture u_{ij}^0 and u_{ij}^T values has been set to a large value and zero, respectively. These values kept these parameters away from the regression process.

Table 5-3. $u_{ij}^0 = u_{ji}^0$ Parameters used for calculating UNIQUAC interaction energy parameters. Values in bold are obtained in this work.

Species	H_2O	CO_2	MDEA	OH^-	H^+	HCO_3^-	CO_3^{2-}	$MDEAH^+$
H_2O	0^a							
CO_2	8.83825^b	302.25^b						
MDEA	**-561.6682**	**10^{10}**	**-1489.795**					
OH^-	600.4952^a	10^{10b}	**10^{10}**	1562.881^a				
H^+	10^{5a}	10^{10b}	**10^{10}**	10^{10a}	0^a			
HCO_3^-	577.0502^c	526.31^b	**10^{10}**	10^{10a}	$10^{10\,a}$	771.0377^c		
CO_3^{2-}	361.3877^c	10^{10b}	**10^{10}**	1588.025^c	10^{10a}	800.0081^c	1458.344^c	
$MDEAH^+$	**-294.3952**	**-764.52**	**10^{10}**	**10^{10}**	**10^{10}**	**10^{10}**	**10^{10}**	**0**

[a] (Thomsen et al. 1996)

[b] (Garcia et al. 2006)

[c] (Thomsen and Rasmussen 1999)

Table 5-4. $u_{ij}^T = u_{ji}^T$ Parameters used for calculating UNIQUAC interaction energy parameters. Values in bold are obtained in this work.

Species	H_2O	CO_2	MDEA	OH^-	H^+	HCO_3^-	CO_3^{2-}	$MDEAH^+$
H_2O	0^a							
CO_2	$0.86293^{\,b}$	0.3587^b						
MDEA	**0.10616**	**0**	**-2.637**					
OH^-	8.5455^a	0^b	**0**	5.6169^a				
H^+	0^a	0^b	**0**	0^a	0^a			
HCO_3^-	$-0.38795^{\,c}$	-3.734^b	**0**	0^a	0^a	-0.019813^c		
CO_3^{2-}	$3.3516^{\,c}$	0^b	**0**	2.7496^a	0^a	$1.7241^{\,c}$	-1.3448^c	
$MDEAH^+$	**-0.0035922**	**9.473**	**0**	**0**	**0**	**0**	**0**	**0**

[a] (Thomsen et al. 1996)

[b] (Garcia et al. 2006)

[c] (Thomsen and Rasmussen 1999)

Table 5-5 and Table 5-6 show values that have been used for standard state heat capacity of the species present in the system, aqueous and gas phase. As in the original work (Thomsen et al. 1996) a temperature dependent correlation $\left(C_{P,i}^{0} = a_i + b_i\ T + \frac{c_i}{T-200}\right)$ has been used for standard state heat capacity of species present in the aqueous phase. For most of the molecular (neutral) species that exist in aqueous phase, standard state heat capacity is almost constant in a broad temperature range; thus for all molecular (neutral) species, except water, "b" and "c" parameters of equation has been assigned to zero based on the assumption that heat capacity is independent of temperature. Unlike molecular species, for ionic species standard state heat capacity cannot be assumed temperature independent, therefore it is wise to consider "b" and "c" parameters for ionic species. Whenever it is possible to determine coefficients "b" and "c", standard state heat capacity of ionic species is considered temperature dependent, which helps improving model temperature dependency. Parameters "a", "b" and "c" were either fitted to the experimental heat capacity data or were taken from data compilations (Garcia et al. 2005). Data compilations could also contain standard state heat capacity at 25 °C, in such cases "a" coefficient is set to the value from data compilation and b and c are fixed to zero (Garcia et al. 2005). Heat capacity parameters for H_2O, OH^-, H^+ are values reported by (Thomsen, Rasmussen et al. 1996). (Thomsen, Rasmussen et al. 1996) estimated "a", "b" and "c" parameters for water from the 5 parameter (DIPPR) (version 1983) correlation for the heat capacity of pure water. (Thomsen, Rasmussen et al. 1996) fitted a, b and c parameters for OH^- to the experimental data and set all parameters for H^+ to zero as H^+ is a reference point. HCO_3^- and CO_3^{2-} heat capacity parameters are adopted from (Thomsen and Rasmussen 1999). Heat capacity arameters for CO_2 (aq) are taken from (Garcia, Thomsen et al. 2006), these values had been taken values from (NIST) tables.

Table 5-5 represents values of heat capacity parameters (a, b and c) that has been used for calculation of standard state heat capacity of species i (C_{pi}^{0}) present in the aqueous phase from the mentioned correlation above which yields C_{pi}^{0} in $J.mol^{-1}.K^{-1}$. The "a" parameter given for MDEA is the C_p^0 (at T = 25 °C) presented by (Hawrylak et al. 2006). The "a" parameter for $MDEAH^+$ standard state heat capacity has been calculated from the difference between standard state heat capacity value of $MDEAH^+Cl^-$ measured by (Hawrylak et al. 2000) and Cl^- standard state heat capacity value presented by (Thomsen et al. 1996). From equation (5-11) standard state heat capacity of $MDEAH^+$ was obtained. b and c parameters for $MDEAH^+$ were assigned to zero.

$$C^0_{p,MDEAH^+\,Cl^-}(T = 25\,℃) = 194.31\ J\ mol^{-1}K^{-1} \quad (5\text{-}9)$$

$$C^0_{p,Cl^-}(T = 25\,℃) = -126.16\ J\ mol^{-1}K^{-1} (a = 400.35, b = -1.1312, c = -18574) \quad (5\text{-}10)$$

$$C^0_{p,MDEAH^+}(T = 25\,℃) = C^0_{p,MDEAH^+\,Cl^-}(T = 25\,℃) - C^0_{p,Cl^-}(T = 25\,℃) = 321.1582 J\ mol^{-1}K^{-1} \quad (5\text{-}11)$$

Table 5-5. Standard state heat capacity parameters for species in aqueous phase, C^0_{pi} (J mol^{-1}K^{-1}). Values in bold are obtained in this study.

Species	a (J mol^{-1} K^{-1})	b (J mol^{-1} K^{-2})	c (J mol^{-1})
MDEA (aq)	385[a]	0[a]	0[a]
$MDEAH^+$(aq)	**321.1582**	**0**	**0**
H_2O (l)	58.36952[b]	0.0389611[b]	523.8794[b]
OH^-(aq)	1418.157[b]	-3.445769[b]	-51473.13[b]
H^+(aq)	0[b]	0[b]	0[b]
HCO_3^-(aq)	-0.6770971[c]	0.2737451[c]	-10089.51[c]
CO_3^{2-}(aq)	894.6877[c]	-2.827237[c]	-21149.44[c]
CO_2(aq)	243[d]	0[d]	0[d]

[a] (Hawrylak et al. 2000)

[b](Thomsen et al. 1996)

[c](Thomsen and Rasmussen 1999)

[d](Garcia et al. 2006)

For molecular species present in the gas phase standard state heat capacities are taken from (DIPPR) data base. It is assumed that standard state heat capacity of molecular species in the gas phase is temperature independent and is constant over the wide range of temperature.

Table 5-6. Standard state heat capacities of species in the gas phase C^0_{pi} (J mol^{-1}K^{-1})

Species	C^0_{pi} (J mol^{-1} K^{-1})
MDEA (g)	100[b]
H_2O (g)	33.577[b]
CO_2 (g)	37.11[b]

[b](DIPPR)

Table 5-7 includes standard state Gibbs free energy of formation (G_f^0) and standard state enthalpy of formation (H_f^0). Most of the values were taken from (NIST) tables and (DIPPR). Standard state thermodynamic properties that could not found in (NIST) and (DIPPR) data bases were fitted to experimental data. It is noted that in (NIST) and (DIPPR) data bases, mainly standard state Gibbs free energy of formation (standard state chemical potential) are available at 25 °C. At temperatures other than 25 °C, standard state Gibbs free energy of formation has been calculated from the integration of Gibbs-Helmholtz equation using heat capacity and enthalpy data.

Table 5-7. Standard state properties G_f^0 and H_f^0 in (kJ mol^{-1}) at T = 25 °C. Values in bold are obtained in this study.

Species	G_f^0(kJ mol^{-1})	H_f^0(kJ mol^{-1})
MDEA (aq)	**-214.8709**	**-491.5275**
MDEA (g)	-169[a]	-380[a]
$MDEAH^+$ (aq)	**-264.1016**	**-528.4562**
H_2O (l)	-237.129[b]	-285.83[b]
H_2O (g)	-228.572[b]	-241.818[b]
OH^-(aq)	-157.2481[b]	-230.2433[b]
H^+(aq)	0	0
HCO_3^-(aq)	-586.77[b]	-691.99[b]
CO_3^{2-}(aq)	-527.81[b]	-677.14[b]
CO_2 (aq)	-385.98[b]	-413.8[b]
CO_2 (g)	-394.359[b]	-393.509[b]

[a](DIPPR)

[b](NIST)

5.2.3.2 CO_2-MEA-H_2O System

Similar to MDEA system, physical and chemical equilibrium should be considered for thermodynamic modeling of vapor-liquid behavior of mixtures of CO_2, MEA and H_2O.

Physical Equilibrium

Vapor-liquid equilibrium condition for the molecular species is the same as MDEA system. Equations (5-2) and (5-3) are kept and equation (5-4) is replaced by (5-12). Notice that MEA is shown as RNH_2 where R: $CH_2 - CH_2 - OH$

$$RNH_2(aq) \leftrightarrow RNH_2\ (g) \qquad (5\text{-}12)$$

Chemical Equilibrium

The principle reactions in the MEA-CO_2-H_2O system are like the reactions for MDEA-CO_2-H_2O system. One more reaction occurs in addition to the reactions in the MDEA system. Because MEA is a primary amine, it reacts with bicarbonate and forms MEA carbamate:

$$HCO_3^-(aq) + RNH_2(aq) \leftrightarrow RNHCOO^-(aq) + H_2O\ (l) \quad (5\text{-}13)$$

The mentioned reactions are generally taken into account for detailed modeling of mentioned systems. Although further reactions may happen, the amounts of these further side components are very small and could be neglected. For example MEA is able to form a very small amount of a component called 2-oxazolidone, nevertheless formation reaction of oxazolidone is neglected in this study (Boettinger et al. 2008).

Table 5-8 to Table 5-13 list parameters used for modeling equilibrium thermodynamic properties of CO_2-MEA-H_2O system. Some parameters were obtained in this work and some were taken from literature. Parameters that are shown in bold were determined in this work. Table 5-8 shows adjusted volume parameter (r) and surface area parameter (q) for MEA, $MEAH^+$ and $MEACOO^-$. Values for H_2O, OH^-, H^+, HCO_3^-, CO_3^{2-} and CO_2 are tabulated in Table 5-2.

Table 5-8. UNIQUAC volume parameter (r) and surface area parameter (q). Bold parameters are determined in this work.

Species	r	q
MEA	**3.0646**	**3.5394**
$MEAH^+$	**0.70865**	**1.3546**
$MEACOO^-$	**3.0005**	**2.1871**

Table 5-9 and Table 5-10 present u_{ij}^0 and u_{ij}^T parameters used for calculating UNIQUAC binary interaction energy parameters ($u_{ij}=u_{ji}$). For the pairs that are not present together in the mixture u_{ij}^0 and u_{ij}^T values were assigned to a large value and zero, respectively. Therefore these pairs were being kept away from the regression process.

Table 5-9. $u_{ij}^0 = u_{ji}^0$ Parameters used for calculating UNIQUAC interaction energy parameters. Values in bold are obtained in this work.

Species	H_2O	CO_2	MEA	OH^-	H^+	HCO_3^-	CO_3^{2-}	$MEAH^+$	$MEACOO^-$
H_2O	Table 5-3								
CO_2	Table 5-3	Table 5-3							
MEA	**188.3175**	**1688.45**	**427.4998**						
OH^-	Table 5-3	Table 5-3	**10^{10}**	Table 5-3					
H^+	Table 5-3	Table 5-3	**10^{10}**	Table 5-3	Table 5-3				
HCO_3^-	Table 5-3	Table 5-3	**475.3**	Table 5-3	Table 5-3	Table 5-3			
CO_3^{2-}	Table 5-3	Table 5-3	**10^{10}**	Table 5-3	Table 5-3	Table 5-3	Table 5-3		
$MEAH^+$	**159.3751**	**2.25**	**41.14279**	**10^{10}**	**10^{10}**	**446.46**	**10^{10}**	**0**	
$MEACOO^-$	**151.95**	**10^{10}**	**10^{10}**	**10^{10}**	**10^{10}**	**10^{10}**	**10^{10}**	**10^{10}**	**10^{10}**

Table 5-10. $u_{ij}^T = u_{ji}^T$ Parameters used for calculating UNIQUAC interaction energy parameters. Values in bold are determined in this work.

Species	H_2O	CO_2	MEA	OH^-	H^+	HCO_3^-	CO_3^{2-}	$MEAH^+$	$MEACOO^-$
H_2O	Table 5-4								
CO_2	Table 5-4	Table 5-4							
MEA	**1.6182**	**5.845**	**2.1171**						
OH^-	Table 5-4	Table 5-4	**0**	Table 5-4					
H^+	Table 5-4	Table 5-4	**0**	Table 5-4	Table 5-4				
HCO_3^-	Table 5-4	Table 5-4	**0.91**	Table 5-4	Table 5-4	Table 5-4			
CO_3^{2-}	Table 5-4	Table 5-4	**0**	Table 5-4	Table 5-4	Table 5-4	Table 5-4		
$MEAH^+$	**-2.9268**	**16.156**	**0.61711**	**0**	**0**	**4.258**	**0**	**0**	
$MEACOO^-$	**13.191**	**0**	**0**	**0**	**0**	**0**	**0**	**0**	**0**

Table 5-11 and Table 5-12 present the standard state heat capacity parameters for species present in the aqueous and gas phase, respectively. Values for H_2O (aq), OH^- (aq), H^+ (aq), HCO_3^- (aq), CO_3^{2-} (aq) and CO_2 (aq) are tabulated in Table 5-5. Values for H_2O (g) and CO_2 (g) are presented in Table 5-6. To avoid adding more adjustable parameters for MEA(aq) , $MEAH^+$(aq) and $MEACOO^-$(aq) only parameter "a" of heat capacity has been adjusted to experimental data and parameters "b" and "c" of heat capacity were assigned to zero. Fitting parameter "b" of heat capacity for the mentioned ions has been tried, but adding this parameter did not improve calculation results therefore it has been decided to consider the heat capacity of MEA, MEAH+ and $MEACOO^-$ temperature independent.

Table 5-11. Standard state heat capacity parameters for species in aqueous phase, C_{pi}^0 (J $mol^{-1}K^{-1}$). Values in Bold are obtained in this work.

Species	a (J $mol^{-1}K^{-1}$)	b (J $mol^{-1}K^{-2}$)	c (J mol^{-1})
MEA (aq)	**170.5628**	**0**	**0**
$MEAH^+$ (aq)	**59.56242**	**0**	**0**
$MEACOO^-$ (aq)	**-120.5933**	**0**	**0**

For molecular species present in the gas phase standard state heat capacities were taken from DIPPR data base (DIPPR).

Table 5-12. Standard state heat capacities of species in the gas phase C_{pi}^0 (J $mol^{-1}K^{-1}$)

Species	C_{pi}^0 (J mol^{-1} K^{-1})
MEA (g)	85.75[b]

[b](DIPPR)

Table 5-13 shows values of standard state Gibbs free energy of formation (G_f^0) and standard state enthalpy of formation (H_f^0). Values for H_2O (l), H_2O (g), OH^- (aq), H^+ (aq), HCO_3^- (aq), CO_3^{2-} (aq) , CO_2 (aq) and CO_2 (g) are tabulated in Table 5-7.

Table 5-13. Standard state properties G_f^0 and H_f^0 in (kJ mol^{-1}) at T = 25 °C. Values in bold are obtained in this work.

Species	G_f^0(kJ.mol^{-1})	H_f^0(kJ. mol^{-1})
MEA (aq)	**-135.6199**	**-274.9381**
MEA (g)	-103.3[a]	-206.7[a]
$MEAH^+$ (aq)	**-190.9034**	**-312.2365**
$MEACOO^-$(aq)	**-493.1112**	**-705.2981**

[a](DIPPR)

5.2.3.3 MDEA-MEA-H_2O System

Mixture of MDEA-MEA-H_2O was modeled based on combination of developed models for MDEA-H_2O and MEA-H_2O systems and from regression binary interaction parameter between MEA and MDEA to experimental data. Aqueous mixture of MDEA-MEA-H_2O has been modeled by fixing all the parameters at the values determined for binary MDEA-H_2O and MEA-H_2O subsystems and adjusting binary interaction parameter between MEA and MDEA to VLE and SLE data of ternary MDEA-MEA-H_2O system. Below table reports values required to calculate binary interaction parameters between MDEA and MEA.

Table 5-14. $u_{ij}^0 = u_{ij}^0$ and $u_{ij}^T = u_{ij}^T$ Parameters used for calculating UNIQUAC energy interaction parameters. Values in bold are obtained in this work.

Interaction parameter	$u_{ij}^0 = u_{ij}^0$	$u_{ij}^T = u_{ij}^T$
MDEA-MEA	**1574.44**	**5.867**

5.2.3.4 CO_2-MDEA-MEA-H_2O System

A model for CO_2-MDEA-MEA-H_2O system has been created based on combination of developed models for CO_2-MDEA-H_2O, CO_2-MEA-H_2O and MDEA-MEA-H_2O systems and without adjusting any additional parameter.

5.3 Equilibrium Constant for MDEA

In this work, the equilibrium constant for the MDEA protonation reaction was fitted to the experimental data. It is worth to mention that in this study standard state Gibbs energy of formation and standard state enthalpy of formation for MDEA and $MDEAH^+$ were regressed to the all kinds of experimental data available in regression data base. As it was mentioned in section 3.7 for components that values of standard state properties were not available in NITS tables, standard state properties were determined by fitting to all kinds of experimental data available in the regression data base. Therefore it is of high importance to check the fitted equilibrium constant against the available experimental equilibrium constants. It is noted that equilibrium constant affects the calculation results especially at low loading region, because in dilute solutions, the solution is close to ideal solution and activity coefficients are close to unity, therefore the role of Extended UNIQUAC is less noticeable. Thus, at low loading region equilibrium calculations are mainly based on equilibrium constants. The role of Extended UNIQUAC is more pronounced at higher concentration where the condition is far from ideal and activities need to take into account. The

results of fit for equilibrium constant of MDEA protonation reaction at 25 °C, and the increments in standard state Gibbs energies of formation and standard state enthalpies of formation of MDEA protonation reaction at 25 °C are compared with the experimental data measured by (Kamps and Maurer 1996). Table 5-15 summarizes the radjusted values in this study with the measured data from (Kamps and Maurer 1996). Obviously there is a good agreement between the two.

Table 5-15. Comparison between values obtained in this study with literature data for MDEA protonation reaction at 25 °C

Reference	(Kamps and Maurer 1996)	This Study
ΔG_f (kJ/mole)	48.81	49.2
ΔH_f (kJ/mole)	34	36.9
K (equilibrium Constant)	2.81E-9	2.37E-9

5.4 Regression Data Base and Results

In this work pure, binary and ternary VLE, SLE, heat capacity, excess enthalpy and heat of absorption data were used for regression model parameters. In order to create a data base which covers extensive pressure, temperature, amine concentration and acid gas loading range, it was attempted to collect almost all the available data in the open literature. Although there are a high number of data, especially VLE, available in the open literature, only some of them are qualified and consistent. Many of the published data show discrepancies. Therefore in order to obtain a good fit, it is crucial to create a reliable and consistent data base for parameter optimization. There are many ways to distinguish between consistent and inconsistent data. In this work four different ways were tried to analyze consistency of data:

- *Literature study*: a literature survey on the data source citations often provide good information about reliability of the data source.
- *Comparing different data sources*: Comparing data from different publications at the same conditions is a way to test quality of the data. In case of disagreement with other sources or a difference in trends, the data were discarded from regression data base. A direct comparison between measurements from different sources at the same conditions, make it possible to determine which measurements within a given data set are errant. However, a large number of parameters varying from measurement to measurement make this comparison risky, but this is one of the few available methods to determine beforehand the reliability of data points.

- *Analyze the data by itself*: Details of experimental procedure, uncertainty value reported for the data can be used for determining the quality of data.
- *Comparison with optimized model*: After optimization of the model, in principle, there will be a small deviation from the calculated values and most of the values obtained from experimental measurements. Hence, by plotting the calculated values versus the experimental ones (parity plot), a line with tangent of unity forms. The majority of the data is close to this line and can be considered as reliable and those which are far from unity are outliers, hence, most probably are erroneous. It is of high importance to note that when the experimental data at certain conditions is scarce this method may suffer from misjudgment. Hence, by including as many data sources as possible into the regression data base, the outliers can be indicated and confidently excluded.

Not all the data were used for parameter optmization. Consistent and accurate data were chosen for parameter optimization. Data that are inconsistent with other sources were discarded from regression data base. Data that including them in the parameter regression affect other sources results, were also excluded from data base. Data sources used for parameter regression with model deviations are presented in following sections. Average absolute relative deviation (AARD) is calculated from the following formula:

$$AARD = \frac{\sum_{i=1}^{N} \frac{\left(\left|Z_{i,exp} - Z_{i,calc}\right|\right)}{Z_{i,exp}}}{N} \tag{5-14}$$

$$AARD\% = AARD \times 100$$

N is the total number of data, $Z_{i,exp}$ is the experimental value and $Z_{i,calc}$ is the calculated value with the model.

As mentioned by (Thomsen and Rasmussen 1999) typical accuracy for vapor pressure measurements using modern equipment is up to $\pm 5\%$ (Rumpf et al. 1994). The usual accuracy of partial pressure measurements is about 5-10% (Goppert and Maurer 1988) and can increase to 15% in some conditions. According to Rochellle (Rochelle 1991) acid gas solubility in MDEA data have an average error of around 10% (Chang et al. 1993). Hence it is expected that the model calculates vapor pressure and partial pressure data within acceptable accuracy (less than 10%). In the following sections the data used for the parameter optimization are discussed and compared with the modeling results.

5.5 MDEA System

The parameters required for modeling CO_2-MDEA-H_2O system were fitted based on totally 1597 data points. Different kinds of data of pure amine, binary water-amine and ternary CO_2-amine-water mixtures have been used for adjusting model parameters. As mentioned previously modeling of CO_2-MDEA-H_2O system has been started by creating a model for MDEA-H_2O system. Based on parameters of binary MDEA-H_2O, the model is further developed for ternary system. In the following, different types of data that have been used for regression model parameters and modeling results are given.

5.5.1 Pure MDEA Vapor Pressure Data and Modeling Results

An overview over the experimental pure MDEA vapor pressure used for parameter optimization and the modeling results are given in Table 5-16. Totally 13 pure vapor pressure data points were used for model parameters optimization. Vapor pressure of pure components is very important for calculation of activity coefficients (Kim et al. 2008). As mentioned in chapter 3, this kind of data helps to get better prediction for infinite dilution activity coefficient. Pure MDEA vapor pressure data could improve optimization of MDEA r and q parameters, and MDEA-MDEA and MDEA-water interaction parameters.

Table 5-16. Regression results for MDEA vapor pressure

Temperature , °C	Reference	Number of Data Points	AARD%
147.3 to 194.7	(VonNiederhausern et al. 2006)	7	3.53
136.54 to 157.33	(Kim et al. 2008)	6	8.89

Figure 5-1 shows regressing results for vapor pressure of pure MDEA. The model represents vapor pressure of pure MDEA with an average absolute relative devaiaton of 6.21 %.

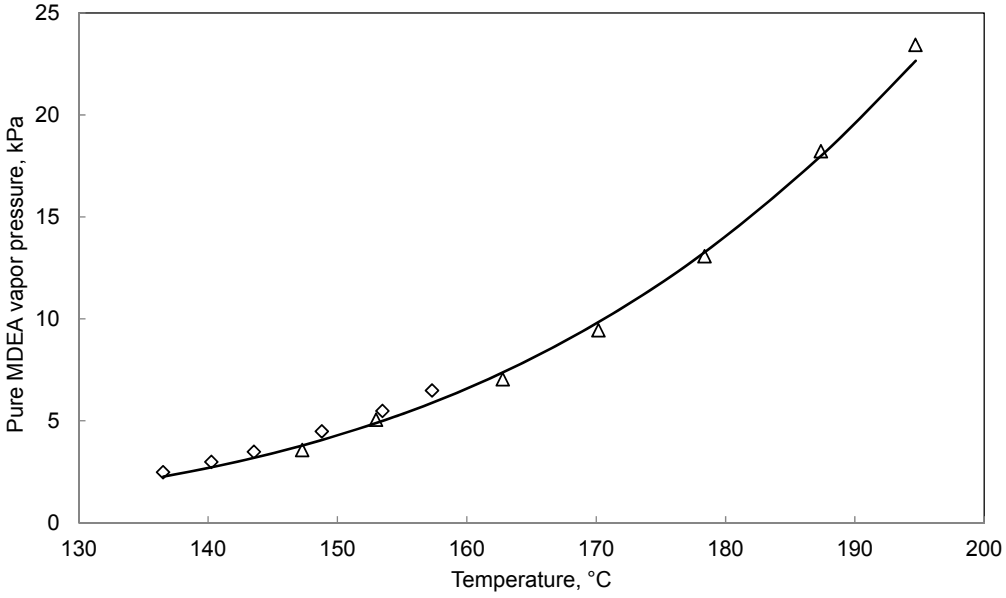

Figure 5-1. Vapor pressure of pure MDEA. Symbols stand for the experimental data and curve (line) refer to the calculated values using the developed thermodynamic model. ◊**,** (Kim et al. 2008)**;** Δ**,** (VonNiederhausern et al. 2006)

Data from (VonNiederhausern et al. 2006) at temperatures higher than 200 °C were discarded from regression data base, because majority of data for CO_2-MDEA-H_2O systems were available up to 140°C. Therefore it was not so relevant to model the pure component vapor pressure to higher temperatures.

5.5.2 Binary MDEA-H_2O Data and Modeling Results

As the loading in CO_2-MDEA-H_2O system approaches zero, a binary mixture of amine and water forms. As mentioned in section 5.2.1, interaction parameters of MDEA-water system were established prior to treat the loaded solution. UNIQUAC parameters required for modeling MDEA-water system were fitted to pure MDEA vapor pressure and data of binary MDEA-H_2O system. This section will discuss the modeling results of the created model for binary MDEA-Water system. In addition to pure MDEA vapor pressure data, 534 binary MDEA-H_2O data points including total pressure, freezing point depression (SLE), H^E and heat capacity have been used to determine model parameters. Total pressure of amine-water mixtures is dominated by the water vapor pressure since

the vapor pressures of amines are very low compared to water (Posey 1997). 90% (or more) of the total pressure of amine-water solutions is due to water, so that an error of 10% in total pressure measurements can hide the amine contribution of total pressure (Posey 1997). Thus, experimental total pressure data for amine-water solutions are not so sensitive to amine activity coefficients and as a result activity coefficients cannot be precisely determined from total pressure data (Posey 1997). In addition, partial pressure data for amine-water mixtures are scarce, due to low volatility of the amines which brings about difficulties in the measurements of partial pressure. Thus the uncertainty associated with the partial pressure measurements is usually high. (Posey 1997) showed that fitting NRTL model parameters to freezing point and heat of mixing data along with total pressure data significantly improve modeling of binary amine-water systems. In this study freezing point depression, heat capacity and Excess enthalpy (H^E) data have been regressed with total pressure data to develop a strong UNIQUAC model of the binary amine-water system. Table 5-17 lists the data sets upon which the parameters were optimized. In what follows modeling results for different kinds of data are given.

Table 5-17. Review over binary MDEA-H_2O data used for model parameter optimization and modeling results

MDEA Concentration, wt%	T ,°C	P, kPa	Data Type	Reference	Number of Data Points	AARD%
25.68 to 46.85	25,40,75	2.7 to 5.47 (P_{Total})	VLE	(Sidi-Boumedine et al. 2004,a)	5	5.22
77.05 to 185.55	77 to 185.5	40, 53.3, 66.7 (P_{Total})	VLE	(Voutsas et al. 2004)	27	10
3 to 78.61	40 to 100	7.27 to 100 (P_{Total})	VLE	(Kim et al. 2008)	57	0.76
9.98, 19.99, 29.98, 49.92, 70.02	53.1 to 108.05	13.08 to 101.67 (P_{Total})	VLE	(Xu et al. 1991)	34	2.69
18.84, 32.11	120, 140	186.2 to 346.4 (P_{Total})	VLE	(Kuranov et al. 1996)	4	0.72
23 , 50	25, 50, 75	Na*	C_P	(Hayden et al. 1983)	6	3.58
62.3, 81.51,90.84,96.35	30 to 80	Na*	C_P	(Chen et al. 2001)	44	4.78
16.82 to 99.01	5 to 95	Na*	C_P	(Zhang et al. 2002)	228	2.38
23 to 50	30 to 80	Na*	C_P	(Chiu and Li 1999)	22	1.43
1.41 to 20.47	10 to 55	100 (P_{Total})	Apparent C_P	(Hawrylak et al. 2006)	37	3.65
29.99, 40, 49.99, 59.99	25	Na*	C_P	(Weiland et al. 1997)	4	1.86
5.17 to 39.65	-1 to -15	101.3 (P_{Total})	Freezing point	(Fosbol et al. 2011)	6	6.54
26.34 to 39.15	-7 to -14	101.3 (P_{Total})	Freezing point	(Chang et al. 1993)	6	12
17.5 to 98.92	25, 40	Na*	H^E	(Maham et al. 1997)	26	16
16.25 to 65.94	65	Na*	H^E	(Maham et al. 2000)	9	41
9.58 to 94.91	25, 69.3	Na*	H^E	(Posey 1997)	19	14

Not available

5.5.2.1 Total pressure data

For low volatile species like MDEA, partial pressure measurements are difficult to carry out and usually results are uncertain. Therefore, like (Hessen et al. 2010), for binary mixture of water and MDEA, model parameters have been regressed to total pressure data. Total pressure data of (Sidi-Boumedine et al. 2004, a), (Voutsas et al. 2004), (Kim et al. 2008) and (Xu et al. 1991) have been used for parameter regression. Figure 5-2 shows that total pressure data for binary system fit quiet well.

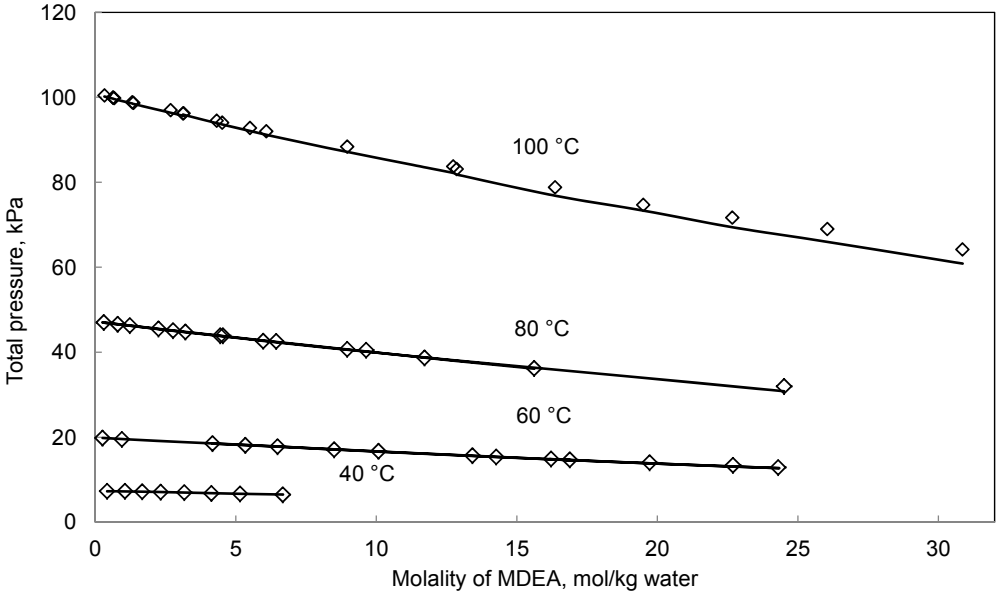

Figure 5-2. Total vapor pressure of MDEA-H_2O solutions. Symbols stand for the experimental data and curves (lines) refer to the calculated values using the developed thermodynamic model. □, (Kim et al. 2008)

Figure 5-3 is a parity plot which represents model calculated results against experimental data from (Xu et al. 1991), (Sidi-Boumedine et al. 2004, a) and (Kim et al. 2008) at various conditions. The curve has the slope of 0.98 which confirms model capability for well representing total pressure of MDEA-water subsystem.

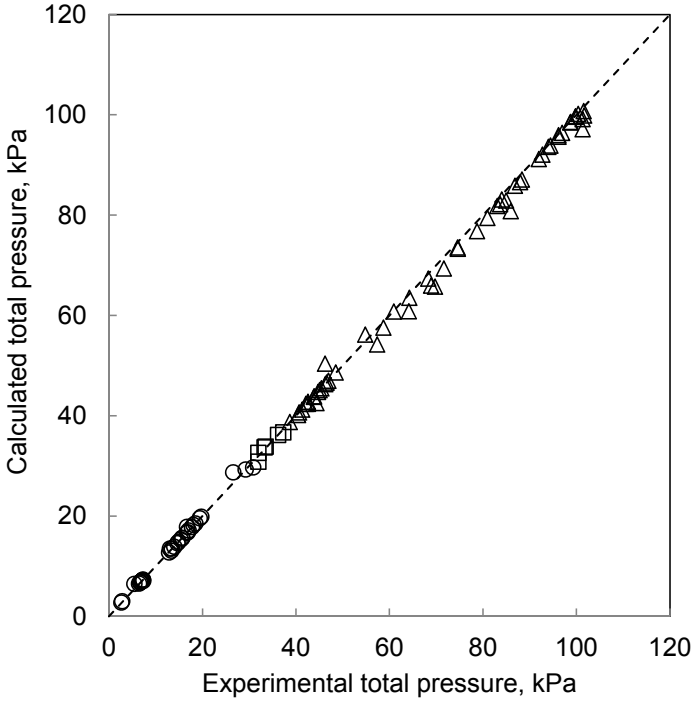

Figure 5-3. Parity plot for binary MDEA-H_2O system. ○**,** (Xu et al. 1991)**;** □**,** (Sidi-Boumedine et al. 2004, a)**;** Δ**,** (Kim et al. 2008)

Overall, model reproduce total pressure of MDEA-water mixture within 3.87 AARD%.

5.5.2.2 Excess Enthalpy Data

Excess enthalpy data is directly related to temperature dependence of excess Gibbs energy. Thus using excess enthalpy data for optimizing parameters of a G^E model will provide a more accurate temperature dependence of excess Gibbs energy. Data of (Maham et al. 1997), (Maham et al. 2000) and (Posey 1997) have been used for adjusting model parameters. Figure 5-4 displays the excess enthalpy data for mixtures of MDEA and water at 25 °C. Altogether, model fit excess enthalpy data within 23 AARD%.

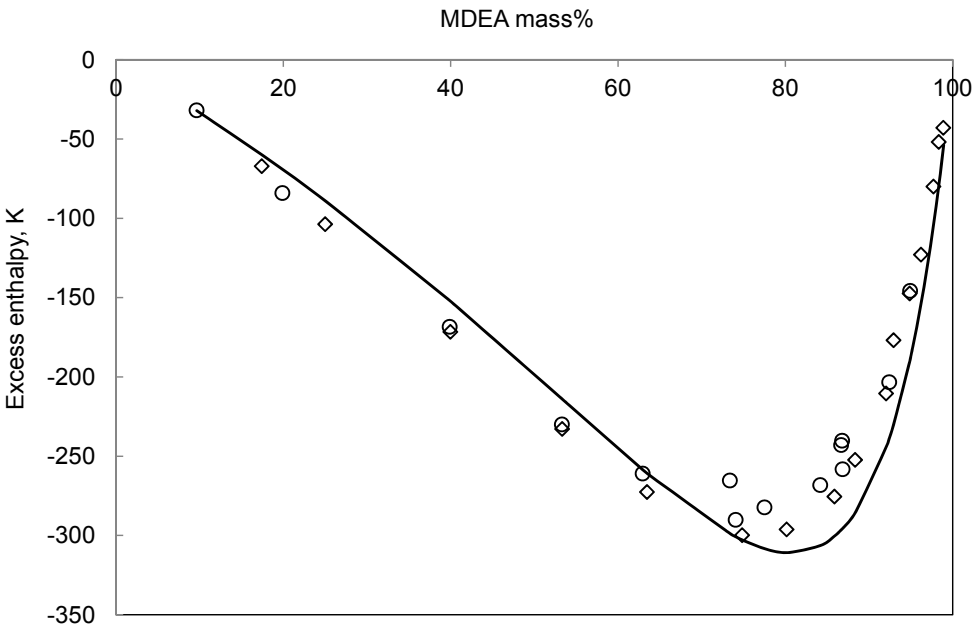

Figure 5-4. Excess enthalpy of MDEA-H_2O solutions at T = 25 °C. Symbols stand for the experimental data and curve (line) refers to the calculated values using the developed thermodynamic model.◊, (Maham et al. 1997)**; ○,** (Posey 1997)

As it can be seen in Figure 5-4, calculated results fit the experimental data well at all concentrations except 70 to 90 wt% MDEA. (Maham et al. 2000) estimated that the uncertainty of the measurements of molar excess enthalpy is 2% over whole amine concentration range. Since there is a good agreement between the experimental data provided by two different sources and the uncertainty of the reported measurement is small, it is most probably a shortcoming of the model that under predicts the excess enthalpy. Though the origin of this effect is not well-understood yet, it is pointed out (Posey 1997) that simultaneous regression of H^{ex} and VLE data for solutions far away from ideality, causes notable deviation of model prediction from experimental data.

5.5.2.3 Heat Capacity Data

The liquid phase heat capacity of a mixture is obtained by taking the derivative of the liquid enthalpy at constant pressure. Mixture heat capacity data as a function of temperature and

concentration has been used to adjust water and MDEA activity coefficients through the simultaneous optimization of the binary interaction parameters. Data of (Hayden et al. 1983), (Chen et al. 2001), (Zhang et al. 2002), (Chiu and Li 1999), (Weiland et al. 1997) and (Hawrylak et al. 2006) have been used for adjusting model parameters. Figure 5-5 plots heat capacity of binary MDEA-water mixture calculated by the model together with the experimental data from (Zhang et al. 2002). Results at selected temperatures; 5, 50 and 95 °C, are shown in the Figure 5-5.

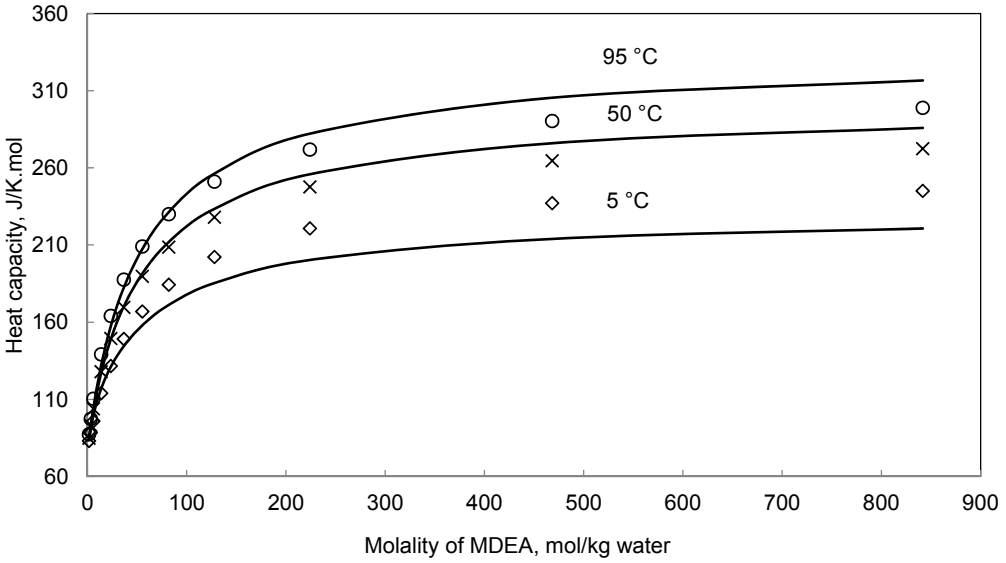

Figure 5-5. Heat capacity of MDEA-H_2O solutions at 5 °C, 50 °C and 95 °C. Symbols stand for the experimental data and curves (lines) refer to the calculated values using the developed thermodynamic model.◊, 5 °C (Zhang et al. 2002)**; ×, 50 °C** (Zhang et al. 2002)**; ○, 95 °C** (Zhang et al. 2002)

Altogether, model fist heat capacity data with average absolute relative deviation of 2.94%.

5.5.2.4 Freezing Point Depression Data

This kind of data is useful to get a better prediction for water activity. Activity of water is directly related to the freezing point depression of water. Two different freezing point data sources have been used for adjusting model parameters. It is noted that (Chang et al. 1993) have used two different methods (methods A and B) for measurement of freezing point depression of MDEA-water system. In a thorough study by (Fosbol et al. 2011) it is shown that only the result of one of

the methods was accurate (Method B by (Chang et al. 1993)). Hence, in this study the results of method A is not used i.e. the 6 data points measured by method B are included in the regression data base. Figure 5-6 represents freezing point of aqueous MDEA mixture calculated by the model against different experimental sources. Calculated results are in good agreement with the experimental data. Overall, model represent freezing point of aqueous MDEA solution within 9.61 AARD%.

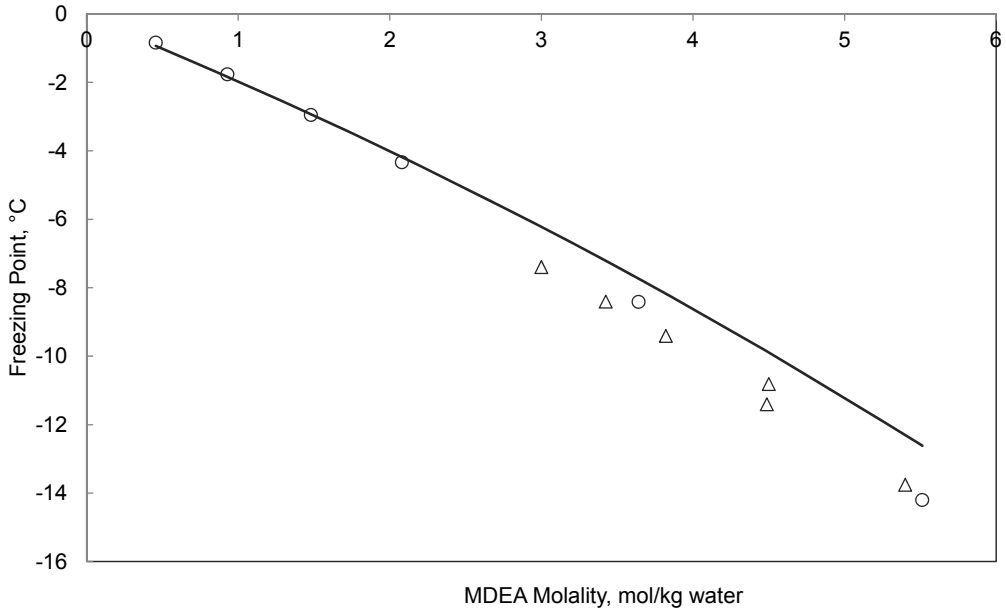

Figure 5-6. Comparison between experimental and regressed values of MDEA-H_2O freezing point. Symbols stand for the experimental data and curve (line) refers to the calculated values using the developed thermodynamic model. Δ**,** (Chang et al. 1993)**;** ○, (Fosbol et al. 2011)

5.5.2.5 MDEA Partial Pressure, Model Predictions

Some amine loss is expected in any amine plant, but huge amine losses can increase the plant cost. Understanding and controlling the amount of amine loss is vital for successful plant operation (Stewart and Lanning May 1994). Amine plant losses mainly stem from vaporization. The amine losses due to vaporization are associated with all types of alkanolamines used in treatment of gas streams, however for more volatile amines like MEA the amount of loss is higher. It is useful that the developed thermodynamic model can predict the amount of amine loss due to vaporization. As

previously mentioned for less volatile amines like MDEA, accurate MDEA partial pressure measurements are scarce in the literature. This section only shows model predictions for MDEA partial pressure. It should be noted that calculated results were not verified to experimental data because of lack of certain measured data at the time of this study. Figure 5-7 and Figure 5-8 show model predictions for MDEA volatility at 9.98, 19.99, 29.98, 49.92 and 70.02 wt% MDEA aqueous solutions versus temperature. The temperature range shown in the figure covers absorber and stripper operational conditions.

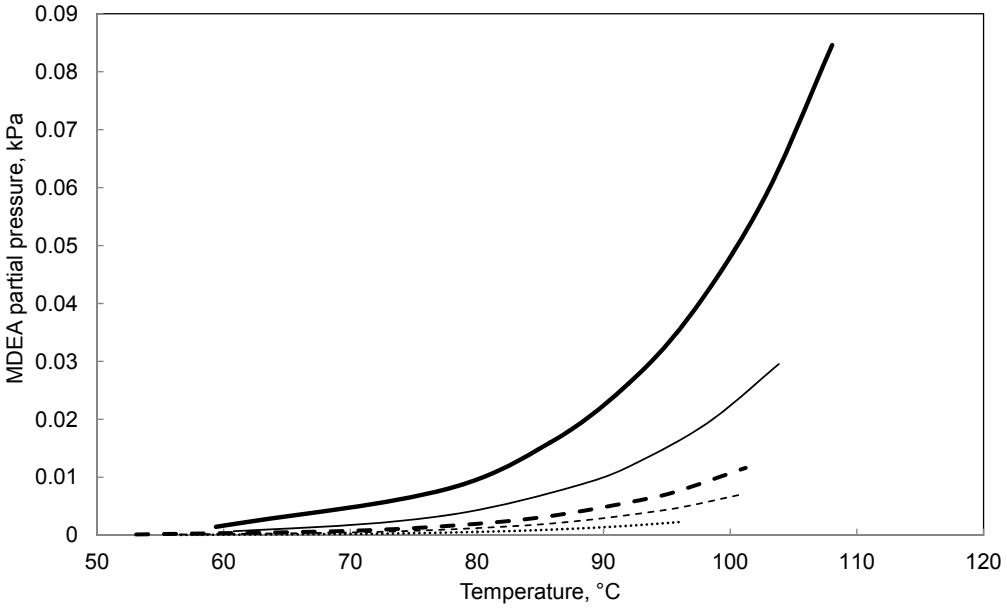

Figure 5-7. Predicted MDEA volatility in 9.98, 19.99, 29.98, 49.92 and 70.02 wt% MDEA aqueous solutions. Curves (lines) refer to the calculated values using the developed thermodynamic model. Dot Line, 9.98 wt% MDEA; Dash Line, 19.99 wt% MDEA; Bold Dash Line, 29.98 wt% MDEA; Solid Line, 49.92 wt% MDEA; Bold Solid Line, 70.02 wt% MDEA

To have better illustration of the predicted MDEA volatility, results were shown also in a semi-log plot (logarithmic y axis).

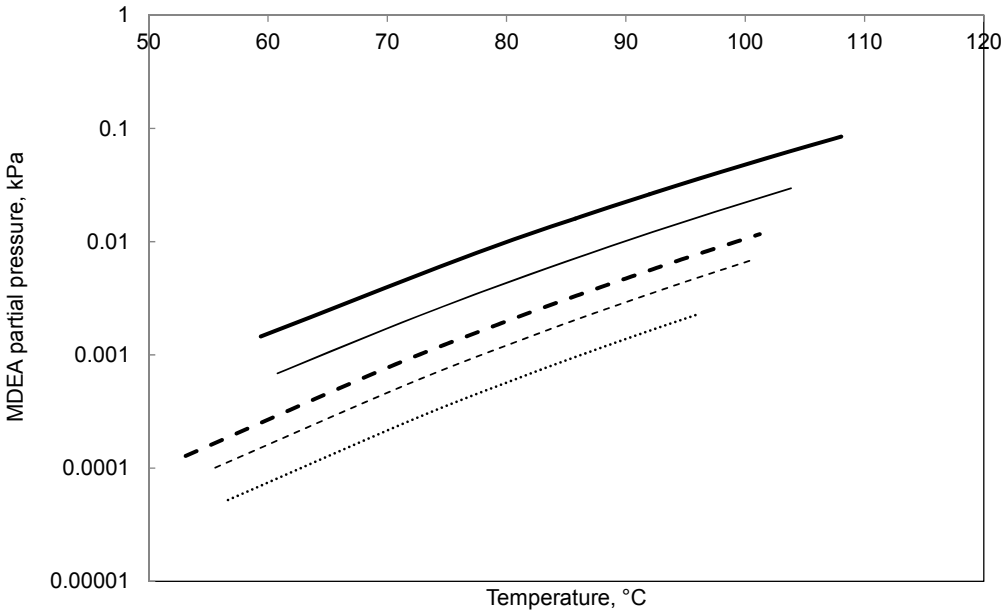

Figure 5-8. Semi-log plot-predicted MDEA volatility in 9.98, 19.99, 29.98, 49.92 and 70.02 wt% MDEA aqueous solution. Curves (lines) refer to the calculated values using the developed thermodynamic model. Dot Line, 9.98 wt% MDEA; Dash Line, 19.99 wt% MDEA; Bold Dash Line, 29.98 wt% MDEA; Solid Line, 49.92 wt% MDEA; Bold Solid Line, 70.02 wt% MDEA

Overall, the results presented above indicate that the Extended UNIQUAC model, through simultaneous regression gave a set of optimum parameters for the binary mixture of MDEA-water. Model parameters for binary MDEA-H_2O system are valid in the temperature range of -15 to 140℃, the total pressure range of 2 to 347 kPa and the whole concentration range of MDEA. The developed model represents all kinds of used binary data within AARD% of 7.91.

5.5.3 Ternary CO_2-MDEA-H_2O Data and Modeling Results

To this point modeling results have been presented for pure MDEA and MDEA-water subsystem. Model parameters associated with CO_2-MDEA-H_2O system have been determined through simultaneous regression of total pressure, CO_2 solubility (CO_2 partial pressure), heat capacity and heat of absorption data with the Extended UNIQUAC model. Speciation data from NMR analysis have not been used for regression model parameters, since the availability of this kind of data are low and the uncertainty associated with these measurements is significant; whereas these data have

been used to compare with model predictions. pH data were also excluded from the data base used for optimization parameters, since these data are rarely available in open literature. As stated by (Hessen et al. 2010), it should be discussed whether or not pH is a good measure of the proton activity since single ions activity cannot be measured directly (Hessen et al. 2010). 1050 number of ternary data composed of total pressure and CO_2 partial pressure, heat capacity and heat of absorption over vast range of temperature, pressure and composition were used to fit parameters associated with the loaded solution. Table 5-18 represents a summary of the ternary data used for parameter optimization. The remainder of this section will discuss different kinds of data used for adjusting model parameters; in addition modeling results for CO_2-MDEA-H_2O system will be presented.

Table 5-18. Overview on ternary MDEA-CO_2-H_2O data used for parameter optimization and regression results

MDEA , wt%*	T (°C)	P (kPa)	Data Type	Reference	Number of Data Points	AARD%
19, 32.11	40 to 140	139 to 5037 (P_{Total})	VLE	(Kuranov et al. 1996)	77	8.60
26, 47	25, 40, 75	3 to 4559 (P_{Total})	VLE	(Sidi-Boumedine et al. 2004, a)	80	10
19	40	791 to 4739 (P_{Total})	VLE	(Kamps et al. 2002)	5	4.26
32, 49	40, 80, 120	176.5 to 7565 (P_{Total})	VLE	(Kamps et al. 2001)	28	15
24	40	1155 to 3029 (P_{Total})	VLE	(Addicks et al. 2002)	3	7
24	40	12 to 3029 (P_{Total})	VLE	(Silkenbaumer et al. 1998)	10	13
19, 32, 48	40, 80, 120	0.12 to 69.3 (P_{CO_2})	VLE	(Ermatchkov et al. 2006)	101	8.22
5, 20, 50, 75	50, 75, 100	0.775 to 268.3 (P_{CO_2})	VLE	(Rho et al. 1997)	99	18
23, 47	40	0.005 to 93.6 (P_{CO_2})	VLE	(Austgen et al. 1991)	13	14
35	40, 100	0 to 262 (P_{CO_2})	VLE	(Jou et al. 1993)	37	27
50	25, 50, 75, 100	8.27 to 95.83 (P_{CO_2})	VLE	(Park and Sandall 2001)	29	19
23, 50	40	0 to 0.55 (P_{CO_2})	VLE	(Rogers et al. 1998)	27	18
23, 50	40, 70, 100, 120	0.002 to 5188 (P_{CO_2})	VLE	(Huang and Ng 1998)	66	21
11.8, 20, 23	25,38,50,65.5,115.5	11.1 to 6161.5 (P_{CO_2})	VLE	(Maddox et al. 1987)	99	21
50	55, 70, 85	65.75 to 813.4 (P_{CO_2})	VLE	(Ma'mun et al. 2005)	31	8.83
10, 20, 30, 40	20, 40, 60	80 to 298 (P_{CO_2})	VLE	(Kicrzkowska-Pawlak 2007)	24	19
23.6	24.5	0.02 to 1.6 (P_{CO_2})	VLE	(Lemoine et al. 2000)	13	19
34, 38.5, 47	40, 55, 70, 80, 90, 100	0.8 to 1013 (P_{CO_2})	VLE	(Xu et al. 1998)	65	32
23, 29	30, 40, 50	2.9 to 94.7 (P_{CO_2})	VLE	(Kundu and Bandyopadhyay 2005)	43	24
19, 47	100, 140, 160, 180, 200	103 to 4930 (P_{CO_2})	VLE	(Chakma and Meisen 1987)	76	28
23, 28	25, 40, 70	101 to 2320 (P_{CO_2})	VLE	(Jenab et al. 2005)	10	40
30, 40, 50, 60	25	Na**	C_P	(Weiland et al. 1997)	39	1.25
15, 30	49.3	Na**	H_{abs}	(Arcis et al. 2008)	75	3.45

**MDEA concentration indicates the concentration of MDEA in the aqueous MDEA solution, before loading the solution with CO_2.*

***Not available*

5.5.3.1 Total Pressure Data

Equations that relate total pressure data to model parameters have been already illustrated. 203 total pressure data of ternary system that were used for parameter optimization are listed in Table 5-18. Figure 5-9 shows the results of fit for experimental total pressure at 40 °C and 19.9 wt% MDEA versus loading (mole CO_2/mole MDEA), experimental data are from (Kuranov et al. 1996) and (Kamps et al. 2002).

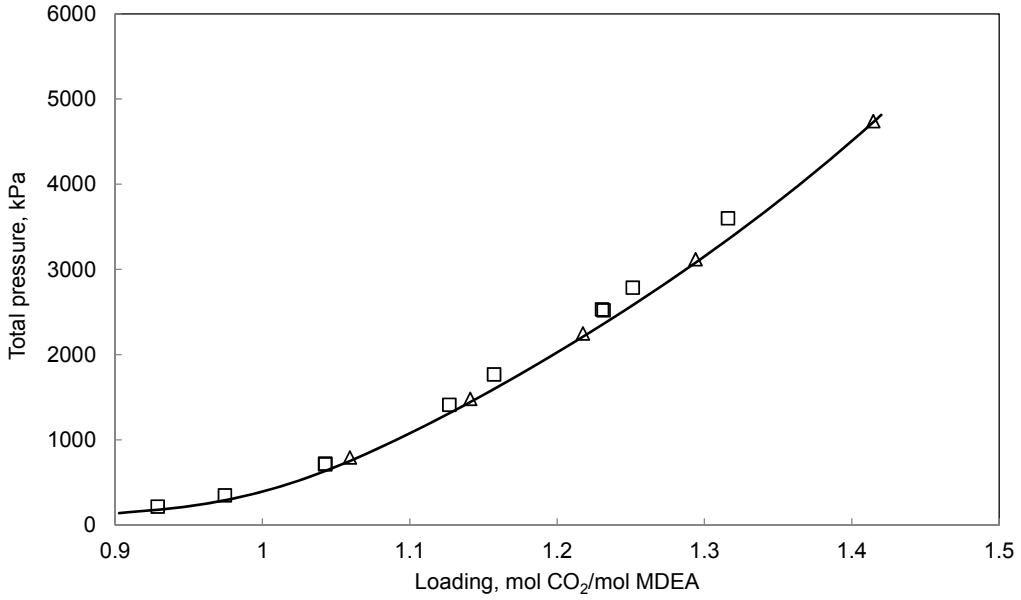

Figure 5-9. Comparison between experimental and regressed total pressure for CO_2-MDEA-H_2O solutions in 19.19 wt% MDEA and at 40 °C. Symbols stand for the experimental data and curve (line) refers to the represented values using the developed thermodynamic model. Δ**,** (Kamps et al. 2002)**,** □**,** (Kuranov et al. 1996)

Figure 5-10 and Figure 5-11 plot calculated results of the developed model against experimental measurements of total pressure for CO_2-MDEA-H_2O solution at 50 wt% MDEA and from 80 to 120 °C, over a broad loading range.

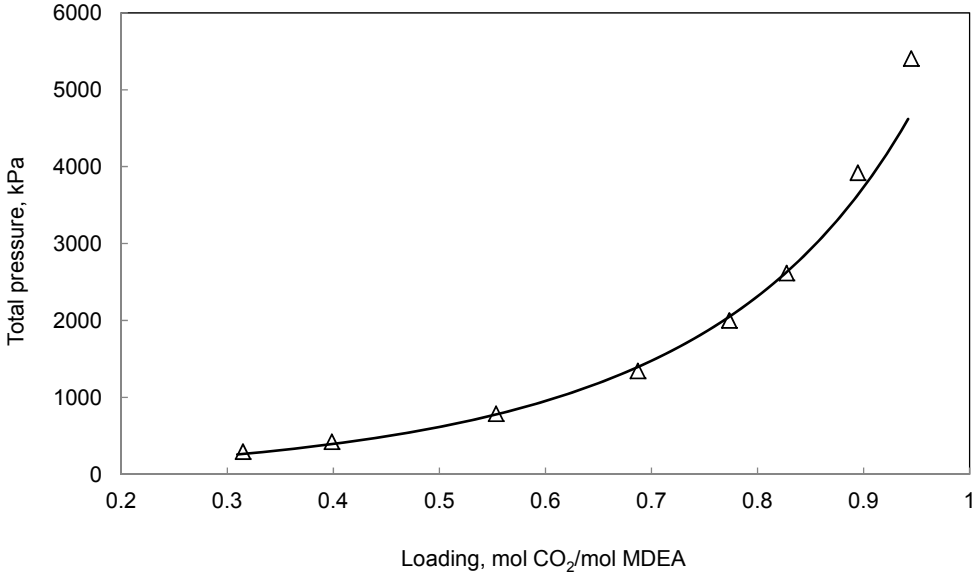

Figure 5-10. Comparison between experimental and regressed total pressure for CO_2-MDEA-H_2O solutions in 50 wt% MDEA and at 80 °C. Symbols stand for the experimental data and curve (line) refers to the represented values using the developed thermodynamic model. Δ**,** (Kamps et al. 2001)

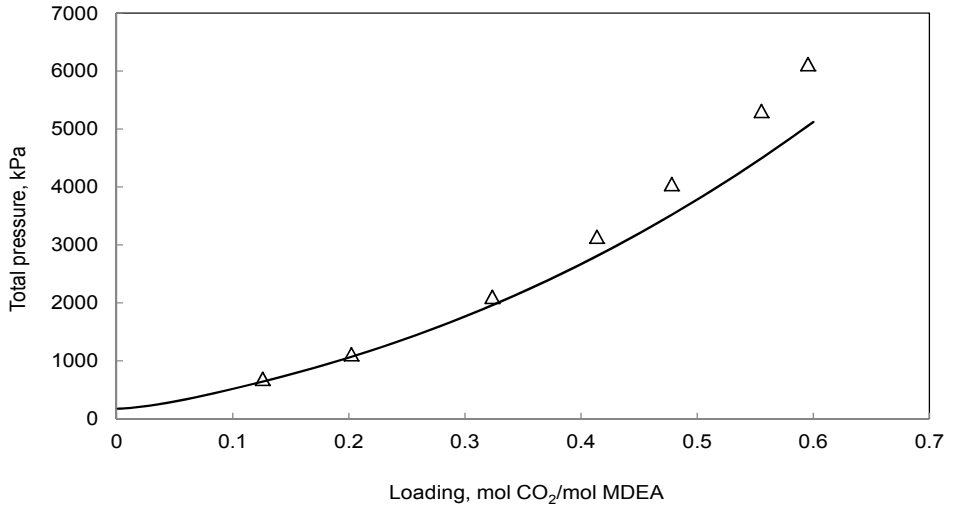

Figure 5-11. Comparison between experimental and regressed total pressure for CO_2-MDEA-H_2O solutions in 50 wt% MDEA and at 120 °C. Symbols stand for the experimental data and curve (line) refers to the represented values using the developed thermodynamic model. Δ**,** (Kamps et al. 2001)

As it can be seen from Figure 5-9 to Figure 5-11, in terms of industrial applications the developed model can adequately represent total pressure of CO_2-MDEA-H_2O solutions. Overall the model describes total pressure of CO_2-MDEA-H_2O mixtures with an average absolute relative deviation of 9.64 %.

It is worth to mention that the data provided by (Baek and Yoon 1998) have been excluded from regression data base. As can be seen in Figure 5-12 the reported experimental values are outliers of both other sources and model prediction. In addition, (Mathonat et al. 1997) have indirectly obtained high pressure data from calorimetric measurements. Even though, to the best of author knowledge, there is no other report in open literature for pressures as high as 10 MPa, the provided data has a huge deviation from the model prediction (AARD% of 86). In the absence of other reports it is not possible to determine whether the deviation stems from experimental error or it is due to the model shortcoming at very high pressures. Hence, the provided data is excluded from the regression data base and the upper pressure limit of model validity is set to 8 MPa.

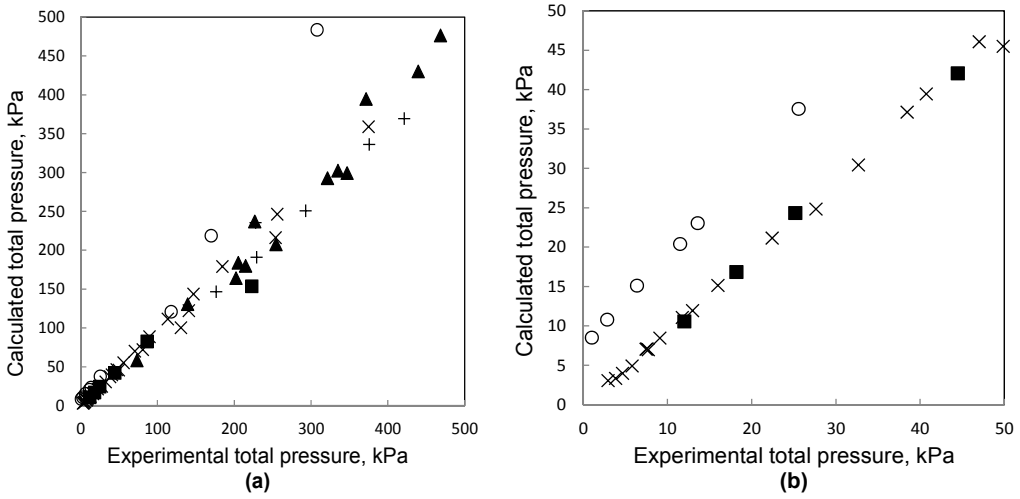

Figure 5-12. (a) Parity plot for total pressure of ternary CO_2-MDEA-H_2O mixture. (b) is magnified of figure (a) in low pressure region ■, (Silkenbaumer et al. 1998); ▲, (Kuranov et al. 1996); ×, (Sidi-Boumedine et al. 2004, a); +, (Kamps et al. 2001); ○, (Baek and Yoon 1998)

5.5.3.2 CO_2 Solubility Data

CO_2 solubility data refers to the measurements of CO_2 partial pressure (P_{CO2}) over an aqueous mixture of MDEA. Though the open literature is rich of this type of data, many of them are

uncertain and inconsistent. Hence, it is of importance to only use reliable data. Accordingly, based upon a thorough evaluation, data sets which are listed in Table 5-18 are chosen for optimization of the model parameters.

In the following, the results of fit for experimental CO_2 solubility at different conditions are presented. Regarding the modeling of the absorber column, it is of high importance that the model describes CO_2 partial pressure accurately at absorber temperature in order to assess the efficiency of the absorber column. To have better design of stripper column, it is very important to have precise prediction of CO_2 partial pressures at elevated temperatures (stripper operational temperatures). Figure 5-13 and Figure 5-15 show calculated results against experimental data for 50 wt% MDEA and at 40 °C and 100 °C, respectively. Figure 5-14 is the magnified images of Figure 5-13**,** in low loading range region.

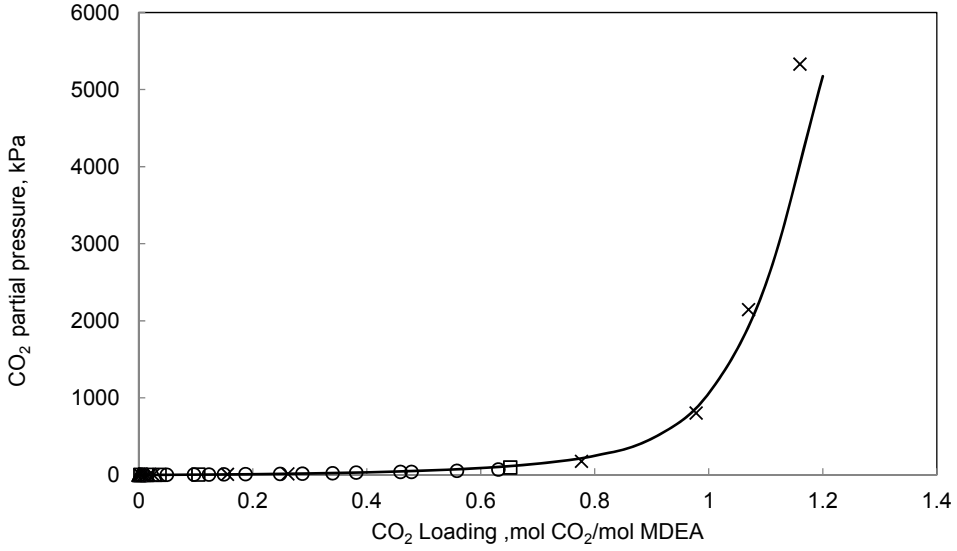

Figure 5-13. Comparison between experimental and regressed CO_2 solubility in aqueous MDEA solutions in 50 wt% MDEA and at 40°C. Symbols stand for the experimental data and curve (line) refers to the represented values using the developed thermodynamic model. ○, (Ermatchkov et al. 2006); □**,** (Austgen et al. 1991)**;** Δ**,** (Rogers et al. 1998)**;** ×**,** (Huang and Ng 1998)

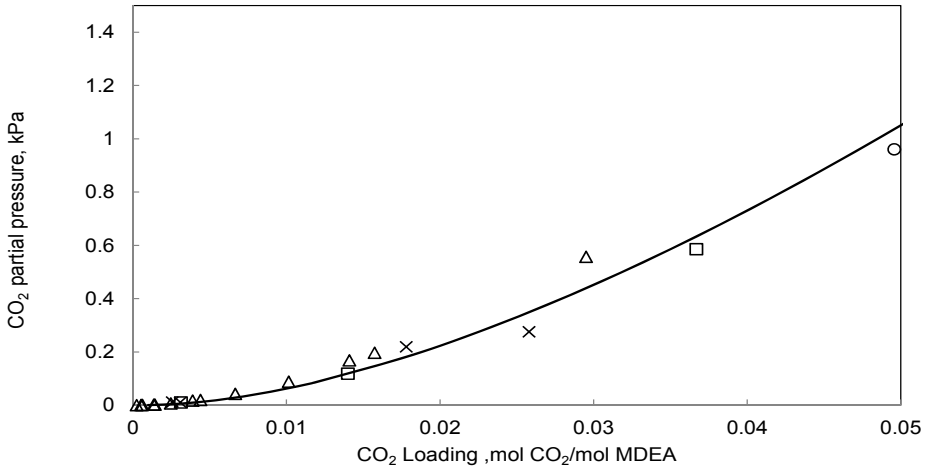

Figure 5-14. Magnified images of Figure 5-13, **in low loading range region. Comparison between experimental and regressed CO_2 solubility in aqueous MDEA solutions in 50 wt% MDEA and at 40°C. Symbols stand for the experimental data and curve (line) refers to the represented values using the developed thermodynamic model.** □**,** (Austgen et al. 1991)**;** Δ**,** (Rogers et al. 1998)**;** ×**,** (Huang and Ng 1998)

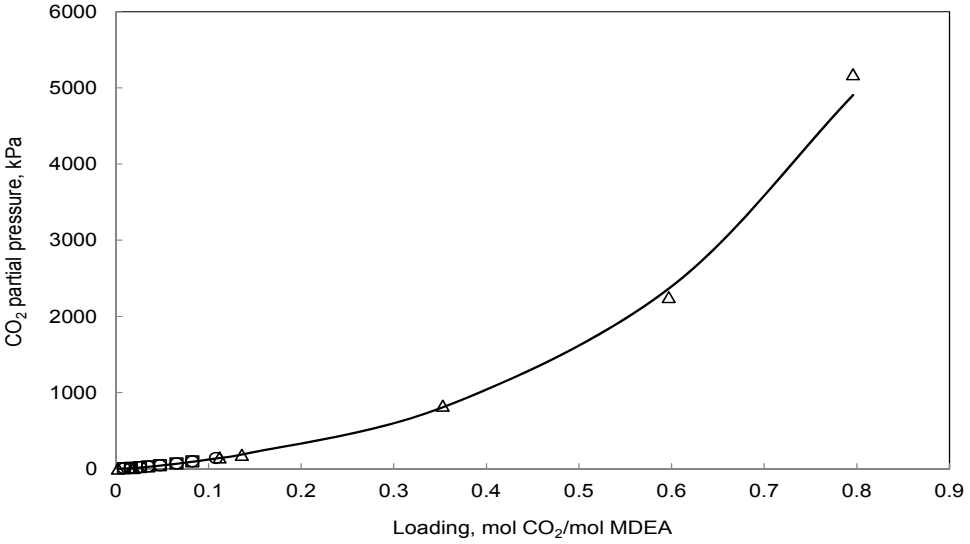

Figure 5-15. Comparison between experimental and regressed CO_2 solubility in aqueous MDEA solutions in 50 wt% MDEA and at 100°C. Symbols stand for the experimental data and curve (line) refers to the represented values using the developed thermodynamic model. ○, (Rho et al. 1997); □**,** (Park and Sandall 2001)**,** Δ**,** (Huang and Ng 1998)

Figure 5-16 (a) and (b) give results of fit for the experimental CO_2 partial pressure as a function of loading at 5 and 75 wt% MDEA and from 50 °C to 100 °C. To the best of our knowledge, at the time of this work, measurements of (Rho et al. 1997) for CO_2 solubility in aqueous MDEA solutions cover the lowest and highest values available in open literature for MDEA concentration, 5 to 75 wt%. Hence, it is worthwhile to present the results of fit for this source to evaluate model performance in a wide span of amine concentration.

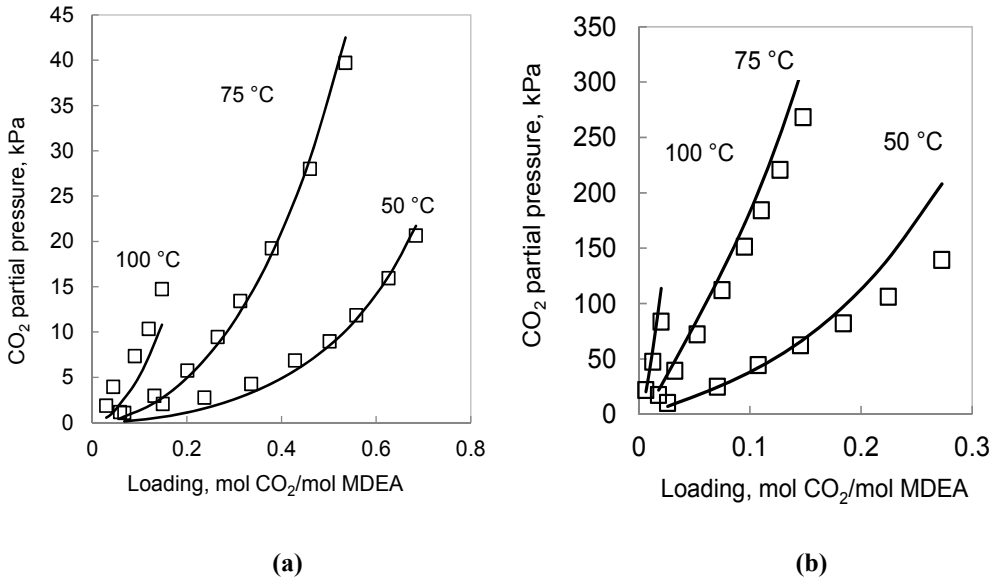

Figure 5-16. Comparison between experimental and regressed CO_2 solubility in 5 wt% (figure (a)) and 75 wt% (figure (b)) MDEA aqueous solutions and at 50 °C, 75 °C and 100°C. Symbols stand for the experimental data and curves (lines) refer to the represented values using the developed thermodynamic model. □, (Rho et al. 1997)

As it can be seen from Figure 5-16 the model is capable of representing CO_2 solubility in very low and very high concentrations of aqueous MDEA solutions. Figure 5-17 shows results of fit for very low pressure data of (Lemoine et al. 2000). As it can be observed in Figure 5-17 the developed model fairly represent CO_2 partial pressures in very low loading region.

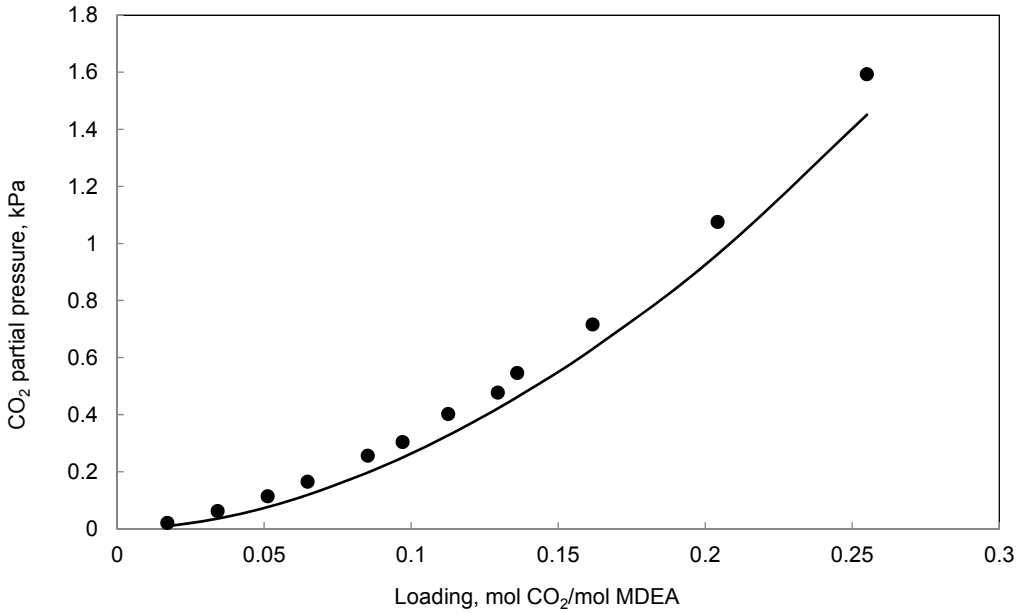

Figure 5-17. Comparison between experimental and regressed CO_2 solubility in 23 wt% MDEA aqueous solutions at 25 °C. Symbols stand for the experimental data and curve (line) refers to the represented values using the developed thermodynamic model. ●, (Lemoine et al. 2000)

All in all, the model adequately represents CO_2 solubility in aqueous MDEA solutions. The average absolute relative deviation for estimated CO_2 solubility in aqueous MDEA is 22 %.

It is worth mentioning that the data provided by (Jou et al. 1982) were discarded from regression data base since these data have a systematical error. This is shown in the parity plot in Figure 5-18 , where the experimental data of (Jou et al. 1982) is an outlier both to other data sources and the optimized model. It is noted that, the same observation was made by (Huttenhuis et al. 2007) and they postulated that the contamination of MDEA is at least one source of the error. Similarly, the experimental data provided by (Shen and Li 1992), especially at low partial pressure region, has a large deviation from other sources (see Figure 5-19). (Posey 1997) and (Hessen et al. 2010) have also disregarded (Shen and Li 1992) data, and that adds more justification for evaluating the data as erroneous.

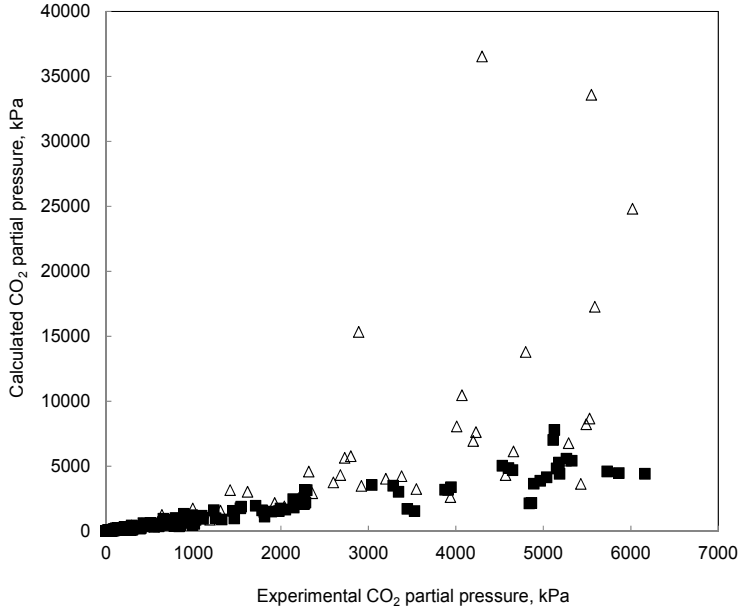

Figure 5-18. Parity plot for ternary mixture of CO_2-MDEA-H_2O. Δ, (Jou et al. 1982)**; ■, all the used data for CO_2 partial pressure listed in Table 5-18**

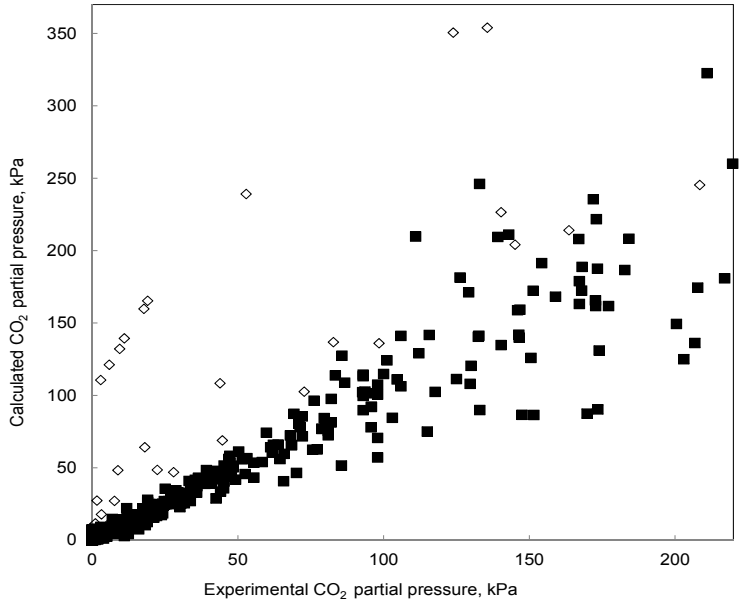

Figure 5-19. Parity plot for ternary mixture of CO_2-MDEA-H_2O. ◊, (Shen and Li 1992)**; ■, all the used data for CO_2 partial pressure listed in Table 5-18**

Moreover there is a discrepancy between the data provided by (Ali and Aroua 2004) and other sources, such as (Ermatchkov et al. 2006) and (Austgen et al. 1991), see Figure 5-20. Furthermore, there is a large deviation from the model predictions, i.e. AARD% = 378. In addition, the model developed by (Ermatchkov et al. 2006) showed larger deviations to (Ali and Aroua 2004) experimental data. Accordingly, this data set is excluded from the regression data base.

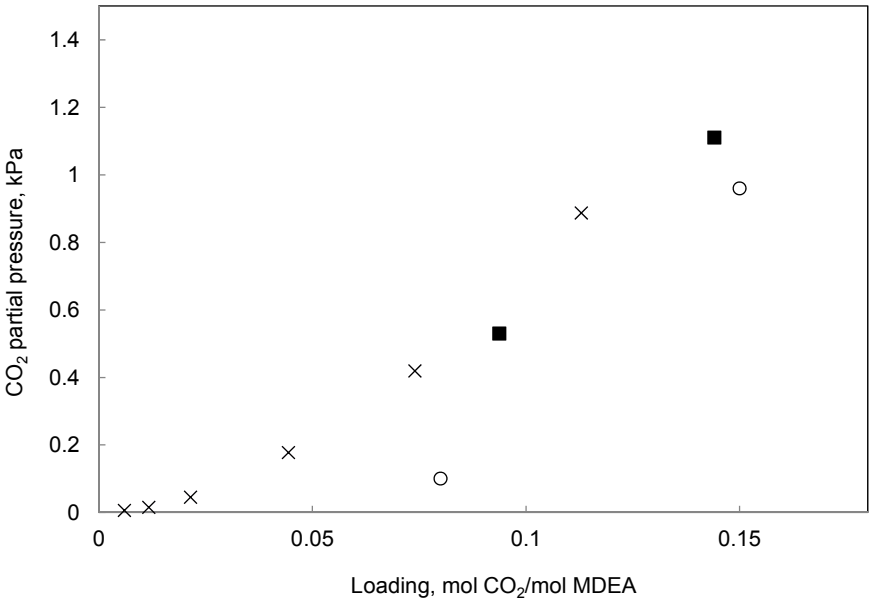

Figure 5-20. Comparison between CO_2 solubility data of (Ali and Aroua 2004) in 20 wt% MDEA aqueous solution at 40 °C with literature. ○, (Ali and Aroua 2004); ■, (Ermatchkov et al. 2006), ×, (Austgen et al. 1991)

Finally, the data provided by (Macgregor and Mather 1991) show a deviation from experimental results provided in other sources such as (Silkenbaumer et al. 1998) and (Kuranov et al. 1996) and the model developed in this study (see Figure 5-21). The deviation is more pronounced at loadings close and higher than unity. In this region, the pressure has a strong dependency on loading, hence, a slight error in measurement of pressure and/or loading is highly magnified. Similarly, (Hessen et al. 2010) pointed out the large deviation of data by (Macgregor and Mather 1991) from other sources. (Posey 1997) has also not used the mentioned data. Hence, based on comparison with other experimental data, the model developed in this study and models developed previously, the data

provided by (Macgregor and Mather 1991) is considered as erroneous and excluded from the regression data base.

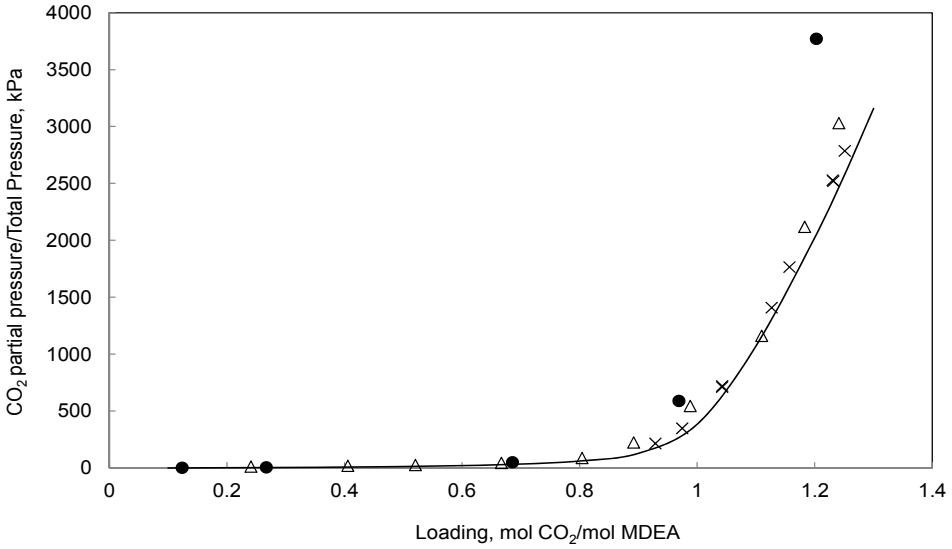

Figure 5-21. Comparison between CO_2 partial pressure data of (Macgregor and Mather 1991) in 19 wt% MDEA aqueous solution at 40 °C with literature and calculated results of model. ●, (Macgregor and Mather 1991) **(CO_2 partial pressure);** Δ, (Silkenbaumer et al. 1998) **(total pressure);** ×, (Kuranov et al. 1996) **(total pressure); Solid line, Extended UNIQUAC model (CO_2 partial pressure)**

5.5.3.3 Heat Capacity Data and Regression Results

Using Heat capacity data for parameter optimization improves model temperature dependency. Figure 5-22 compares experimental data from (Weiland et al. 1997) to the regressed results at 25 °C and 29.99, 40, 49.99 and 59.99 wt% MDEA. To the best of our knowledge, this data set is the only measurements available for heat capacity of CO_2-MDEA-H_2O system. As it can been from the figure there is a good agreement between calculated and experimental results.

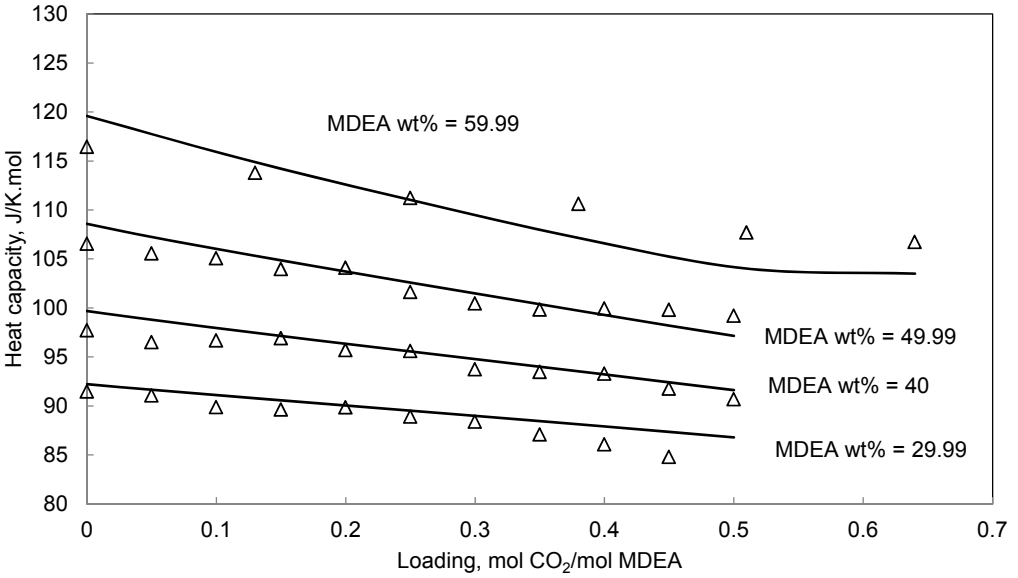

Figure 5-22. Comparison between experimental and regressed heat capacity at 25 °C and for ternary mixtures of CO_2-MDEA-H_2O for different MDEA concentrations. Symbols stand for the experimental data and curves (lines) refer to the represented values using the developed thermodynamic model. Δ, (Weiland et al. 1997)

5.5.3.4 Heat of Absorption Data, Regression Results

Optimizing model parameters to heat of absorption data helps to improve temperature dependency of the model. Notice that model parameters have been adjusted to the integral heat of absorption data. Hence, differential heat of absorption data is transformed to integral type of data before using for optimization parameters. In this study, heat of absorption data that are obtained from direct calorimetric measurements were used for parameter optimization. Calorimetric measurements provide values of enthalpy of absorption which reflects both the heat effects because of chemical reactions between acid gas and amine and the heat effects due to physical dissolution of gas in the solvent (Kim and Svendsen 2007). To explain enthalpy of absorption data, measured points of (Arcis et al. 2008) are plotted in Figure 5-23. This figure shows the measured values of enthalpy of absorption by (Arcis et al. 2008) at 50 °C and total pressure of 980 kPa. In this figure, heat of absorption provided as of both kJ/mole CO_2 and kJ/mole MDEA is plotted against mol CO_2/mol MDEA (which is the total molar flow rate of CO_2 divided by total molar flow rate of MDEA). The graph can be separated into two parts: **1)** The first part corresponds to a total dissolution of CO_2

(unsaturated region) **2)** The second part corresponds to partial dissolution of CO_2 (saturated region) (Arcis et al. 2009). The intersection between these two parts corresponds to the saturation point (acid gas solubility limit). Saturation point is the point where acid gas is completely absorbed and the aqueous alkanolamine solution is saturated with acid gas (Loading point, equilibrium point) and is dependent on the temperature and amine solution concentration (Mathonat et al. 1997). The explanation of the two parts of graph is more evident when enthalpy of absorption is provided per mole of amine. As it can be seen from Figure 5-23, the enthalpy of absorption (presented as of kJ/mole amine) increases with flow rate ratio (mole CO_2/mole MDEA) as more or less linearly up to limit of solubility of CO_2 in MDEA which corresponds to complete absorption of CO_2 in the aqueous MDEA solution. Then enthalpy of absorption grow slower and becomes constant after the saturation point since the aqueous MDEA solution is saturated with CO_2 and no more CO_2 is absorbed (Mathonat et al. 1997). When enthalpies of solution are presented as enthalpies per mole of amine, the graphs exhibit plateaus for saturation region and when enthalpies of solution are plotted as enthalpies per mole of acid gas, the plateaus corresponds to unsaturated region (Arcis et al. 2009).

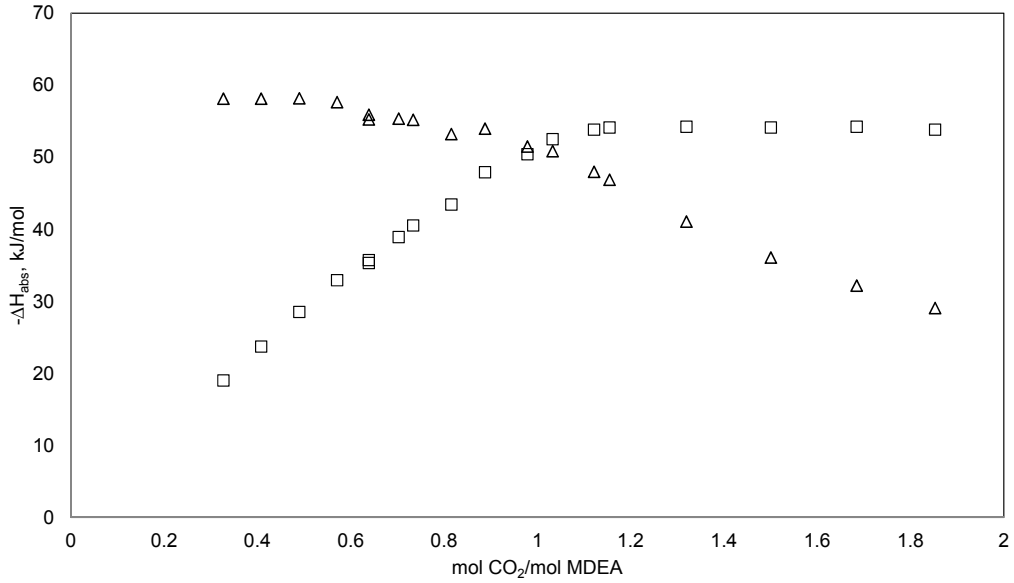

Figure 5-23. Measured heat of CO_2 absorption into 15 wt% MDEA aqueous solutions at temperature of 49.35 °C and total pressure of 980 kPa. Experimental data are from (Arcis et al. 2008)**. □, Enthalpies of absorption per mole of amine (-ΔH_{abs}, kJ/mol MDEA); Δ, Enthalpies of absorption per mole of acid gas (-ΔH_{abs}, kJ/mol CO_2)**

Heat of CO_2 absorption data from (Arcis et al. 2008) has been used simultaneously with other kinds of data to optimize model parameters. Figure 5-24 shows the result of fit for the experimental data at 49.35 °C, in 15 wt% MDEA and at different total pressures, 520 kPa, 980 kPa and 5170 kPa.

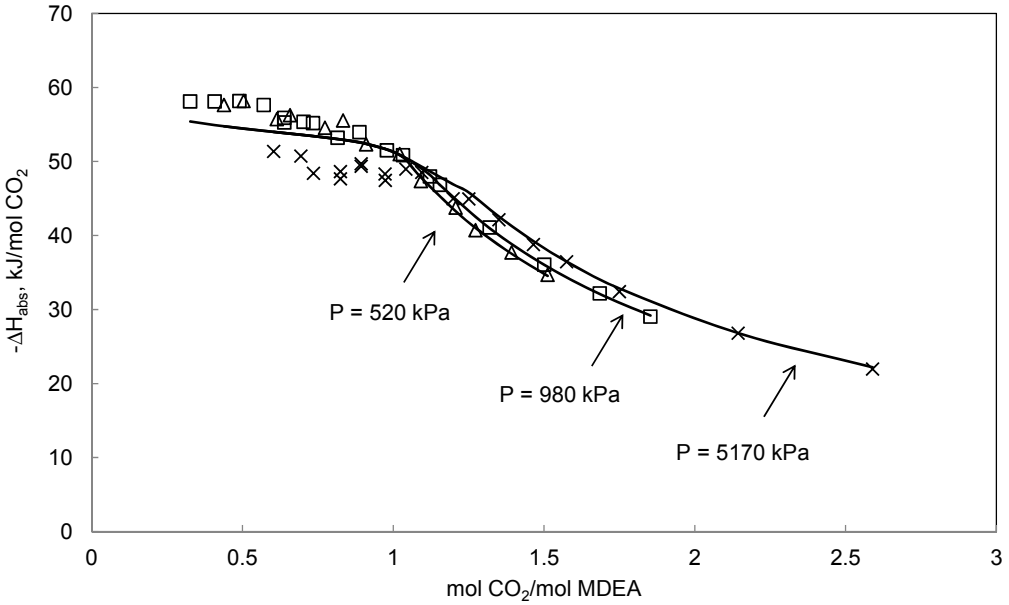

Figure 5-24. Comparison between calculated and measured heat of CO_2 absorption into 15wt% MDEA aqueous solutions at temperature of 49.35 °C and total pressure of 520, 980 and 5170 kPa. Symbols stand for the experimental data and curve (line) refers to the represented values using the developed thermodynamic model. Δ (P = 520 kPa), □ (P = 980 kPa), × (p = 5170 kPa), (Arcis et al. 2008)

Heat of CO_2 absorption data from (Oscarson et al. August, 1995) and (Arcis et al. 2009) have been used to verify the model; these data have been used to examine ability of the model as a predictive tool. Model predictions against the experimental values for data of (Oscarson et al. August, 1995) and (Arcis et al. 2009) are shown in Figure 5-25 and Figure 5-26, respectively. Figure 5-25 shows the effect of temperature on heat of CO_2 absorption into aqueous MDEA solution and Figure 5-26 demonstrates the effect of pressure on enthalpy of CO_2 absorption.

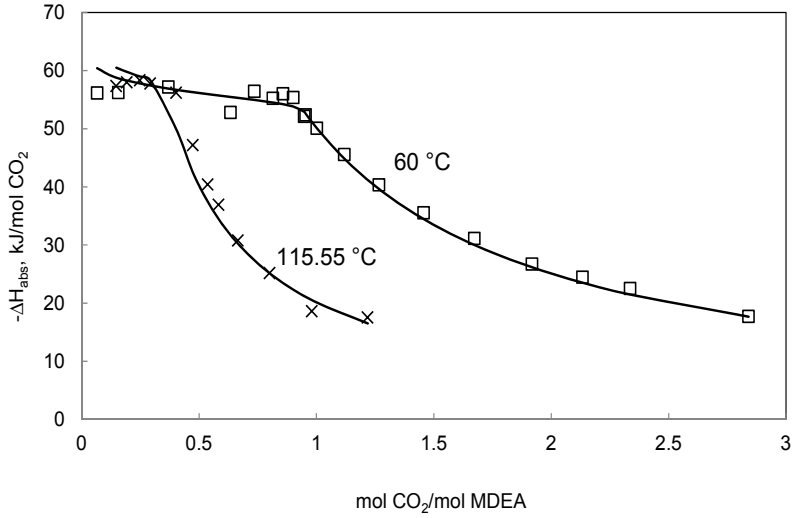

Figure 5-25. Comparison between model predictions and measured heat of CO_2 absorption into 40 wt% MDEA aqueous solution at 1120.96 kPa and at 60 and 115.55 °C. Symbols stand for the experimental data and curves (lines) refer to the represented values using the developed thermodynamic model. □ (T = 60°C), × (T = 115.55 °C), (Oscarson et al. August, 1995)

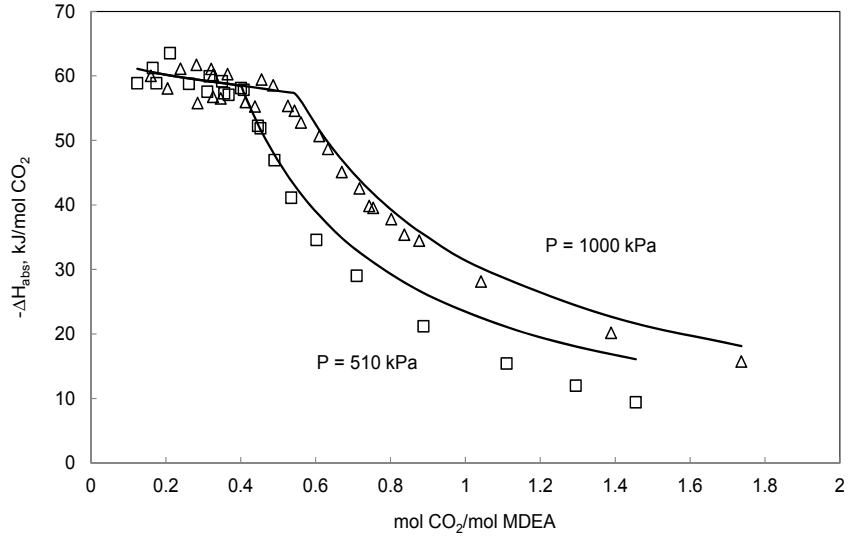

Figure 5-26. Comparison between model predictions and measured heat of CO_2 absorption into 30 wt% MDEA aqueous solution at 99.75 °C and at 510 and 1000 kPa. Symbols stand for the experimental data and curves (lines) refer to the represented values using the developed thermodynamic model. □ (P = 510 kPa), Δ (P = 1000 kPa), (Arcis et al. 2009)

As it can be seen in Figure 5-25 Generally, for all MDEA concentration, temperature increase results in slight increase of heat of CO_2 absorption in aqueous MDEA solutions (slight increase in exothermic effect). As it can be observed in Figure 5-26 and as stated by (Arcis et al. 2008), for all MDEA concentrations, pressure rise leads to slight decrease of heat of CO_2 absorption into aqueous MDEA solutions (slight decrease in exothermic effect). Table 5-19 shows experimental heat of CO_2 absorption data that have been used for verification of the developed model.

Table 5-19. Heat of CO_2 absorption data used for model verification

MDEA Concentration, wt%	T ,°C	Total Pressure, kPa	Reference	Number of Data Points	AARD%
20, 40, 60	15.5, 60, 115.5, 148.8	155.8, 1120.9, 1465.6	(Oscarson et al. August, 1995)	296	12
15, 30	99.7	510, 1000, 3160, 5290	(Arcis et al. 2009)	170	10

*Not available

Overall calculation results show that the model could accurately predict heat of CO_2 absorption into aqueous MDEA solution.

5.5.3.5 NMR Speciation Data and Prediction Results

As it was mentioned in section earlier, speciation data have not used in regression process, however model predictions were checked against available experimental NMR speciation data. The below figure demonstrates prediction results for NMR speciation data at temperature of 20 °C and for MDEA mass% of 23. Notice that the experimental values were only available for MDEA, CO_2, HCO_3^-.and CO_3^{2-}. For $MDEAH^+$ only model predictions are shown.

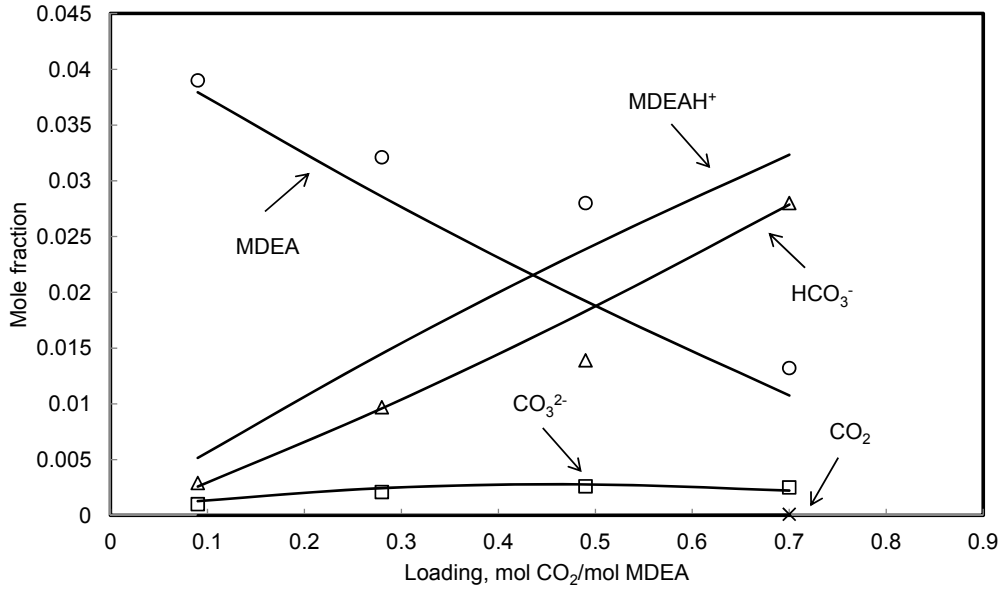

Figure 5-27 .Comparison between model predictions and NMR speciation data at T = 20 °C and MDEA wt% = 23. Symbols stand for the experimental data and curve (line) refers to the represented values using the developed thermodynamic model. ○ **(MDEA),** Δ **(HCO_3^-),** □ **(CO_3^{2-}),** × **(CO_2),** (Jakobsen et al. 2005)

Table 5-20 shows deviations of prediction of the model from the experimental speciation data for each species.

Table 5-20. AARD% for the predicted NMR speciation data

Species	**AARD%**
MDEA	14
CO_2	39
HCO_3^-	12
CO_3^{2-}	40

Model parameters for ternary CO_2-MDEA-H_2O system are valid in the temperature range of 20 to 200 ℃, the CO_2 partial pressure range of 0 to 7565 kPa, loading of 0.0002 to 1.4 and MDEA mass% of 5 to 75. Further experiments are carried out in this study (cf. section 7.6) and it is shown that the model is valid up to MDEA mass% of 90.

The developed model represents all kinds of used ternary data within AARD% of 16.

5.5.4 Comparison between Different Models

This section compare the results of the developed Extended UNIQUAC model in this study with the Extended UNIQUAC model with parameters from (Faramarzi et al. 2009) and e-NRTL model with parameters from (Hessen et al. 2010) for some selected sources. Table 5-21 shows comparison between different models results for some selected sources for CO_2 solubility in aqueous solutions of MDEA

Table 5-21. Comparison between different models results for CO_2-MDEA-H_2O system

Reference	MDEA Concentration, wt%	T, °C	Pressure, kPa	AARD%		
				Extended UNIQUAC		e-NRTL
				This Study	*(Faramarzi et al. 2009)*	*(Hessen et al. 2010)*
(Austgen et al. 1991)	23, 47	40	0.005 to 93.6 (P_{CO_2})	14	51	21
(Rho et al. 1997)	5, 19, 49, 75	50, 75, 100	0.77 to 264 (P_{CO_2})	18	42	25
(Ermatchkov et al. 2006)	19, 32, 48	40, 80, 120	0.12 to 69.3 (P_{CO_2})	8	24	18

As it can be seen from the above table, the developed model in this study has the lowest AARD% compare to the other two models. (Hessen et al. 2010) used E-NRTL, whereas (Faramarzi et al. 2009) used Extended UNIQUAC model. The reason behind better results of this work compare to (Faramarzi et al. 2009) can be summarized as **1)** Converting the volumetric VLE data in a correct way **2)** Use both partial pressure data and total pressure data for optimization parameters **3)** Use heat of absorption data in regression data base. Regression data base and fitting procedure also affect the modeling results.

5.6 MEA System

Model parameters for CO_2-MEA-H_2O system were fitted to various types of data. Model parameters were adjusted to 690 data points of pure MEA, binary aqueous MEA solution and CO_2 loaded mixtures. The modeling was started by creating a strong model for binary MEA-H_2O system; later on a model for CO_2-MEA-H_2O was developed based on the model parameters for MEA-H_2O mixture. In what follows, different types of data that have been used for adjusting model parameters and modeling results are provided.

5.6.1 Pure MEA Vapor Pressure Data and Modeling Results

Table 5-22 provides a summary of the experimental pure MEA vapor pressure data used for parameter regression. Deviations between model calculations and experimental data are also provided in Table 5-22. Totally 45 pure vapor pressure data points were used for adjusting model parameters.

Table 5-22. Regression results for MEA pure vapor pressure

Temperature , °C	Reference	Number of Data Points	AARD%
89.85 to 166.85	(Tochigi et al. 1999)	26	0.89
78 and 91.7	(Nath and Bender 1983)	2	6.11
158.24 and 170.23	(Cai et al. 1996)	2	1.66
84.31 to 158.46	(Kim et al. 2008)	15	0.70

Table 5-22 shows model regression results for vapor pressure of pure MEA. Alltogether the model represent pure MEA vapor pressure with average 2.34 AARD%.

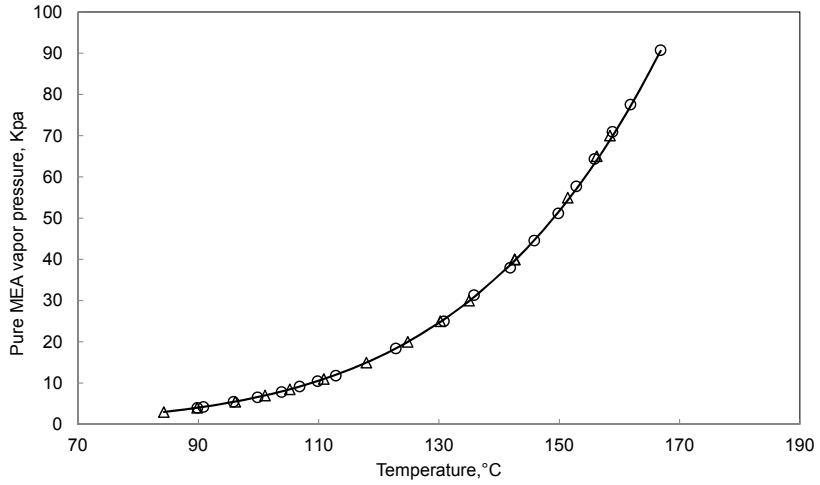

Figure 5-28. Vapor pressure of pure MEA. Symbols stand for the experimental data and curve (line) refers to the calculated values using the developed thermodynamic model.○,(Tochigi et al. 1999)**;** Δ**,** (Kim et al. 2008)

5.6.2 Binary MEA-H_2O Data and Modeling Results

In addition to pure MEA vapor pressure, 260 binary MEA-H_2O data points have been used for adjusting model parameters for MEA-H_2O system. The same as MDEA-H_2O system, different types

of binary data including total pressure, freezing point (SLE) and heat capacity were used for fitting MEA-H_2O model parameters. Regressing model parameters to freezing point depression and heat capacity data along with total pressure data leads to creation of a strong model for binary MEA-H_2O system. Table 5-23 lists the data sets upon which MEA-water model parameters were adjusted. In what follows modeling results for different kind of data of binary system are given.

Table 5-23. Review over binary MEA-H_2O data used for model parameter optimization and modeling results for binary mixture

MEA Concentration, wt%	T ,°C	P, kPa	Data Type	Reference	Number of Data Points	AARD%
42.5 to 97.86	89.85	4.02 to 68.15 (P_{Total})	VLE	(Tochigi et al. 1999)	10	21
16.74 to 97.86	60, 78, 90.7	1.31 to 69.1 (P_{Total})	VLE	(Nath and Bender 1983)	36	3.09
53.05, 77.24, 91.04	37.51 to 137.49	4.32 to 92.2 (P_{Total})	VLE	(Kling and Maurer 1991)	20	4.22
14.68 to 97.69	89.66 to 158.7	66.66, 101.33 (P_{Total})	VLE	(Cai et al. 1996)	25	7.02
3.98 to 75.58	40, 60, 80, 100	7.28 to 46 (P_{Total})	VLE	(Kim et al. 2008)	85	1.51
10, 20, 30, 40	25	Na*	C_p	(Weiland et al. 1997)	4	1.10
45.87, 69.32, 83.56, 93.13	30 to 80	Na*	C_p	(Chiu and Li 1999)	44	1.91
5.03 to 30.64	-1.6 to -16.27	Na*	Freezing point	(Fosbol et al. 2011)	6	1.80
9.01 to 35.87	-3.11 to -20.48	Na*	Freezing point	(Chang et al. 1993)	30	3.57

Not available

5.6.2.1 Total pressure data

Totally 176 experimental data points for total pressure of binary mixture of MEA and water have been used to adjust model parameters of MEA-H_2O system. Figure 5-29 shows the results of fit for total pressure of binary mixture of MEA and water at temperatures of 40 to 100 °C.

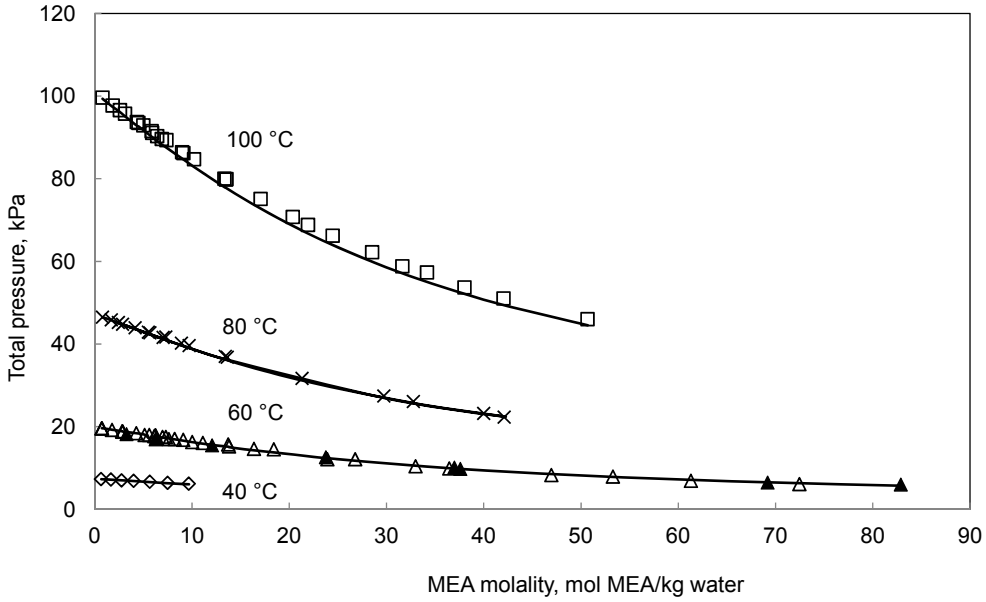

Figure 5-29. Comparison between experimental and fitted results for total pressure of MEA-H_2O solutions. **Symbols stand for the experimental data and curves (lines) refer to the calculated values using the developed thermodynamic model. ◊ (T = 40 °C), Δ (T = 60 °C), × (T = 80 °C), □ (T = 100 °C),** (Kim et al. 2008)**; ▲(T = 40 °C),** (Nath and Bender 1983)

As it is shown in the above figure, total pressure of aqueous mixture of MEA and water rises with increasing temperature. Total pressure of MEA-water solution is mainly dominated by water vapor pressure, about 90% of total pressure of binary MEA-Water mixture is because of water. With increasing MEA molality the share of water vapor pressure in total solution pressure decreases which results in total pressure drop.

Figure 5-30 is a parity plot shows model calculated results versus regressed experimental data; the curve has the slope of 0.96 which confirms model capability for representing total pressure of MEA-water subsystem. Overall the model represents total pressure of MEA-H_2O subsystem with an average absolute relative deviation of 7.36 %.

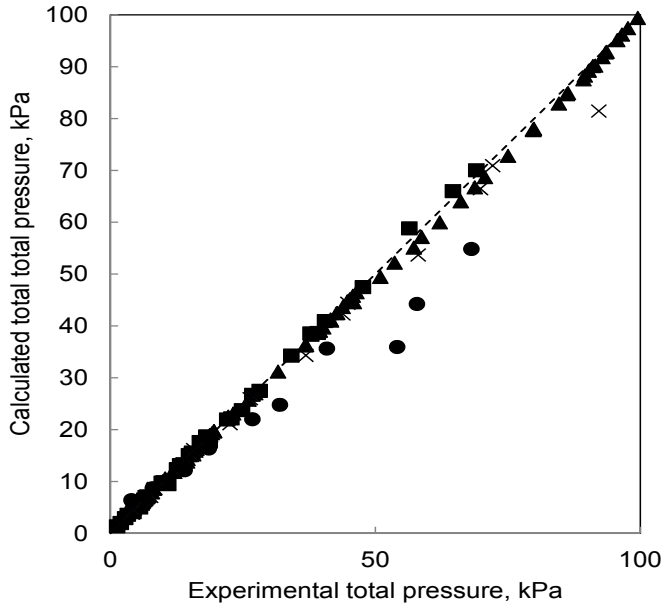

Figure 5-30. Parity plot for binary MEA-H_2O system.■, (Nath and Bender 1983)**; ▲,** (Kim et al. 2008)**; ×,** (Kling and Maurer 1991)**; ●,** (Tochigi et al. 1999)

5.6.2.2 Heat Capacity Data

(Weiland et al. 1997) and (Chiu and Li 1999) heat capacity data for binary mixture of MEA-H_2O have been used simultaneously with other data types to adjust model parameters. Figure 5-31 compares results of fit for heat capacity of MEA-water mixture with the experimental data from (Chiu and Li 1999). All in all, average AARD% for results of fit of heat capacity of binary MEA-H_2O system is 1.50 %.

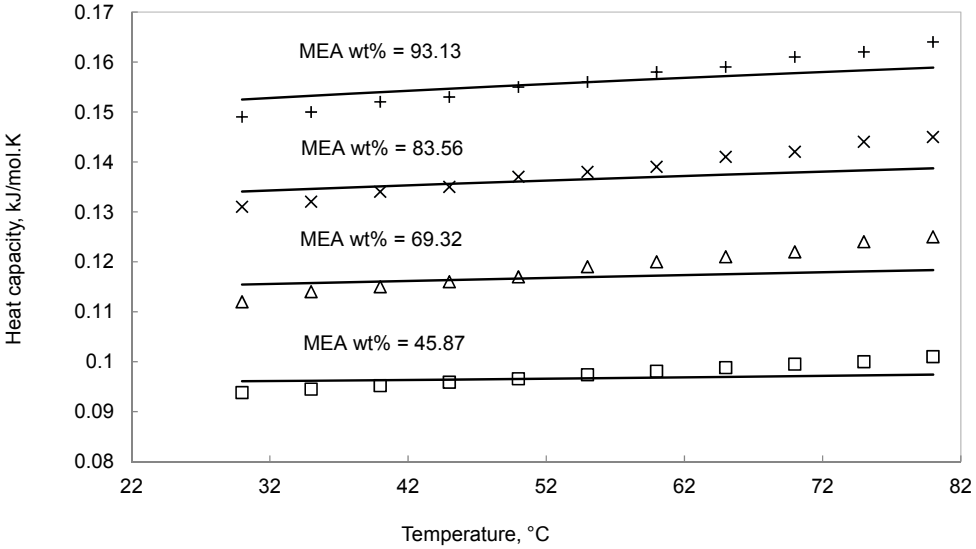

Figure 5-31. Comparison between experimental and calculated values of heat capacity of MEA-H_2O solutions at 45.87, 69.32, 83.56 and 93.13 wt% MEA. Symbols stand for the experimental data and curves (lines) refer to the calculated values using the developed thermodynamic model. □ (45.87 wt% MEA), Δ (69.32 wt% MEA),× (83.56 wt% MEA), + (93.13 wt% MEA), (Chiu and Li 1999)

Figure 5-31 shows that the heat capacity of aqueous MEA mixture rises as the temperature increases and also as the MEA concentration increases.

5.6.2.3 Freezing Point Depression Data

MEA-H_2O freezing point data of (Fosbol et al. 2011) and (Chang et al. 1993) have been used to optimize model parameters. Figure 5-32 shows freezing point of aqueous MEA mixture calculated by the model against different experimental sources. As it can be seen from the Figure 5-32, calculated results are in good agreement with the experimental data. All in all, the developed model calculates freezing point of MEA-H_2O solution within 4.01 AARD%.

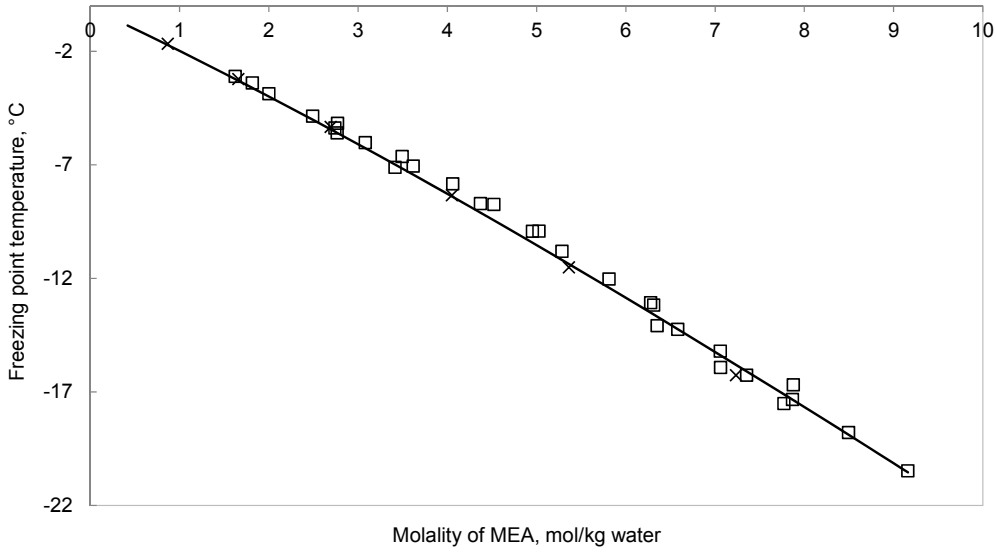

Figure 5-32. Freezing point of MEA-H_2O solutions. Symbols stand for the experimental data and curve (line) refers to the calculated values using the developed thermodynamic model. ×,(Fosbol et al. 2011); □, (Chang et al. 1993)

5.6.2.4 MEA Vapor Pressure, Model Predictions

MEA is more volatile than MDEA and the amount of MEA losses from absorber and stripper columns are greater than MDEA. Accurate prediction of MEA volatility at absorber and stripper conditions leads to efficient plant design. Thus it is of great need that thermodynamic model could represent MEA vapor pressure over operational conditions accurately. Figure 5-33 plots model predictions for MEA vapor pressure over aqueous mixtures of MEA at 53.05, 77.22 and 91.04 wt% MEA. The temperature range shown in the figure covers absorber and stripper operational conditions.

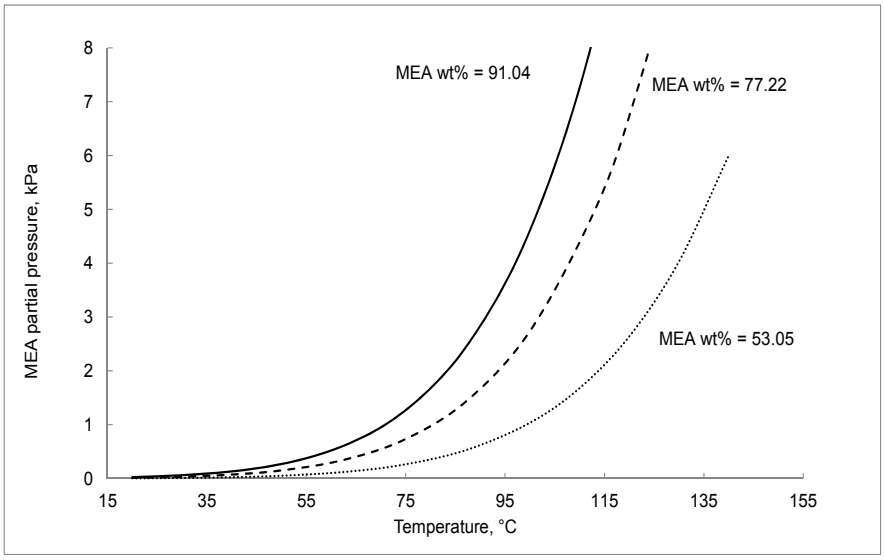

Figure 5-33. Predicted MEA volatility for MEA-H_2O solutions in 53.05, 77.22 and 91.04 wt% MEA. Curves (lines) refer to the predicted values using the developed thermodynamic model. Dot Line, 53.05 wt% MEA; Dash Line, 77.22 wt% MEA; Solid Line, 91.04 wt% MEA

As it can be seen from Figure 5-33, MEA losses become larger with increasing temperature. Increasing MEA concentration also leads the amount of loss to rise.

Overall, the Extended UNIQUAC model, through simultaneous regression gave a set of optimum parameters for the binary MEA- H_2O system. Model parameters for binary MEA-H_2O system are valid in the temperature range of -21 to 159℃, the total pressure range of 1 to 101 kPa and the whole concentration range of MEA. The developed model represents all kinds of used binary data within AARD% of 5.

5.6.3 Ternary CO_2-MEA-H_2O Data and Modeling Results

Modeling results for MEA-water subsystem were presented in previous section. This section will go through CO_2 loaded system results. Data that have been used to adjust model parameters and modeling results will be described in what follows. Interaction parameters involved in CO_2-MEA-H_2O system have been determined through simultaneous regression of total pressure, CO_2 solubility (CO_2 partial pressure), heat capacity, heat of absorption and freezing point depression data with the

Extended UNIQUAC model. 385 numbers of data over vast range of temperature, pressure and composition were used to fit model parameters.

Table 5-24 presents a summary of the data that were used for parameter optimization.

Table 5-24.Overview on ternary CO_2-MEA-H_2O data used for parameter optimization and regression results.

MEA Concentration, wt%	T (°C)	P (kPa)	Data Type	Reference	Number of Data Points	AARD%
15.17	25, 60, 80	6.84 to 6085.46 (P_{CO_2})	VLE	(Maddox et al. 1987)	60	14
15.29, 30	40, 60, 80, 100	1.1 to 2550 (P_{CO_2})	VLE	(Shen and Li 1992)	61	18
15.17	40, 80	0.09 to 228.7 (P_{CO_2})	VLE	(Austgen et al. 1991)	8	9.66
15.20	40, 60, 80, 100, 120, 140	1.33 to 2786.44 (P_{CO_2})	VLE	(Lawson and Garst 1976)	20	14
30	120	7.3 to 191.9 (P_{CO_2})	VLE	(Ma'mun et al. 2005)	19	20
15.29	0.43, 40, 80, 100, 120, 140	0.002 to 930.99 (P_{CO_2})	VLE	(Jones et al. 1959)	54	34
10, 20, 30, 40	25	Na*	C_p	(Weiland et al. 1997)	24	14
9.99, 20, 29.99	25	Na*	H_{abs}	(Carson et al. 2000)	40	1.68
29.99	40, 80, 120	Na*	H_{abs}	(Kim and Svendsen 2007)	84	3.37
29.99	-15.55 to -15.09	Na*	Freezing Point	(Nielsen 2011)	4	2.13
29.99	-16.42 to -14.88	Na*	Freezing Point	(Jepsen and Petersen 2011)	11	2.74

Not available

The remainder of this section will present different kinds of data that have been used for fitting model parameters of CO_2-MEA-H_2O system.

5.6.3.1 CO_2 Solubility Data

CO_2 partial pressure data over aqueous mixture of MEA have been used to adjust model parameters. After a thorough evaluation, sources that are listed in

Table 5-24 were chosen for parameter optimization. Figure 5-34, Figure 5-35 and Figure 5-36 represent modeling results for CO_2 solubility in aqueous MEA solutions at 40 and 80 and 120 °C, respectively.

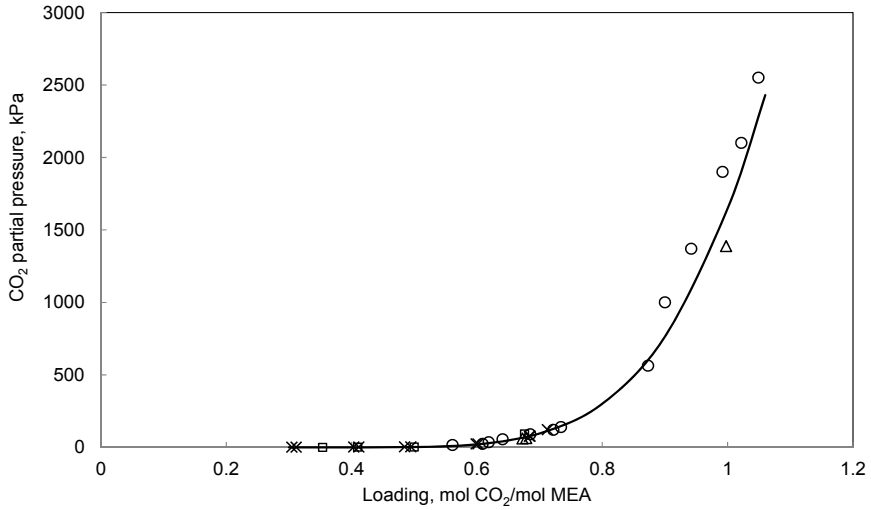

Figure 5-34. Comparison between experimental and regressed CO_2 solubility in 15 wt% aqueous MEA solutions at 40 °C. Symbols stand for the experimental data and curve (line) refers to the represented values using the developed thermodynamic model. ○, (Shen and Li 1992); □, (Austgen et al. 1991); Δ, (Lawson and Garst 1976); ×, (Jones et al. 1959)

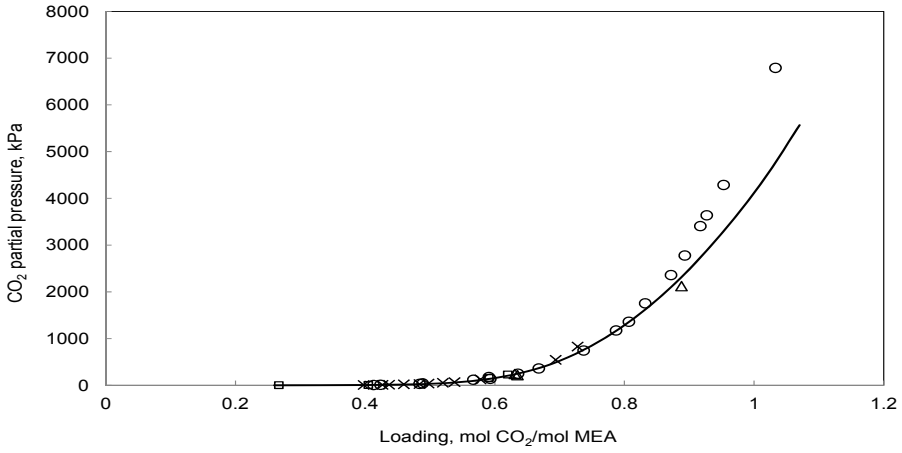

Figure 5-35. Comparison between experimental and regressed CO_2 solubility in 15 wt% aqueous MEA solutions at 80 °C. Symbols stand for the experimental data and curve (line) refers to the represented values using the developed thermodynamic model. ○,(Maddox et al. 1987); □, (Austgen et al. 1991); Δ, (Lawson and Garst 1976); ×, (Jones et al. 1959)

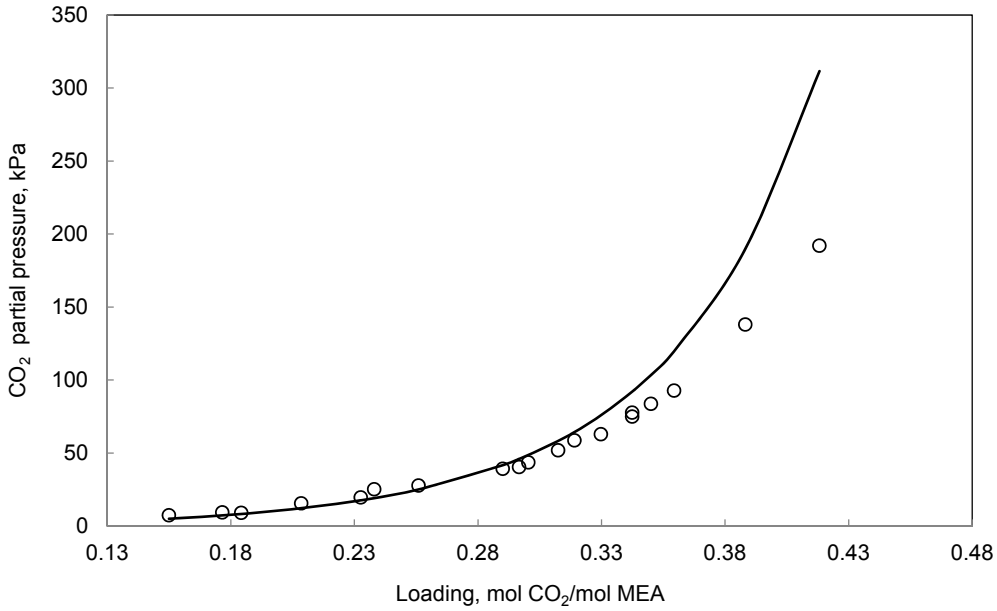

Figure 5-36. Comparison between experimental and regressed CO_2 solubility in 30 wt% aqueous MEA solutions at 120 °C. Symbols stand for the experimental data and curve (line) refers to the represented values using the developed thermodynamic model.○, (Ma'mun et al. 2005)

All in all model represent CO_2 solubility in aqueous MEA solution within 18% AARD.

It is worth mentioning that the data provided by (Lee et al. 1976) give large deviation from the optimized model (AARD of 80%). (Jou et al. 1995), also reported the inaccuracy of experimental procedure of (Lee et al. 1976) and indicated that loading is biased. In addition, (Hessen et al. 2010) stated that the mentioned data was not useable fully even after biasing. Hence, based on the deviation from the optimized model and agreement of scientific community on errors of the data reported by (Lee et al. 1976), the data were not included in the data base of this study.

The data provided by (Jou et al. 1995) show a significant scatter from the optimized model (see parity plot in Figure 5-37, and has an AARD of 95%. Due to the same reason, (Faramarzi et al. 2009) have also excluded the mentioned data. Thus, the data reported by (Jou et al. 1995) were not used in this study too.

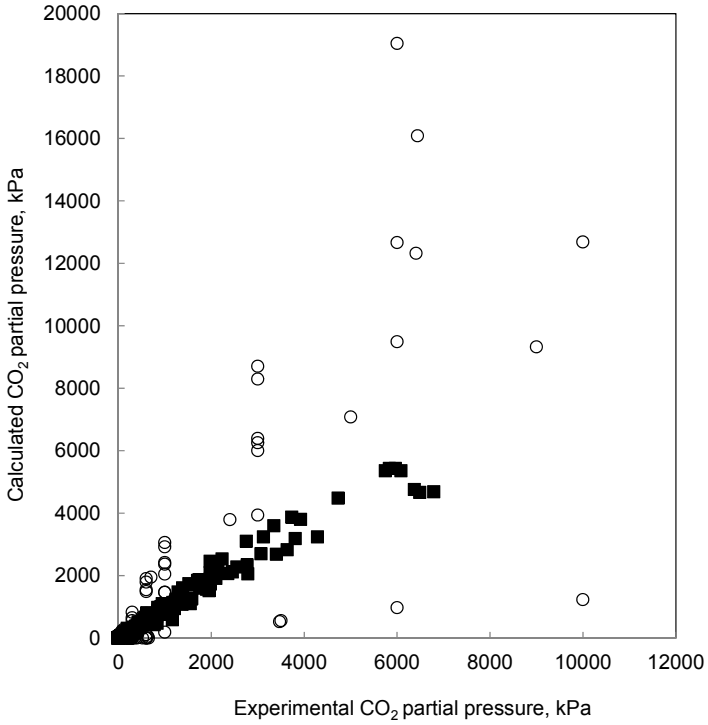

Figure 5-37. Parity plot for ternary mixture of CO_2-MEA-H_2O. ○, (Jou et al. 1995)**; ■, all the used data for CO_2 partial pressure listed in table 5-24**

It is pointed out by (Weiland et al. 1993) that the experimental data provided by (Isaacs et al. 1980) is not reliable. And even after exclusion of 30% of the data which was obviously erroneous, the rest of data set still showed large deviation from the model. Similarly, (Hessen et al. 2010) have reported AARD% of 123 for the mentioned data set. In this study, the absolute average deviation is relatively lower, but still unacceptable, 84%, hence, it is excluded from regression data base.

The experimental data reported by (Daneshvar et al. 2004) show notable deviation from the optimized model, the parity plot is shown in Figure 5-38 (AARD% of 243). It is worth to mention that, due to the same reason (Faramarzi et al. 2009) have not included the mentioned data.

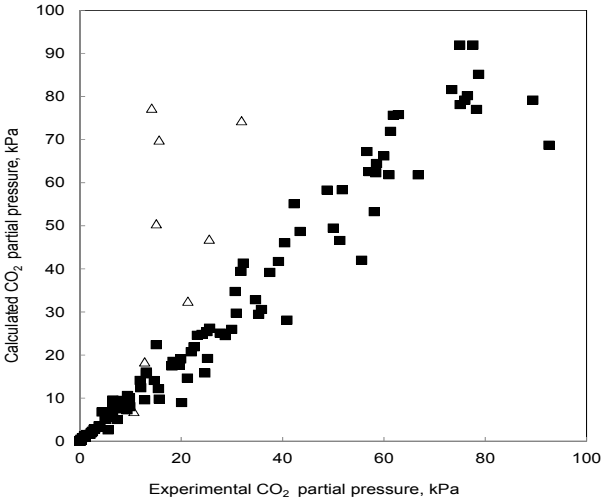

Figure 5-38. Parity plot for ternary mixture of CO_2-MEA-H_2O. Δ, (Daneshvar et al. 2004)**; ■, all the used data for CO_2 partial pressure listed in table 5-24**

5.6.3.2 Heat of Absorption Data

Figure 5-39 presents the result of fit for heat of CO_2 absorption data at 40, 80 and 120 °C, in 30 wt% aqueous MEA solutions.

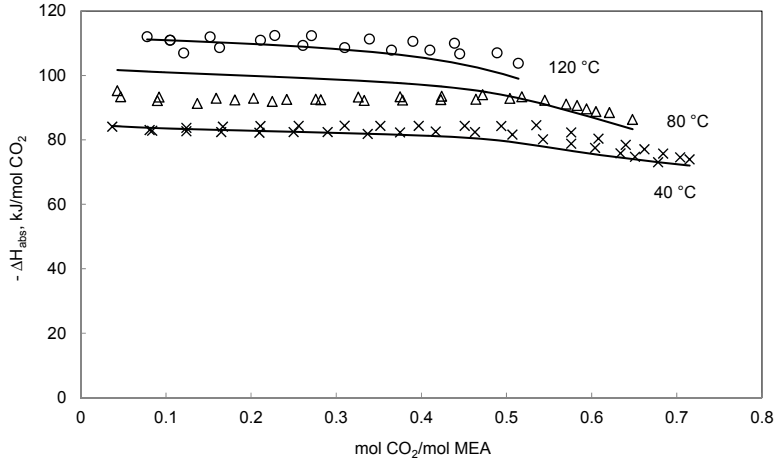

Figure 5-39. Comparison of the heat of CO_2 absorption at 40, 80 and 120 °C and in 30 wt% aqueous MEA solutions. Symbols stand for the experimental data and curves (lines) refer to the represented values using the developed thermodynamic model. × (T = 40 °C), Δ (T = 80 °C), ○ (T = 120 °C), (Kim and Svendsen 2007)

As it is shown in Figure 5-39 the agreement between model and experiments are satisfactory. All in all model represents CO_2 heat of absorption in aqueous MEA solutions within 2.52 AARD%.

5.6.3.3 Freezing Point Depression Data

Figure 5-40 shows results of fit for freezing point of CO_2 loaded solution. The experimental data have not been published yet. Freezing point depression data of CO_2-MEA-H_2O mixtures have been used simultaneously with other data types to adjust model parameters. Including these data in the regression data base improve model capability to represent freezing point of the loaded solution.

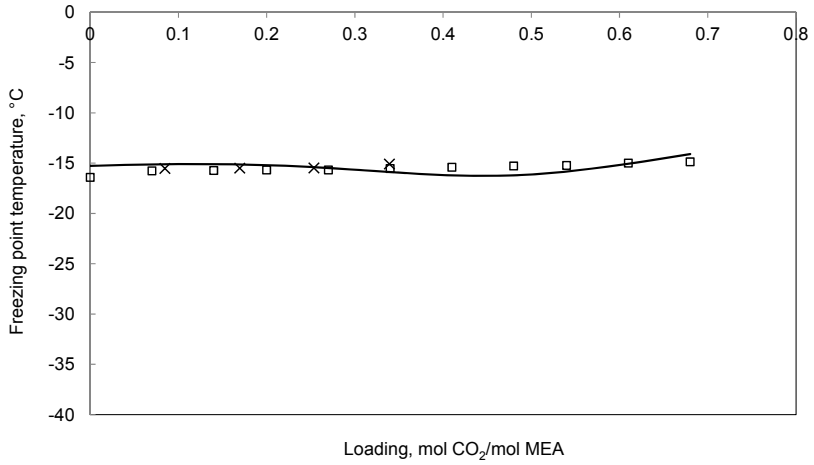

Figure 5-40. Comparison between estimated and experimental freezing point in 30 wt% aqueous MEA solutions. Symbols stand for the experimental data and curve (line) refers to the represented values using the developed thermodynamic model. ×**,** (Nielsen 2011)**;** □**,** (Jepsen and Petersen 2011)

Overall the model represent freezing point of CO_2-MEA-H_2o mixture within 2.43 AARD%.

5.6.3.4 NMR Speciation Data, Prediction Results

This section show model predictions for NMR speciation data, like MDEA system these data have not been used for adjusting model parameters. Figure 5-41 plots model predictions against NMR speciation data for 30 wt% MEA and at 40 °C. Due to fast proton transfer between MEA and MEA protonated, it was not possible to experimentally determine MEA and $MEAH^+$ concentrations, therefore only sum of MEA and $MEAH^+$ concentrations were presented by (Boettinger et al. 2008). Despite this, the model can calculate concentration of all constituents of liquid phase. Figure 5-42

shows model predictions for liquid phase distribution in solution of CO_2-MEA-H_2O for 30 wt% MEA and at 40 °C.

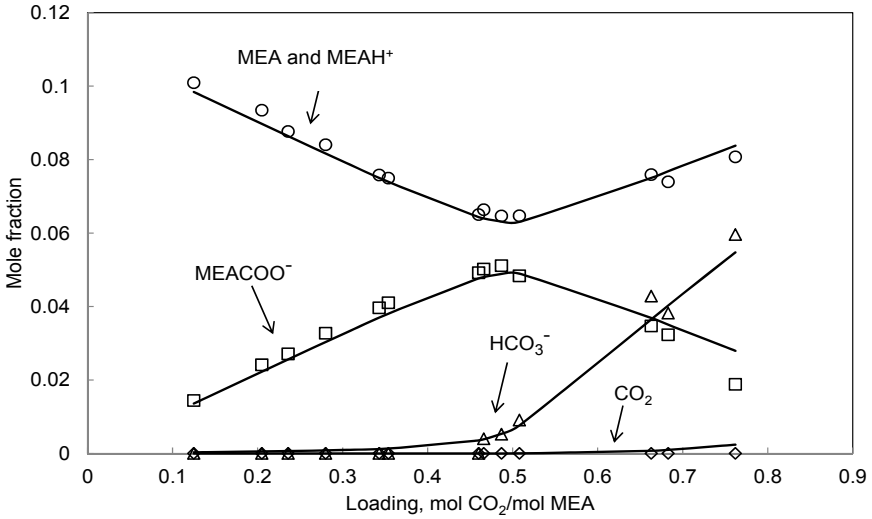

Figure 5-41. Comparison between model predictions and speciation NMR data at 40 °C and in 30 wt% MEA. Symbols stand for the experimental data and curves (lines) refer to the calculated values using the developed thermodynamic model.○ (MEA and $MEAH^+$), Δ (HCO_3^-), □ ($MEACOO^-$), ◊ (CO_2) ,(Boettinger et al. 2008)

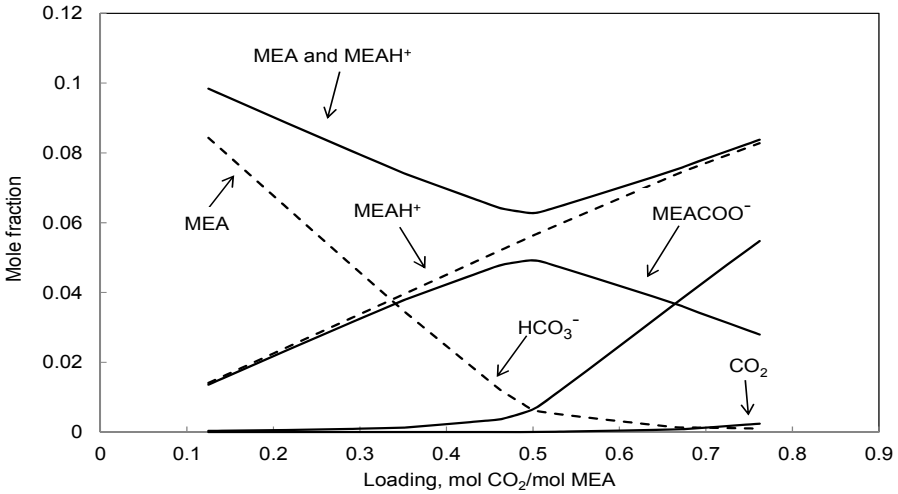

Figure 5-42. Model predictions for liquid phase distribution in CO_2-MEA-H_2O solution at 40 °C and in 30 wt% MEA.

When CO_2 is added to the system, many reactions will occur in the system. Reactions between CO_2 and aqueous MEA form $MEACOO^-$ and $MEAH^+$ as primary products. The concentration of MEA drops while the MEA carbamate and MEA protonated concentrations rise. At loading around 0.5 MEA concentration almost becomes zero since MEA totally consumed by the reactions. However $MEAH^+$ concentration continues to increase with the loading. Thus $MEACOO^-$ starts to decline after loading 0.5. This makes more MEA available for the formation of $MEAH^+$. It also creates more HCO_3^- and consequently more CO_2. Table 5-25 shows deviations between model predictions and NMR speciation data from (Boettinger et al. 2008) for the concentration of the species present in the liquid phase.

Table 5-25. AARD% for the NMR speciation data

Species	AARD%
MEA and $MEAH^+$	2.41
$MEACOO^-$	8.94
HCO_3^-	3.93

Figure 5-42 and Table 5-25 show that the developed model accurately predicts distribution of species in the liquid phase considering that no parameters were adjusted to the speciation data.

Model parameters for ternary CO_2-MEA-H_2O system are valid in the temperature range of -16 to 140℃, the CO_2 partial pressure range of 0 to 6086 kPa, loading of 0.01 to 1.3 and MEA mass% of 10 to 40. The developed model represents all kinds of used ternary data within AARD% of 12.

5.6.4 Comparison between Different Models

This section compare the results of the developed Extended UNIQUAC model in this study with the Extended UNIQUAC model with parameters from (Faramarzi et al. 2009) and e-NRTL model with parameters from (Hessen et al. 2010). Table 5-26 shows comparison between different models results for some selected sources for CO_2 solubility in aqueous MEA solutions.

Table 5-26. Comparison between different models results for CO_2 solubility in aqueous MEA solutions

Reference	MDEA Concentration., wt%	T, °C	Pressure, kPa	AARD%		
				Extended UNIQUAC		e-NRTL
				This Study	*(Faramarzi et al. 2009)*	*(Hessen et al. 2010)*
(Austgen et al. 1991)	15.17	40, 80	0.09 to 228.7 (P_{CO_2})	9.66	36	28
(Shen and Li 1992)	15.29, 30	40, 60, 80, 100	1.1 to 2550 (P_{CO_2})	18	29	53
(Maddox et al. 1987)	15.17	25, 60, 80	6.48 to 6085.46 (P_{CO_2})	14	15	Na*
(Ma'mun et al. 2005)	30	120	7.3 to 191.9 (P_{CO_2})	20	64	31

Na : Not available

5.7 Blend of MDEA and MEA System

As it was mentioned earlier, only binary interaction parameter between MDEA and MEA has been adjusted to the experimental data of the MDEA-MEA-H_2O systems and the rest of the parameters remained fixed at the determined values for subsystems. 219 data points have been used to fit MDEA-MEA interaction parameter. Next section show data sources that were used for regression MDEA-MEA interaction parameter. Regression results are shown afterwards.

5.7.1 Ternary MDEA-MEA-H_2O Data and Modeling Results

Ternary MDEA-MEA-H_2O data including total pressure, freezing point and heat capacity have been used for model parameter determination. Table 5-27 lists the data sets upon which the parameters are regressed. In what follows modeling results for different kind of data have been shown.

Table 5-27. Review over ternary MDEA-MEA-H_2O data used for model parameter regression

Molar ratio, MEA:MDEA	Water Mole Fraction	T ,°C	P, kPa	Data Type	Reference	Number of Data Points	AARD %
1:3, 2:2, 3:1	0.6	40 to 100	5.98 to 90.3 (P_{Total})	VLE	(Kim et al. 2008)	11	0.80
4:16 to 64:16	0.2 to 0.8	30 to 80	Na*	C_p	(Chen et al. 2001)	176	4.15
1:1, 1:2, 2:1, 1:4, 4:1	0.86 to 0.99	-0.96 to -20.15	Na*	Freezing Point	(Fosbol et al. 2011)	32	3.52

Na: Not Available

5.7.1.1 Total Pressure Data

Total pressure data of (Kim et al. 2008) have been used to adjust binary interaction parameter between MEA and MDEA. Results of the fit are shown in Figure 5-43.

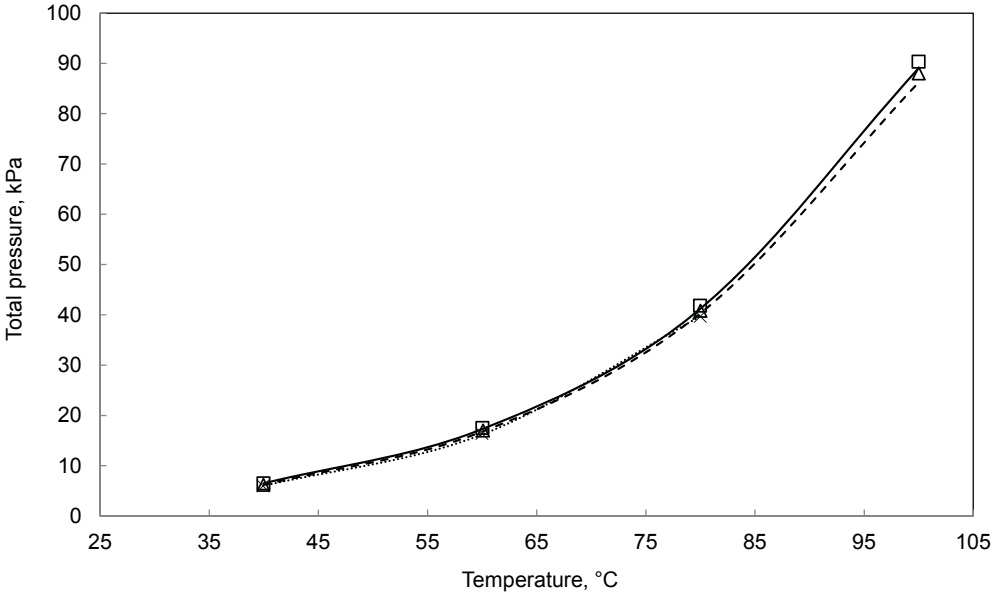

Figure 5-43. Comparison between calculated and experimental total pressure of MDEA-MEA-H_2O solutions. Symbols stand for the experimental data and curves (lines) refer to the calculated values using the developed thermodynamic model. □ (Molar ratio, MEA:MDEA=1:3), Δ (Molar ratio, MEA:MDEA=1:1), × (Molar ratio, MEA:MDEA=3:1), (water mole fraction = 0.6), (Kim et al. 2008)**; Solid line (Molar ratio, MEA:MDEA=1:3), Dash line (Molar ratio, MEA:MDEA=1:1), Dot line (Molar ratio, MEA:MDEA=3:1),**

As it can be seen from the above figure agreement between experimental and calculated values by Extended UNIQUAC model are very satisfactory.

5.7.1.2 Heat Capacity Data

Heat capacity data from (Chen et al. 2001) for mixtures of MDEA-MEA-H_2O have been used to tune MDEA-MEA binary interaction parameters. Figure 5-44 plots estimated values against the experimental data at water mole fraction of 0.4.

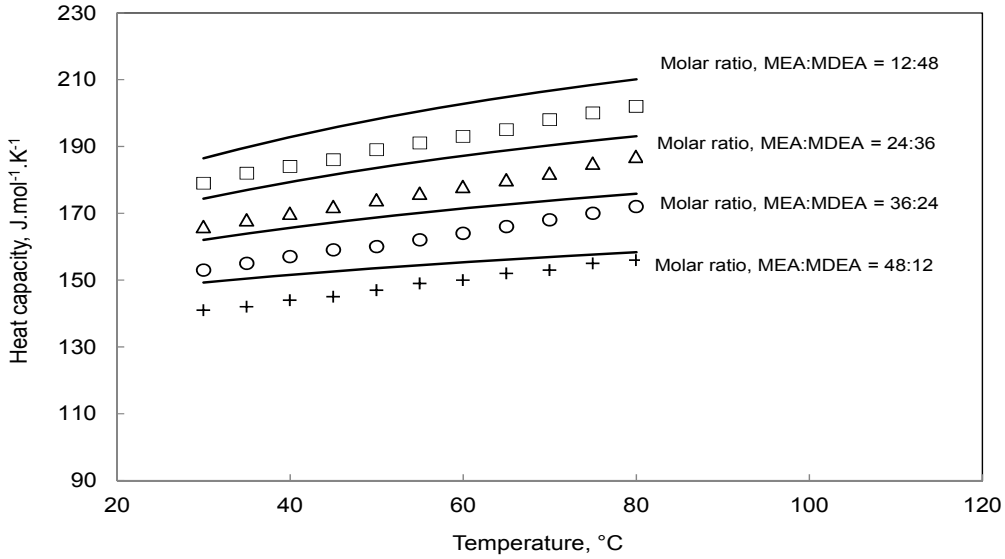

Figure 5-44. Heat capacity of MDEA-MEA-H_2O solutions for water mole fraction = 0.4. **Symbols stand for the experimental data and curves (lines) refer to the calculated values using the developed thermodynamic model. □ (Molar ratio, MEA:MDEA=12:48), Δ (Molar ratio, MEA:MDEA=24:36), ○ (Molar ratio, MEA:MDEA=36:24), + (Molar ratio, MEA:MDEA=48:12), (water mole fraction = 0.2 to 0.8),** (Chen et al. 2001)

As it can be seen from Figure 5-44, heat capacity of aqueous mixture of MDEA and MEA is over predicted by the model. (Chen et al. 2001) estimated the uncertainty of their measurements of heat capacity equal to $\pm 2\%$. The model calculates the data of (Chen et al. 2001) within 3.5 AARD% which is larger than the estimated uncertainty of the measurements.

5.7.1.3 Freezing Point Data

Freezing point depression data of (Fosbol et al. 2011) have been simultaneously used to adjust binary interaction parameter between MDEA and MEA. Regression results are plotted in Figure 5-45.

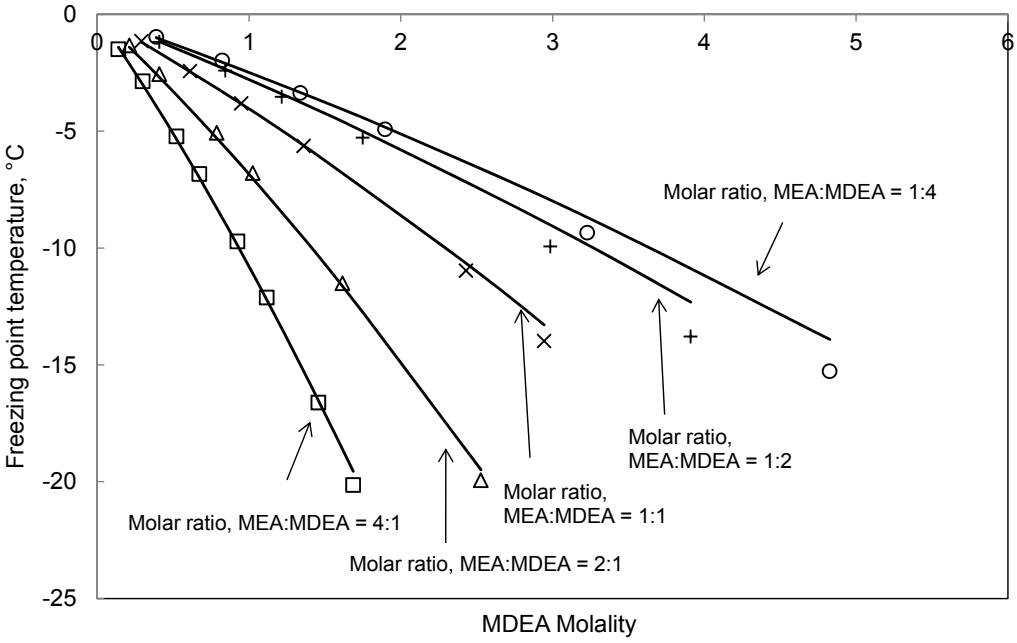

Figure 5-45. Freezing point of MDEA-MEA-H_2O solutions. **Symbols stand for the experimental data and curves (lines) refer to the calculated values using the developed thermodynamic model. □ (Molar ratio, MEA:MDEA=4:1), Δ (Molar ratio, MEA:MDEA=2:1), × (Molar ratio, MEA:MDEA=1:1), + (Molar ratio, MEA:MDEA=1:2), ○ (Molar ratio, MEA:MDEA=1:4), (water mole fraction = 0.86 to 0.99),** (Fosbol et al. 2011)

Model parameters for ternary MDEA-MEA-H_2O system are valid in the temperature range of -20 to 100 ℃, the total pressure range of 5 to 90 kPa and molar ratio of MEA to MDEA from 1:4 to 4:1 while mole fraction of water varies from 0.2 to 0.99. The developed model represents all kinds of used ternary data within AARD% of 2.82.

5.7.2 Quaternary CO_2-MDEA-MEA-H_2O Data and Prediction Results

Parameters of CO_2-MDEA-MEA-H_2O system consist of model parameters for CO_2-MDEA-H_2O, CO_2-MEA-H_2O and MDEA-MEA-H_2O systems. Table 5-28 shows model prediction results for quaternary CO_2-MDEA-MEA-H_2O system. Model prediction results for CO_2 solubility in aqueous mixture of MDEA and MEA are shown in Figure 5-46.

Table 5-28. Review over prediction results for quaternary CO_2-MDEA-MEA-H_2O data

Molar ratio, MEA:MDEA	Water Mole Fraction	T ,°C	P, kPa	Data Type	Reference	Number of Data Points	AARD %
4:3, 9:1	0.9	40, 60, 80, 100	0.9 to 2016(P_{CO_2})	VLE	(Shen and Li 1992)	94	44
0.8:3.4, 2.1:2.1	0.5, 0.81	70, 100, 120, 140, 160, 180	137 to 3876 (P_{CO_2})	VLE	(Dawodu and Meisen 1994)	68	45
2:2	0.9	40,80	0.05 to 258.2 (P_{CO_2})	VLE	(Austgen et al. 1991)	16	54

Figure 5-46 compares results of fit with experimental data from (Shen and Li 1992).

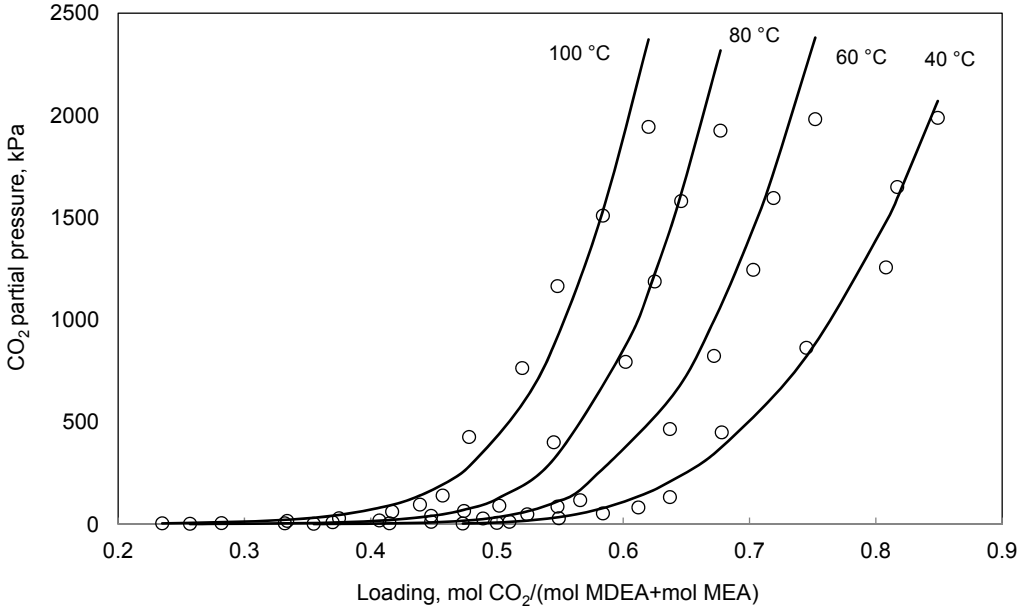

Figure 5-46. Comparison between calculated and experimental values of CO_2 solubility in aqueous mixture of MDEA-MEA at 40, 60, 80 and 100 °C and with molar ratio, MEA:MDEA of 0.71 to 6.5. (water mole fraction = 0.9). Symbols stand for the experimental data and curve (line) refers to the calculated values using the developed thermodynamic model. ○, (Shen and Li 1992)

Three data sources are used to validate the model predictions for quaternary CO_2-MDEA-MEA-H_2O system. These data are in the temperature range of 40 to 180℃, CO_2 partial pressure range of 0 to 3876 kPa and molar ratio of MEA to MDEA from 0.8:3.4 to 9:1 while mole fraction of water varies from 0.5 to 0.9.

Overall, model predicts CO_2 partial pressure in aqueous MDEA-MEA solution within 47% average absolute relative deviation.

5.8 Conclusion

In this chapter Extended UNIQUAC models for CO_2-MDEA-H_2O, CO_2-MEA-H_2O and CO_2-Blend of MDEA and MEA-H_2O systems were developed. Three improvements were utilized in the model of this study and the model parameters were fitted to a more various and extensive data base than preexisting model (Faramarzi et al. 2009). The experimental data available in the open literature were found to be discrepant and scattered, the regression data base was selected after evaluation of the available data. The modeling of CO_2-amine-H_2O system begins with creating a strong model for the amine-water system. Model parameters for the amine-H_2O subsystems have been adjusted to pure amine vapor pressure and binary total pressure, excess enthalpy, heat capacity and freezing point data. Regressing excess enthalpy, heat capacity and freezing point data along with total pressure data, improve model predictions of amine activity coefficient in aqueous amine solutions. Amine activity coefficients are required to calculate amine concentration in the vapor phase, also are important in the acid gas VLE calculations (Posey 1997). Good values for amine activity coefficients lead to accurate prediction of amine losses from the top of the absorber and stripper which is one of important operational considerations. The overall fit of the two subsystems were quiet good and the developed models adequately represent thermodynamic and thermal properties of the subsystems. The models also properly predict amine volatility. Models for CO_2-amine-water systems were developed based on parameters for amine-water subsystems and by adjusting additional interaction parameters associated with the ternary systems. Total pressure, CO_2 partial pressure, heat capacity, heat of absorption and in case of MEA system, freezing point data of ternary systems were regressed to adjust interaction parameters associated with the ternary systems. Regression of heat capacity and heat of absorption data improves temperature dependency of the model. The models were confirmed to be able to represent thermodynamic and thermal properties of ternary mixtures of CO_2-amine-H_2O over a broad range of conditions. Moreover, a model for MDEA-MEA-H_2O system was developed based on combination of model parameters for MDEA-

H_2O and MEA-H_2O systems, and by adjusting additional MDEA-MEA parameter. Finally, model for CO_2-MDEA-MEA-H_2O system was constructed by combining parameters of CO_2-MDEA-H_2O, CO_2-MEA-H_2O and MDEA-MEA-H_2O systems. Results of fit for CO_2-blend of MDEA and MEA-H_2O system were found to be satisfactory, although the deviations are larger than binary and ternary systems.

Overall the presented results indicate that simultaneous regression to different kind of data, gave a set of optimum parameters for MDEA-H_2O, MEA-H_2O, MDEA-MEA-H_2O CO_2-MDEA-H_2O, CO_2-MEA-H_2O and CO_2-MDEA-MEA-H_2O systems. The developed Extended UNIQUAC models adequately represent thermodynamic and thermal properties of the mentioned systems. The developed models are demonstrated to be thermodynamically consistent by comparison to NMR speciation data that were not regressed. Modeling results show that the developed models improved significantly over previously existing models.

Chapter 6

Thermodynamic Modeling of H_2S-MDEA-H_2O and Acid gas-Methane-MDEA-Water

Chapter 6

Thermodynamic Modeling of H_2S-MDEA-H_2O and Acid gas-Methane-MDEA-Water

6 Thermodynamic Modeling of H_2S-MDEA-H_2O and Acid gas-Methane-MDEA-Water

6.1 Chapter Overview

The optimization of model parameters for H_2S containing systems is more difficult and complicated than that of CO_2. It is due to the fact that less data is available for H_2S systems and also because the concentration of some of the present ions in the system is very small. In natural gas cleaning industry, in the absorber column the pressure is normally high and therefore it is of high importance to model effect of high pressure on the solubility of acid gas in aqueous MDEA. In this chapter, optimization of Extended UNIQUAC model parameters for H_2S-H_2O, CH_4-H_2O, H_2S-MDEA-H_2O, H_2S-CH_4-MDEA-H_2O and CO_2-CH_4-MDEA-H_2O systems are discussed in the following manner. Modeling of pure H_2S and H_2S-H_2O binary subsystem are discussed first. Based on the proposed model for H_2S-H_2O and MDEA-H_2O subsystems (MDEA-H_2O model was already discussed in chapter 5) the model is further developed for H_2S-MDEA-H_2O systems. Afterwards, modeling of CH_4-H_2O system is presented. The last section describes model predictions for H_2S-CH_4-MDEA-H_2O and CO_2-CH_4-MDEA-H_2O systems. Finally the effect of high pressure on acid gas solubility is investigated quantitatively.

6.2 Evaluation of Parameters

This section represents the fitting procedure, selection of interaction parameters for fitting and the adjusted value of parameters.

6.2.1 Fitting Procedure

Available data in the open literature were first evaluated and then used to fit the Extended UNIQUAC model parameters. The type of data was as follows: pure H_2S vapor pressure, VLE (total and partial pressure) and heat of absorption (H_{abs}). The model for H_2S-MDEA-H_2O system is developed based on the parameters of MDEA-H_2O and H_2S-H_2O systems and by adjusting

additional binary interaction parameters to ternary data. The parameters of H_2S-MDEA-H_2O mixture are determined in a two-stage approach. In the first stage model parameters for binary H_2S-H_2O, r and q and binary interaction parameters, are adjusted by regressing pure H_2S vapor pressure and binary VLE data of H_2S-H_2O. In the second stage, binary interaction parameters associated with the ternary system are fitted to ternary VLE and H_{abs} data, while parameters for H_2S-H_2O system were fixed at the fitted values obtained in the stage 1 and parameters of MDEA-H_2O were retained at the determined values in chapter 5. The modeling was continued by developing a model for H_2S-CH_4-MDEA-H_2O system based on the combination of parameters of H_2S-MDEA-H_2O and CH_4-H_2O systems. CH_4-H_2O system was modeled by fitting r and q parameters for CH_4 and CH_4-H_2O interaction parameter to binary VLE data of CH_4-H_2O system.

The evaluation of model parameters was performed by minimizing the objective function (equation (6-1)).

$$S = \sum_{VLEdata}\left[\frac{P_{calc}-P_{exp}}{w_1\,(P_{exp}+(0.01\ bar))}\right]^2 + \sum_{P^{vap}data}\left[\frac{P_{cal}^{vap}-P_{exp}^{vap}}{w_2\,P_{exp}^{vap}}\right]^2 + \sum_{H^{Abs}data}\left[\frac{H_{calc}^{Abs}-H_{exp}^{Abs}}{w_3\,y}\right]^2 \qquad (6\text{-}1)$$

In the equation (6-1) "calc" and "exp" represent calculated and experimental values, respectively. w_1 to w_3 indicate the weight numbers used for each kind of data. In equation (6-1), P is either the solution total pressure (bar) or in most cases acid gas partial pressure (bar), P^{Vap} is the pure H_2S vapor pressure (bar) and H^{Abs} is the heat of absorption of H_2S into aqueous MDEA solution (J). y = 1 J is included to make the equation dimensionless. 0.01 bar is added to the denominator of the VLE term to limit the influence of the low pressure data. Table 6-1 shows weighting factors that have been used for VLE, pure H_2S vapor pressure and heat of absorption data in the objective function. Different types of data were weighted the same way as modeling the CO_2 system (section 5.2.1).

Table 6-1. Weights for different kinds of data in the objective function used for optimization model parameters

Data Type	Weight Number
VLE*	0.05
Pure H_2S vapor pressure	0.0075
Heat of H_2S absorption	0.02

**Total and partial pressure data used for regression parameters of H_2S-H_2O, CH_4-H_2O, H_2S-MDEA-H_2O systems.*

The approach used in this study for optimizing parameters of H_2S-MDEA-H_2O system comprises of two steps. In the first step, r and q parameters and effective interaction parameters in the binary system were fitted to the pure H_2S vapor pressure and binary H_2S-H_2O data. This step leads to a model for H_2S-H_2O binary system. Eventually the effective interaction parameters in the ternary system were tuned to the ternary data while the parameters of H_2S-H_2O and MDEA-H_2O systems were retained at the adjusted values obtained in previous step and chapter 5, respectively. In the other words, first a strong model for H_2S-H_2O binary system was proposed, and based on the H_2S-H_2O binary model, a model for H_2S-MDEA-H_2O was developed. Altogether, 8 parameters (including 4 pure component (r and q) and 4 interaction parameters) for H_2S-H_2O binary subsystem were adjusted to the experimental data. H_2S-H_2O model parameters were fitted to pure H_2S vapor pressure data, total pressure data of H_2S-H_2O system and H_2S solubility in water data (H_2S partial pressure). Total pressure, H_2S solubility and heat of H_2S absorption data in aqueous MDEA have been regressed to adjust 8 interaction parameters involved in ternary H_2S-MDEA-H_2O system. Altogether, 16 parameters were adjusted to model the behavior of H_2S-MDEA-H_2O system (8+8=16). Thermodynamic modeling continued by development of a model for H_2S-CH_4-MDEA-H_2O system based on combination of models for H_2S-MDEA-H_2O and CH_4-H_2O systems. For the CH_4-H_2O system, CH_4-H_2O binary interaction parameters (u^0 and u^T) were fitted to binary total pressure data of CH_4-H_2O system, r and q parameters for methane were taken from (Addicks et al. 2002). Adjusted parameters for H_2S-MDEA-H_2O and CH_4-H_2O systems have been used to model (predict) the behavior of H_2S-CH_4-MDEA-H_2O system; no additional parameter was adjusted on quaternary H_2S-CH_4-MDEA-H_2O data.

6.2.2 Determination of Effective Interaction Parameters, Selection of Interaction Parameters for Fitting

In the H_2S-MDEA-H_2O system, there are 3 molecular and 4 ionic species present in the liquid phase, for H_2S-CH_4-MDEA-H_2O system, one more component (CH_4) is added to the number of molecular species present in the liquid solution. Hence an achingly large number of possible interactions could be formulated in the system. For example in the system of CO_2-H_2S-primary or secondary amine-H_2O, 78 possible interactions (by considering for symmetry) could be specified (Weiland et al. 1993). Fitting this large number of parameters is not a realistic goal. Therefore, it is necessary to disregard ineffective interaction parameters in order to reduce the number of adjustable parameters to a manageable set. Knowing the chemistry of solution and calculating concentration of species in ideal solution helps to discard ineffective parameters. Concentration of some of the

species is quiet small, thus, parameters associated with them have negligible effect on representation the behavior of system (when the concentration is low, even if the interactions were strong, they make negligible contribution to the total interaction term). The choice of important parameters of the system, those that affected representation of system behavior, arises from experience with the model, sensitivity studies of parameters and necessity to adequately fit the experimental data. Finally, the following set of effective parameters was chosen to tune to experimental data. For ineffective interaction parameters, u^0 is fixed at 10^{10} and u^T is assigned at 0.

- **H_2S- H_2O System**
  - ✓ H_2S-H_2S
  - ✓ H_2S-H_2O
- **H_2S-MDEA-H_2O System**
  - ✓ MDEA-HS^-
  - ✓ $MDEAH^+$-HS^-
  - ✓ HS^--HS^-
  - ✓ H_2O-HS^-
  - ✓ MDEA-H_2O (Determined in previous chapter)
  - ✓ MDEA-MDEA (Determined in previous chapter)
  - ✓ $MDEAH^+$-H_2O (Determined in previous chapter)
- **CH_4- H_2O System**
  - ✓ CH_4-H_2O

It is notable that concentration of HS^- ion is very low in the binary H_2S-H_2O system, however in the ternary H_2S-MDEA-H_2O mixture, its concentration is notable. Therefore parameters associated with HS^- are adjusted to data of ternary mixture of H_2S-MDEA-H_2O.

The mentioned interaction parameters were fitted to the experimental data, by using the fitting procedure illustrated in section 6.2.1, values of adjusted parameters are presented in section 6.2.3.

6.2.3 Fitted Parameters

The parameters required by the UNIQUAC equation for modeling the H_2S-MDEA-H_2O and H_2S-CH_4-MDEA-H_2O system include volume parameter, r, surface parameter, q, for the components present in the liquid phase and the binary interaction parameters representing energies of interaction between liquid phase species. Model parameters were adjusted to the evaluated data base. In

following section the adjusted values for the parameters involved in H_2S-MDEA-H_2O and CH_4-H_2O system (required for predicting the behavior of H_2S-CH_4-MDEA-H_2O system) are presented.

6.2.3.1 H_2S-MDEA-H_2O System

This section illustrates the proposed equations to correlate H_2S solubility in aqueous MDEA solution. Modeling the behavior of such a system is rather complex as chemical and physical equilibria are coupled. To perform thermodynamic modeling of this system rigorously, both physical and chemical equilibrium should be taken into account.

Physical Equilibrium

As it was mentioned, physical equilibrium should be included in equilibrium representation of the system. Dissolution of gaseous H_2S into the solution and vaporization of liquid MDEA and water creates the following vapor-liquid equilibria equations:

$$H_2S(aq) \leftrightarrow H_2S\,(g) \tag{6-2}$$

$$H_2O\,(l) \leftrightarrow H_2O\,(g) \tag{6-3}$$

$$MDEA(aq) \leftrightarrow MDEA\,(g) \tag{6-4}$$

Chemical Equilibrium

Dissolution of H_2S in the aqueous MDEA solution is accompanied with different acidic and basic reactions which are listed below. “Due to chemical reactions in the solution hydrogen sulfide is dissolved in the liquid phase not only in neutral, but also in nonvolatile, ionic form (Kuranov et al. 1996).”

Ionization of water: $H_2O\,(l) \leftrightarrow OH^-\,(aq) + H^+(aq)$ (6-5)

Hydrogen sulfide dissociation: $H_2S\,(aq) \leftrightarrow H^+(aq) + HS^-(aq)$ (6-6)

Bisulfide ion dissociation: $HS^-\,(aq) \leftrightarrow H^+(aq) + S^{2-}(aq)$ (6-7)

Protonation of MDEA: Equation (5-8)

S^{2-} concentration is very small in the solution since dissociation constant for equation (6-7) is three to four orders of magnitude smaller than the dissociation constant for equation (6-6) (Li and Furst 2000). Ideal solution calculations also show the concentration of sulfide ion is extremely low.

Owing to the extremely low concentration of S^{2-} in the aqueous phase, its presence in the aqueous phase is neglected; hence reaction (6-7) is disregarded. This realistic assumption yields to reduce the number of adjustable interaction parameters. Table 6-2 and Table 6-4 represent parameters that have been determined in this work for modeling behavior of H_2S-MDEA-H_2O system. Table 6-2 shows determined UNIQUAC r and q parameters for H_2S and HS^-. Values for MDEA, $MDEAH^+$, H_2O, OH^- and H^+ are tabulated in Table 5-2.

Table 6-2. UNIQUAC volume parameter (r) and surface area parameter (q). Bold parameters are obtained in this work.

Species	r	q
H_2S	**0.64453**	**0.11014**
HS^-	**9.9317**	**15.031**

Table 6-3 and Table 6-4 list u_{ij}^0 and u_{ij}^T parameters determined for calculating UNIQUAC binary interaction energy parameters for the named pairs, respectively. For the pairs that are less probable to coexist in the mixture u_{ij}^0 and u_{ij}^T values has been set to a large value and zero, respectively. These assigned values eliminate the effect of these parameters over other parameters.

Table 6-3. $u_{ij}^0 = u_{ji}^0$ Parameters for calculating UNIQUAC interaction energy parameters. Values in bold are obtained in this work.

Species	H_2O	H_2S	MDEA	OH^-	H^+	HS^-	$MDEAH^+$
H_2O	Table 5-3						
H_2S	**-183.341**	**-1499.484**					
MDEA	Table 5-3	**10^{10}**	Table 5-3				
OH^-	Table 5-3	**10^{10}**	Table 5-3	Table 5-3			
H^+	Table 5-3	**10^{10}**	Table 5-3	Table 5-3	Table 5-3		
HS^-	**113.5498**	**10^{10}**	**-216.2905**	**10^{10}**	**10^{10}**	**58.7296**	
$MDEAH^+$	Table 5-3	**10^{10}**	Table 5-3	Table 5-3	Table 5-3	**-51.41282**	Table 5-3

Table 6-4. $u_{ij}^T = u_{ji}^T$ Parameters for calculating UNIQUAC interaction energy parameters. Values in bold are obtained in this work.

Species	H_2O	H_2S	MDEA	OH^-	H^+	HS^-	$MDEAH^+$
H_2O	Table 5-4						
H_2S	**-5.8785**	**-31.563**					
MDEA	Table 5-4	**0**	Table 5-4				
OH^-	Table 5-4	**0**	Table 5-4	Table 5-4			
H^+	Table 5-4	**0**	Table 5-4	Table 5-4	Table 5-4		
HS^-	**-0.76892**	**0**	**-0.1475**	**0**	**0**	**-0.93466**	
$MDEAH^+$	Table 5-4	**0**	Table 5-4	Table 5-4	Table 5-4	**-4.993**	Table 5-4

Values of standard state heat capacity of species present in the aqueous phase and gas phase are presented in Table 6-5 and Table 6-6, respectively. Values for H_2O (l), OH^- (aq), H^+ (aq), MDEA (aq), $MDEAH^+$ (aq) are tabulated in Table 5-5. Values for MDEA (g) and H_2O (g) are presented in Table 5-6.

Table 6-5. Standard state heat capacity parameters for species in aqueous phase, C_{pi}^0 (J $mol^{-1}K^{-1}$).

Species	a (J mol^{-1} K^{-1})	b (J mol^{-1} K^{-2})	c (J mol^{-1})
H_2S (aq)	110[b]	0[b]	0[b]
HS^- (aq)	-94[a]	0[a]	0[a]

[a] (Marcus 1997)

[b](Lindholdt 2008)

Table 6-6. Standard state heat capacities of species in the gas phase C_{pi}^0 (J $mol^{-1}K^{-1}$)

Species	C_{pi}^0 (J mol^{-1} K^{-1})
H_2S(g)	34.23[a]

[a] (NIST)

Values of standard state Gibbs free energy of formation (G_f^0) and standard state Enthalpy of formation (H_f^0) are presented in Table 6-7. Values for H_2O (l), H_2O (g), OH^- (aq), H^+ (aq), MDEA (aq), MDEA (g), $MDEAH^+$ (aq) are tabulated in Table 5-7.

Table 6-7. Standard state properties G_f^0 and H_f^0 in (kJ mol^{-1}) at T = 25 °C

Species	G_f^0(kJ mol^{-1})	H_f^0(kJ mol^{-1})
H_2S(aq)	-27.83[a]	-39.7[a]
HS^- (aq)	12.08[a]	-17.6[a]
H_2S(g)	-33.56[a]	-20.63[a]

[a] (NIST)

6.2.3.2 CH_4-H_2O System (Required for predictions of H_2S-CH_4-MDEA-H_2O System)

Methane dissolved only physically in the water. Therefore it is important to take the vapor-liquid equilibrium for the dissolved methane into account:

$$CH_4(g) \leftrightarrow CH_4(aq) \tag{6-8}$$

To model the CH_4-H_2O system, binary interaction parameter between CH_4 and H_2O has been fitted to the binary VLE data of CH_4-H_2O while r and q parameters for methane are taken from (Addicks

2002). Table 6-9 and Table 6-9 show r and q parameters for CH_4 and adjusted parameters required for calculation of binary interaction parameter between CH_4 and H_2O, respectively.

Table 6-8. UNIQUAC volume parameter (r) and surface area parameter (q)

Species	r	q
CH_4	5*	5*

*(Addicks 2002)

Table 6-9. $u_{ij}^0 = u_{ij}^0$ and $u_{ij}^T = u_{ij}^T$ parameters required for calculating UNIQUAC energy interaction parameters. Values are determined in this work.

Interaction parameter	u_{ij}^0	u_{ij}^T
CH_4-H_2O	44.16483	1.4836

Values of standard state heat capacity of methane in the aqueous phase and gas phase are reported in Table 6-10.

Table 6-10. Standard state heat capacity parameters for species in aqueous and gas phase, C_{pi}^0 (J mol^{-1}K^{-1}).

Species	a (J mol^{-1} K^{-1})	b (J mol^{-1} K^{-2})	c (J mol^{-1})
$CH_4(aq)$	0*	0*	0*
$CH_4(g)$	35.309[a]	0	0

[a] (NIST)

*The author was not able to find the value for heat capacity of $CH_4(aq)$ in open literature and open data bases. To proceed with the modeling study, heat capacity of dissolved methane in aqueous phase was assigned to zero. This is a reasonable approximation since methane is almost insoluble in water (solubility is very low).

Values of standard state Gibbs free energy of formation (G_f^0) and standard state Enthalpy of formation (H_f^0) for methane are presented in Table 6-11.

Table 6-11. Standard state properties G_f^0 and H_f^0 in (kJ mol^{-1}) at T = 25 °C

Species	G_f^0(kJ mol^{-1})	H_f^0(kJ mol^{-1})
$CH_4(aq)$	-34.33[a]	-89.04[a]
$CH_4(g)$	-50.72[a]	-74.81[a]

[a] (NIST)

6.3 H_2S-MDEA-H_2O ternary system

Modeling of H_2S-MDEA-H_2O ternary system was initiated by creating a strong model for binary H_2S-H_2O system. A model for H_2S-MDEA-H_2O is then developed based on combination of parameters of H_2S-H_2O and MDEA-H_2O systems and by adjusting additional parameters associated with the ternary system to the ternary data. Model parameters required for representing behavior of H_2S-MDEA-H_2O system were adjusted to totally 1143 data points. Regression data base consists of pure H_2S vapor pressure, VLE data of H_2S-H_2O binary system, VLE and heat of absorption data of H_2S-MDEA-H_2O ternary system. This section addresses regression data base and modeling results for Pure H_2S, H_2S-H_2O and H_2S-MDEA-H_2O systems.

6.3.1 Pure H_2S Vapor Pressure Data and Modeling Results

Table 6-12 provides an overview over experimental pure H_2S vapor pressure data used for parameter optimization, model deviations are also shown in this table. Totally 64 pure H_2S vapor pressure data points have been used for fitting model parameters. As previously explained, modeling H_2S-MDEA-H_2O ternary system starts with creating a model for H_2S-H_2O binary subsystem. Pure H_2S vapor pressure data and VLE data of binary H_2S-H_2O were utilized to adjust model parameters for H_2S-H_2O binary system.

Table 6-12. Regression results for H_2S pure vapor pressure

Temperature, °C	Reference	Number of Data Points	AARD%
4.44 to 100.39	(Reamer et al. 1950)	9	0.98
0 to 96.85	(West 1948)	19	1.04
0 to 100.4	(Cardoso 1921)	16	0.72
-28.51 to 29.98	(Clarke and Glew 1970)	20	0.39

Figure 6-1 shows a comparison between calculated and experimental H_2S pure vapor pressure data. Overall, all the calculation results of the model for pure H_2S vapor pressure are within an AARD of 0.78 % . As expected H_2S vapor pressure increases with increasing temperature.

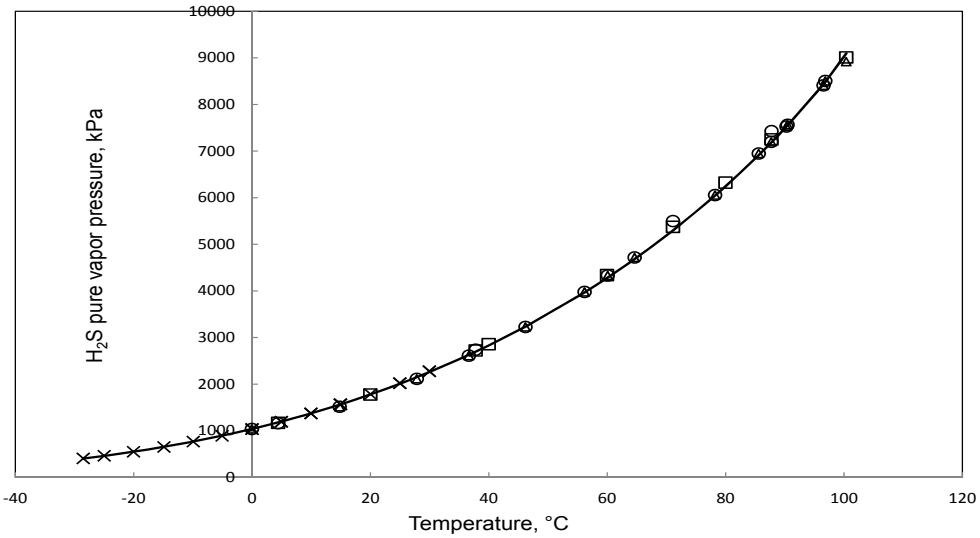

Figure 6-1. Comparison between calculated and experimental pure H_2S vapor pressure. Symbols stand for the experimental data and curve (line) refers to the calculated values using the developed thermodynamic model.○**,**(West 1948)**;** Δ**,** (Cardoso 1921)**;** □**,** (Reamer et al. 1950)**;** ×**,** (Clarke and Glew 1970)

6.3.2 Binary H_2S-H_2O Data and Modeling Results

In addition to pure H_2S vapor pressure data, 496 binary H_2S-H_2O data points have been regressed to obtain the UNIQUAC parameters required to model H_2S-H_2O binary system. Total pressure and H_2S partial pressure data were used to determine model parameters. Table 6-13 shows H_2S-H_2O binary data used for model parameters adjustment. Evaluation analysis over these data and other data sources listed in Table 6-13 shows that regressed binary data are fairly accurate and in agreement with each other. For example, (Kuranov et al. 1996) compares their data with (Lee and Mather 1977) data; their comparison showed that relative deviation in total pressure is below 3 %.

Table 6-13. Overview over binary H_2S-H_2O data

H_2S Concentration, wt%	T, °C	P, kPa	Data Type	Reference	Number of Data Points	AARD%
0.81 to 6.43	25.01 to 65.19	483 to 3475 (P_{Total})	VLE	(Chapoy et al. 2005)	30	3.74
0.06 to 7.20	10 to 180	154.8 to 6670.4 (P_{Total})	VLE	(Lee and Mather 1977)	325	4.50
0.82 to 7.51	37.77 to 148.88	344.73 to 3102.64 (P_{Total})	VLE	(Gillespie and Wilson 1982)	11	5.18
1.12 to 5.53	40	470.4 to 2489.5 (P_{Total})	VLE	(Kuranov et al. 1996)	9	1.89
0.09 to 0.57	0 to 50	46.76 to 96.29 (P_{Total})	VLE	(Clarke and Glew 1971)	36	2.02
0.12 to 1.40	5 to 60	35.73 to 474.36 (P_{H_2S})	VLE	(Wright. and Maass 1932)	52	3.56
0.54 to 8.41	37.77 to 171.11	548.96 to 8329.71 (P_{H_2S})	VLE	(Selleck et al. 1952)	33	5.18

6.3.2.1 Total pressure data

Model parameters have been regressed to 411 total pressure data of binary mixture of H_2S-H_2O and results of fit are shown in Figure 6-2. Figure 6-3 shows the magnified portion of Figure 6-2 in the low pressure range.

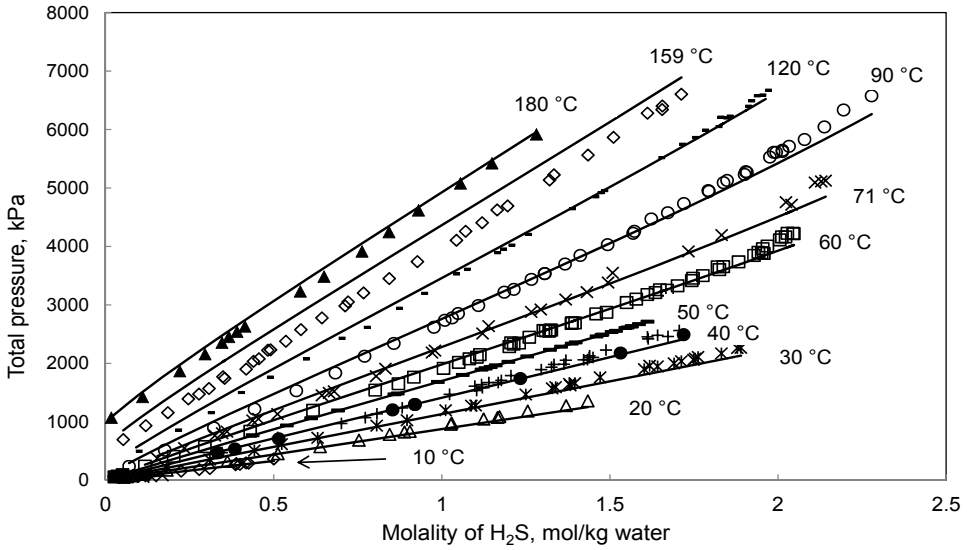

Figure 6-2. Comparison between experimental and fitted results for total pressure of H_2S-H_2O solutions. Symbols stand for the experimental data and curves (lines) refer to the calculated values using the developed thermodynamic model. ○ (T = 0 °C), ♦ (T = 10 °C), ▲ (T = 20 °C), * (T = 30 °C), + (T = 40 °C), - (T = 50 °C), (Clarke and Glew 1971)**; ● (T = 40 °C),** (Kuranov et al. 1996)**; ◊ (T = 10 °C), Δ (T = 20 °C), * (T = 30 °C), + (T = 40 °C), ■ (T = 50 °C), □ (T = 60 °C), × (T = 71 °C), ○ (T = 90 °C), - (T = 120 °C), ◊ (T = 159 °C), ▲ (T = 180 °C),** (Lee and Mather 1977)

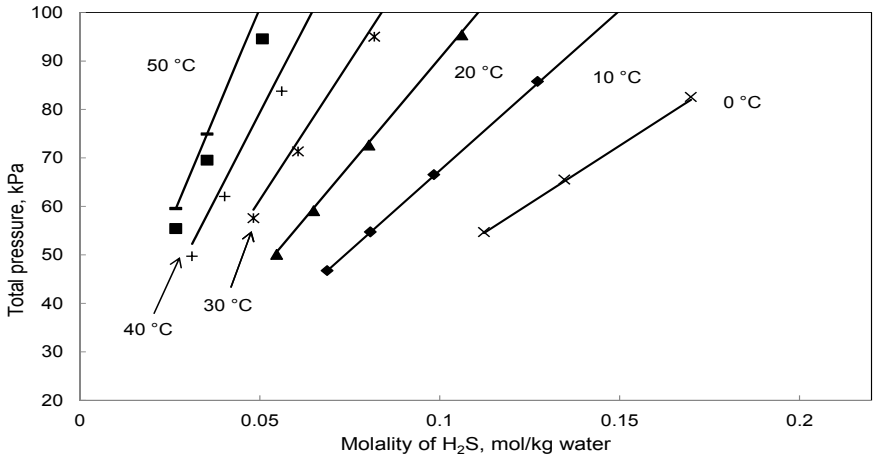

Figure 6-3. Magnified portion of Figure 6-2 in low pressure region. Symbols stand for the experimental data and curves (lines) refer to the calculated values using the developed thermodynamic model. ○ (T = 0 °C), ♦ (T = 10 °C), ▲ (T = 20 °C), * (T = 30 °C), + (T = 40 °C), ■ (T = 50 °C), (Clarke and Glew 1971)**; - (T = 50 °C),** (Lee and Mather 1977)

H_2S is in gaseous phase at the studied conditions, hence, has much higher pressure than water vapor. Thus, total pressure of binary H_2S-H_2O mixture is governed by H_2S pressure. This explains the almost linear increase of total pressure by increase of H_2S concentration (Figure 6-2). The model represents total pressure of H_2S-H_2O subsystem with an average absolute relative deviation of 3.46 %.

6.3.2.2 H_2S Partial Pressure Data

Model parameters have been adjusted to H_2S partial pressure data of (Wright. and Maass 1932) and (Selleck et al. 1952). Figure 6-4 compares model results to regressed data set of (Wright. and Maass 1932).

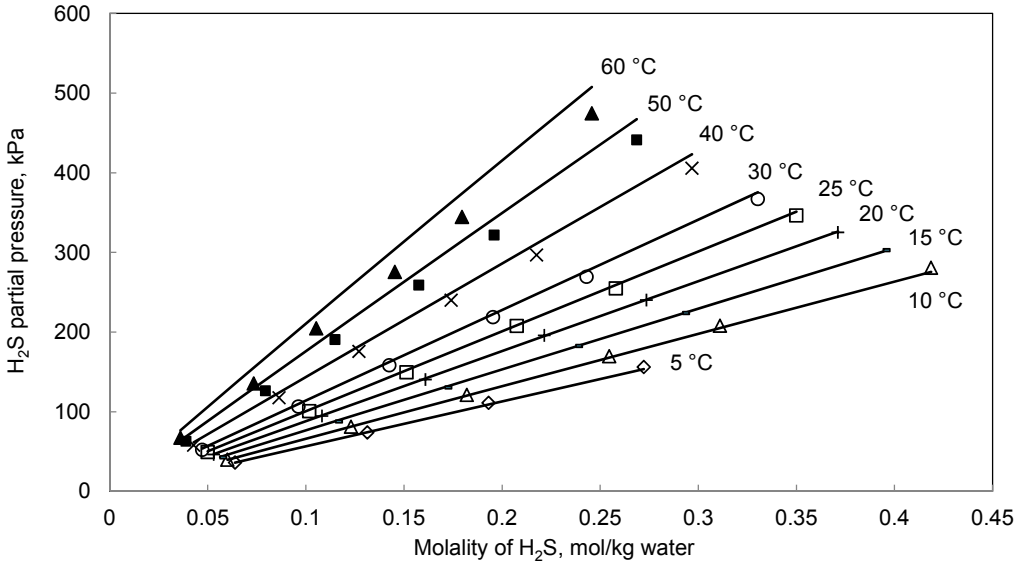

Figure 6-4. Comparison between experimental and fitted results for H_2Ssolubility in water. Symbols stand for the experimental data and curves (lines) refer to the calculated values using the developed thermodynamic model. ◊ (T = 5 °C), Δ (T = 10 °C), - (T = 15 °C), + (T = 20 °C), □ (T = 25 °C), ○(T = 30 °C),×(T = 40 °C), ■(T = 50 °C),▲(T = 60 °C), (Wright. and Maass 1932)

Figure 6-5 is a parity plot for H_2S partial pressure over binary mixture of hydrogen sulfide and water. The figure plots model calculated results against regressed experimental data points; the

trend line curve has the slope of 0.96 which shows how well the model can represent H_2S solubility in water.

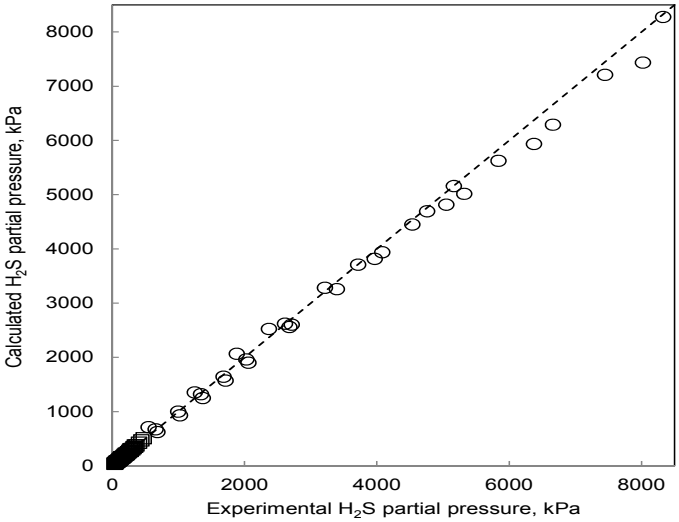

Figure 6-5. Parity plot for H_2S partial pressure over H_2S-H_2O mixture. ○,(Selleck et al. 1952); □, (Wright. and Maass 1932)

Overall the model represents H_2S partial pressure over binary mixture of H_2S and H_2O within 8.74 AARD%.

Model parameters for binary H_2S-H_2O system are valid in the temperature range of 0 to 180℃, the H_2S partial pressure range of 35 to 8330 kPa and H_2S mass% of 0 to 8.4. The developed model represents all kinds of used binary data within AARD% of 3.

6.3.3 Ternary H_2S-MDEA-H_2O Data and Modeling Results

Modeling results for H_2S-H_2O subsystem were described in previous section. In this section, modeling results for H_2S-MDEA-H_2O ternary system are presented. The model is created based on combination of the parameters for H_2S-H_2O and MDEA-H_2O systems and from adjusting parameters associated with the ternary system to the ternary experimental data. Model parameters

are determined by regressing total pressure, H_2S solubility (H_2S partial pressure) and H_2S heat of absorption data. Totally 583 data points are used. Table 6-14 presents a summary of the regressed data.

Table 6-14. Overview on ternary, H_2S-MDEA-H_2O, data used for parameter adjustment and regression results

MDEA Concentration, wt%	T, °C	P, kPa	Data Type	Reference	Number of Data Points	AARD%
18.68, 32.20	40 to 140	165.2 to 4895.9 (P_{Total})	VLE	(Kuranov et al. 1996)	71	3.83
48.80	40, 80, 120	147.9 to 2783 (P_{Total})	VLE	(Kamps et al. 2001)	26	6.87
11.82, 19.99	25 to 115.5	13.23 to 1536.6 (P_{H_2S})	VLE	(Maddox et al. 1987)	47	10
23.10, 49.99	40 to 120	0.0033 to 3673 (P_{H_2S})	VLE	(Huang and Ng 1998)	42	20
11.82, 23.6	25, 40	0.04 to 1.091 (P_{H_2S})	VLE	(Lemoine et al. 2000)	29	26
11.35, 21.63, 33.88	26.65 to 126.65	87 to 1121 (P_{Total})	H_{abs}	(Oscarson and lzatt 1990)	368	12

6.3.3.1 Total Pressure Data

Total pressure data of two sources, (Kuranov et al. 1996) and (Kamps et al. 2001) are used for adjusting interaction parameters in the ternary system. Figure 6-6, shows total pressure of H_2S-MDEA-H_2O mixtures for two different MDEA concentration, 32.20 and 48.80 wt% MDEA at 40 and 120 °C.

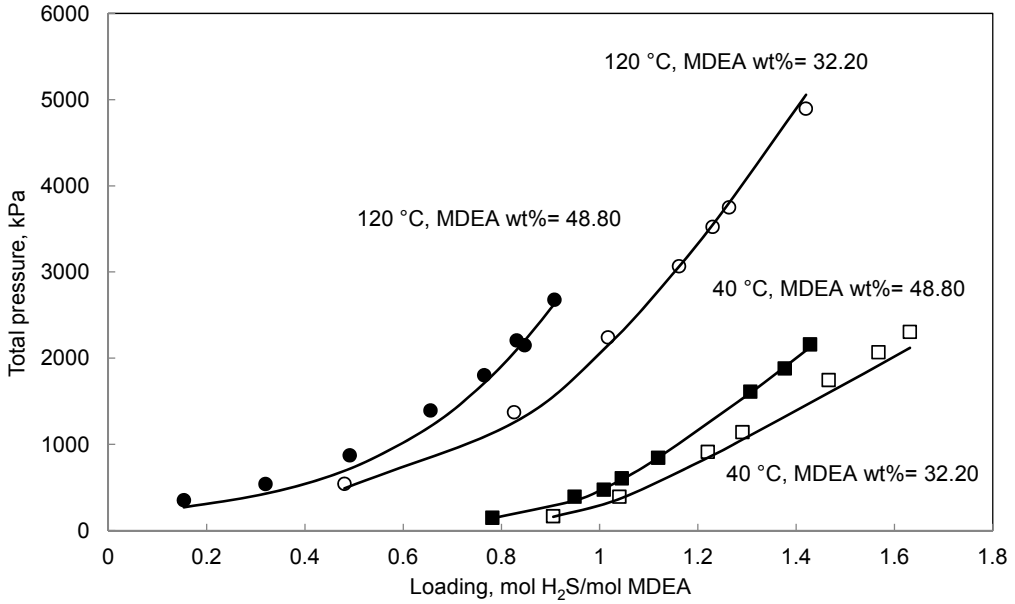

Figure 6-6. Comparison between experimental and fitted results for total pressure of H_2S-MDEA-H_2O solutions for 32.20 and 48.80 wt% MDEA and at 40 and 120 °C. Symbols stand for the experimental data and curves (lines) refer to the calculated values using the developed thermodynamic model. □ (T = 40 °C, MDEA wt% = 32.20), ○ **(T = 120 °C MDEA, wt% = 32.20),** (Kuranov et al. 1996)**; ■ (T = 40 °C, MDEA wt% = 48.80), ● (T = 120 °C, MDEA wt% = 48.80),** (Kamps et al. 2001)

Figure 6-7 exhibits effect of temperature on the absorption capacity for 18.68 wt% MDEA. It shows that at a fixed pressure and amine concentration, by decrease of temperature absorption capacity increases. Following basic thermodynamics, for exothermic reactions lowering the temperature would cause the equilibrium shift towards heat generation. The reaction between acid gas and aqueous alkanolamine is exothermic, reducing temperature, brings about absorption of more acid gas in the aqueous phase in forms of ionic nonvolatile species.

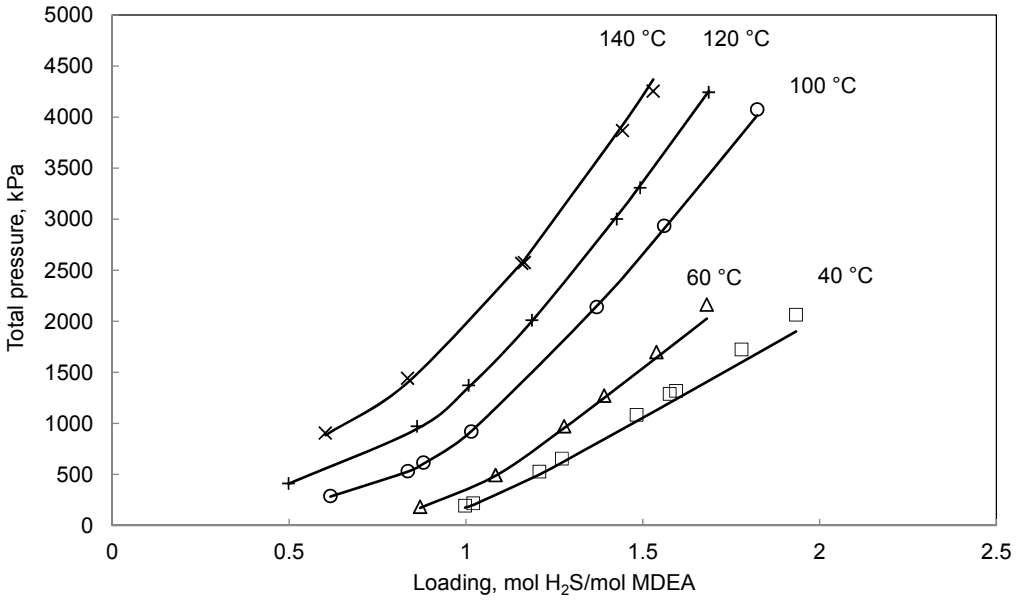

Figure 6-7. Results of fit for total pressure of H_2S-MDEA-H_2O solutions for 18.68 wt% MDEA solvent. Symbols stand for the experimental data and curves (lines) refer to the calculated values using the developed thermodynamic model. □ (T = 40 °C), Δ (T = 60 °C),),○ (T = 100 °C), + (T = 120 °C),× (T = 140 °C), (Kuranov et al. 1996)

Altogether, the model developed model fits the total pressure data of H_2S-MDEA-H_2O solutions within 5.35 AARD%.

6.3.3.2 H_2S Solubility Data

The available data for H_2S solubility in aqueous MDEA solution are not abundant in the open literature and more importantly, there are discrepancies between different sources. Hence it is of high importance to evaluate the data before regression. For the H_2S partial pressure, three data sets were regressed to obtain Extended UNIQUAC parameters. 118 data points of H_2S partial pressure were regressed. Results of fit for 19.99 and 49.99 wt% MDEA at different temperatures span from 37.8 to 120 °C are shown in Figure 6-8 and Figure 6-9, respectively. Figure 6-10, shows the modeling results for H_2S solubility in low loading region.

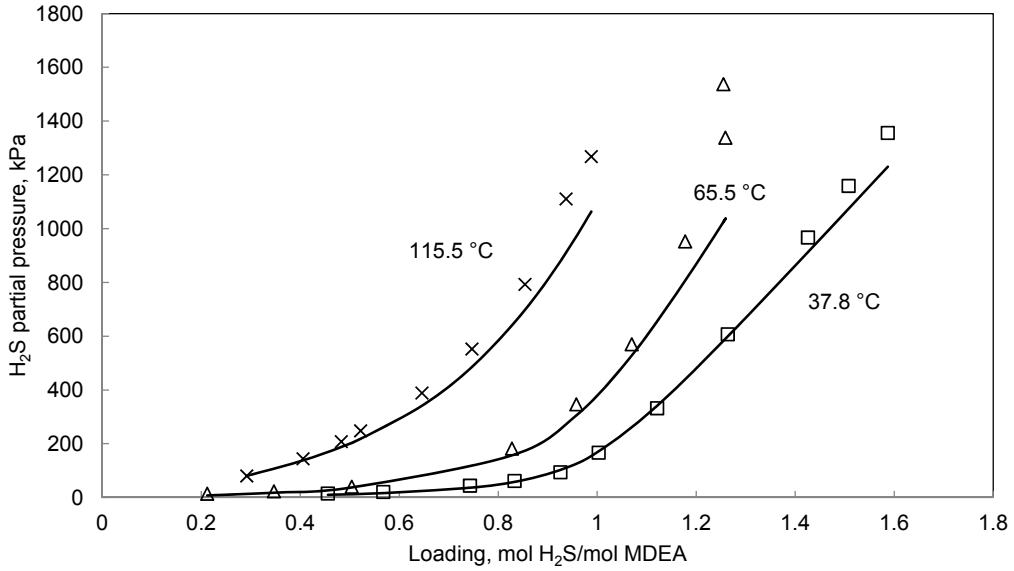

Figure 6-8. Comparison between experimental and regressed H_2S solubility in 19.99 wt% aqueous MDEA solutions and at different temperatures. Symbols stand for the experimental data and curves (lines) refers to the represented values using the developed thermodynamic model. □, (T=37.8 °C), Δ, (T=65.5 °C),×, (T=115.5 °C), (Maddox et al. 1987)

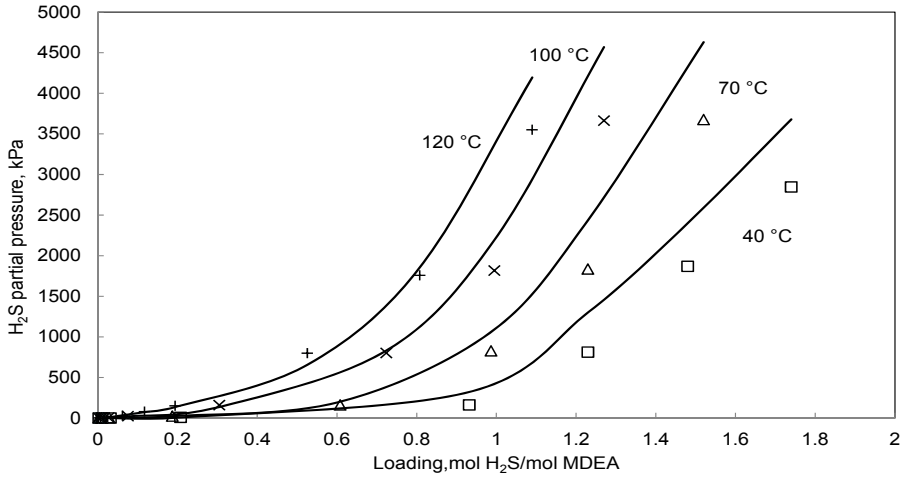

Figure 6-9. Comparison between experimental and regressed H_2S solubility in 49.99 wt% aqueous MDEA solutions and at different temperatures. Symbols stand for the experimental data and curves (lines) refers to the represented values using the developed thermodynamic model. □, (T=40°C), Δ, (T=70°C), ×, (T=100 °C), + (T=120 °C), (Huang and Ng 1998)

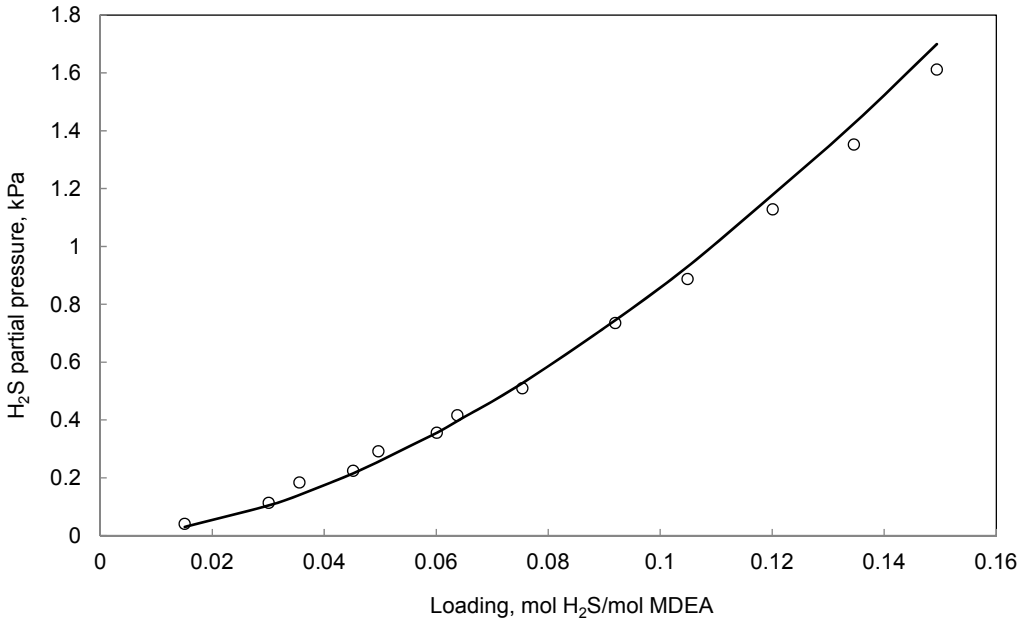

Figure 6-10. Comparison between experimental and predicted H_2S solubility in 23.6 wt% aqueous MDEA solutions and at 40 °C. Symbols stand for the experimental data and curves (lines) refers to the represented values using the developed thermodynamic model. ○**,** (Lemoine et al. 2000)

As it can be seen from the Figure 6-8 to Figure 6-10, results of fit well agree with the expermental data points. Altogether model calculates H_2S partial pressure over aqueous MDEA mixture within 18% AARD.

Four data sets for H_2S-MDEA-H_2O mixtures were excluded from regression data: (Macgregor and Mather 1991) , (Li and Shen 1993), (Jou et al. 1993) and (Jou et al. 1982). Data of (Macgregor and Mather 1991) and (Li and Shen 1993) show rather large deviation from the optimized model, AARD% of 45 and 70. Figure 6-11 shows a comparison between the data provided by (Macgregor and Mather 1991), (Huang and Ng 1998) and (Lemoine et al. 2000). Evidently the former has a trend different from the latter two. Figure 6-12 (a) and (b), are the parity plots that show a comparison between model the model calculated results, all the regressed data and data provided by (Li and Shen 1993). As it can be seen, there is a large deviation between data of (Li and Shen 1993), the model and other regressed data sources, both at high and low pressure. It is noted that, (Posey and Rochelle 1997) have also reported the deviation of these two sources from other ones

and postulated that the error in the reported H_2S partial pressure may be due to H_2S adsorption onto the walls of equilibrium cell or analytical devices.

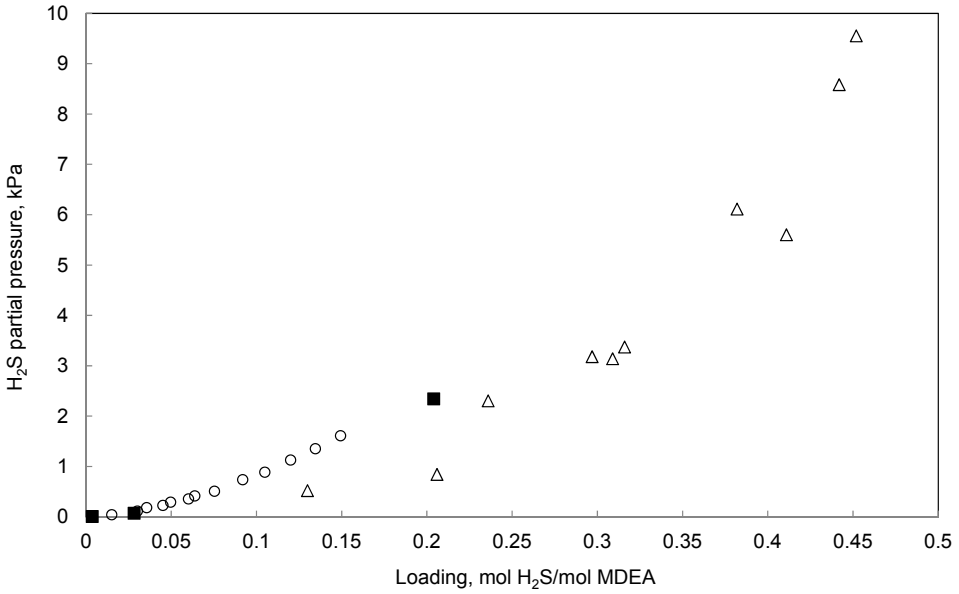

Figure 6-11. Comparison between experimental H_2S solubility in 23 wt% MDEA and at 40 °C. ○, (Lemoine et al. 2000); ■, (Huang and Ng 1998); Δ, (Macgregor and Mather 1991)

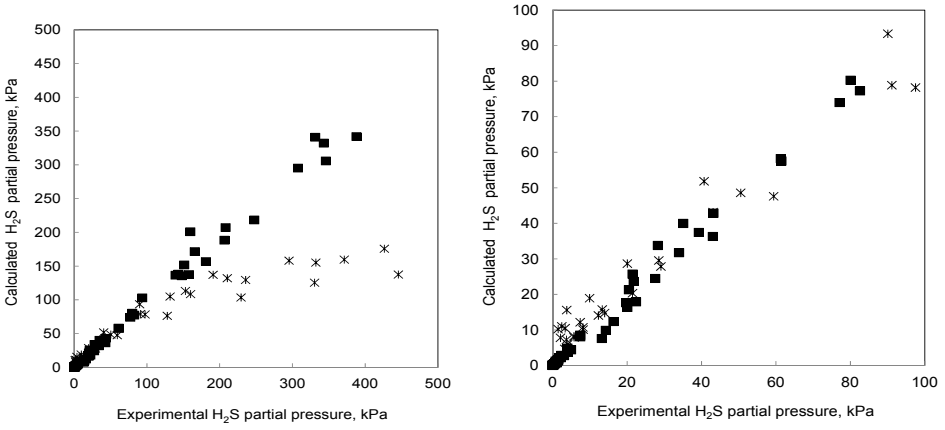

(a) **(b)**

Figure 6-12. (a) Parity plot for ternary mixture of H_2S-MDEA-H_2O. *, (Li and Shen 1993)**; ■, all the regressed H_2S partial pressure data listed in Table 6-14. (b) Low pressure region of (a) in higher magnification.**

The data provided by (Jou et al. 1982) and (Jou et al. 1993) were also omitted from regression data base due to the large deviation from the optimized model (AARD% of 82 and 66, respectively) and in accordance with the rest scientific community opinion ((Kamps et al. 2001), (Posey and Rochelle 1997), (Ter Maat et al. 2004), (Kuranov et al. 1996)) about questionable reliability of the mentioned data. Figure 6-13 shows the comparison between different data sources in low loading region from (Huang and Ng 1998), (Rogers et al. 1998), (Ter Maat et al. 2004) and (Jou et al. 1982). It is apparent that the first three are in agreement whereas (Jou et al. 1982) data deviates from the rest.

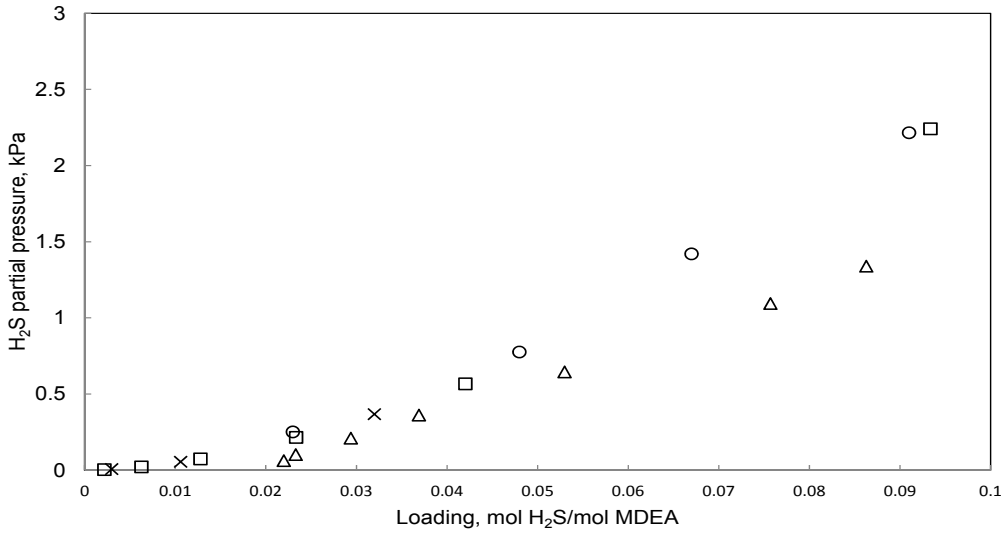

Figure 6-13. Comparison between H_2S partial pressure from different data sets at 40 °C and 50.02 wt% MDEA. □, (Rogers et al. 1998); Δ ,(Jou et al. 1982);○,(Ter Maat et al. 2004); ×, (Huang and Ng 1998)

6.3.3.3 Heat of Absorption Data and Modeling Results

368 data of heat of H_2S absorption into aqueous MDEA solution were fitted within an average absolute relative deviation of 12%. Regression results at 126.65 °C and 1121 kPa at 20, 35 and 50 wt% MDEA are demonstrated in Figure 6-14.

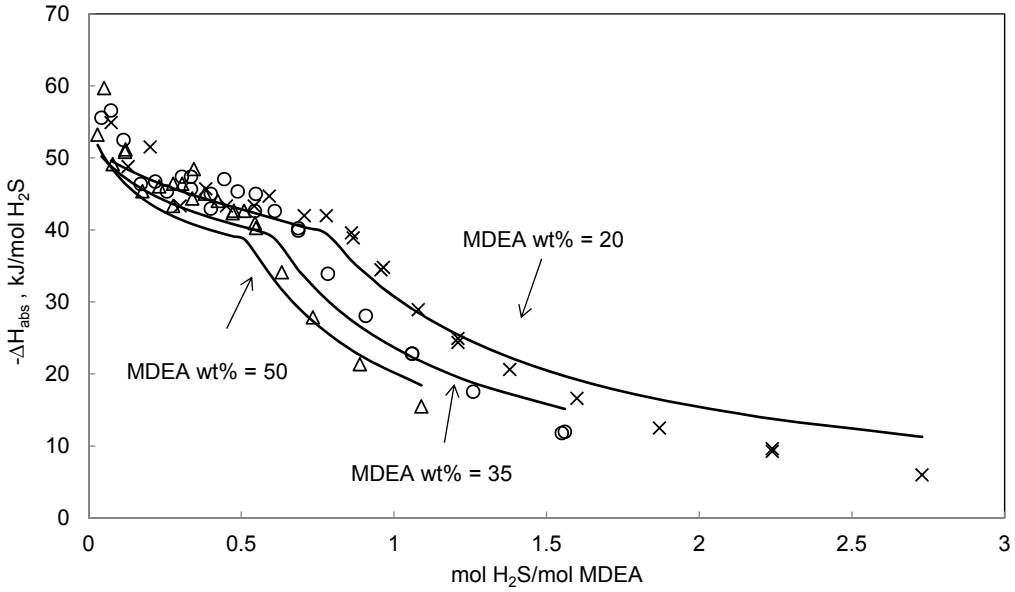

Figure 6-14. Comparison of the enthalpy of H_2S absorption at 126.65 °C and 1121 kPa and in 20, 35 and 50 wt% aqueous MDEA solutions. Symbols stand for the experimental data and curves (lines) refer to the represented values using the developed thermodynamic model. × (MDEA wt% = 20), ○ (MDEA wt% = 35), Δ (MDEA wt% = 50), (Oscarson and lzatt 1990)

As it is shown in Figure 6-14, the agreement between model and experiments are satisfactory. The developed model can describe the heat of H_2S absorption into aqueous MDEA solution quiet well. Altogether, results of fit show that developed models for H_2S-H_2O and H_2S-MDEA-H_2O systems consistently well represent thermodynamic and thermal properties of the binary and ternary systems.

Model parameters for ternary H_2S-MDEA-H_2O system are valid in the temperature range of 25 to 140 ℃, the H_2S partial pressure range of 0 to 4900 kPa, loading of 0.01 to 2.17 and MDEA mass% of 11 to 50. The developed model represents all kinds of used ternary data within AARD% of 13.

6.4 CH_4 System

This section will describe modeling results for absorption of H_2S and CO_2 into aqueous MDEA solutions for systems that have methane as a makeup gas. Before quaternary systems of H_2S-CH_4-MDEA-H_2O and CO_2-CH_4-MDEA-H_2O could be modeled, first CH_4-H_2O binary system has to be studied. Models for acid gas-methane-MDEA-water are developed by combining parameters of acid gas-MDEA-water and methane-water systems.

6.4.1 CH_4-H_2O System and Modeling Results

Methane is physically dissolved in water. The hydrocarbon solubility, i.e. methane, is an important parameter for the correct design of high pressure gas treating equipment. CH_4-H_2O binary interaction parameter is required to model CH_4-H_2O system. In addition to CH_4-H_2O interaction parameter, r and q parameter for CH_4 should be determined in order to model the CH_4-H_2O binary system. The value of the interaction parameter is determined by adjusting the interaction parameter to total pressure data of CH_4-H_2O system, r and q values are taken from (Addicks 2002). Values of adjusted parameters were shown in Table 6-9. Table 6-15 lists data sets upon which the CH_4-H_2O interaction parameter was adjusted. In what follows modeling results for total pressure data of CH_4-H_2O system have been shown.

Table 6-15. Review over binary CH_4-H_2O data used for regression

CH_4 Concentration, Molality	T ,°C	P, kPa	Data Type	Reference	Number of Data Points	AARD%
0.02 to 0.09	25, 50	3000 to 8000 (P_{Total})	VLE	(Yokoyama et al. 1988)	6	1.86
0.03 to 0.22	10, 20, 30	2000 to 40030 (P_{Total})	VLE	(Wang et al. 2003)	17	7.61
0.01 to 0.09	25, 41	993 to 9981(P_{Total})	VLE	(Awan et al. 2010)	8	5.06

Results of fit for total pressure of CH_4-H_2O binary system at 25 and 50 °C plotted in Figure 6-15.

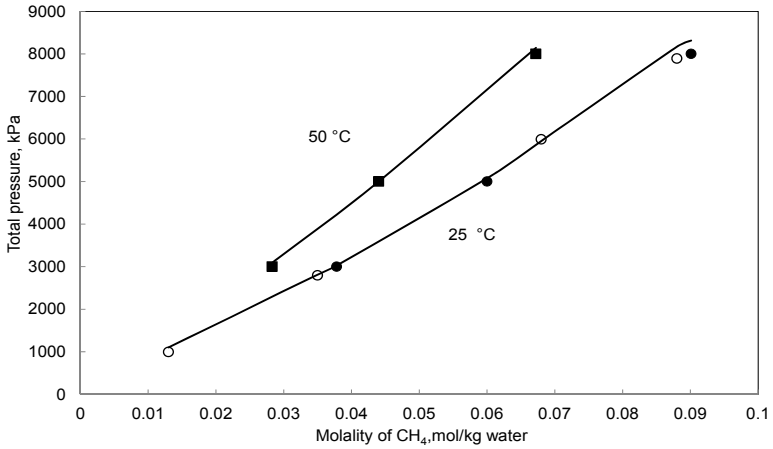

Figure 6-15. Comparison of measured total pressure of CH_4-H_2O solutions with the calculated values from model. Symbols stand for the experimental data and curves (lines) refer to the calculated values using the developed thermodynamic model.● (T = 25 °C), ■ (T = 50 °C), (Yokoyama et al. 1988)**; ○ (T = 25 °C),** (Awan et al. 2010)

Model parameters for binary CH_4-H_2O system are valid in the temperature range of 10 to 50℃, the total pressure range of 993 to 40030 kPa and CH_4 mass% of 0 to 0.35. The developed model represents all kinds of used binary data within AARD% of 4.

6.4.2 H_2S-CH_4-MDEA-H_2O System and prediction Results

In natural gas treatment process, typical absorber pressure is around 70 to 100 bar, whereas stripper pressure is between 1 to 2 bar. In the absorber, mixtures of acid gas-hydrocarbons (mainly methane) are contacted counter currently with mixtures of amine-water while in the stripper mixtures of acid gas-amine-water are present as methane is already separated. Therefore it is very important that the model adequately represents acid gas solubility at high pressures, where methane is present as a makeup gas. Also it is required to investigate the influence of methane on acid gas solubility.

Model parameters for acid gas-CH_4-MDEA-H_2O are obtained by combining parameters of acid gas-MDEA-H_2O and CH_4-H_2O systems. In this case, it is of high importance to find out whether additional interaction parameters of CH_4-MDEA and CH_4-$MDEA^+$ are necessary for modeling the behavior of acid gas-CH_4-MDEA-H_2O system or there is no need to add more adjustable parameters. Therefore, four regression cases are applied for modeling MDEA-CH_4-H_2O system. In each case the interaction parameter of the mentioned species are optimized: **(I)** only CH_4-H_2O; **(II)**

CH_4-H_2O and CH_4-MDEA; **(III)** CH_4-H_2O and CH_4-$MDEA^+$; **(IV)** all three CH_4-H_2O, CH_4-MDEA and CH_4-$MDEA^+$. It is noted that CH_4-MDEA and CH_4-$MDEA^+$ parameters were fitted to CH_4-MDEA-H_2O ternary data of (Jou et al. 1998). Comparing results of four regression cases demonstrates that by considering CH_4-H_2O interaction parameter and parameters of acid gas-MDEA-H_2O system, the model could satisfactorily describe the behavior of the quaternary system of acid gas-CH_4-MDEA-H_2O, and there is no need to add more adjustable parameters.

A model for H_2S-CH_4-MDEA-H_2O system is developed based on combination of parameters for CH_4-H_2O and H_2S-MDEA-H_2O systems. Figure 6-16 shows model predictions for (Ter Maat et al. 2004) data for 50 wt% MDEA and at temperature of 40 °C and total pressure of 350 kPa.

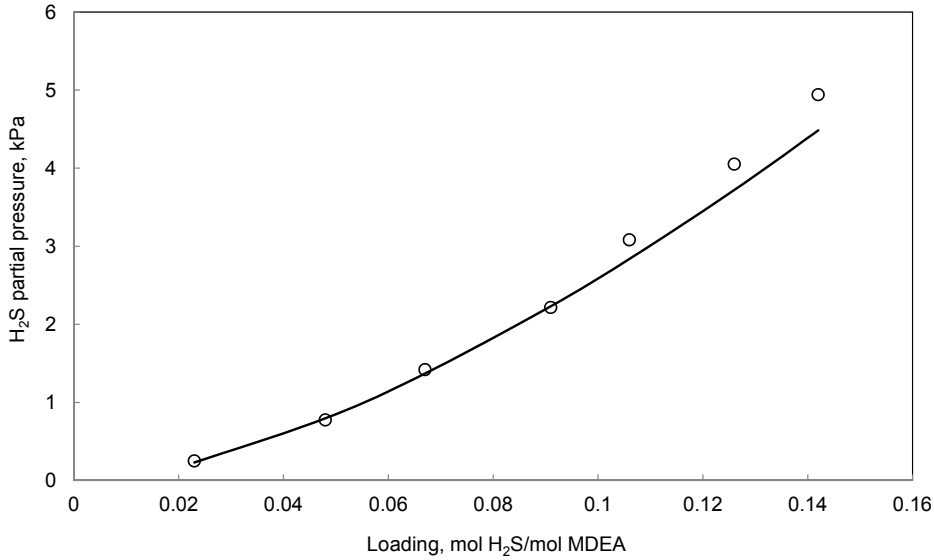

Figure 6-16. Comparison between experimental and calculated H_2S solubility in 50 wt% aqueous MDEA and at 40 °C and total pressure of 350 kPa with methane as a makeup gas. Symbols stand for the experimental data and curve (line) refers to the calculated values using the developed thermodynamic model. ○, (Ter Maat et al. 2004)

Figure 6-17 and Figure 6-18 depict model predictions at total pressures of 3450 and 6900 kPa. Figure 6-17 shows model predictions for data of (Huttenhuis et al. 2007) for 49.99 wt% MDEA, at temperature of 10 and 25 °C and at total pressure of 3450 kPa.

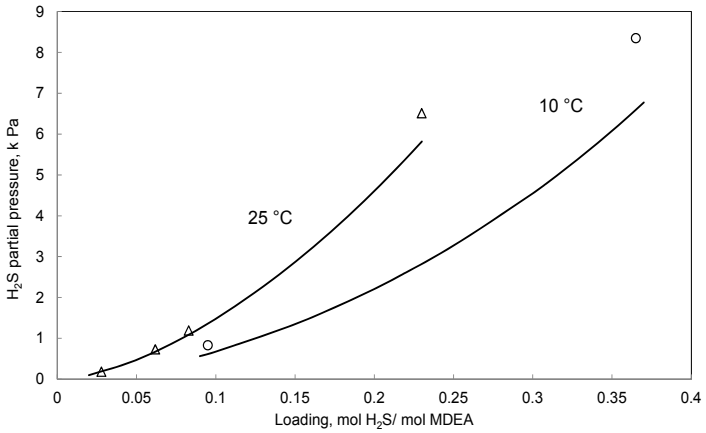

Figure 6-17. Comparison between experimental and predicted values for H_2S solubility in 49.99 wt% aqueous MDEA and at 10 and 25°C and total pressure of 3450 kPa with methane as a makeup gas. Symbols stand for the experimental data and curves (lines) refer to the calculated values using the developed thermodynamic model. ○, (T=10 °C), Δ, (T=25 °C), (Huttenhuis et al. 2007)

Figure 6-18 compares model predictions with data of (Huttenhuis et al. 2007) at total pressure of 6900 kPa which is a typical absorber pressure in natural gas treatment process.

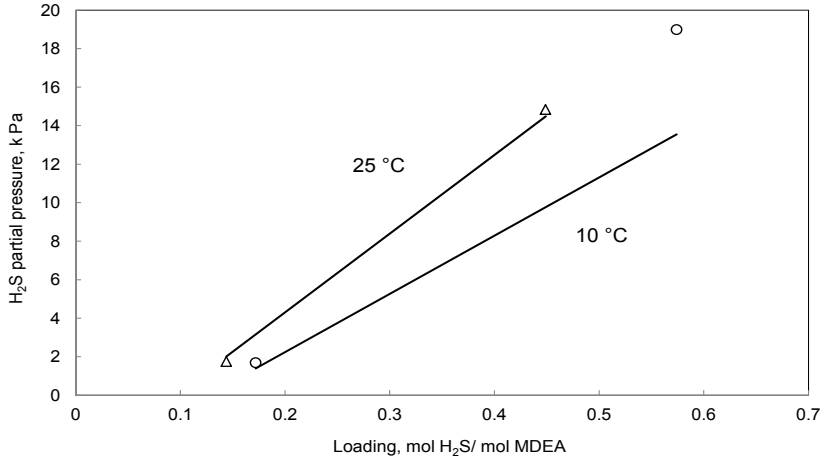

Figure 6-18. Comparison between model prediction results and experimental data for H_2S solubility in 34.99 wt% aqueous MDEA and at 10 and 25°C and total pressure of 6900 kPa with methane as a makeup gas. Symbols stand for the experimental data and curves (lines) refer to the calculated values using the developed thermodynamic model. ○, (T=10 °C), Δ, (T=25 °C), (Huttenhuis et al. 2007)

Table 6-16 shows deviations between model predictions and data for quaternary system of H_2S-CH_4-MDEA-H_2O.

Table 6-16. Prediction results for H_2S-CH_4-MDEA-H_2O system

MDEA Concentration, Wt%	T ,°C	Total Pressure, kPa	H_2S partial pressure (kPa)	Data Type	Reference	No. of Data Points	AARD%
50	50	499 to700	3 to 278	VLE (P_{H_2S})	(Dicko et al. 2010)	5	15
34.99, 49.99	10, 25	690, 3450, 6900	0.1 to 18	VLE (P_{H_2S})	(Huttenhuis et al. 2007)	30	15
50	40	350	0.2 to 4.9	VLE (P_{H_2S})	(Ter Maat et al. 2004)	7	5.76

Two data sources are used to validate the model predictions for quaternary H_2S-CH_4-MDEA-H_2O system. These data are in the temperature range of 10 to 50 ℃, H_2S partial pressure range of 0 to 278 kPa, total pressure up to 7000 kPa and MDEA mass% of 35 and 50. Further experiments are carried out in this study (cf. chapter 9) and it is shown that the model is valid up to temperature of 70 ℃ and H_2S partial pressure up to 1000 kPa.

All in all, in presence of methane, model predicts H_2S solubility in aqueous MDEA solutions within average absolute relative deviation of 11%.

6.4.3 CO_2-CH_4-MDEA-H_2O System and prediction Results

Model parameters for CO_2-CH_4-MDEA-H_2O system consist of parameters of CO_2-MDEA-H_2O and CH_4-H_2O systems. Table 6-17 shows prediction results for CO_2 solubility in mixtures of MDEA-H_2O in presence of methane as a makeup gas.

Table 6-17. Prediction results for CO_2-CH_4-MDEA-H_2O systems

MDEA Concentration, wt%	T ,°C	Total Pressure, kPa	CO_2 partial pressure (kPa)	Data Type	Reference	Number of Data Points	AARD%
30, 50	40, 80	10000, 15000, 20000	11 to 5066	VLE (P_{CO_2})	(Addicks et al. 2002)	31	21
50	50	1268 to 1558	6 to 434	VLE (P_{CO_2})	(Dicko et al. 2010)	5	30

Figure 6-19 plots predicted CO_2 partial pressure against loading at total pressure of 100 bar, where methane is present as a makeup gas.

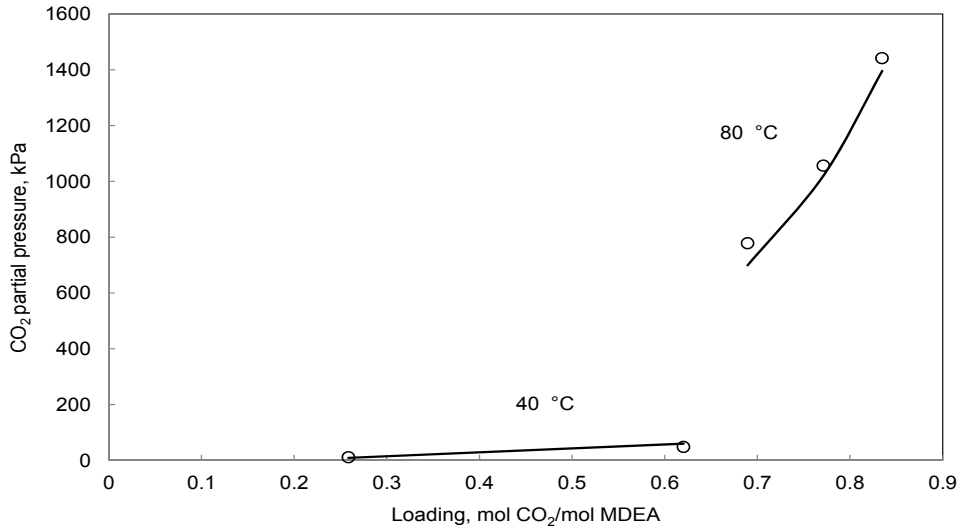

Figure 6-19. Comparison between model prediction results and experimental data for CO_2 solubility into 30 wt% aqueous MDEA and at 40 and 80°C and 10000 kPa with methane as a makeup gas. Symbols stand for the experimental data and curves (lines) refer to the calculated values using the developed thermodynamic model. ○**,** (Addicks et al. 2002)

Two data sources are used to validate the model predictions for quaternary CO_2-CH_4-MDEA-H_2O system. These data are in the temperature range of 40 to 80 ℃, CO_2 partial pressure range of 6 to 5066 kPa, total pressure up to 20000 kPa and MDEA mass% of 30 and 50.

Overall, in presence of methane, the developed model predict CO_2 solubility within 25 AARD%.

6.5 Effect of high pressure on Acid Gas Solubility

Acid gas solubility data are limited to low pressures, where there are no hydrocarbons or inert gases like nitrogen present in the system. Despite of this fact, in natural gas treatment industry typically hydrocarbons foremost methane is present in the absorber column and typical absorber pressure is high (70 to 100 bar). Therefore, it is crucial to investigate the high pressure effect (effect of methane) on acid gas solubility. To achieve this goal, literature data for H_2S-CH_4-MDEA-H_2O at different total pressures (methane partial pressure) were compared. Figure 6-20 shows H_2S partial

pressure as a function of methane partial pressure for a definite loading, temperature and MDEA concentration, experimental data points are taken from (Dicko et al. 2010). Figure 6-21 plots H_2S partial pressure as a function of methane partial pressure at different loadings (mole H_2S/mole MDEA); data are from (Huttenhuis et al. 2007). As it can be seen in the figures, at constant H_2S loading, H_2S partial pressure increases when system total pressure (or methane partial pressure) is increased. It is concluded that at constant H_2S loading, H_2S partial pressure increase with increasing total pressure. This conclusion is in an agreement with literature studies, (Huttenhuis et al. 2007), (Addicks et al. 2002) and (Dicko et al. 2010). Measurements of (Dicko et al. 2010) show that at loading of 0.74 and at 50 °C and for 50 wt% MDEA solution, a variation of approximately 6 MPa in the CH_4 partial pressure leads to a variation of 30 % in H_2S partial pressure. From Figure 6-21 it can be concluded that at 25 °C and in 50 wt% MDEA aqueous solution, an increase of 6 MPa in CH_4 partial pressure, causes about 40 % increase in H_2S partial pressure. Comparing H_2S partial pressure does not allow determining which phase (gas or liquid) is mainly affected by methane presence. Hence, further study is required to clarify whether the increase in H_2S partial pressure is the result of increasing system pressure in the gas phase or is due to dissolution of little amount of methane in the liquid phase (decrease in H_2S solubility).

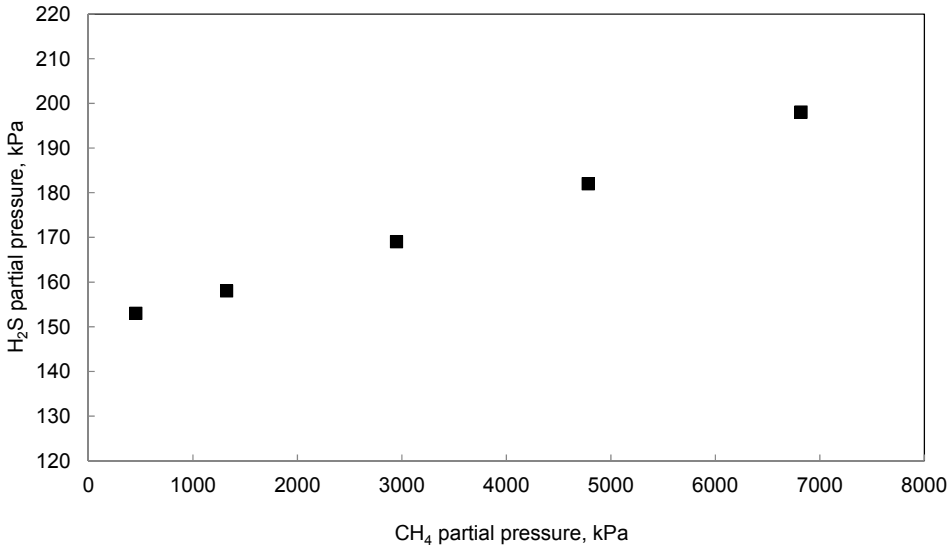

Figure 6-20. Experimental investigation on effect of high pressure methane on H_2S partial pressure over aqueous solution of 50 wt% MDEA at 50 °C and at loading (mole H_2S/mole MDEA) of 0.74. ■, (Dicko et al. 2010)**.**

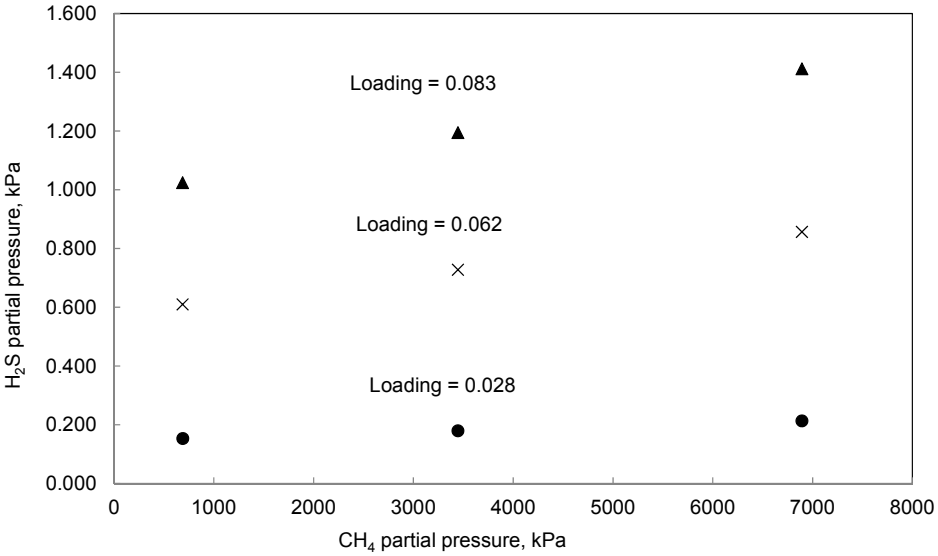

Figure 6-21. Experimental investigation on effect of high pressure methane on H_2S partial pressure over aqueous solution of 50 wt% MDEA at 25 °C and for three different loadings (mole H_2S/mole MDEA). ● (Loading = 0.028), × (Loading = 0.062), ▲ (Loading = 0.083), (Huttenhuis et al. 2007)

In order to assess the methane effect on acid gas equilibrium in liquid and gas phase, H_2S fugacity at low and high pressures should be compared. To investigate this, a gas mixture of H_2S and methane is considered (MDEA and water presence in the gas phase is neglected). It is knwon that at equilibrium H_2S fugacity in liquid and gas phase is the same. H_2S fugacity in the gas mixture of H_2S-CH_4 is calculated by SRK equation at the correspondence experimental conditions (temperature, total pressure, gas phase composition) to (Dicko et al. 2010) and (Huttenhuis et al. 2007). Figure 6-22 shows H_2S fugacity calculations for mixture of CH_4 and H_2S at temperature, total pressure and vapor phase composition similar to what is reported in (Dicko et al. 2010). Calculations are done using SRK EoS.

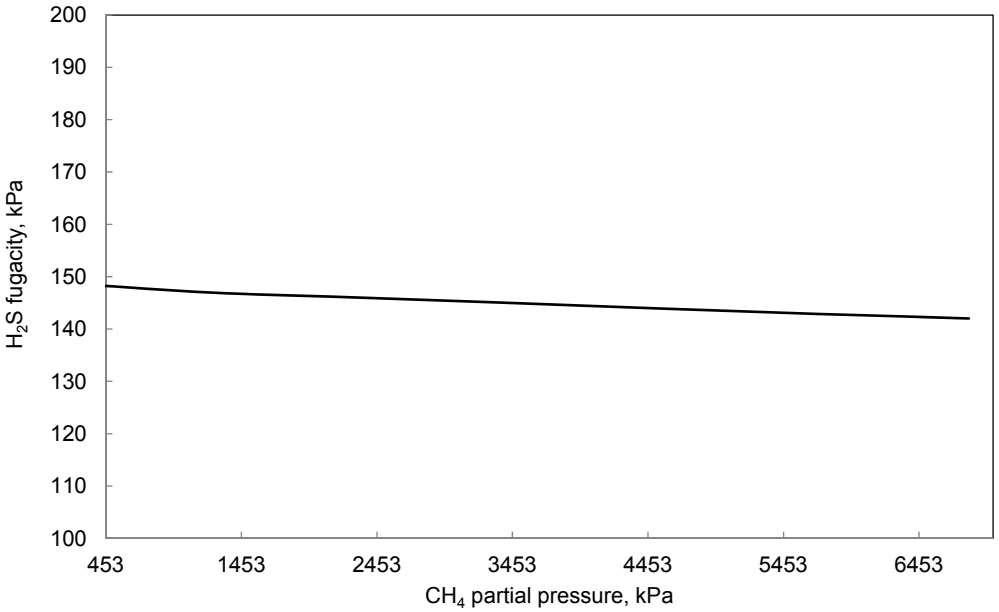

Figure 6-22. Modeling investigation on influence of methane partial pressure on H_2S fugacity for H_2S-CH_4 mixture at T, P_{Total}, y_i corresponds to Figure 6-20. Solid line, calculated H_2S fugacity using SRK EoS.

As it can be seen from Figure 6-22, H_2S fugacity is constant and equal to 1.45 ± 0.03 bar in the pressure range of 6 MPa, the result of calculations of this study is in agreement with the (Dicko et al. 2010). (Dicko et al. 2010) calculated H_2S fugacity with PR EoS, their calculations shows that H_2S fugacity is constant at 1.48 ± 0.01 bar at the studied pressure range. Figure 6-23 shows calculated results for H_2S fugacity in mixture of CH_4 and H_2S at (Huttenhuis et al. 2007) reported experimental conditions (temperature, total pressure, and vapor phase composition). Calculations are performed using SRK EoS.

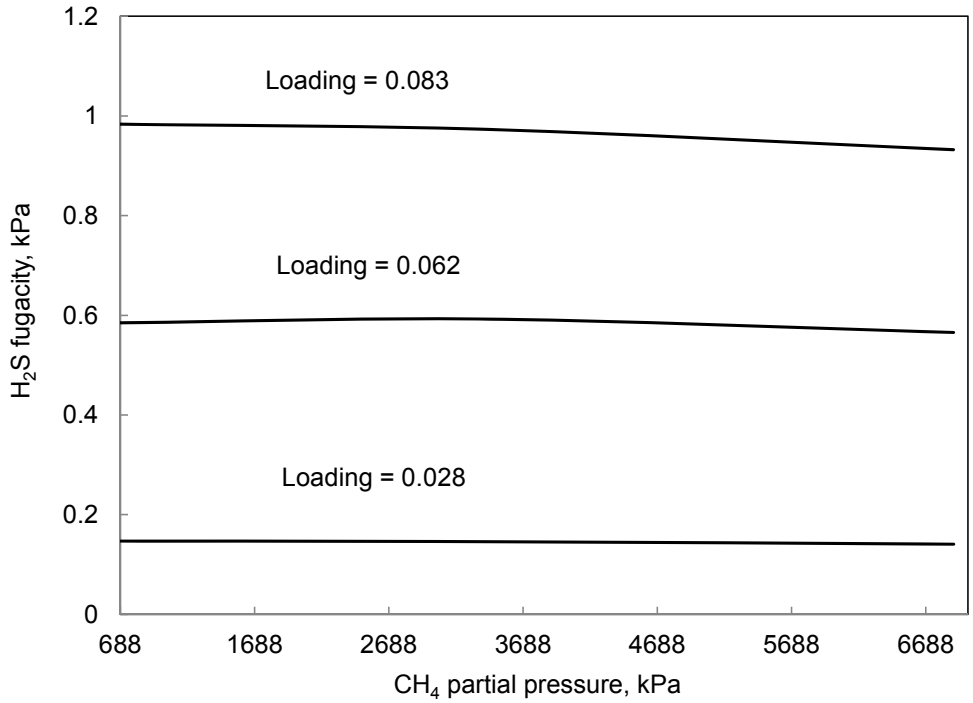

Figure 6-23. Modeling investigation on influence of methane partial pressure on H_2S fugacity for H_2S-CH_4 mixture at T, P_{Total}, y_i correspond to Figure 6-21. Solid line, calculated H_2S fugacity using SRK EoS.

Figure 6-23 shows that H_2S fugacity at the same conditions as (Huttenhuis et al. 2007) is independent of total pressure. From Figure 6-22 and Figure 6-23, it can be concluded that at constant H_2S loading, H_2S fugacity does not change with methane partial pressure in the studied pressure range. At equilibrium H_2S fugacity in gas and liquid phase is equal, therefore at a given loading and temperature, increasing pressure over the liquid phase by inserting methane in the gas phase, does not change the H_2S fugacity in liquid phase. Depending on equilibrium calculations approach, non-ideality in the liquid phase is defined by fugacity coefficients (when EoS is used for the liquid phase) or activity coefficients (when liquid phase is modeled by G^E models). Liquid phase is nearly incompressible, for this reason fugacity coefficients or activity coefficients in the liquid phase are assumed to be pressure independent. In the other hand, the amount of methane dissolved in the liquid phase is very small and should not have significant influence on the liquid phase activity or fugacity coefficient. Hence, high pressure over the liquid phase and presence of

methane in the liquid phase do not significantly change H_2S solubility in the liquid phase. Thus, the influence of methane on the gas phase is of importance.

Methane Influence on the gas phase:

Figure 6-24 plots the calculated fugacity, partial pressure and fugacity coefficient of H_2S in the gas phase (left axis) and H_2S solubility in the liquid phase (right axis) for MDEA-H_2S-CH_4-H_2O mixture, with 50 wt% MDEA and at temperature of 50 °C and liquid loading of 0.74 as a function of methane partial pressure (calculations are performed using SRK EoS). It can be seen in Figure 6-24 that at constant H_2S loading and constant temperature, H_2S fugacity is independent of methane partial pressure. However, with increasing methane partial pressure, H_2S partial pressure is increasing while H_2S fugacity coefficient in the gas phase is decreasing. Therefore, at constant H_2S loading, an increase in H_2S partial pressure with an increase in methane partial pressure can be attributed to a decrease in H_2S fugacity coefficient gas phase. H_2S solubility also remains constant with methane partial pressure.

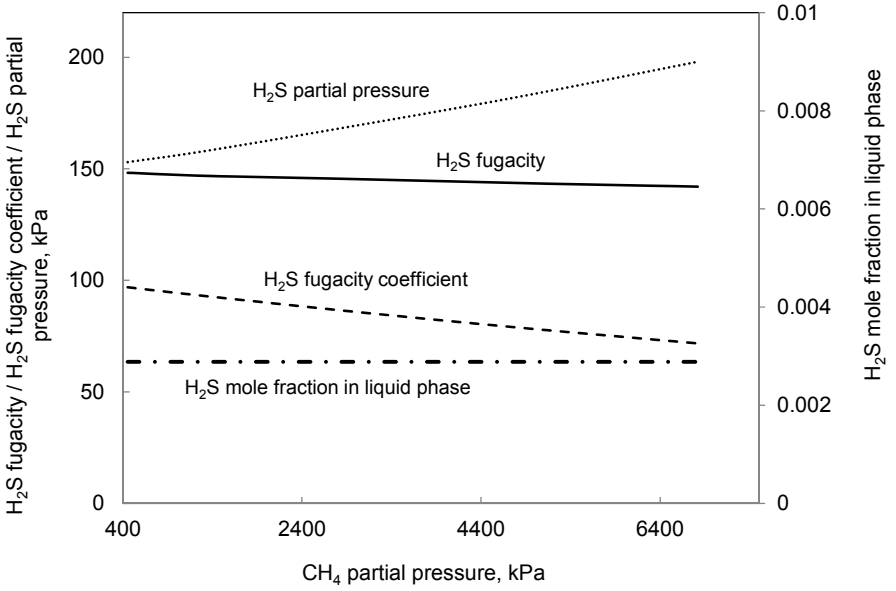

Figure 6-24. Calculated fugacity, partial pressure, fugacity coefficient of H_2S (left axis) and H_2S mole fraction in the liquid phase (right axis) in a 50 wt% MDEA aqueous solution and a liquid loading of 0.74 and at 50 °C. Solid line: H_2S fugacity, Dash line: H_2S fugacity coefficient, Dotted line: H_2S partial pressure; Dash-Dotted line: H_2S mole fraction in the liquid phase. Calculations are performed using SRK EoS.

It is worthwhile to mention that the same behavior was observed for CO_2 partial pressure in aqueous MDEA solutions (Huttenhuis et al. 2008). Experiments by (Huttenhuis et al. 2009) demonstrate that H_2S partial pressure is sensitive to the type of inert gas (nitrogen or methane). However, type of inert gas does not affect CO_2 partial pressure (Huttenhuis et al. 2009).

6.6 Conclusion

In this chapter, the optimized parameters for H_2S-MDEA-H_2O and H_2S-CH_4-MDEA-H_2O and CO_2-CH_4-MDEA-H_2O systems are presented and the results are discussed. Modeling of H_2S-MDEA-H_2O and H_2S-CH_4-MDEA-H_2O systems began with strong underlying models for H_2S-H_2O and CH_4-H_2O subsystems. Model parameters for H_2S-H_2O subsystem have been fitted to the experimental data of pure H_2S vapor pressure, total pressure data of H_2S-H_2O system and H_2S solubility data in water. The optimized model for H_2S-H_2O system accurately predicts thermodynamic properties of the binary H_2S-H_2O mixture. Based on the determined parameters for H_2S-H_2O subsystem, a model for H_2S-MDEA-H_2O system was developed, additional interaction parameters were adjusted to ternary VLE and H_2S heat of absorption data. The optimized model is valid over broad range of amine concentration, temperature, pressure and loading. Model parameters for CH_4-H_2O subsystem have been adjusted to the experimental total pressure data of CH_4-H_2O binary system. The overall fit of the CH_4-H_2O system was satisfactory and the optimized model represents thermodynamic properties of the CH_4-H_2O binary system well. Model parameters for CH_4-H_2O and H_2S-MDEA-H_2O systems were combined to model H_2S-CH_4-MDEA-H_2O system. H_2S-CH_4-MDEA-H_2O model predicts H_2S solubility at high pressures and in presence of methane (typical absorber condition in natural gas treatment process). The same as H_2S system, model parameters for CO_2-CH_4-MDEA-H_2O were obtained based on combination of parameters of CH_4-H_2O and CO_2-MDEA-H_2O systems. The CO_2-CH_4-MDEA-H_2O model predicts CO_2 solubility at high pressures where methane is present in the gas phase. The predictions results proved that optimized models accurately represent acid gas, CO_2 and H_2S, solubility in aqueous MDEA solutions at high pressures. Finally, at constant H_2S loading, effect of high pressure (methane influence) on acid gas solubility was investigated. It is concluded that at constant acid gas loading, increasing methane partial pressure or system total pressure results in an increase in acid gas partial pressure while acid gas solubility remains constant. Therefore the effect of high pressure (methane partial pressure) on acid gas partial pressure is due to the non-ideality of the gas phase and not because of dissolution of methane in the liquid phase. The calculations show that at constant acid

gas loading, acid gas fugacity coefficient in the gas phase is changing by pressure whereas acid gas fugacity is independent of the pressure.

Chapter 7

Measurement: VLE of CO_2-MDEA-H_2O and Density of MDEA-H_2O

Chapter 7

Measurement: VLE of CO_2-MDEA-H_2O and Density of MDEA-H_2O

---

7 Measurement: VLE of CO_2-MDEA-H_2O and Density of MDEA-H_2O

7.1 Chapter Overview

Solubility data of acid gases in aqueous alkanolamines are essential to improve the design of the processes. It is determined by measurement of the vapor-liquid equilibrium at a certain temperature and pressure. There are plenty of experimental data available for CO_2 solubility in aqueous solutions of MDEA especially in the range 20 to 50 wt% which is the industrially applied range. Most of the G^E thermodynamic models encounter problems in representing acid gas solubility at high amine concentrations because these models are not predictive and their parameters should adjust to proper experimental data. Accordingly, stronger models can be optimized if the experimental data was richer out of the industrial concentration range. Experimental measurements carried out by (Rho et al. 1997) is one of the few reports, investigating larger MDEA concentration range (5 to 75 wt%). To enrich the experimental data, CO_2 solubility data are measured in this study for aqueous MDEA solutions of 10 to 100 wt%. The data nearly cover the whole amine concentration range and can be used for validation of the developed models and if necessary for refitting the model parameters.

In this chapter provides the details of the experimental procedure used for measurement of CO_2 solubility and density. Furthermore, the measured data are used to validate optimized thermodynamic model of CO_2-MDEA-H_2O presented in the chapter 5. It noted that, though in principle possible, model parameters are not adjusted to the newly measured data, because the main aim was model validation.

7.2 Review on Experimental Techniques for Study of the Acid Gas Solubility

The methods involved in measuring acid gas solubility could be classified in three techniques, static, circulation and flow method (Anufrikov et al. 2007).

7.2.1 Static Method

In this measurement method, at constant temperature, amine aqueous solution with known composition is put into the cell, a required amount of the acid gas is introduced into the cell, the system is kept until equilibrium is attained. After equilibrium established (when temperature, pressure and composition become constant), equilibrium pressure and mole fractions of components in each of the coexisting phases are recorded (Anufrikov et al. 2007). This technique is widely used for measuring gas solubility data.

7.2.2 Circulation Method

In this method, a circulation pump is used to bubble the gas through the amine solution. The temperature is maintained constant with a thermostat during the experiments. The same as static method the amounts of each components of the system are fixed, the equilibrium pressure and phase compositions are recorded in the course of an experiment. The difference of this method with the static method is that in this method the vapor phase or the liquid phase or both phases are circulated and usually an inert gas is present in the system (Anufrikov et al. 2007).

7.2.3 Flow Method

Flow method is occasionally used to measure gas solubility. In this method, the partial pressure of the acid gas in the gas flow is set during the experiment and the liquid phase composition (the phase that gas passes through it) changes until equilibrium reached. In this method, temperature, numbers of moles of water and amine in the solution and partial pressure of the acid gas are the quantities which are set in the experiments (Anufrikov et al. 2007).

In summary, static method is sufficiently accurate, however the accuracy of the method decrease at low acid gas concentrations, that is due to the significant adsorption of gases to the apparatus wall. In contrast to static method, the flow method application is limited to low pressures. The circulation method is applicable at low and medium pressures. Unlike flow method it does not need a carrier gas. At elevated pressures, the circulation method is less accurate than the static method.

7.3 Experimental Design

The advantages of MDEA over the primary and secondary amines, like lower heat of reaction with acid gas, lower vapor pressure, lower corrosive tendency and capability of selective absorption of H_2S, make the process of natural gas treatment with MDEA more economically feasible. Solving problems associated with natural gas treatment process requires information on phase behavior of acid gas-alkanolamine-water systems mainly with MDEA as an alkanolamine. There are lots of data available for vapor-liquid equilibria of CO_2-MDEA-H_2O system. Table 7-1 summarized the available published experimental VLE data for CO_2-MDEA-H_2O system. It is noted that collected data in Table 7-1 were gathered to the best of author knowledge and at the time of this work.

Table 7-1. Published VLE data for CO_2-MDEA-H_2O systems

MDEA Concentration, wt%	T, °C	P, kPa	Data Type	Reference
19, 32.11	40 to 140	139 to 5037 (P_{Total})	VLE	(Kuranov et al. 1996)
26, 47	25, 40, 75	3 to 4559 (P_{Total})	VLE	(Sidi-Boumedine et al. 2004, a)
19	40	791 to 4739 (P_{Total})	VLE	(Kamps et al. 2002)
32, 49	40, 80, 120	176.5 to 7565 (P_{Total})	VLE	(Kamps et al. 2001)
24	40	1155 to 3029 (P_{Total})	VLE	(Addicks et al. 2002)
24	40	12 to 3029 (P_{Total})	VLE	(Silkenbaumer et al. 1998)
19, 32, 48	40, 80, 120	0.12 to 69.3 (P_{CO_2})	VLE	(Ermatchkov et al. 2006)
5, 20, 50, 75	50, 75, 100	0.775 to 268.3 (P_{CO_2})	VLE	(Rho et al. 1997)
23, 47	40	0 to 93.6 (P_{CO_2})	VLE	(Austgen et al. 1991)
35	40, 100	0 to 262 (P_{CO_2})	VLE	(Jou et al. 1993)
50	25, 50, 75, 100	8.27 to 95.83 (P_{CO_2})	VLE	(Park and Sandall 2001)
23, 50	40	0 to 0.55(P_{CO_2})	VLE	(Rogers et al. 1998)
23, 50	40, 70, 100, 120	0.002 to 5188 (P_{CO_2})	VLE	(Huang and Ng 1998)
11.8, 20, 23	25,38,50,65.5,115.5	11.1 to 6161.5(P_{CO_2})	VLE	(Maddox et al. 1987)
50	55, 70, 85	65.75 to 813.4(P_{CO_2})	VLE	(Ma'mun et al. 2005)
34, 38.5, 47	40, 55, 70, 80, 90,	0.8 to 1013	VLE	(Xu et al. 1998)

	100	(P_{CO_2})		
23, 28	25, 40, 70	101 to 2320 (P_{CO_2})	VLE	(Jenab et al. 2005)
23	40, 60, 80	0.06 to 95.61 (P_{CO_2})	VLE	(Ali and Aroua 2004)
23.8, 29.9	30, 40, 50	2.9 to 94.7 (P_{CO_2})	VLE	(Kundu and Bandyopadhyay 2005)
22.98, 47.01	25, 40, 70, 100, 120	0.001 to 6020 (P_{CO_2})	VLE	(Jou et al. 1982)
29.99	40	1.02 to 1169 (P_{Total})	VLE	(Baek and Yoon 1998)
23.63	25	0.02 to 1.6 (P_{CO_2})	VLE	(Lemoine et al. 2000)
30	40, 80, 120	2000 to 10000 (P_{Total})	VLE	(Mathonat et al. 1997)
19.55, 47.01	100, 140, 160, 180, 200	103 to 4930 (P_{CO_2})	VLE	(Chakma and Meisen 1987)
10, 20, 30, 40	20, 40, 60	80 to 298 (P_{CO_2})	VLE	(Kicrzkowska-Pawlak 2007)
18.96	40	1.17 to 3770 (P_{CO_2})	VLE	(Macgregor and Mather 1991)
30	40, 60, 80, 100	1.1 to 1979 (P_{CO_2})	VLE	(Shen and Li 1992)

As expected majority of CO_2 solubility data in MDEA aqueous solutions are reported for 30 wt% to 50 wt% MDEA concentrations. Bibliographic study shows that (Rho et al. 1997) data contains the lowest and highest MDEA concentration for which CO_2 solubility is reported for. The main objective of this work is to fill the gaps in the available data and to provide the necessary data in order to make a reliable data base. As a result of this bibliographic study, it has been concluded that it is crucial to determine CO_2 solubility up to higher amine concentrations. As it was mentioned earlier, CO_2 solubility in high concentrated amine solutions could be used to validate available G^E models since most of the G^E models do not show good results at high amine concentrations. It is worth to mention that nowadays industry starts to investigate higher MDEA concentrations. New data are measured herein for CO_2 solubility in aqueous MDEA solutions for MDEA wt% vary between 10 to 100, at constant pressure of 110 kPa (1.10 bar) and from 40 to 80 °C. The results of this study could serve as the basis for furthermore developing thermodynamic models for the acid gas removal process studies and the models can then be used for the design or optimization of acid gas treating plants.

7.4 Experimental Section

7.4.1 Chemicals

The chemicals used in this work include MDEA (Acros Organics, ≥ 99 % pure), CO_2 (Yara, ≥ 99 % pure) and Acetone (VWR (BDH PROLABO), ≥ 99 % pure). All chemicals were used without any further purification.

7.4.2 Experimental Apparatus

The apparatus used for measuring CO_2 solubility in aqueous MDEA solutions was called "low pressure cell" and already exists in Statoil laboratories. The Low pressure cell was designed to give information on relative kinetics and phase equilibria. It could be used both for measuring rate of reaction and equilibrium CO_2 solubility in different solvents. It was designed to operate between 20° C and 80° C and between 100 and 7000 kPa (1 and 70 bar). However the rig safety valve was set to 1800 kPa (18 bar). Figure 7-1 shows a schematic configuration of the low pressure cell.

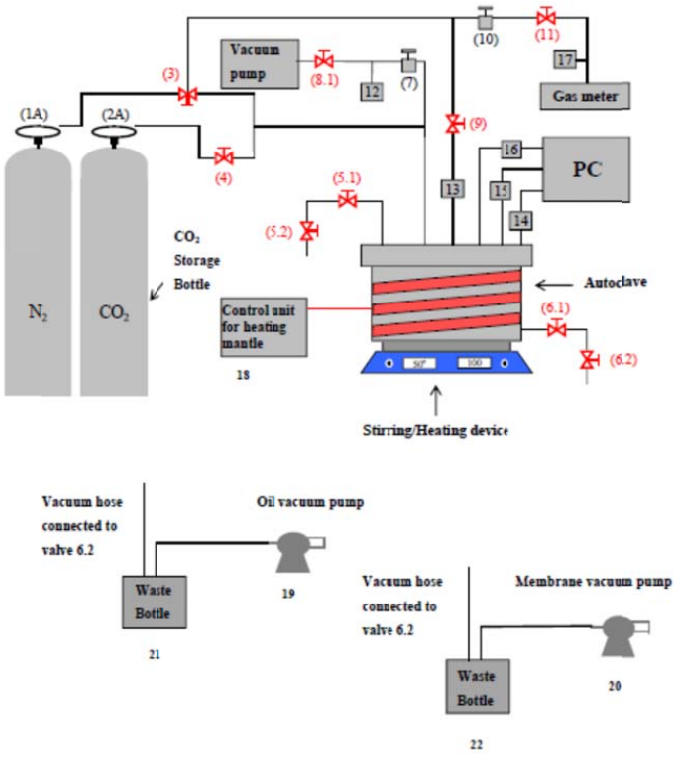

Figure 7-1. Sketch of the low pressure cell setup.

The main parts of the low pressure cell were a stainless steel autoclave, CO_2 gas storage bottle, a gas meter, a membrane vacuum pump, an oil vacuum pump, a stirring/heating device (combined hot plate and magnetic stirrer), autoclave heating mantle (there were heating cables surrounding the autoclave) and a PC with a control program for the rig, autoclave safety valve that was set to 1800 kPa (18 bar), a thermocouple in the gas phase inside the autoclave (T_1), a thermocouple in the liquid phase inside the autoclave (T_2), a temperature sensor in the Gas meter (T_{Gm}), a pressure sensor for measuring the pressure of the gas phase inside the autoclave (P_1), a pressure sensor for measuring gas pressure inside the gas meter (P_{Gm}) and the safety valve for the gas meter which operates at 130 kPa (1.3 bar). Different parts of the system are connected with several valves. Figure 7-1 is the sketch of the Low pressure cell set up; the corresponding numbers in Figure 7-1 refer to:

1. Nitrogen gas storage bottle
2. Carbon dioxide gas storage bottle
3. Ball valve to release nitrogen gas.
4. Ball valve to release carbon dioxide gas
5. Valves for filling the solvent. 5.1 is a needle valve and 5.2 is a ball valve.
6. Valves for the withdrawal of liquid samples, emptying, washing and vacuuming the autoclave. 6.1 is a ball valve and 6.2 is a needle valve.
7. Needle valve for withdrawal of gas sample and the suction of the vacuum.
8. Ball valve for withdrawal of gas samples. 8.1 and 8.2 are two different options for connecting a hose to a vacuum pump. Note that in this work, cell was vacuumed by connecting valve 6.2 with a hose to vacuum pumps.
9. Ball valve for connecting autoclave to the gas meter.
10. Needle valve for connecting autoclave to the gas meter.
11. Needle (Regulator) valve connected to the gas meters.
12. Pressure display
13. Safety valve set to 1800 kPa (18 bar). The release part of the safety valve was connected to the central exhaust system.
14. A thermocouple in the liquid phase inside the autoclave (T_2).
15. A thermocouple sensor in the gas phase inside the autoclave (T_1).
16. Pressure transducer for the autoclave (P_1).
17. Gas meter safety valve, set at 130 kPa (1.3 bar). The release part of the safety valve was connected to the central exhaust system.

18. Autoclave heating mantle, manufactured by Julabo (Julabo LC 3).
19. Oil vacuum pump.
20. Membrane vacuum pump.
21. Waste bottle connected to the oil vacuum pump.
22. Waste bottle connected to the membrane vacuum pump.

There were two vacuum pumps that were used for emptying and vacuuming the autoclave. A membrane vacuum pump which was made by VACUUBRAND GMBH+CO KG and it created the maximum vacuum of 0.9 kPa (9 mbar). The oil vacuum pump was a rotary pump which created maximum 0.00004 kPa (0.0004 mbar) vacuum and was made by the same manufacture as the membrane pump. Pictures of the equipment are included in appendix.

7.4.2.1 Autoclave

As it was mentioned autoclave was one of the main parts of the low pressure cell (Figure 7-2) which was made of stainless steel. Figure 7-2 shows the autoclave more in detail. Figure 7-2 (a) shows the different parts of the autoclave and Figure 7-2 (b) presents the dimensions inside the autoclave. Autoclave was equipped with a stirring/heating device (which mixed the solution on a combined hotplate and magnetic stirrer device), surrounding electrical heat tracing, two K-type thermocouples and two pressure indicators. Autoclave and all linings connected to it were covered by insulated materials. Two thermometers were placed in the autoclave, one in the liquid phase and other one in the vapor phase. Both gas and liquid phase temperatures were measured with the two thermocouples within the accuracy of ± 0.1 °C. A pressure sensor was located outside the autoclave which measured the autoclave pressure within accuracy of $\pm$ 0.01 bar. The pressure in sampling port was read by a pressure indicator (0-4 bar, Keller, type: LE03/8104-0.2) within accuracy of $\pm$ 0.01 bar.

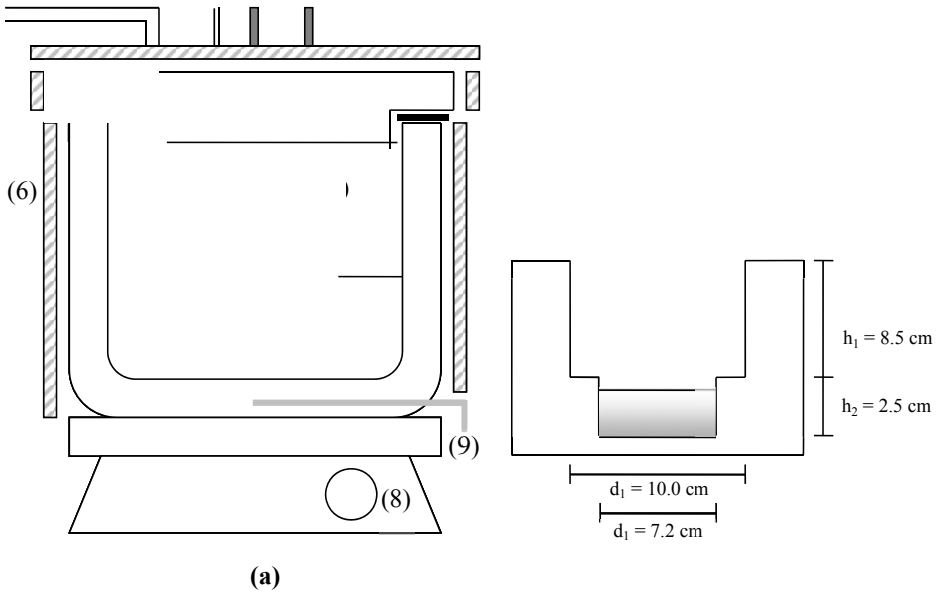

Figure 7-2. (a) Sketch of the internal part of the autoclave: (1) thermocouple measuring temperature of gas phase inside autoclave, (2) thermocouple measuring temperature of liquid phase inside autoclave, (3) tube to insert solvent in the rig, (4) CO_2 gas inlet, (5) Washer, (6) insulation material, (7) stirring bar, (8) stirring and heating plate, (9) liquid withdrawal tube. (b) Dimensions inside the autoclave

The stir bar is manufactured by IKA RET, it monitors the temperature from 0 to 340 °C and the stirring rate could change from 0 to 1500 rpm[32].

7.4.2.2 Gas Meter

Gas meter is another main part of the rig which was manufactured by ROP France, temperature and pressure electronic devices (monitoring/reading) are from Eurotherm. The gas meter consists of a glass vessel with a piston to alter its volume, a volume meter, a temperature sensor, a pressure sensor, two vent valves and a safety valve set at 130 kPa (1.3 bar). The piston was driven by a motor. The volume of the gas was measured in a Pyrex tube with diameter of 100 ± 0.002 mm, in which the volume was measured within accuracy of ± 100 cm^3. The capacity of gas meter is 4000 cm^3. The gas meter is made of glass and therefore could not withstand high pressures; the maximum acceptable pressure in the gas meter was 130 kPa (1.3 bar). A safety valve set at 130 kPa (1.3 bar)

[32] rpm: Round per Minute

was connected to the gas meter to prevent it from breaking in case the pressure increases above 1.3 bar. During this study the gas meter pressure was set to be fixed at 110 kPa (1.1 bar). The temperature of the gas meter was measured with thermometer within the accuracy of $\pm 0.01°C$. The pressure sensor has 0 to 4 bar pressure range and its accuracy was ± 0.01. Figure 7-3 shows the configuration of the gas meter. The gas meter can be operated in two modes: Manual and Automatic. In the manual mode the piston movement was done manually and in the automatic mode the piston movement was triggered automatically to keep the pressure constant. In this work, experiments were performed with the gas meter operated in the automatic mode. The gas meter allows for the automatic measurements of volumes of CO_2 at constant pressure.

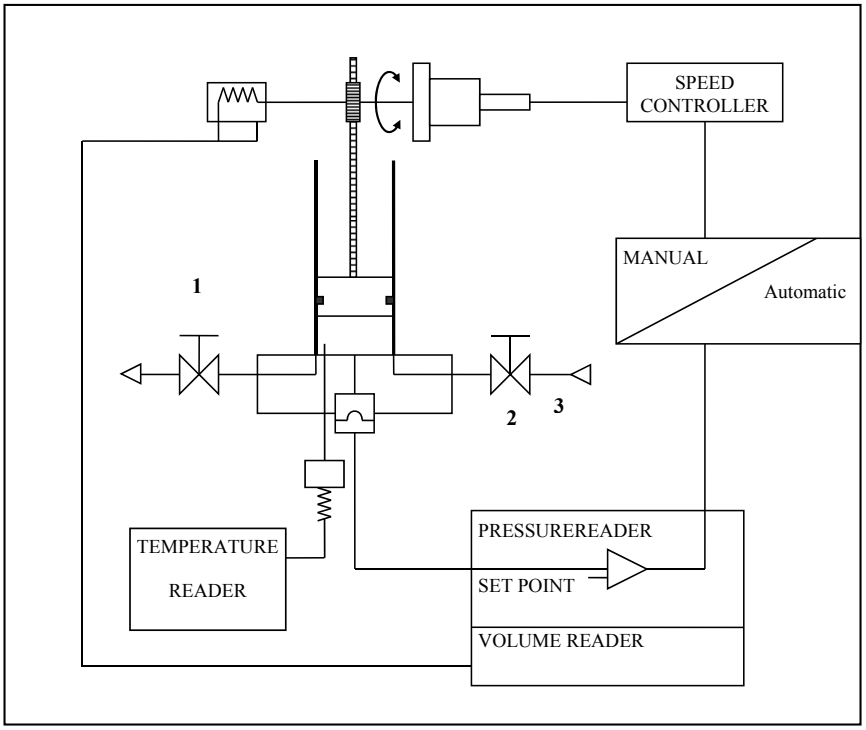

Figure 7-3. Sketch of the gas meter. (1) Valve connects the gas meter to the autoclave (corresponds number in Figure 7-1 is 11), (2) Vent valve, (3) Vent valve

7.4.3 Experimental Procedure

The experiments were performed using the static-synthetic method. Briefly, the rig was initially vacuumed and known amount of preloaded solvent with known composition (approximately 30 g of the aqueous amine solution, note that for conditions where absorption capacity is low (low and high MDEA concentrations and high temperatures, the amount of solvent was increased to approximately 120 g in order to decrease the results inaccuracy (It will be discussed later in section 7.5.4)) was inserted through the valves 5.1 and 5.2. The solvent was continuously stirred during the experiment. The gas meter was filled with approximately 3.5 L pure CO_2. When the desired temperature was reached in the cell, the valves connecting the autoclave and the gas meter were opened, and the volume of the autoclave was filled with CO_2. The experiments were performed under constant pressure while volume of absorbed CO_2 per time was logged. Monitoring the temperature, the pressure and the CO_2 volume ensured that the sample was withdrawn at equilibrium. Volume was always the last quantity that became constant. Stirring was very important to ensure while the system was approaching equilibrium. Due to slow mass transfer at the interface of gas and liquid, without stirring, pressure, temperature and volume could be unchanged without achieving equilibrium. A detailed procedure of performing experiments is as follows:

- Set the desired temperature: Both heaters (the hot plate and surrounded heater) were set to the target temperature.
- Clean the autoclave (Empty, Wash and Dry): Any remaining solvent from previous tests was removed by creating vacuum in the autoclave. The vacuum hose from the waste bottle (waste bottle which was connected to the membrane pump) was attached to the sampling port (valve 6.2). Membrane vacuum pump was turned on and the solvent was moved to the waste bottle. After emptying the autoclave, the cell was rinsed with approximately 600 cm^3 distilled water. Water was filled in a beaker and placed under the injection port (valve 5.2). The beaker was connected to the cell through the plastic hose attached to valve 5.2. At the same time the cell was vacuumed by attaching the vacuum hose from the waste bottle to the valve 6.2 and turning the membrane vacuum pump on. Water pulled in and was collected in a waste bottle. To dry water droplets remained in the cell, autoclave was rinsed with around 300 cm^3 acetone. Afterwards the autoclave was vacuumed for a while with the oil vacuum pump in order to remove all the small droplets of the water or acetone remaining in the cell. The cell was furthermore dried by CO_2. The cell was filled with CO_2 up to 250 kPa (2.5 bar)

pressure, afterwards valves 5.1 and 5.2 were opened (or valves 6.2 and 6.1). Note that valve 5.2 (or 6.2) had been closed before the autoclave pressure went below atmospheric pressure to avoid the air entering the cell. Releasing CO_2 through valve 6.2 or valve 5.2 also flushes the piping system.

- Fill the gas meter with CO_2: Gas meter was filled with CO_2 (approximately 3500 cm^3) through the autoclave. First autoclave was filled with CO_2. Notice that whenever there was CO_2 flow from storage bottle to autoclave, gas meter was isolated (all the valves between autoclave and gas meter were closed to avoid pressure build up inside the gas meter). Afterwards CO_2 was released to gas meter by opening valves 9, 10 and (slightly) valve 11. CO_2 flew from autoclave to gas meter until the pressure of the autoclave dropped to 1.1 bar. All the connection valves between CO_2 storage bottle and autoclave were closed during transferring CO_2 from autoclave to gas meter. As previously mentioned, gas meter was made of glass and was operated at constant pressure of 1.1 bar., it could not stand higher or lower pressures as the regulated one (1.1 bar).
- Injecting the solvent: Before injecting the solvent, cell was vacuumed through valve 6.2 while all valves except valve 5.2 and 11 were opened. A disposable syringe was filled with approximately 30cm^3 of the prepared solvent. The possible formed air bubbles inside the syringe were removed to avoid air bubbles entering the autoclave. The weight of filled syringe before injection was noted (w_1). Through valves 5.2 and 5.1 solvent was injected to the cell. After injection syringe was weighted again (w_2) in order to calculate exact amount of injected solvent.
- Start the experiments: A new log file was created and logging was started. The stirrer was turned on. After about 20 to 30 minutes when the solvent reached the stable temperature and thermal equilibrium between the gas phase and the solvent was attained (whenever P_1, T_1 and T_2 became constant with time) $CO_2$was introduced into the cell. Valves 10 and 11 were completely opened to let the CO_2 freely flow through the connecting pipes; gas meter volume and temperature were noted. Finally by opening valve 9, CO_2 was introduced to the cell and volume of the autoclave was filled with CO_2. The gas meter volume was continuously logged during the experiment and when this volume stopped changing with time, equilibrium was assumed. Logging was stopped and connecting valve between gas meter and autoclave, valve 9, was closed. The final values of gas meter volume and temperature were noted down.

7.4.3.1 Solvent Preparation

All solvent solutions were prepared gravimetrically from distilled and degassed water. Water was degassed by vacuum. Based on the desired composition of the solution, required amounts of MDEA and degassed water were mixed to create a homogeneous solvent solution. Solvents were kept in a closed bottle and their exposure to air was minimized to avoid contamination with CO_2 from the air. According to (Huang and Ng 1998) the total residual amount of CO_2 in a freshly prepared amine solution will increase to 0.0005 mole CO_2/mole MDEA if the solution is exposed to air for 6 hours in an Erlenmeyer. Therefore in this study the influence of residual CO_2 in the prepared amine solutions on experimental results were safely neglected since the exposure of the prepared solution to atmosphere was few minutes and the studied loading range was much greater than 0.0005. An analytical balance (Mettler Toledo) with resolution of 0.0001 g was used for the preparation of the solvent solutions

7.4.3.2 Set up Preparation

Calibration

The autoclave was connected to two temperature thermocouples and one pressure sensor. One thermocouple was used to measure the temperature of the gas phase, while the other was immersed in the liquid phase. The criterion to confirm that the system has reached thermal equilibrium was that these two K-type thermocouples probes show the same temperature within the correspondence experimental uncertainty. Both thermocouples were calibrated against a reference thermometer and the calibration parameters were entered into the calibration file used by the program that controls the rig and logs the results. The temperature calibrator is from Ametek (Type: ATC-650 B), the reference platinum probe (Type: STS-100 A 901) had a temperature range of -150 to 650 °C and an accuracy of $\pm 0.01\,°C$. The pressure transducer and the pressure indicator connected to the autoclave were calibrated using a reference pressure gauge. The DPI 610 pressure calibrator from GE Druck, with a pressure range of -1.01 to 413.68 bar and an accuracy of 0.025% full scale range was used to calibrate the pressure sensor. The calibration of temperature, pressure and volume sensors in the gas meter was done by the supplier prior to these experiments. Two safety valves connected to the setup were also calibrated before starting the experiments.

Leak Test

Both gas meter and autoclave were tested against leakage. The test involves filling the autoclave with CO_2 and pressurization of the autoclave to the specified test pressure. Leak was tested by observing whether there is a pressure loss in the autoclave. In the same way, gas meter was filled with certain volume of CO_2 and leak was tested by observing whether or not there is a volume loss. Autoclave, linings and gas meter were regularly checked for leakage.

Gas Meter Clean up

The gas meter was washed with CO_2 to be certain that there is no other gas e.g. nitrogen or oxygen present in the gas meter. The gas meter was washed following two different methods. In the first method the gas meter was fully filled with CO_2 to the highest level and then emptied. The procedure was repeated for 5 times. This method allowed the gas diluted with respect to any possible impurities. In the Second method the piston was at its lowest level and CO_2 was purged through the gas meter.

7.4.3.3 Measuring Cell Volume

Volume refers to the volume of a cavity inside the autoclave and tubing. Volume of the autoclave was considered as the volume of cavity between valve 5.1 and 6.1. Volume of the autoclave (volume of cavity between valve 5.1 and 6.1) was measured by filling the autoclave with water. Volume of water that filled the autoclave was recorded as autoclave volume. This procedure was repeated for 5 times. Overall the average of repeat tests was considered as the cell volume. Cell volume was estimated to be 599.34 $cm^3 \pm 2.11$ cm^3. The reported expanded uncertainty is based on a standard uncertainty multiplied by a coverage factor k = 2, providing a level of confidence of approximately 95%.

7.4.3.4 Measuring Cell Dead Volumes

Dead volume refers to the volume of a cavity inside the autoclave and tubing that does not have the possibility to meet acid gas or solvent. Low pressure cell total dead volume consists of two parts: **1)** Volume of the tube between valve 5.1 and 5.2 (sampling port) **2)** Volume of the tube that connects valve 9 to the autoclave (Notice that during the experiments volume of gas meter was recorded while valves 10 and 11 were opened and valve 9 was closed. Hence the volume of tube between valve 9 and gas meter was already included in gas meter volume).

- Volume of the tube between valve 5.1 and 5.2 (sampling port)

During the injection of solvent, some of the solvent may trapped in the tube connected valve 5.1 to 5.2. Therefore the mass of injected solvent should be corrected for the trapped amount. To measure the amount of solvent that may be trapped in the tubing, solvent with 50 wt% MDEA concentration (50 mass% was the average of injected solvent concentrations) was injected to the rig and mass of solvent that trapped in the tube was measured. The procedure was repeated in 4 parallels, average of the 4 measurements was considered as the amount of the solvent that during the injection trapped in tube connected valve 5.1 to valve 5.2. The trapped amount was estimated to be $0.50\ \mathrm{g} \pm 0.06\ \mathrm{g}$. Note that depending on the viscosity of the solvent and injection conditions, the trapped amount of solvent could be lower or higher than the estimated value. It was not possible to measure exact amount of trapped solvent for each experiment, therefore the estimated amount of 0.5 g was considered as the trapped amount for all experiments. Bearing in mind that the amount of solvent that trapped in sampling tubing is one of the sources of the uncertainty of these measurements, however compare to the amount of injected solvent this amount is very little but not negligible (about 1.5 % of the injected solvent).

- Volume of the tube that connects valve 9 to the autoclave

The volume of tube volume that connects valve 9 to autoclave was neglected as it was very small compare to autoclave volume (The length of tube was approximated to be 20 cm with outer diameter of 1/8 inch). Keep in mind that this dead volume did not affect the final results of these particular measurements and therefore was neglected. In case of using the cell for other types of measurements, it is recommended to investigate the effect of the mentioned dead volume on final results.

7.5 Results

7.5.1 Validation

In order to test the experimental set up and procedure, some validation (introductory) experiments were performed. In these measurements the pressure was kept constant at 1.1 bar. In contrast to this study, almost all the data available in the open literature were measured at constant volume. This inherent difference impedes meaningful comparison of the measured data of this study to the very scarce literature data of the same conditions. Therefore, some measurements that have been

validated in Statoil laboratories earlier are chosen to validate the newly conducted experiments. The validation tests were conducted at 50 °C with 50 and 30 wt% MDEA. Comparison of the results shows that the new measurements are well in line with previous results. The uncertainty of the validation measurements for loading (mole CO_2/mole MDEA) at 50 °C and 50 mass% MDEA was estimated to be ±0.02 and at 50 °C and 30 wt% MDEA the uncertainty was estimated to be ±0.01.

7.5.2 Results Analysis

7.5.2.1 Volumetric Analysis

In these experiments generally liquid phase loading has been calculated from the volume of CO_2 absorbed in the liquid phase. Avoiding liquid phase analysis was one of the advantages of the used method. In this work the mentioned method is called volumetric analysis. This section demonstrates how loading was calculated from volumetric data. Loading indicates mole numbers of CO_2 absorbed in the liquid phase per MDEA moles present in the liquid phase.

$$Loading = \frac{CO_2 \text{ mole numbers present in the liquid phase}}{MDEA \text{ mole numbers present in the liquid phase}} \tag{7-1}$$

The amount of CO_2 absorbed in the liquid phase was calculated from the total mole balance. CO_2 mole numbers in the liquid phase was calculated from the difference between total moles of CO_2 introduced to the system and number of moles present in the vapor phase.

$$n_{CO_2,Liquid\ phase} = n_{CO_2,\text{Introduced}} - n_{CO_2,Vapr\ phase} \tag{7-2}$$

Total mole numbers of CO_2 introduced to the system were calculated from the volume of CO_2 transferred from gas meter to the autoclave and by considering the pure CO_2 inside the gas meter as an ideal gas. This assumption seemed realistic as the pressure of gas meter was low (1.1 bar), therefore:

$$n_{CO_2,\text{Introduced}} = \frac{P_{G\_m} V_{CO_2}}{R T_{G\_m}} \tag{7-3}$$

Where P_{G_m} is the pressure of gas meter which is equal to 1.1 bar, V_{CO_2} is the volume of CO_2 introduced to the cell, R is the gas constant and T_{G_m} is the temperature of gas meter. Volume of CO_2 introduced to the cell was obtained from the recorded values of initial and final volume of CO_2 inside the gas meter.

$$V_{CO_2} = V_{G_m,Initial} - V_{G_m,Final} \tag{7-4}$$

Number of moles of CO_2 present in the vapor phase was calculated based on the ideal gas assumption for the vapor phase which is in equilibrium with the liquid phase inside the autoclave. Hence:

$$n_{CO_2,Vapor\ phase} = \frac{P_{CO_2} V_{Vapor\ phase}}{RT_{Autoclave}} \quad (7\text{-}5)$$

Where R is the gas constant, $T_{Autoclave}$ is the temperature of autoclave, P_{CO_2} is the partial pressure of CO_2 and $V_{Vapor\ phase}$ is the volume of the vapor phase. $V_{Vapor\ phase}$ was calculated through equation (7-6):

$$V_{Vapor\ phase} = V_{Cell\ total\ volume} - V_{Solvent} \quad (7\text{-}6)$$

$V_{Cell\ total\ volume}$ is the cell volume and as already illustrated was measured equal to 599.34 $cm^3 \pm 2.11\ cm^3$. $V_{Solvent}$ is the solvent volume calculated by the following equation:

$$V_{Solvent} = m_{Solvent}.d_{Solvent} \quad (7\text{-}7)$$

Where $m_{Solvent}$ is mass of solvent inside the autoclave and was calculated from equation (7-8):

$$m_{Solvent} = m_{Injected\ solvent} - m_{Trapped\ solvent} \quad (7\text{-}8)$$

Where $m_{Injected\ solvent}$ is the mass of injected solvent and $m_{Trapped\ solvent}$ is the mass of solvent that trapped in the tube between valve 5.1 and valve 5.2. As already illustrated $m_{Trapped\ solvent}$ was considered equal to 0.5 g. $d_{Solvent}$ is the solvent density, note that instead of density of loaded solution, density of unloaded solvent was measured by Anton-Paar density meter and was considered as density of solvent. This is a reasonable assumption as density of unloaded solution at the conditions of this work was almost similar to the density of loaded solution. Density of liquid sample withdrawn from the cell at 70 °C and MDEA mass% of 50 and 60 and at 80 °C and MDEA mass% of 20 was measured by Anton- Paar method and compared to density of unloaded solution at the same conditions. Comparison between densities of unloaded and loaded solutions demonstrated that densities of loaded solutions were in average 2.1170 % (0.0210 g/cm^3) higher than densities of unloaded solutions. Therefore because density of unloaded solvent was very close to the density of loaded solution and since loading calculations was not sensitive to density of solvent, density of unloaded solutions were measured and utilized in loading calculations.

Partial pressure of CO_2 was calculated through the following equation. MDEA presence in the vapor phase was neglected because the studied temperature range was far below MDEA boiling point.

$$P_{CO_2} = P_{Total} - P_{H_2O} \tag{7-9}$$

Where P_{Total} is the total pressure (1.1 bar) and P_{H_2O} is the partial pressure of water. Partial pressure of water was calculated form the Rault's law and by considering both liquid and vapor as ideal phases, hence:

$$P_{H_2O} = P_{Total} \cdot y_{H_2O} = x_{H_2O} \cdot P_{H_2O}^{Sat} \tag{7-10}$$

Where y_{H_2O} is the mole fraction of water in the vapor phase, x_{H_2O} is the mole fraction of water in the liquid phase and $P_{H_2O}^{Sat}$ is the vapor pressure of water at the interested temperature. x_{H_2O} was calculated from the following equations.

$$x_{H_2O} = \frac{n_{H_2O}}{n_{H_2O} + n_{MDEA}} \tag{7-11}$$

MDEA mole numbers in the liquid phase, n_{MDEA} , was calculated from :

$$n_{MDEA,Liquid\ phase} = \frac{m_{MDEA}}{Mw_{MDEA}} \tag{7-12}$$

Mw_{MDEA} is MDEA molecular weight and is equal to 119.1628 g/mole and m_{MDEA} is the mass of MDEA in the solution and calculated by:

$$m_{MDEA} = \left(\frac{MDEA\ wt\%}{100}\right) . m_{Solvent} \tag{7-13}$$

Water mole numbers, n_{H_2O} , was calculated from :

$$n_{H_2O} = \frac{m_{H_2O}}{Mw_{H_2O}} \tag{7-14}$$

Mw_{H_2O} is water molecular weight and equal to 18.01532 g/mole and m_{H_2O} is the mass of water in the solution and calculated from the total mass balance:

$$m_{H_2O} = m_{Solvent} - m_{MDEA} \tag{7-15}$$

Inserting values of equations (7-2) and (7-12) into equation (7-1) yields to obtain the value of loading.

Applying above procedure results in calculation of loading (equation (7-1)) from volumetric data obtained from set up. Note that after CO_2 absorption, solvent composition and MDEA mass% was calculated again and subsequent loading was obtained. However calculation results showed that solvent composition and consequently loading almost remained unchanged, therefore to avoid further calculations, loading was obtained as illustrated above, based on the initial solvent composition.

7.5.2.2 Titration Analysis

Loading results presented here were calculated based on the volumetric data obtained from the set up and calculations were done according to the procedure presented in section 7.5.2. However in order to validate the method used to calculate CO_2 solubility from volumetric data, liquid phase was also analyzed by precipitation titration method, note that this method is very time consuming thus only few measurements were done with this method. In precipitation titration method liquid phase sample withdrawn from the cell was mixed with NaOH. Therefore CO_2 and HCO_3^- present in the liquid phase react with NaOH and create CO_3^{2-}. Then $BaCl_2$ was added to the mixture, which made CO_3^{2-} precipitate as $BaCO_3$. The created solution was heated in order to agglomerate the $BaCO_3$ particles. Then the solution was cooled to ambient temperature and filtered. The filter and filtrate were placed in distilled water and $BaCO_3$ was dissolved by the addition of HCl. Then the solution was boiled in order to remove CO_2. Afterwards the solution was cooled to ambient temperature and titrated with NaOH to find the amount of HCl that was not used for dissolving $BaCO_3$. From the amount of HCl found by titration and the amount used for dissolving $BaCO_3$, the amount of CO_2 present in the solution was calculated. The titration was performed with automate titrator (Metrohm 809 Titrando). As it will be shown in Table 7-9 to Table 7-12 later on, the titration results confirmed volumetric results except for 10 mass% MDEA in which suspected results were obtained. The reason behind the inaccuracy of results at 10 mass% MDEA is unknown.

7.5.3 Measured Values

The VLE experiments for CO_2-MDEA-H_2O system as defined in section 7.3 were executed at constant total pressure 110 kPa (1.1 bar), for 10 to 100 wt% MDEA concentrations and from 40 to 80 °C. As illustrated in section 7.5.2 information on density of solution is required for converting volume based data to mass based data, density experiments were carried out for MDEA-H_2O solutions for 10 to 100 wt% MDEA and at 40 to 80 °C. The remainder of this section will demonstrate results of density and VLE experiments in figures and tables.

7.5.3.1 Density Experiments

Before starting VLE experiments, density of prepared aqueous MDEA solutions were measured using Anton-Paar (DMA 4500 M) density meter. To test the accuracy of the procedure and equipment some validation experiments were performed and compared to literature data. The validation runs were carried out for 20 and 30 wt% MDEA and at 40, 50 and 60 °C. Table 7-2 presented comparison between introductory experiments with data of (Li and Lie 1994).

Table 7-2. Comparison between this study and literature densities of aqueous MDEA solutions

T (°C)	ρ ($g.cm^{-3}$)			
	20 mass% MDEA		30 mass% MDEA	
	This study	(Li and Lie 1994[33])	This study	(Li and Lie 1994)
40	1.0087	1.0089	1.0172	1.0171
50	1.0037	1.0040	1.0116	1.0116
60	0.9984	0.9983	1.0057	1.0057
AAD%	**0.02**		**0.0082**	

AAD refers to average absolute deviation between two sources of data. AAD is calculated by the following formula:

$$AAD = \sum_{i=1}^{n} \frac{abs\left(x_{i,source\,1} - x_{i,source\,2}\right)}{n} \quad (7\text{-}16)$$

$$AAD\% = AAD * 100$$

Where $x_{i,source}$ refers to the value from the specified source and n represents the number of data. The uncertainty of the measured densities was estimated to be ± 0.0001 $g.cm^{-3}$, on the basis of comparison with literature data. Densities of 10 to 50 mass% MDEA aqueous solutions at temperature of 15 to 60 °C have been studied by (Alghawas et al. 1989), (Rinker et al. 1994) studied densities at the same concentration range but from 20 to 100 °C. (Li and Lie 1994) measured densities of 20 to 30 mass% MDEA aqueous solutions from 30 to 60 °C. (Bernal-García et al. 2003) measured densities of MDEA aqueous solutions over whole amine concentration range from 10 to 90 °C. (Hawrylak et al. 2000) measured densities of MDEA-water solution (0 to 100 wt% MDEA) at temperatures of 25, 35 and 45 °C. In this work density measurements were done for 10 to 90 mass% MDEA aqueous solutions from 40 to 80 °C. Measured results of this study and literature sources are tabulated in Table 7-3 to Table 7-7. As previously mentioned the uncertainty

[33](Li and Lie 1994) data were in good agreement with Alghawas et al.(Alghawas et al. 1989).

of the density measurements in this work was estimated to be $\pm 0.0001\ \mathrm{g.cm^{-3}}$ (± 0.01 %) on the basis of comparison with literature data.

Table 7-3. Density measurements for MDEA-H_2O systems at 40 °C

MDEA mass%	$\rho\ (g.cm^{-3})$					
	This study, Test 1	**This study, Test 2**	**This study, Test 3**	**This study, Average of tests (Reported value)**	**(Alghawas et al. 1989)**	**(Bernal-García et al. 2003)**
10.00	1.0001	1.0002	1.0002	1.0002	1.0007	1.000686
20.00	1.0087	1.0089	1.0087	1.0088	1.0091	Na*
29.88	1.0172	1.0173	1.0172	1.0172	1.018	1.017291
39.99	1.0256	1.0257	1.0260	1.0258	1.0266	1.025563
49.96	1.0330	1.0331		1.0330	1.0331	1.032899
60.00	1.0384	1.0387		1.0385		1.038284
64.27	1.0400	1.0403		1.0401		Na*
69.87	1.0416	1.0417		1.0417		1.041088
79.88	1.0394	1.0396		1.0395		1.039983
90.00	1.0352	1.0342		1.0347		1.033797
100.00	1.0251			1.0251		1.026523

Na: Not Available

Table 7-4. Density measurements for MDEA-H_2O systems at 50 °C

MDEA mass%	$\rho\ (g.cm^{-3})$				
	This study, Test 1	**This study, Test 2**	**This study, Average of tests (Reported value)**	**(Alghawas et al. 1989)**	**(Bernal-García et al. 2003)**
10.00	0.9956	0.9958	0.9957	0.996	0.996136
20.00	1.0038		1.0038	1.0047	Na*
29.88	1.0117		1.0117	1.013	1.011677
39.99	1.0195		1.0195	1.0204	1.019309
49.96	1.0265		1.0265	1.0269	1.025957
60.00	1.0313		1.0313		1.030901
64.27	1.0325		1.0325		Na*
69.87	1.0338		1.0338		1.033364
79.88	1.0326		1.0326		1.032233
90.00	1.0275		1.0275		1.026125
100.00	1.0176		1.0176		1.018877

Na: Not Available

Table 7-5. Density measurements for MDEA-H_2O systems at 60 °C

MDEA mass%	$\rho\ (g.cm^{-3})$				
	This study, Test 1	This study, Test 2	This study, Average of tests (Reported value)	(Alghawas et al. 1989)	(Bernal-García et al. 2003)
10.00	0.9901	0.99071	0.9904	0.9912	0.990972
20.00	0.9984		0.9984	0.9993	Na*
29.88	1.0058		1.0058	1.0069	1.005577
39.99	1.0129		1.0129	Na*	1.012651
49.96	1.0195		1.0195	1.0199	1.01864
60.00	1.0234		1.0234		1.023242
69.87	1.0259		1.0259		1.025407
79.88	1.0245		1.0245		1.024272
90.00	1.0194		1.0194		1.01833
100.00	1.0098		1.0098		1.01143

Na: Not Available

Table 7-6. Density measurements at for MDEA-H_2O systems 70 °C

MDEA mass%	$\rho\ (g.cm^{-3})$	
	This study	(Bernal-García et al. 2003)
10.00	0.9848	0.985251
20.00	0.9920	Na*
29.88	0.9989	0.999025
39.99	1.0057	1.005595
49.96	1.0112	1.011201
60.00	1.0154	1.015304
69.87	1.0177	1.017215
79.88	1.0163	1.016154
90.00	1.0114	1.010371
100.00	1.0018	1.003321

Na: Not Available

Table 7-7. Density measurements for MDEA-H_2O systems at 80 °C

MDEA mass%	$\rho\ (g.cm^{-3})$	
	This study	**(Bernal-García et al. 2003)**
10.00	0.9784	0.979011
20.00	0.9855	Na*
29.88	0.9922	0.992036
39.99	0.9984	0.998157
49.96	1.0035	1.003386
60.00	1.0071	1.007085
69.87	1.0092	1.008784
79.88	1.0079	1.007635
90.00	1.0032	1.002236
100.00	0.9946	0.995408

Na: Not Available

Figure 7-4 presents measured densities against MDEA mass% at four different temperatures. As expected, densities of aqueous MDEA solutions decrease with increasing temperature.

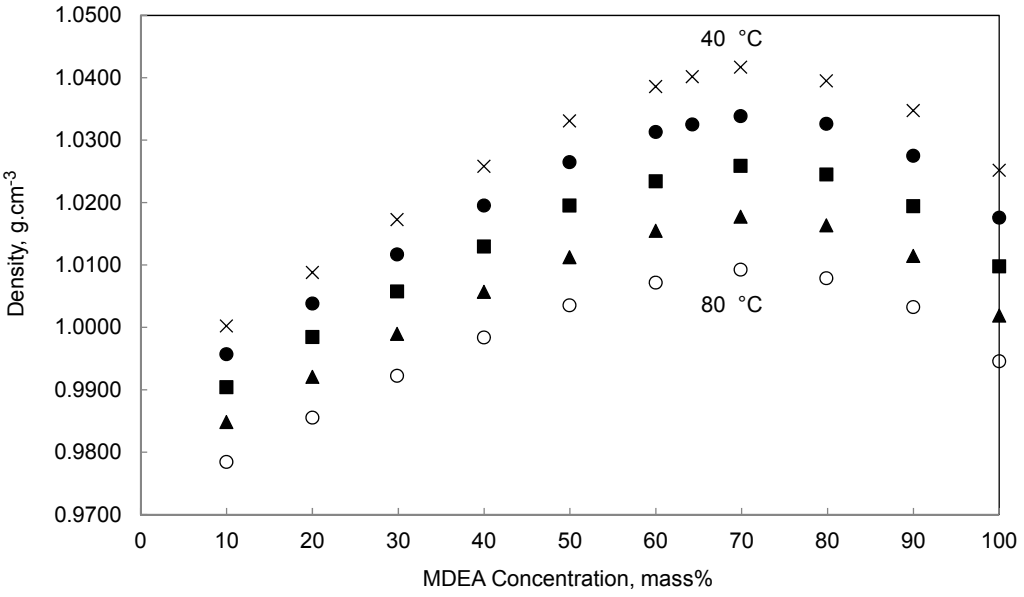

Figure 7-4. Measured densities of aqueous MDEA solutions at 40, 50, 60, 70 and 80 °C. ×, T = 40 °C; ●, T = 50 °C, ■, T = 60 °C; ▲, T = 70 °C; ○, T = 80 °C

7.5.3.2 VLE Experiments

This section illustrates CO_2 solubility data obtained for 10 different amine solutions with concentration of MDEA from 10 mass% to pure at five different temperatures, 40 to 80 °C and at constant total pressure of 110 kPa (1.1 bar). The experimental data are reported in tables and plotted in figures. Tables and figures contain the results obtained from volumetric and titration analyses. It is worth to note both volumetric and titration values presented in tables and figures are the average between tests. Generally most of the measurements were repeated two or three times (repeatability tests), and the average between tests was considered as the final reported value.

Table 7-8. Measured solubility of CO_2 in an aqueous solution of MDEA at 40.00 °C and 110.00kPa (1.10 bar)

MDEA mass%	$\alpha(\frac{\text{mol } CO_2}{\text{mol MDEA}})$[34]	
	Volumetric Analyses	Titration Analysis
10.06	0.91	1.13*
20.00	0.78	
29.88	0.76	
39.99	0.70	
49.96	0.62	
64.27	0.45	
69.87	0.38	
79.88	0.24	
90.00	0.12	
100.00	0.04	

**As mentioned, this value does not validate the volumetric method.*

Figure 7-5 shows the obtained experimental CO_2 solubility data at 40.00 °C and 110.00 kPa (1.1 bar). Results are plotted as loading against MDEA mass%.

[34] α represents loading, mole CO_2 per mole MDEA

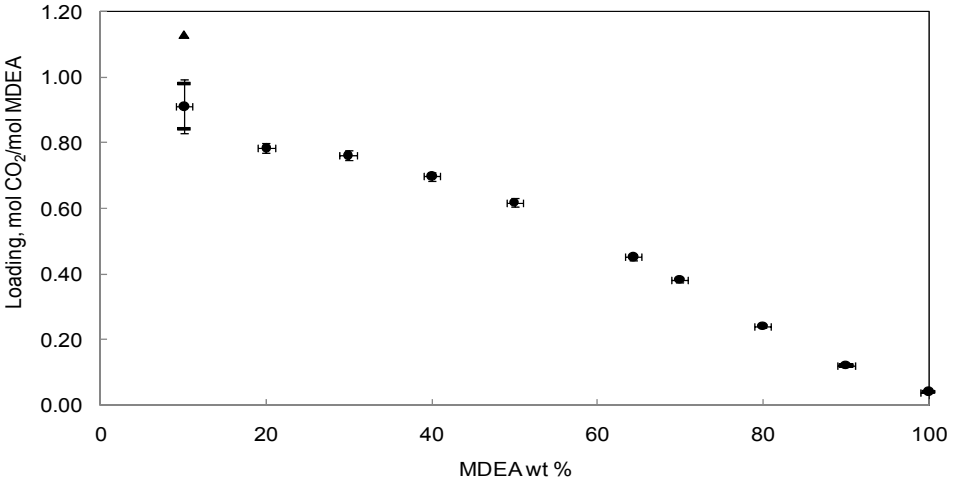

Figure 7-5. Measured solubility data of CO_2 at 40.00 °C and 110.00 kPa.●, Volumetric Analyses; ▲, Titration analysis; ═, Repeatability Tests

Table 7-9 shows the measured CO_2 solubility data at 50.00 °C and 110.00 kPa (1.1 bar).

Table 7-9. Measured solubility of CO_2 in an aqueous solution of MDEA at 50.00 °C and 110.00 kPa (1.10 bar)

MDEA mass%	$\alpha(\frac{\text{mol } CO_2}{\text{mol MDEA}})$	
	Volumetric Analyses	**Titration Analysis**
10.06	0.80	
20.00	0.67	
29.88	0.59	
39.99	0.52	0.54
49.96	0.42	
64.27	0.30	
69.87	0.24	
79.88	0.16	
90.00	0.07	
100.00	0.02	

Figure 7-6 presents the obtained experimental CO_2 solubility data at 50.00 °C and 110.00 kPa (1.1 bar).

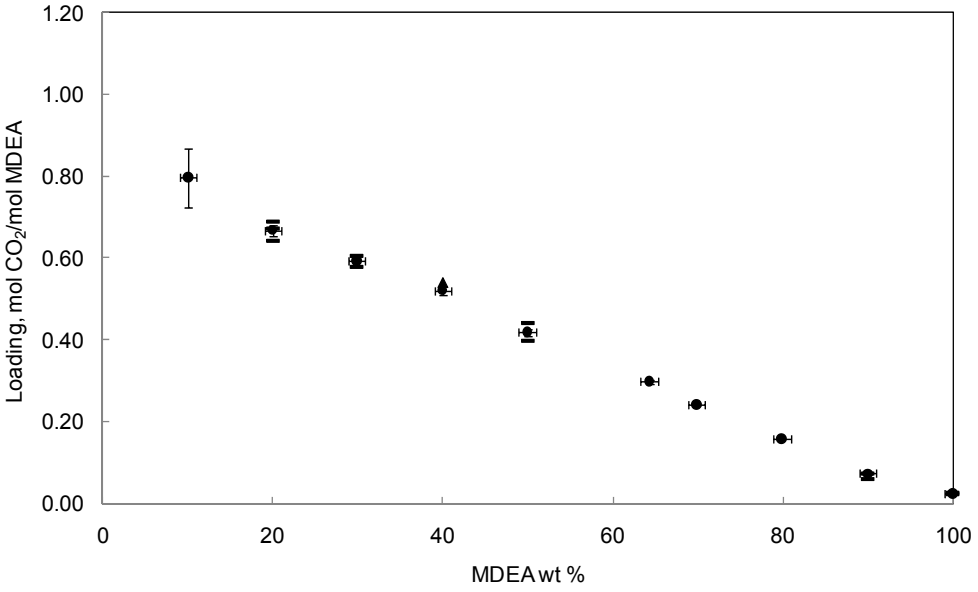

Figure 7-6. Measured solubility data of CO_2 at 50.00 °C and 110.00 kPa.●, Volumetric Analyses; ▲, Titration analysis; ▬, Repeatability Tests

Table 7-10 shows the measured CO_2 solubility data at 60.00 °C and 110.00 kPa (1.1 bar).

Table 7-10. Measured solubility of CO_2 in an aqueous solution of MDEA at 60.00 °C and 110.00 kPa (1.10 bar)

MDEA mass%	$\alpha(\frac{\text{mol } CO_2}{\text{mol MDEA}})$	
	Volumetric Analyses	**Titration Analysis**
10.00	0.72	0.98*
20.00	0.58	
29.88	0.47	
39.99	0.39	
49.96	0.31	
60.00	0.23	0.25
69.87	0.15	
79.88	0.08	
90.00	0.04	
100.00	0.01	

** As mentioned, this value does not validate the volumetric method.*

Figure 7-7 represents the experimental loading against MDEA concentration data at 60.00 °C and 110.00 kPa (1.10 bar).

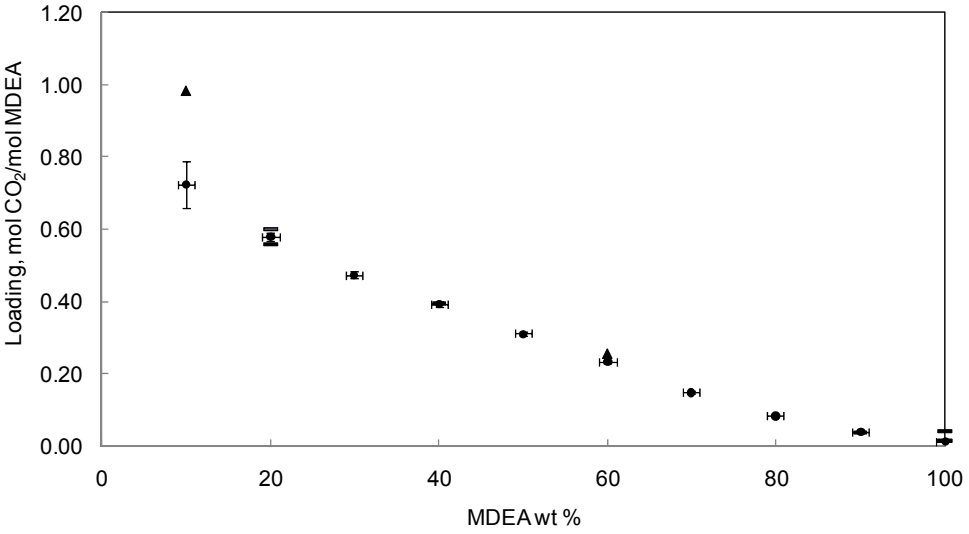

Figure 7-7. Measured solubility data of CO_2 at 60.00 °C and 110.00 kPa.●, Volumetric Analyses; ▲, Titration analyses; ▬, Repeatability Tests

Table 7-11 represents the measured CO_2 solubility data at 70.00 °C and 110.00 kPa (1.1 bar).

Table 7-11. Measured solubility of CO_2 in an aqueous solution of MDEA at 70.00 °C and 110.00 kPa (1.10 bar)

MDEA mass%	$\alpha(\frac{\text{mol } CO_2}{\text{mol MDEA}})$	
	Volumetric Analyses	Titration Analyses
10.00	0.53	0.93*
20.00	0.39	
29.88	0.34	
39.99	0.28	0.27
49.96	0.20	
60.00	0.14	
69.87	0.09	
79.88	0.05	
90.00	0.02	
100.00	0.01	0.01

** As mentioned, this value does not validate the volumetric method.*

Figure 7-8 shows the measured CO_2 solubility at 70.00 °C and 110.00 kPa (1.10 bar).

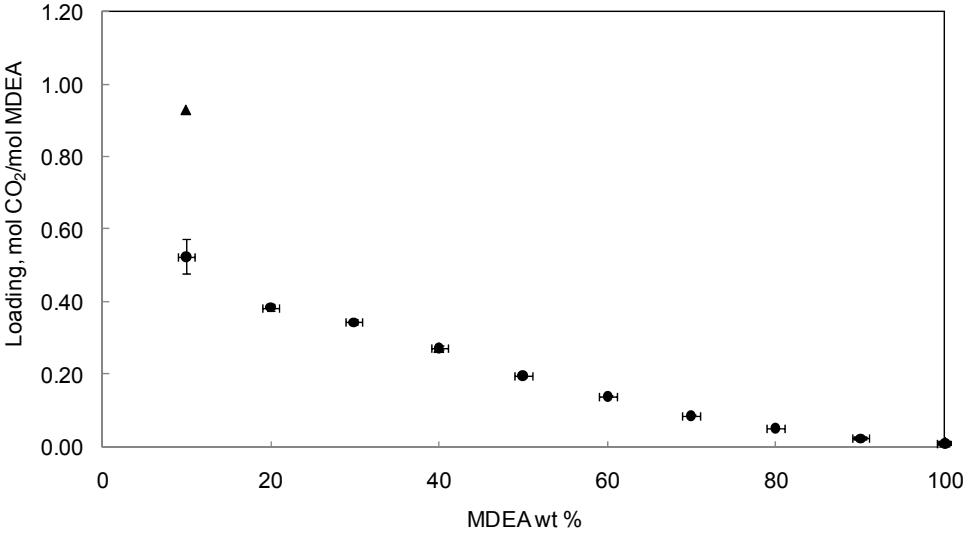

Figure 7-8. Measured solubility data of CO_2 at 70.00 °C and 110.00 kPa.●, Volumetric Analyses; ▲, Titration analyses; ═, Repeatability Tests

Measured CO_2 solubility data at 80.00 °C and 110.00 kPa (1.1 bar) are tabulated in Table 7-12.

Table 7-12. Measured solubility of CO_2 in an aqueous solution of MDEA at 80.00 °C and 110.00 kPa (1.10 bar)

MDEA mass%	$\alpha(\frac{\text{mol } CO_2}{\text{mol MDEA}})$	
	Volumetric Analyses	Titration Analyses
10.00	0.45	
20.00	0.28	
29.88	0.20	
39.99	0.15	0.21
49.96	0.11	0.10
60.00	0.07	0.05
69.87	0.05	
79.88	0.03	
90.00	0.01	0.01
100.00	0.01	0.008

Figure 7-9 represents measured values at 80.00 °C and 110.00 kPa (1.10 bar).

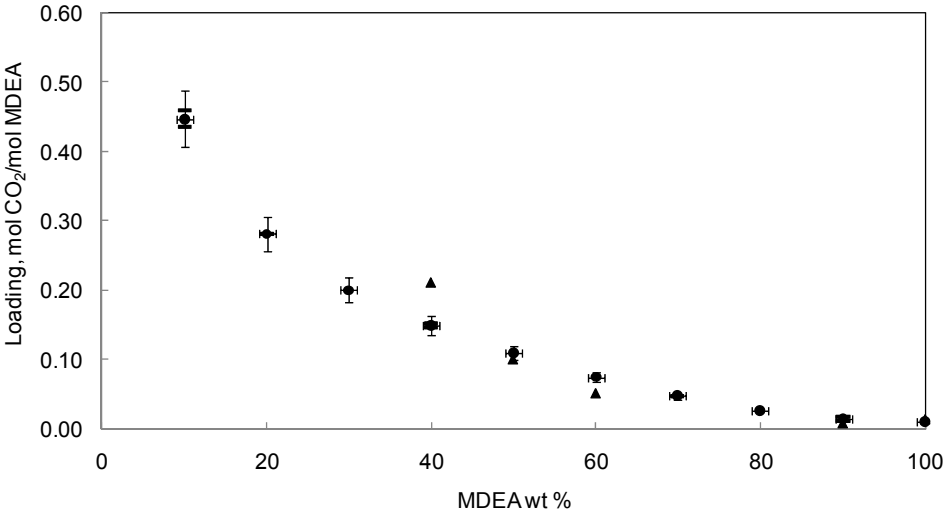

Figure 7-9. Measured solubility data of CO_2 at 80.00 °C and 110.00 kPa.●, Volumetric Analyses; ▲, Titration analyses; ═, Repeatability Tests

At 80 °C, there is a systematic error in the experiments that pulls all the measured points down. The probable reason behind this error is that with increasing temperature the volume of consumed CO_2 decreased to values comparable to cell volume. Therefore the accuracy of experimental data obtained from the cell decrease with increasing temperature. At 80 °C, the volume of consumed CO_2 became very small which caused a decline in accuracy of measured loadings.

As mentioned earlier due to some unknown reasons titration analysis results for 10 wt% MDEA were not accurate. Therefore titration results for 10 wt% MDEA were disregarded, however they were presented in the tables and figures.

7.5.4 Uncertainty Analysis

7.5.4.1 Equipment Uncertainties

The aqueous MDEA solutions were prepared in a flask by dissolving known amounts of amines in distilled degassed water. 500 cm^3 of solvent was prepared and kept in a sealed bottle, for each

experiment the required amount of solvent was taken from the bottle. The amine concentration in the aqueous solution was determined gravimetrically with an uncertainty of $\pm$ 0.0001 g.

The gas meter pressure was measured within $\pm$ 0.01 bar, gas meter temperature was measured with uncertainty of $\pm$ 0.01 °C and volume of gas meter was measured within uncertainty of $\pm$100 cm^3.

The temperature in the autoclave were measured with two thermocouples within $\pm$ 0.1 °C, the autoclave pressure was measured with calibrated pressure sensor within $\pm$ 0.01 bar.

7.5.4.2 Overall Uncertainties

The amount of CO_2 absorbed in the liquid phase was calculated based on volumetric method.

Volumetric Method

As it was mentioned earlier, liquid phase was mainly determined through the volumetric method. The main sources of uncertainty are listed below:

- Cell total volume: Cell total volume is one of the main sources of uncertainty of the solubility data obtained from the volumetric method. At conditions where absorption capacity is low, uncertainty in cell total volume is more pronounced. At high temperatures, low and high amine concentrations, the absorption capacity is low thus the volume of CO_2 that entered the autoclave is small and comparable to the cell total volume. Therefore the amount of CO_2 that entered the autoclave becomes almost similar to the amount of remained CO_2 in the vapor and consequently the amount of CO_2 in the liquid phase will be very small which leads to increase the inaccuracy of solubility data. In conclusion, at these conditions the uncertainty in the total volume played significant role in the overall uncertainty of loading. Notice that this uncertainty could be reduced by using more solvent. Higher amount of solvent leads to more CO_2 absorption.
- Volume measurements in the gas meter.
- Pressure measurements in the gas meter.
- Temperature measurements in the gas meter.
- Temperature measurements in the gas and liquid phase inside the autoclave.
- Mass of the solvent.
- Dead volume in the injection tube (tubing between valve 5.1 and 5.2).

- Isobaric condition of the measurements (autoclave and gas meter should had the same pressure).

Analysis over the mentioned sources of uncertainty showed that cell total volume and gas meter volume measurements are the main effective sources on overall loading uncertainty. However uncertainty in the gas meter volume were taken into account both in initial and final CO_2 volume and the difference between these values was used for loading calculations. The overall of uncertainty of results is estimated to be between 7% and 10% for 10 mass% MDEA and for 20 to 100 mass% MDEA the uncertainty is estimated to be 2%. However the error for the loading results at 80 °C is estimated to increase to 8% to 10%.

7.6 Model Validation

The results of CO_2 solubility experiments of this work were compared to the calculated values by the developed thermodynamic model. Developed thermodynamic model in chapter 5 has been used to predict CO_2 solubility in aqueous solutions of 10 to 90 mass% MDEA at temperatures of 40, 50, 60, 70 and 80 °C and total pressure of 110.00 kPa (1.10 bar). Notice that parameters of the developed model have not been fitted to the measured data of this study; data of this work were utilized to validate the developed model as a predictive tool. Table 7-13 to Table 7-17 summarize predicted and measured values at each studied temperature. Deviations between model and measured values are also shown in tables. Calculated and measured results are also depicted graphically in Figure 7-10 toFigure 7-14.

Table 7-13. Comparison between measured CO_2 solubility in aqueous MDEA and optimized Extended UNIQUAC model predictions at T = 40.00 °C and P = 110.00 kPa

MDEA Concentration, mass%	Experimental Loading* Values	Calculated Loading* Values	Bias Deviation**
10.06	0.91	0.93	0.02
20.003	0.78	0.87	0.08
29.88	0.76	0.81	0.05
39.99	0.70	0.74	0.04
49.96	0.62	0.63	0.01
64.27	0.45	0.43	-0.02
69.87	0.38	0.35	-0.04
79.88	0.24	0.20	-0.04
90	0.12	0.03	-0.09
AARD*%**		**15**	

** *Bias Deviation = loading $_{Calc}$- loading $_{Exp}$*

*** $AARD = \frac{1}{n}\sum_{i=1}^{n}\frac{|Loading_{Exp}-Loading_{Calc}|}{Loading_{Exp}}$

Figure 7-10 plotted model predictions and measured values at 40 °C.

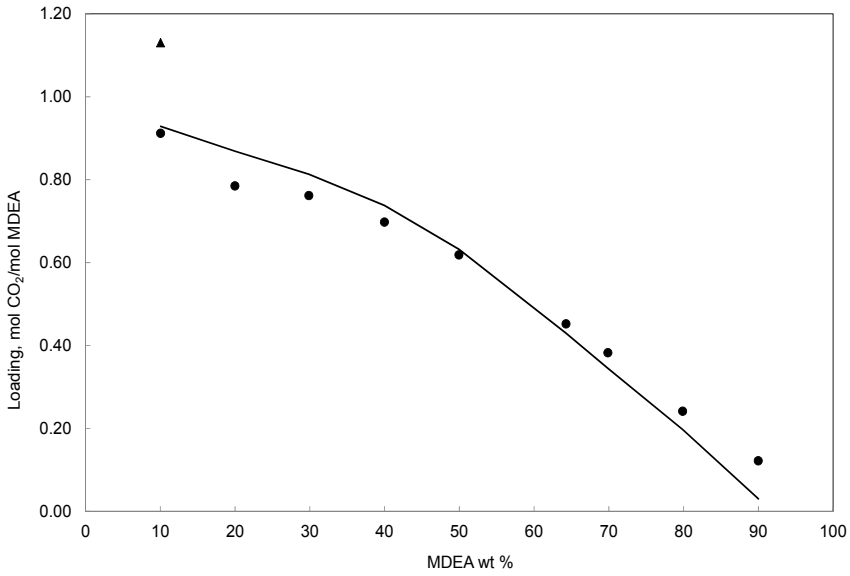

Figure 7-10. Comparison between optimized Extended UNIQUAC model predictions and measured values of CO_2 solubility at 40.00 °C and 110.00kPa. ●, Experimental (Volumetric Analysis); ▲, Experimental (Titration analysis); Solid Line, Extended UNIQUAC

Table 7-14. Comparison between measured CO_2 solubility in aqueous MDEA and optimized Extended UNIQUAC model predictions at T = 50.00 °C and P = 110.00 kPa

MDEA Concentration, mass%	Experimental Loading Values	Calculated Loading Values	Bias Deviation
10.06	0.80	0.86	0.06
20.003	0.67	0.78	0.11
29.88	0.59	0.70	0.11
39.99	0.52	0.61	0.09
49.96	0.42	0.50	0.08
64.27	0.30	0.32	0.02
69.87	0.24	0.25	0.01
79.88	0.16	0.13	-0.02
90	0.07	0.01	-0.06
AARD%[***]		**21**	

Figure 7-11 shows model predictions in comparison with the measured values at 50 °C.

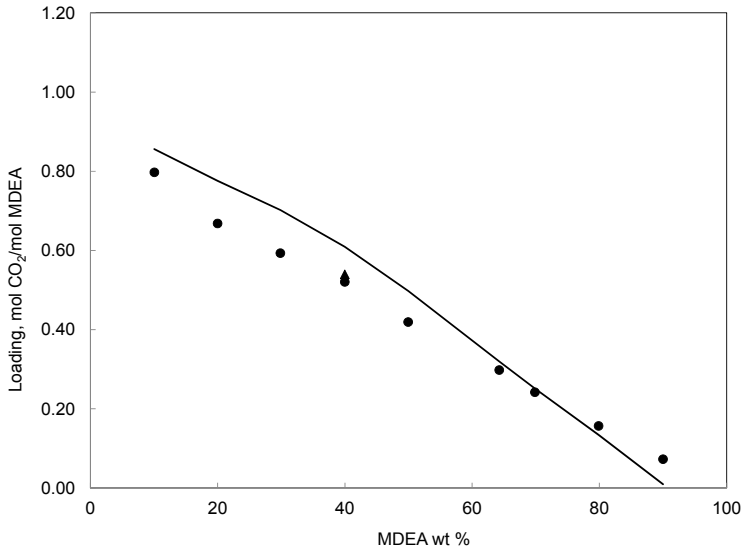

Figure 7-11. Comparison between optimized Extended UNIQUAC model predictions and measured values of CO_2 solubility at 50.00 °C and 110.00 kPa. ●, Experimental (Volumetric Analysis); ▲, Experimental (Titration analysis); Solid Line, Extended UNIQUAC

Table 7-15. Comparison between measured CO_2 solubility in aqueous MDEA and optimized Extended UNIQUAC model predictions at T = 60.00 °C and P = 110.00 kPa

MDEA Concentration, mass%	Experimental Loading Values	Calculated Loading Values	Bias Deviation
10	0.72	0.75	0.03
20.003	0.58	0.65	0.07
29.88	0.47	0.56	0.09
39.99	0.39	0.47	0.07
49.96	0.31	0.37	0.06
60	0.23	0.27	0.03
69.87	0.15	0.17	0.02
79.88	0.08	0.08	0.00
90	0.04	0.01	-0.03
AARD%[***]		**21**	

Figure 7-12 compares developed model prediction results with the measured values obtained in this study at 60 °C.

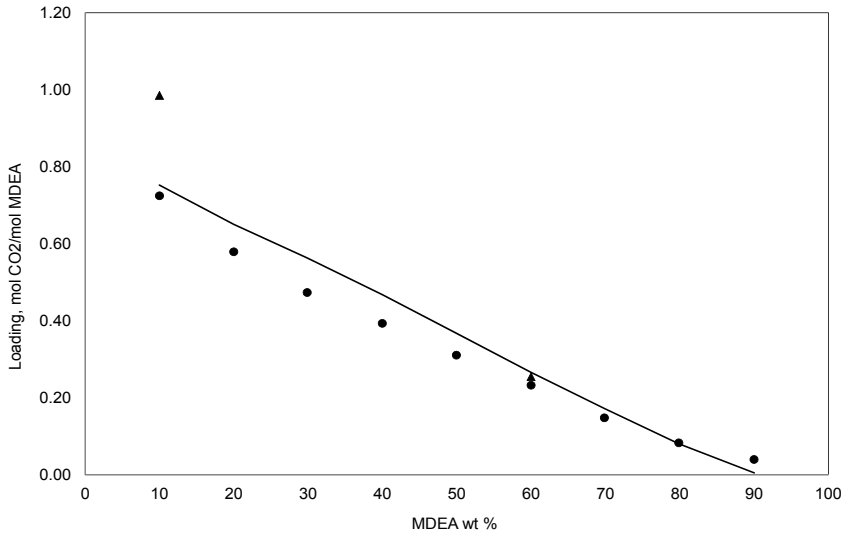

Figure 7-12. Comparison between optimized Extended UNIQUAC model predictions and measured values of CO_2 solubility at 60.00 °C and 110.00 kPa. ●, Experimental (Volumetric Analysis); ▲, Experimental (Titration analysis); Solid Line, Extended UNIQUAC

Table 7-16. Comparison between measured CO_2 solubility in aqueous MDEA and optimized Extended UNIQUAC model predictions at T = 70.00 °C and P = 110.00 kPa

MDEA Concentration, mass%	Experimental Loading Values	Calculated Loading Values	Bias Deviation
10	0.53	0.61	0.09
20.003	0.39	0.50	0.11
29.88	0.34	0.41	0.07
39.99	0.28	0.33	0.05
49.96	0.20	0.25	0.05
60	0.14	0.17	0.03
69.87	0.09	0.11	0.02
79.88	0.05	0.04	-0.01
90	0.02	0.003	-0.02
AARD%***		**29**	

Figure 7-13 represents predicted and measured CO_2 solubility at 70 °C.

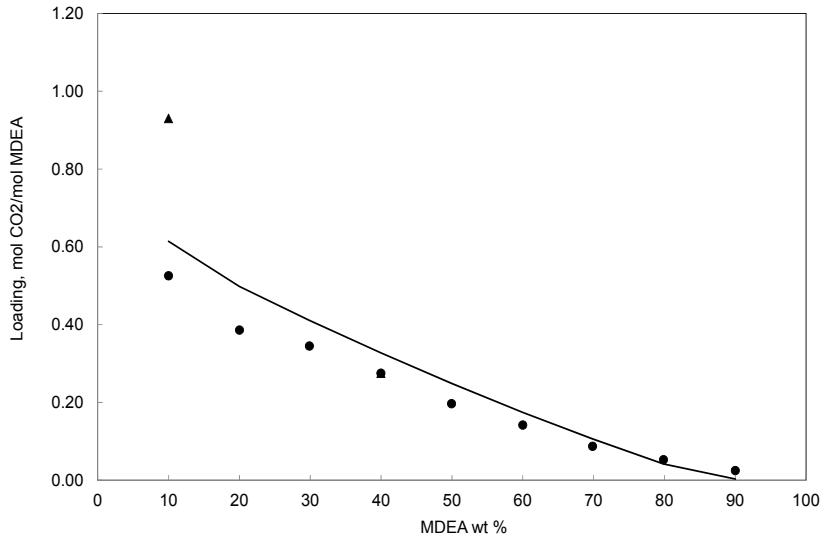

Figure 7-13. Comparison between optimized Extended UNIQUAC model predictions and measured values of CO_2 solubility at 70.00 °C and 110.00 kPa. ●, Experimental (Volumetric Analysis);▲, Experimental (Titration analysis); Solid Line, Extended UNIQUAC

Table 7-17. Comparison between measured CO_2 solubility in aqueous MDEA and optimized Extended UNIQUAC model predictions at T = 80.00 °C and P = 110.00 kPa

MDEA Concentration, mass%	Experimental Loading Values	Calculated Loading Values	Bias Deviation
10	0.45	0.45	0.00
20.003	0.28	0.34	0.06
29.88	0.20	0.27	0.07
39.99	0.15	0.20	0.06
49.96	0.11	0.15	0.04
60	0.07	0.10	0.03
69.87	0.05	0.06	0.01
79.88	0.03	0.02	0.00
90	0.01	0.002	-0.01
AARD%		**32**	

Figure 7-14 presents comparison between predicted values and measured points at 80 °C.

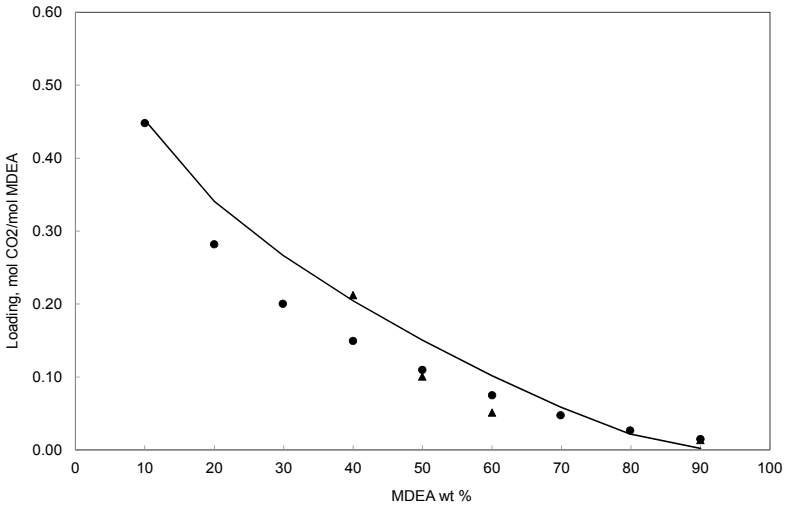

Figure 7-14. Comparison between optimized Extended UNIQUAC model predictions and measured values of CO_2 solubility at 80.00 °C and 110.00 kPa. ●, Experimental (Volumetric Analysis); ▲, Experimental (Titration analysis); Solid Line, Extended UNIQUAC

Comparison between developed model and measured values demonstrated that Extended UNIQUAC appropriately predict CO_2 solubility over the wide amine concentration range. Note that this section showed prediction results for conditions corresponds to measured values (10 to 90

mass% MDEA), Extended UNIQUAC calculation results for 5 and 75 mass% MDEA (data of (Rho et al. 1997)) were already shown in chapter 5. Comparison between Extended UNIQUAC prediction values and experimental data revealed that with rising temperature the deviation between model and experimental data increased. As already explained in section (7.5.3.2) the accuracy of experimental data obtained from the cell decline with increasing temperature. Hence the uncertainties of experiments at higher temperatures may explain the deviation between developed model and experimental data at elevated temperatures. Comparing experimental and modeling results showed that in the studied temperature and pressure range, for MDEA concentrations less than 70 mass%, the developed Extended UNIQUAC model overestimate the CO_2 solubility and from 70 mass% to 90 mass% MDEA, the model underestimate CO_2 solubility.

7.7 Results and Discussion

In this section measured CO_2 solubility data are compared graphically in Figure 7-15 and Figure 7-16. Figure 7-15 shows the loading as mole of absorbed CO_2 per mole of MDEA as a function of MDEA mass% at the different studied temperatures. Figure 7-16 also depicts the measurements graphically however in Figure 7-16 loading is defined as mole of absorbed CO_2 per kg of rich solvent[35]. Because the experiments were performed for different concentrations of MDEA solution, defining loading as mole of CO_2 per kg of rich solvent gives a more consistent basis for comparison between the results.

[35] Rich solvent is defined as the solvent which is loaded by CO_2.

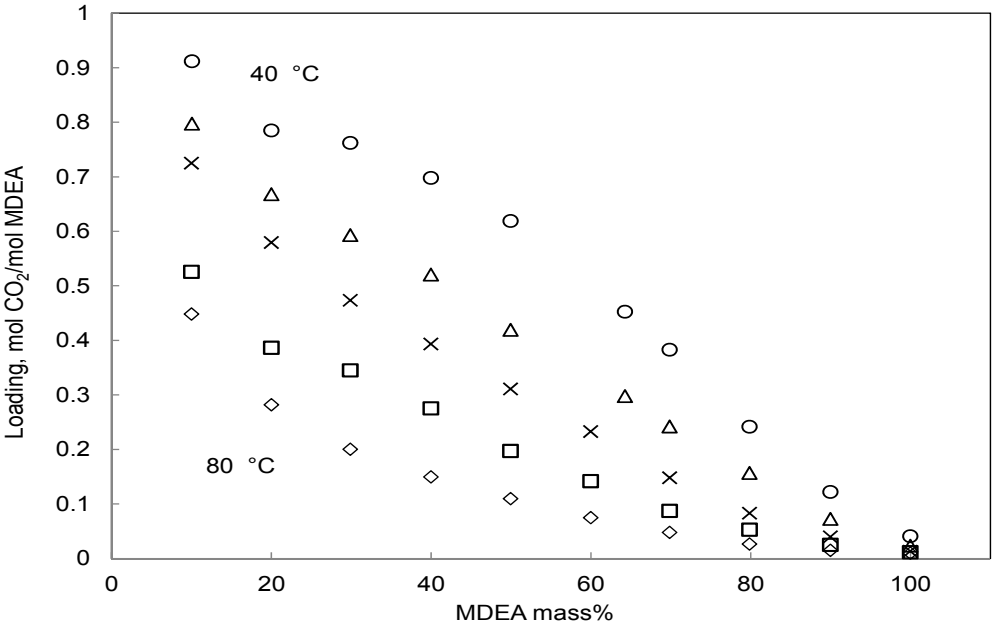

Figure 7-15. Comparison between measured CO_2 Solubility in aqueous MDEA at different temperatures . ○, T = 40 °C; △, T = 50 °C; ×, T = 60 °C; □, T = 70 °C; ◊, T = 80 °C

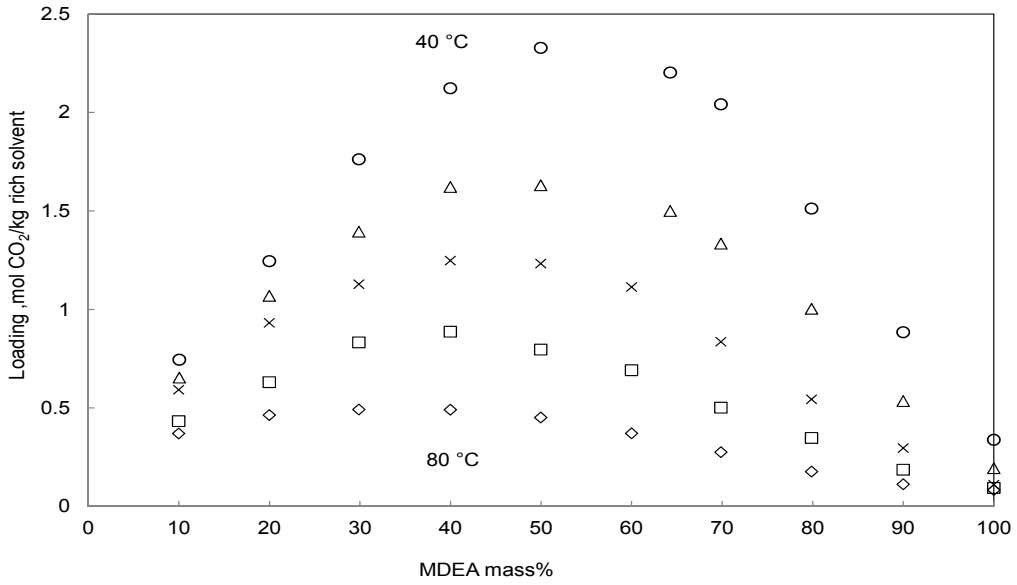

Figure 7-16. Comparison between measured CO_2 Solubility in aqueous MDEA at different temperatures. ○, T = 40 °C; △, T = 50 °C; ×, T = 60 °C; □, T = 70 °C; ◊, T = 80 °C

From the above figures, following observations can be made.

- For a given MDEA concentration and total pressure, the amount of CO_2 that is absorbed in the liquid phase (CO_2 gas solubility in the liquid phase) increase with decreasing the temperature. The behavior is expected since the reaction between CO_2 and MDEA is exothermic, thus at a temperature drop the reaction proceeds to the product side. Continuing the reaction to the product side, makes more molecular forms of CO_2 react with MDEA. Therefore more molecular CO_2, convert to soluble nonvolatile ionic species so that the amount of absorbed CO_2 will increase. As it can be seen from the figures the highest CO_2 is absorbed at the temperature of 40 °C. This observation is in accordance with industrial absorber condition, in industrial installation the most part of CO_2 is absorbed in the temperature range of 40 to 60 °C (Anufrikov et al. 2007). Absorption at lower temperatures of 40 °C is unfeasible because of the very slow rate of reaction.
- For a given temperature and total pressure, the highest absorption capacity was observed for MDEA mass% of 40 to 60.

7.8 Conclusions

To sum up, in this section density data for MDEA-H_2O solutions and new vapor-liquid equilibrium data for CO_2-MDEA-H_2O systems were presented. Density experiments were performed for aqueous MDEA solutions with MDEA concentration of 10 to 100 wt% and at 40 to 80°C. VLE experiments were carried out in a cell named low pressure cell for aqueous solutions of 10 to 100 mass% MDEA at constant pressure of 110 kPa (1.10 bar) and temperatures of 40 to 80 °C. In VLE experiments analysis of the liquid phase was avoided and loading was calculated from the volumetric data obtained from the cell. From these experiments it was concluded that the highest absorption capacity occurs at 40 °C and for MDEA concentration of 40 to 60 mass%. The results of VLE experiments were used to validate the developed thermodynamic model in chapter 5. The developed Extended UNIQUAC model showed promising results at the wide range of MDEA concentration. Overall, the new vapor-liquid equilibrium data obtained in this study covered a broad range of MDEA concentration. These data provide an opportunity for future work on validation of G^E thermodynamic models.

Chapter 8

Measurement: VLE of CO_2-MDEA-PZ-H_2O and Density of MDEA-PZ-H_2O

Chapter 8

Measurement: VLE of CO_2-MDEA-PZ-H_2O and Density of MDEA-PZ-H_2O

---

8 Measurement: VLE of CO_2-MDEA-PZ-H_2O and Density of MDEA-PZ-H_2O

8.1 Chapter Overview

As mentioned in previous chapters, MDEA which is a tertiary amine is the most useful amine in natural gas processing. The main advantages of MDEA over other kind of amines can be addressed as lower heat of reaction with acid gas, lower vapor pressure, lower corrosive tendency and capability of selective absorption of H_2S. Despite these benefits, MDEA has a slow rate of reaction with CO_2. To overcome this problem, piperazine (PZ) which is a cyclic amine is added to MDEA. The PZ activated MDEA is widely applied in CO_2 removal from natural gas processes. This blended solvent, which is called "activated MDEA solvent", has advantage of high rate of reaction of cyclic amine with CO_2 combined with lower heat of reaction and other benefits of MDEA which makes it a successful solvent for natural gas processing. Recently activated MDEA solvent has found widespread application in bulk removal of CO_2 (Derks et al. 2008). Accurate prediction of thermodynamic equilibrium between CO_2 and aqueous blend of MDEA-PZ is crucial for obtaining a good design of amine based acid gas removal process. This chapter presents new CO_2 solubility data in aqueous blend of MDEA-PZ at temperatures from 40 to 70 °C. In addition to VLE data, density data for mixtures of MDEA-PZ-H_2O at temperatures between 40 to 80 °C will be presented in this chapter.

8.1 The reason for Use of Piperazine

Piperazine is so called modifying additive which is used to improve efficiency of absorption of acid gases.

As mentioned earlier, even though the use of MDEA is beneficial compared to other amines, its slow rate of reaction with CO_2 makes it with limited usage of CO_2 absorption. Therefore in order to raise the absorption rate with CO_2, it was aimed to mix aqueous solution of MDEA with other kinds of amine. In 1985 it was suggested to add primary or secondary amine to aqueous solution of MDEA in order to simultaneously take advantage of the benefits of each kind of amine. However addition of primary and secondary amines increased the rate of reaction, but introduced negative factor of rising solvent corrosive power (Bishnoi 2000). In 1982 BASF introduced adding piperazine to aqueous solution of MDEA. The success of the so called"activated MDEA solvent" is based on the high reaction rate of CO_2 with piperazine (Derks et al. 2008). Piperazine is a cyclic amine which has high capacity of protonation (each molecule of piperazine can add two protons) and it can form three different carbamate ions with CO_2. Due to the mentioned features, adding piperazine to aqueous solutions of MDEA highly improve the rate of CO_2 absorption. Addition of piperazine also increases the selectivity of absorption of hydrogen sulfide in a mixture of carbon dioxide and hydrogen sulfide. Note that piperazine increases the heat required for regeneration, but not as much as other common activators. It is worthwhile to mention that addition of piperazine almost does not introduce any negative factor. These advantages made piperazine as a frequent additive to aqueous solutions of MDEA in natural gas treatment process.

8.2 Experimental Design

Table 8-1 summarizes the available published experimental VLE data for CO_2-PZ-MDEA-H_2O system. Notice that collected data in Table 8-1 are gathered according to the best of author knowledge and at the time of this work.

Table 8-1. Published VLE data for CO_2-MDEA-PZ-H_2O systems

MDEA Concentration, wt%	PZ Concentration, wt%	T, °C	P_{CO_2}, kPa	Reference
18, 33, 37, 43, 54.5	1.5, 3, 5, 6, 13	30 to 90	13.16 to 935.3	(Liu et al. 1999)
46	5	40, 80	0.03 to 7.48	(Bishnoi and Rochelle 2002)
16.8	12.1	80	200 to 6400	(Kamps et al. 2003)
21, 22, 23	0.1, 0.4	40, 60, 80	0.1 to 95.78	(Ali and Aroua 2004)
24, 29, 35	3.1, 7.4, 11.7	40,55,70	27.79 to 3938.43	(Jenab et al. 2005)
18.5, 30, 44.2	8.5, 10.3, 11.8	40, 60, 80, 120	200 to 11900	(Böttger et al. 2009)
17 to 47.9	4.1 to 18.8	26.1 to 46.8	0.31 to 146.8	(Speyer et al. 2010)
50	0.9, 2.2, 4.4	101.05 to 104.95	3.83 to 76.77	(Xu et al. 1998)
6, 25, 46	5, 6, 13	25, 30, 40, 50	0.25 to 10.2	(Derks et al. 2010)

As it can be observed from Table 8-1, compared to CO_2-MDEA-H_2O system, there are limited equilibrium data available for CO_2-MDEA-PZ-H_2O mixture. Available VLE data for CO_2-MDEA-PZ-H_2O systems are limited to MDEA concentrations less than 55 mass%. The aim of the present study is to extend the experimental data base available in open literature for the solubility of CO_2 in aqueous mixtures of MDEA and piperazine at wider range of MDEA concentrations. New data are reported herein for CO_2 solubility in aqueous mixtures of MDEA and piperazine with MDEA mass% of 25 to 75, piperazine mass% of 5 and 10, at constant pressure of 110 kPa (1.10 bar) and at temperatures between 40 to 70 °C. The results of this study could be also used to evaluate formerly published thermodynamic models.

8.3 Experimental Section

The chemicals used in this work include MDEA (Acros Organics, ≥ 99 % pure) ,Piperazine Hexahydrate (Fisher Scientific, ≥ 98 % pure), Piperazine Anhydrous (MERCK, ≥ 99 % pure), CO_2 (Yara, ≥ 99 % pure) and Acetone (VWR (BDH PROLABO), ≥ 99 % pure). All chemicals were used without any further purification. Experiments were performed using the same apparatus as in chapter 7. The experimental procedure is similar to what is described in chapter 7. Blended solvents with 40 mass% MDEA-10 mass% PZ, 45 mass% MDEA-5 mass% PZ and 35 mass%

MDEA-5 mass% PZ were prepared using piperazine hexahydrate chemical and the rest were made with piperazine anhydrous. Note that in these experiments 250 $cm^3$of solvent was prepared and kept in a sealed closed bottle, for each experiment the required amount of solvent was taken from the bottle. Recall from chapter 7, due to set up restrictions (the absorption capacity decrease with increasing temperature, and at 80 °C the amount of CO_2 interred in the cell is small and comparable to cell total volume), data obtained from the low pressure cell equipment at 80 °C were not accurate enough. Therefore in this chapter the maximum temperature that data are measured for is 70 °C.

8.4 Results

The VLE experiments for CO_2-MDEA-PZ-H_2O system as described in section 8.2 were performed at 110 kPa (1.1 bar), constant total pressure, temperatures from 40 to 70 °C and for 25, 35, 45, 65, 75 mass% MDEA concentrations mixed with 5 and 10 mass% PZ. As illustrated in section 7.5.2 information on density of solutions is required for converting volume based data to mass based data, therefore density experiments were carried out for MDEA-PZ-H_2O solutions for 25 to 75 wt% MDEA mixed with 5 and 10 wt% PZ, at temperatures between 40 to 80 °C. The remainder of this section explains results of density and VLE measurements in figures and tables. It is noted that all the VLE data reported in this chapter are obtained from the volumetric method as already explained in chapter 7.

8.4.1 Density Experiments

Prior to VLE experiments, density of prepared aqueous activated MDEA solutions were measured using Anton-Paar (DMA 4500 M) density meter. The procedure and equipment was already validated for density measurements of aqueous MDEA solutions. To the best of author knowledge and at the time of this work only two articles reported density of aqueous blend of MDEA-PZ. (Paul and Mandal 2006) measured density of aqueous MDEA-PZ mixtures between 14.85 to 59.85 °C and for mass percent ratio PZ:MDEA of 3:27, 6:24, 9:21 and 12:18. (Derks et al. 2008) determined density of aqueous blends of MDEA-PZ at temperatures from 20 to 50 °C and with concentration of MDEA at 11.9, 23.8, 35.7 and 47.6 mass% while concentration of PZ vary between 0 to 8.6 mass%. In this work density measurements were performed for aqueous solutions of 25 to 75 mass% MDEA mixed with 5 and 10 mass% PZ and at temperatures between 40 to 80 °C. To the best of author knowledge densities of aqueous mixtures of MDEA and PZ at the conditions studied in this study were not published in literature so far. Measurement results are reported in Table 8-2 to Table 8-6 and plotted in Figure 8-1 and Figure 8-2.

Table 8-2. Density measurements for MDEA-PZ-H_2O systems at 40 °C

MDEA mass%	PZ mass%	ρ ($g.cm^{-3}$)			
		Test 1	Test 2	Test 3	Average of tests (Reported value)
25.05	5.00	1.0161	1.0160		1.0160
24.97	9.93	1.0191	1.0194		1.0192
35.33	5.34	1.0250	1.0256		1.0253
35.02	9.96	1.0275	1.0281		1.0278
45.00	4.99	1.0302	1.0325		1.0314
44.90	9.96	1.0341			1.0341
64.94	4.99	1.0401	1.0404		1.0403
64.99	9.98	1.0391	1.0391		1.0391
74.94	4.99	1.0391	1.0390	1.0391	1.0391
74.90	9.99	1.0354	1.0358		1.0356

Table 8-3. Density measurements for MDEA-PZ-H_2O systems at 50 °C

MDEA mass%	PZ mass%	ρ ($g.cm^{-3}$)		
		Test 1	Test 2	Average of tests (Reported value)
25.05	5.00	1.0103	1.0105	1.0104
24.97	9.93	1.0132		1.0132
35.33	5.34	1.0187		1.0187
35.02	9.96	1.0208	1.0215	1.0211
45.00	4.99	1.0251		1.0251
44.90	9.96	1.0270	1.0276	1.0273
64.94	4.99	1.0324		1.0324
64.99	9.98	1.0311	1.0312	1.0311
74.94	4.99	1.0312		1.0312
74.90	9.99	1.0275		1.0275

Table 8-4. Density measurements for MDEA-PZ-H_2O systems at 60 °C

MDEA mass%	PZ mass%	ρ ($g.cm^{-3}$)			
		Test 1	Test 2	Test 3	Average of tests (Reported value)
25.05	5.00	1.0042	1.0044		1.0043
24.97	9.93	1.0067			1.0067
35.33	5.34	1.0120			1.0120
35.02	9.96	1.0138			1.0138
45.00	4.99	1.0179			1.0179
44.90	9.96	1.0193			1.0193
64.94	4.99	1.0243			1.0243
64.99	9.98	1.0231			1.0231
74.94	4.99	1.0231	1.0230	1.0230	1.0230
74.90	9.99	1.0195			1.0195

Table 8-5. Density measurements for MDEA-PZ-H_2O systems at 70 °C

MDEA mass%	PZ mass%	ρ ($g.cm^{-3}$)			
		Test 1	Test 2	Test 3	Average of tests (Reported value)
25.05	5.00	0.9976			0.9976
24.97	9.93	0.9998			0.9998
35.33	5.34	1.0048			1.0048
35.02	9.96	1.0064			1.0064
45.00	4.99	1.0102			1.0102
44.90	9.96	1.0115			1.0115
64.94	4.99	1.0161	1.0163		1.0162
64.99	9.98	1.0149			1.0149
74.94	4.99	1.0150			1.0150
74.90	9.99	1.0113	1.0114		1.0113

Table 8-6. Density measurements for MDEA-PZ-H_2O systems at 80 °C

MDEA mass%	PZ mass%	ρ (g. cm^{-3})		
		Test 1	Test 2	Average of tests (Reported value)
25.05	5.00	0.9908		0.9908
24.97	9.93	0.9927		0.9927
35.33	5.34	0.9973	0.9977	0.9975
35.02	9.96	0.9987		0.9987
45.00	4.99	1.0024		1.0024
44.90	9.96	1.0034		1.0034
64.94	4.99	1.0078		1.0078
64.99	9.98	1.0064		1.0064
74.94	4.99	1.0064	1.0063	1.0064
74.90	9.99	1.0031	1.0030	1.0031

Figure 8-1 presents measured densities for aqueous blended mixtures of MDEA and 5 wt% PZ. Results are plotted against MDEA mass% at five different temperatures. As expected, densities of aqueous blended MDEA-PZ solutions decrease with increasing temperature.

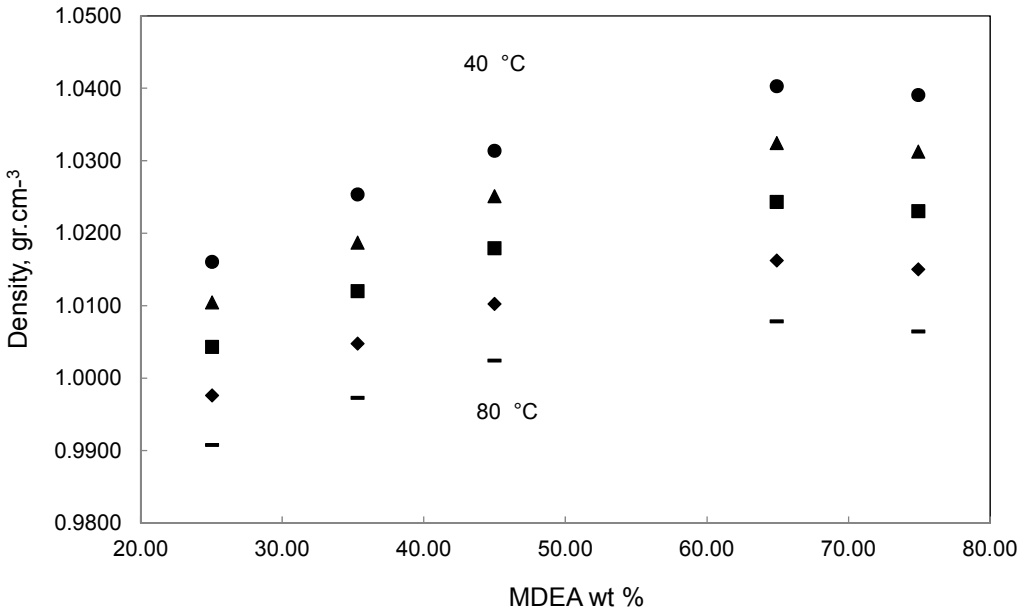

Figure 8-1. Measured densities of aqueous MDEA-PZ (5 mass% PZ) solutions at various temperatures. ● (T = 40 °C), ▲ (T = 50 °C), ■ (T = 60 °C), ♦ (T = 70 °C), - (T = 80 °C)

Figure 8-2 presents measured densities for aqueous blended mixtures of MDEA and 10 wt% PZ. Results are plotted against MDEA mass% at five different temperatures. The same behavior is seen in density as a function of temperature.

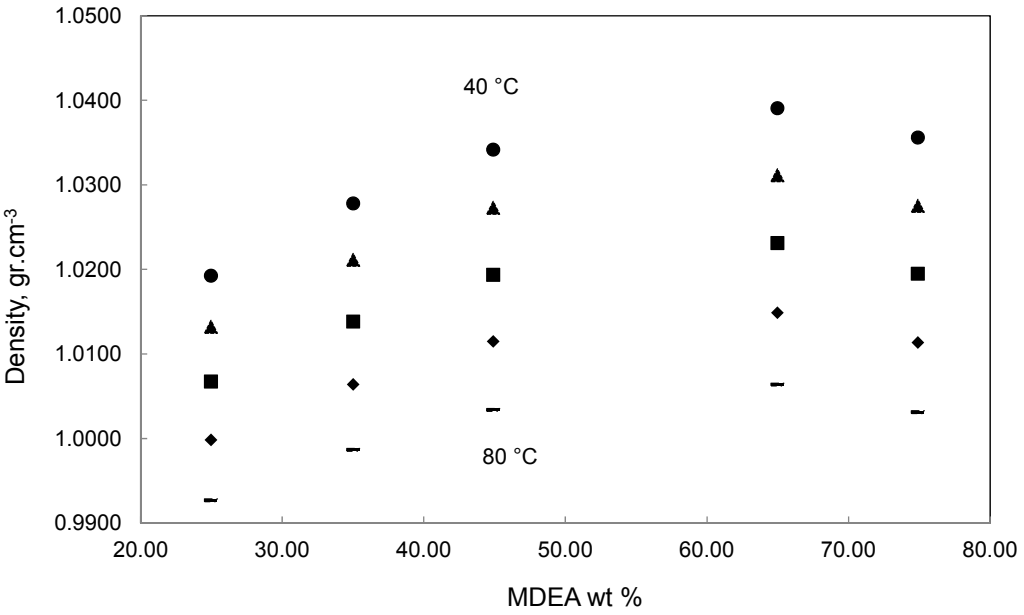

Figure 8-2. Measured densities of aqueous MDEA-PZ (10 mass% PZ) solutions at various temperatures. ● (T = 40 °C), ▲ (T = 50 °C), ■ (T = 60 °C), ♦ (T = 70 °C), - (T = 80 °C)

8.4.2 VLE Experiments

This section illustrates CO_2 solubility data obtained for blend mixtures of MDEA and PZ with concentration of MDEA varying from 25 to 75 mass% while concentration of PZ is kept constant at 5 and 10 mass%, at four different temperatures, 40 to 70 °C and at constant total pressure of 110 kPa (1.10 bar). It is reminded that values presented in tables and figures are average values between repeated tests. Though it is of high interest to compare the measured data with the data provided by other laboratories, unfortunately to the best of author knowledge and at the time of this work, there is no data available in the literature that was measured at the same conditions of this study. Hence, the equipment and experimental procedure (volumetric analysis) were validated in the comparison with the results of Statoil laboratories as explained in chapter 7.

Table 8-7. Measured solubility data of CO_2 in an aqueous blended mixtures of MDEA and PZ at 40.00 °C and 110.00 kPa (1.10 bar)

MDEA mass%	PZ mass%	$\alpha(\frac{\text{mol } CO_2}{\text{mol amine}})$[36]	$\acute{\alpha}(\frac{\text{mol } CO_2}{\text{kg rich solvent}})$[37]
25.05	5.00	0.76	1.86
24.97	9.93	0.77	2.25
35.33	5.34	0.71	2.29
35.02	9.96	0.73	2.63
45.00	4.99	0.66	2.55
44.90	9.96	0.68	2.92
64.94	4.99	0.42	2.30
64.99	9.98	0.43	2.55
74.94	4.99	0.33	2.04
74.90	9.99	0.34	2.29

Figure 8-3 shows the obtained experimental CO_2 solubility data at 40.00 °C and 110.00 kPa. Results are plotted as loading against MDEA mass%, while loading is defined as mole CO_2 per kg of rich solvent.

[36] α represents loading, mole CO_2 per mole amine (where mole amine is the sum of MDEA mole numbers and PZ mole numbers)

[37] $\acute{\alpha}$ represents loading, mole CO_2 per kg rich solvent (where rich solvent indicates the loaded solvent (mixture of CO_2-MDEA-PZ-H_2O))

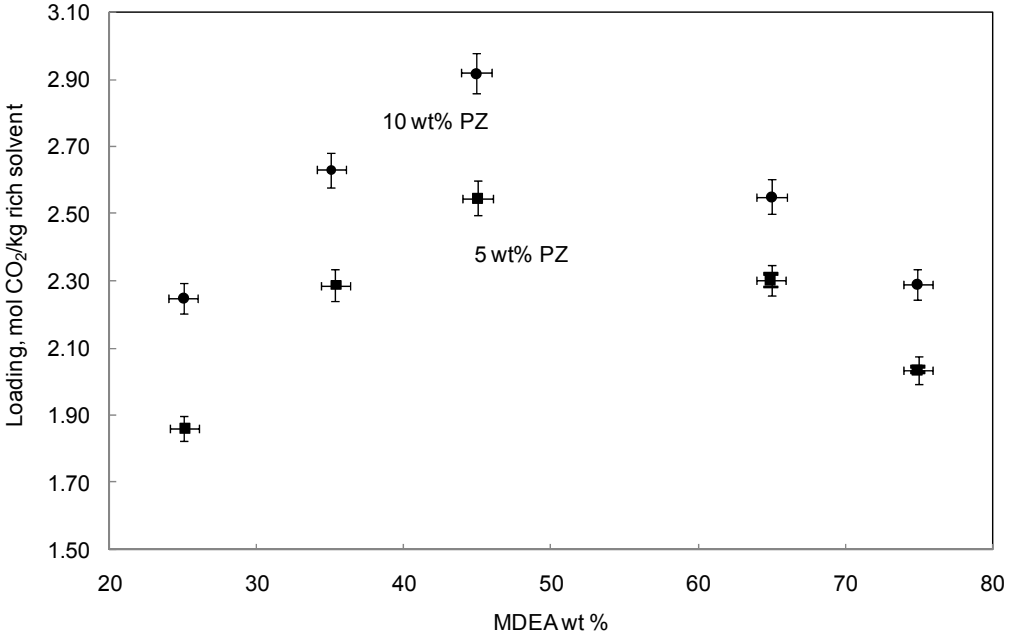

Figure 8-3. Measured solubility of CO_2in blended mixtures of MDEA-PZ at 40.00 °C and 110.00 kPa.■, 5 mass% PZ; ●, 10 mass% PZ; ―, Repeatability Tests. Error bars are added to the measured points.

Table 8-8 presents the measured CO_2 solubility data at 50 °C.

Table 8-8. Measured solubility of CO_2 in an aqueous blended of MDEA and PZ at 50.00 °C and 110.00 kPa (1.10 bar)

MDEA mass%	PZ mass%	$\alpha(\frac{\text{mol } CO_2}{\text{mol amine}})$	$\acute{\alpha}(\frac{\text{mol } CO_2}{\text{kg rich solvent}})$
25.05	5.00	0.68	1.69
24.97	9.93	0.69	2.05
35.33	5.34	0.59	1.94
35.02	9.96	0.61	2.26
45.00	4.99	0.52	2.05
44.90	9.96	0.55	2.41
64.94	4.99	0.34	1.88
64.99	9.98	0.36	2.15
74.94	4.99	0.27	1.69
74.90	9.99	0.29	1.96

Figure 8-4 presents the obtained experimental CO_2 solubility data at 50.00 °C and 110.00 kPa.

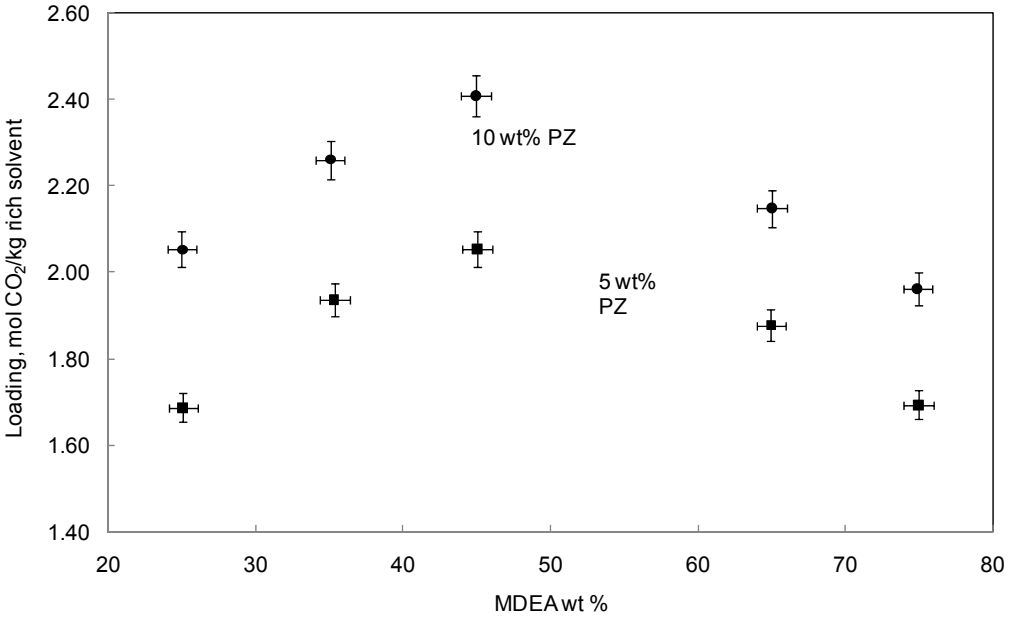

Figure 8-4. Measured solubility of CO_2 in blended mixtures of MDEA-PZ at 50.00 °C and 110.00 kPa.■, 5 mass% PZ; ●, 10 mass% PZ; —, Repeatability Tests. Error bars are added to the measured points.

Table 8-9 shows the measured values at 60 °C.

Table 8-9. Measured solubility of CO_2 in an aqueous blended of MDEA and PZ at 60.00 °C and 110.00 kPa (1.10 bar)

MDEA mass%	PZ mass%	$\alpha(\frac{\text{mol } CO_2}{\text{mol amine}})$	$\acute{\alpha}(\frac{\text{mol } CO_2}{\text{kg rich solvent}})$
25.05	5.00	0.60	1.51
24.97	9.93	0.61	1.82
35.33	5.34	0.53	1.75
35.02	9.96	0.53	1.99
45.00	4.99	0.46	1.84
44.90	9.96	0.47	2.10
64.94	4.99	0.26	1.48
64.99	9.98	0.31	1.88
74.94	4.99	0.20	1.28
74.90	9.99	0.24	1.64

Figure 8-5 represents the experimental loading against MDEA concentration data at 60.00 °C and 110.00 kPa.

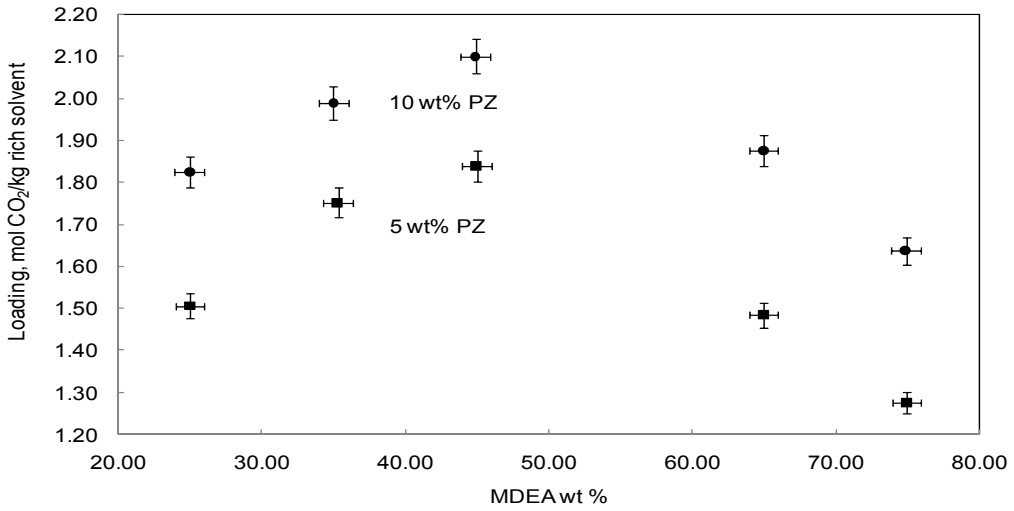

Figure 8-5. Measured solubility of CO_2 in blended mixtures of MDEA-PZ at 60.00 °C and 110.00 kPa.■, 5 mass% PZ; ●, 10 mass% PZ; —, Repeatability Tests. Error bars are added to the measured points.

Table 8-10 shows measured CO_2 solubility data at 70 °C

Table 8-10. Measured solubility of CO_2 in an aqueous blended of MDEA and PZ at 70.00 °C and 110.00 kPa (1.10 bar)

MDEA mass%	PZ mass%	$\alpha(\frac{\text{mol } CO_2}{\text{mol amine}})$	$\acute{\alpha}(\frac{\text{mol } CO_2}{\text{kg rich solvent}})$
25.05	5.00	0.45	1.14
24.97	9.93	0.49	1.50
35.33	5.34	0.37	1.26
35.02	9.96	0.43	1.62
45.00	4.99	0.32	1.31
44.90	9.96	0.35	1.62
64.94	4.99	0.20	1.15
64.99	9.98	0.24	1.49
74.94	4.99	0.15	0.99
74.90	9.99	0.19	1.36

Figure 8-6 shows the measured CO_2 solubility at 70.00 °C and 110.00 kPa.

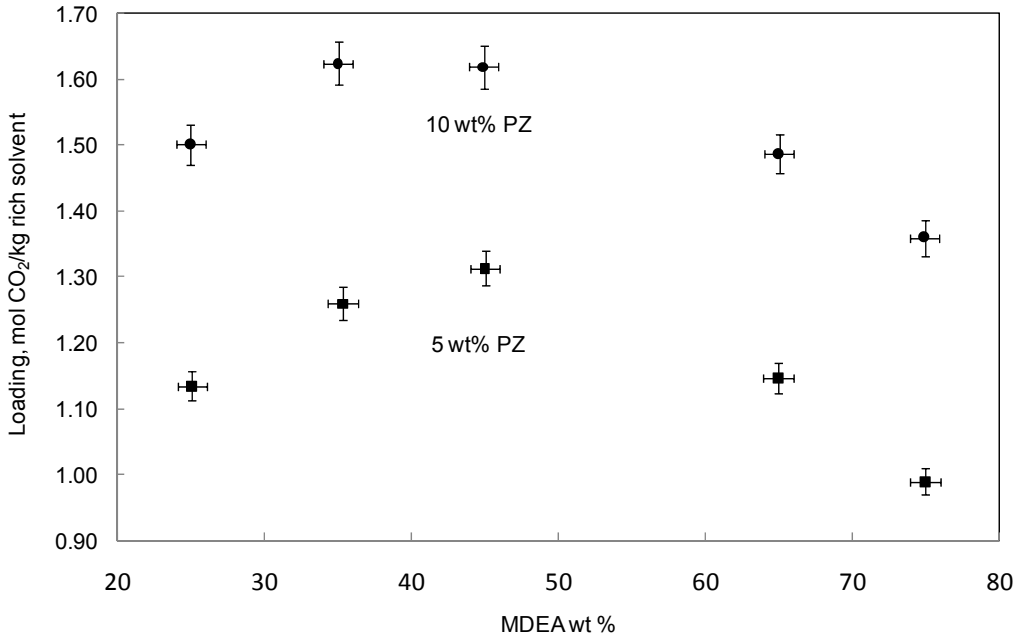

Figure 8-6. Measured solubility data of CO_2 in blended mixtures of MDEA-PZ at 70.00 °C and 110.00 kPa.■, 5 mass% PZ; ●, 10 mass% PZ; ═, Repeatability Tests. Error bars are added to the measured points.

The main sources of uncertainty of the results are as discussed in section 7.5.4. However, it is worthwhile to mention that the CO_2 absorption capacity in aqueous blend of MDEA-PZ is higher compared to aqueous MDEA. Therefore the volume of CO_2 that entered the autoclave is much bigger than the cell total volume and consequently the amount of CO_2 in the liquid phase become greater than the amount of CO_2 in the vapor phase. Hence in case of CO_2 solubility measurements in aqueous activated MDEA, total volume uncertainty has smaller effect in overall uncertainty compared to CO_2 solubility measurements in aqueous MDEA. The overall uncertainty of results is estimated to be about 2 %.

8.5 Results and Discussion

The enhancing effect of PZ on the solubility of CO_2 in aqueous MDEA can be seen in Figure 8-7 to Figure 8-10 where measured data for different PZ concentrations are compared. It is notable that these measured data were provided in chapter 7 and previous sections of this chapter.

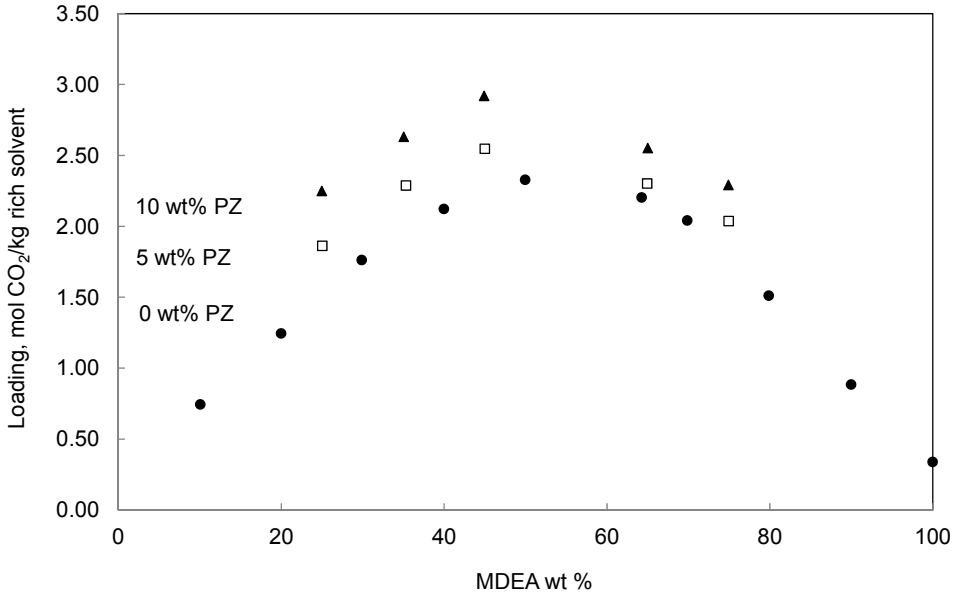

Figure 8-7. Comparison between measured CO_2 solubility data in aqueous MDEA and in presence of 0, 5 and 10 mass% PZ at 40.00 °C and 110.00 kPa. ● (0 wt% PZ), □ (5 wt% PZ), ▲ (10 wt% PZ)

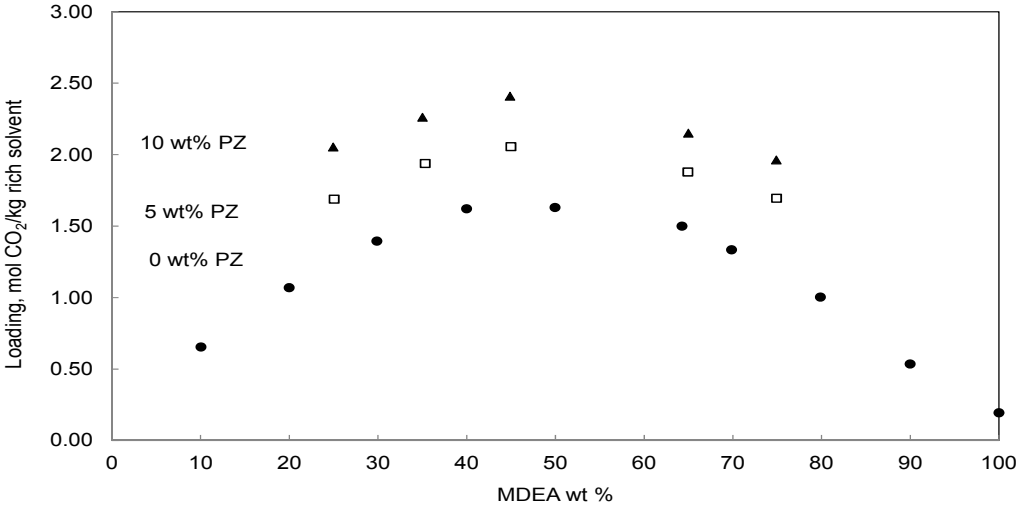

Figure 8-8. Comparison between measured CO_2 solubility data in aqueous MDEA and in presence of 0, 5 and 10 mass% PZ at 50.00 °C and 110.00 kPa. ● (0 wt% PZ), □ (5 wt% PZ), ▲ (10 wt% PZ)

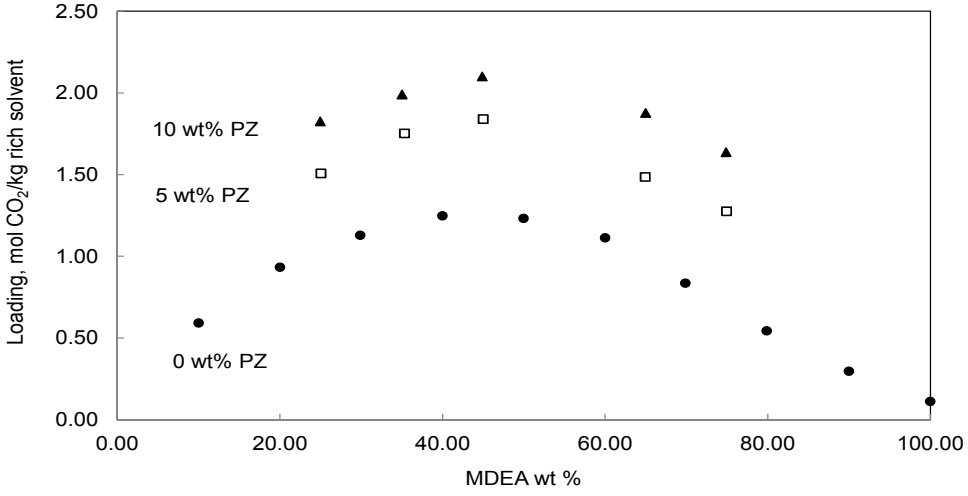

Figure 8-9. Comparison between measured CO_2 solubility data in aqueous MDEA and in presence of 0, 5 and 10 mass% PZ at 60.00 °C and 110.00 kPa. ● (0 wt% PZ), □ (5 wt% PZ), ▲ (10 wt% PZ)

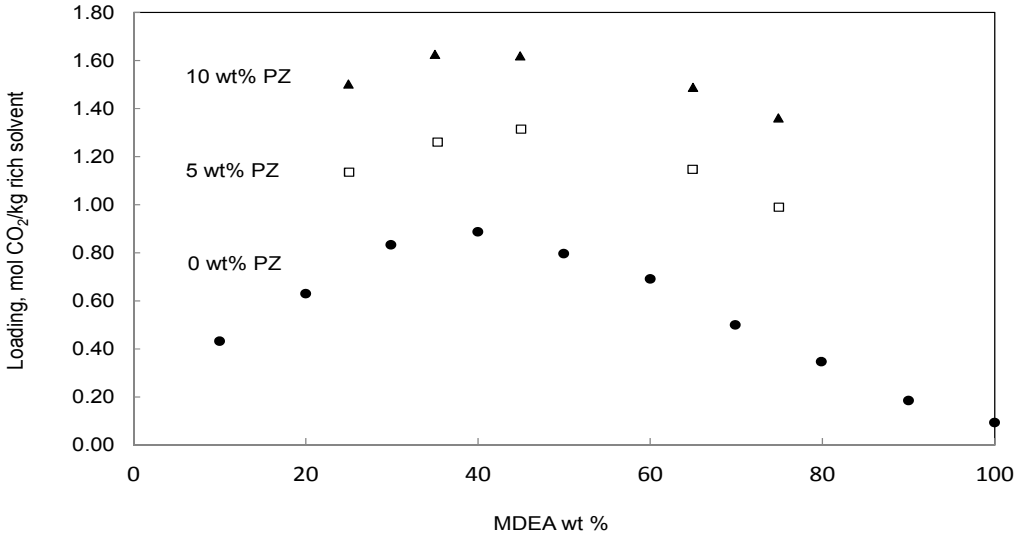

Figure 8-10. Comparison between measured CO_2 solubility data in aqueous MDEA and in presence of 0, 5 and 10 mass% PZ at 70.00 °C and 110.00 kPa. ● (0 wt% PZ), □ (5 wt% PZ), ▲ (10 wt% PZ)

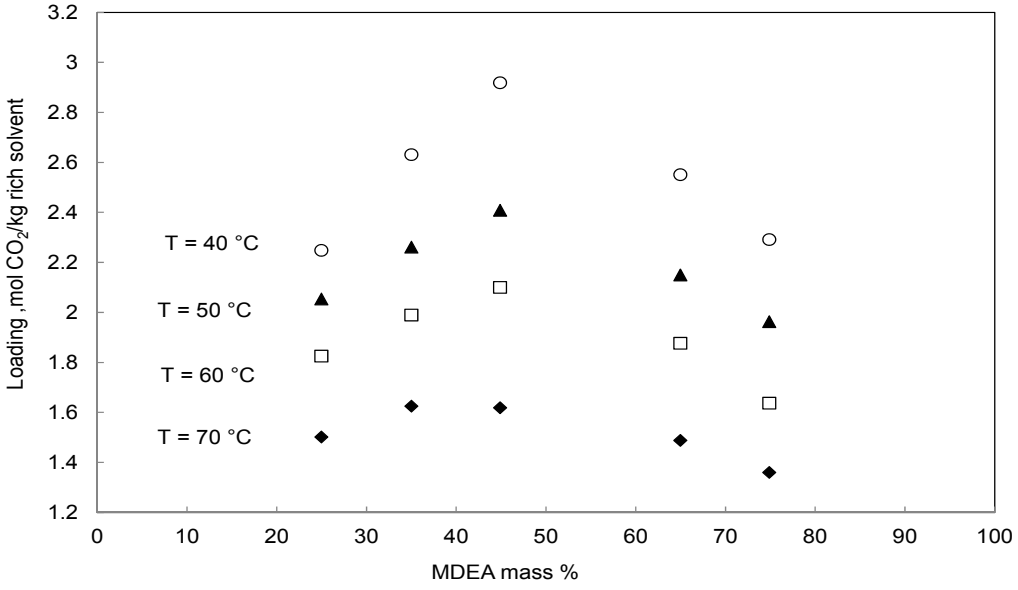

Figure 8-11. Comparison between measured CO_2 solubility in aqueous MDEA mixed with 10 mass% PZ at 40, 50, 60 and 70.00 °C and 110.00 kPa. ○ (T = 40 °C), ▲ (T = 50 °C), □ (T = 60 °C), ♦ (T = 70 °C)

From Figure 8-7 to Figure 8-10 it is obvious that for a given MDEA concentration, temperature and total pressure, adding certain amount of piperazine increase CO_2 absorption capacity in the aqueous MDEA. In addition, the enhancing effect of PZ on CO_2 absorption capacity is more pronounced at higher temperatures (see Table 8-11 for the details). This owes to the influence of PZ on the kinetic reaction.

Table 8-11. Average increase of CO_2 solubility by addition of PZ at various temperatures

Temperature, °C	Average increase of CO_2 solubility by addition of PZ, %	
	5 mass% PZ	10 mass% PZ
40	14.5	31.5
50	31.6	54.3
60	54.0	86.6
70	74.3	128.3

For the sake of easy comparison, the information provided in Figure 8-7 to Figure 8-10 for 10 mass% PZ (the highest absorption capacity at all the mentioned figures) are overlapped in Figure 8-11. It can easily be seen that in the studied conditions, the highest absorption capacity is achieved at the temperature of 40 °C and for blend of 45 mass% MDEA with 10 mass% PZ.

8.6 Conclusions

To sum up, this section presented measured density data for MDEA-PZ-H_2O solutions and new vapor-liquid equilibrium data for CO_2-MDEA-PZ-H_2O systems. Density experiments were carried out for aqueous blends of MDEA-PZ with MDEA concentration of 25 to 75 wt% and PZ mass% of 5 and 10, at temperatures between 40 to 80 °C. VLE experiments were performed for aqueous blends of MDEA-PZ with MDEA concentration of 25 to 75 wt% and PZ mass% of 5 and 10, at constant pressure of 1.1 bar and temperatures range of 40 to 70 °C. In VLE experiments loading were calculated from the volumetric data obtained from the cell without any requirement for liquid phase analysis. From these experiments it was concluded that adding certain amounts of PZ to MDEA significantly increase the solvent absorption capacity occurs. Investigations over the effect of PZ concentration demonstrates that the highest absorption capacity happens in the solutions with 10 mass% PZ.

Chapter 9

Measurement and Modeling of High Pressure Phase Equilibrium of Methane, H_2S and Aqueous Solutions of MDEA

Chapter 9

Measurement and Modeling of High Pressure Phase Equilibrium of Methane, H_2S and Aqueous Solutions of MDEA

9 Measurement and Modeling of High Pressure Phase Equilibrium of Methane, H_2S and Aqueous Solutions of MDEA

9.1 Chapter Overview

As already mentioned aqueous solutions containing alkanolamines are widely used for the removal of acid gases from natural gas. MDEA has many advantages over other amines; so that MDEA is becoming the most common solvent in natural gas industry (Jou et al. 1998), (Anufrikov et al. 2007). One of the most specific advantages of MDEA is its capability for selective separation of H_2S from a gas stream containing CO_2. In natural gas treatment process the absorber is operated at high total pressures (about 70 to 100 bar), but the regenerator operating pressure is low (around 1 to 3 bar) (Huttenhuis et al. 2007). Therefore, it is important to investigate the effect of pressure on the acid gas partial pressure. So if the total pressure affects the acid gas partial pressure, the low pressure experimental partial pressure data could not be used directly (without any correction) in the conditions of high pressure absorber (Huttenhuis et al. 2007). The effect of system pressure on acid gas partial pressure was already discussed in section 6.5 of chapter 6, in this section the effect of total pressure will be examined experimentally through the determined measured data. To design gas cleaning process, equilibrium, mass transfer, and chemical reaction data at industrial conditions are required. The aim of this chapter is to provide experimental data on solubility of H_2S in aqueous MDEA at conditions encountered in natural gas treatment process, 70 bar total pressure. In order to investigate the effect of pressure, H_2S partial pressure data were also determined at 15 bar.

In this chapter, vapor-liquid equilibrium (VLE) data for the systems composed of CH_4 (methane), H_2S, MDEA, and water will be presented at two different total pressures, 15 and 70 bar. Determined data at 70 bar will be presented for partial pressures of H_2S from 0.3 to 9.7 bar, and at 50 and 70 °C. Measured data at 15 bar will be presented at 50 °C for H_2S partial pressures from 0.5 to 3.9 bar. The concentration of the aqueous MDEA solution is 50 mass% for all the experiments. Moreover, the obtained data are used to validate the developed Extended UNIQUAC model in chapter 6. Results of model predictions are compared to the measured data in the remainder of this chapter.

9.2 Experimental Design

Most of the data available in open literature are presented as acid gas partial pressure without specifying the total pressure, because normally data were measured at low total pressures (Huttenhuis et al. 2007). This section contains bibliographic study over the experimental vapor-liquid equilibrium data available in open literature, for H_2S-MDEA-H_2O and H_2S-CH_4-MDEA-H_2O systems. Bibliographic results are summarized in Table 9-1.

Note that collected data in Table 9-1 were gathered to the best of author knowledge and at the time of this work.

Table 9-1. **Overview of published VLE data for H_2S-MDEA-H_2O and H_2S-CH_4-MDEA-H_2O**

MDEA Concentration, wt%	T, °C	P_{H_2S}, kPa	Loading, mole H_2S/mole MDEA	Reference	Number of experiments
11.8, 23.4, 48.9	25, 40, 70, 100, 120	0.0012 to 5890	0.001 to 3.220	(Jou et al. 1982)	153
11.8 , 19.9	25, 37.8, 65.6, 115.6	13.23 to 1536.60	0.180 to 2.1700	(Maddox et al. 1987)	49
23.4	40	52 to 1600	0.130 to 1.725	(Macgregor and Mather 1991)	27
35, 50	40, 100	0.0018 to 313	0.0040 to 1.077	(Jou et al. 1993)	50
30	40, 60, 80, 100	1.498 to 445.7	0.082 to 0.902	(Li and Shen 1993)	43
18.7, 32.2	40, 60, 100, 120, 140	165.2 to 4895.9*	0.480 to1.934	(Kuranov et al. 1996)	71
23, 50	40, 70, 100, 120	0.0033 to 3673	0.0020 to 1.74	(Huang and Ng 1998)	42
11.8, 23.6	25, 40	0.023 to 1.61	0.01 to 0.26	(Lemoine et al. 2000)	29
48.8	40, 81, 122	147.9 to 2783	0.15 to 1.42	(Kamps et al. 2001)	26
29.9	40, 60, 80, 100	1.5 to 445.7	0.08 to 0.9	(Li and Shen 1993)	42
46.7	40, 100	6.21 to 1040	0.03 to 1.1	(Sidi-Boumedine et al. 2004,b)	27
35, 50	10, 25, 40	0.141 to18.98	0.023 to 0.575	(Ter Maat et al. 2004), (Huttenhuis et al. 2007)** (P_{Total} = 690, 3450, 6900 kPa)	37
50	50	3 to 278	0.096 to 0.889	(Dicko et al. 2010)**(P_{Total} = 500 to 700 kPa)	5

* *Bubble pressure is measured (P_{H_2S} + solvent vapor pressure)*

** *Methane is present*

As it can be seen, there are only a few measured points at high total pressure, however there is a requirement for more data points at high pressures, the typical absorber pressure in amine based gas sweetening units. To execute H_2S measurements at high pressures, it is required to have methane or nitrogen as a makeup gas. Existing literature data reveals a gap in high pressure VLE data for H_2S-CH_4/N_2-MDEA-H_2O systems. One objective of this study is to obtain complementary points where there is a lack of data. In chapter 6 the effect of total pressure on H_2S partial pressure in aqueous MDEA was discussed through both modeling and experimental investigations. Notice that it is not very feasible to quantify the effect of total pressure accurately by comparing low pressure data from one source and high pressure data from another source. Experience tells that the deviations between different sources are related to other reasons as well (apparatus, analysis methods, chemicals used, etc.). Therefore another aim of this work was set to study the effect of total pressure on H_2S partial pressure in the same equilibrium cell, with the same chemicals, the same analysis techniques, etc. Hence the effect of pressure on H_2S partial pressure could be quantified more accurately. In this work new VLE data points are measured for H_2S-CH_4-MDEA-H_2O system at 70 and 15 bar, 50 and 70 °C and loading range of 0.28 to 1. To the best of our knowledge there is no measured data at 70 °C and at loadings higher than 1.

9.3 Experimental Section

9.3.1 Chemicals

The chemicals used in this work include MDEA (Merck, ≥ 98 % pure), H_2S (Yara, ≥ 99 % pure) and CH_4 (Yara, ≥ 99 % pure). All chemicals were used without any further purification.

9.3.2 Experimental Apparatus

The experiments were done in the apparatus shown in Figure 9-1. The cell is constructed for a "static-analytic" method with liquid and vapor samplings at constant temperature and pressure. The apparatus already exist in Statoil laboratories. The apparatus is a modified version of the one used by (Addicks 2002) for high pressure VLE measurements for the system CO_2-CH_4-MDEA-H_2O.

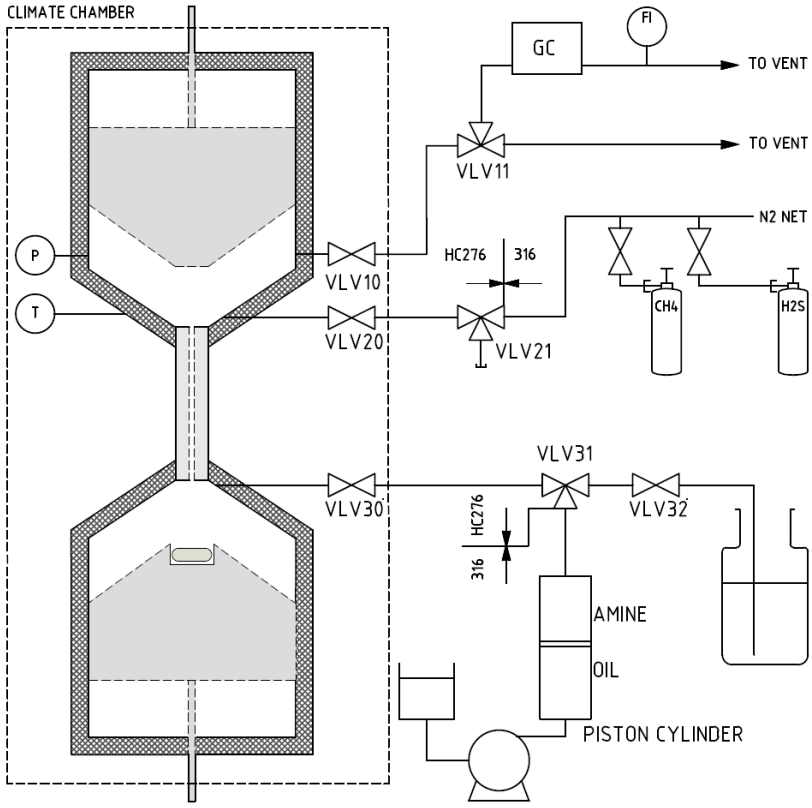

Figure 9-1. Sketch of the equilibrium cell.

The central part of the apparatus is a variable volume cell consisting of two cylindrical compartments connected through a cylindrical sapphire window. Both compartments are equipped with pistons which make it possible to vary the cell volume. A stirrer is fitted inside the lower piston to ensure mixing in the liquid phase. There is hydraulic oil on the back side of the pistons. The maximum volume is 450 cm^3, and the cell can be operated up to 700 bar (70000 kPa) and in the temperature range -50 to 200 °C. The cell is placed inside an air bath to keep the temperature inside the cell constant. The air bath temperature fluctuated with $\pm$ 0.5 °C. The temperature in the cell is measured with a platinum resistance thermometer with an accuracy of $\pm$ 0.1°C, which is placed within the wall the cell. Each piston is driven by the pressure difference between the hydraulic oil and the "process". The pressure in the hydraulic oil is controlled during an experiment. The pressure on the process side is slightly lower than the pressure in the hydraulic oil due to the friction

between the piston and the cell wall. The pressure is measured with a high-pressure sensor up to 1000 bar (100000 kPa), and its accuracy is ± 0.1 % of full scale. All the measuring devices are connected to a PC to store measurements and to control the operation of the cell. In order to avoid leaking between the hydraulic oil and the process side, there are two sets of O-rings on each piston. During operation, the O-rings and the bearings for the stirrer are affected by the harsh environment inside the cell. The cell is therefore emptied and taken apart for cleaning and maintenance every so often. The O-rings and bearings of the stirrer are then changed. Figure 9-1 shows that there are three inlet/outlet valves from the cell. The upper valve was used for gas sampling to a gas chromatograph and for depressurizing of the apparatus. The H_2S in the waste gas was removed with solid adsorbents before the gas was vented. The middle inlet/outlet valve was used for filling of methane and H_2S, and for purging with nitrogen during cleaning. The lower inlet/outlet valve was used for loading of the solvent into the cell, and for taking liquid samples. The liquid sample was taken directly into 1 M NaOH in order to stabilize H_2S in the liquid phase. Methane which had been dissolved in the solvent inside the cell escaped to the atmosphere and was vented. The solvent was pumped into the cell from a separate storage vessel. Valves, tubing and fittings in contact with the H_2S-loaded solvent or in contact with wet gas containing H_2S are made of Hastelloy C276. Some parts of the gas and solvent loading system are made of 316 stainless steel (shown in Figure 9-1). Equipment in more details was explained by (Addicks et al. 2002). Pictures of the equilibrium cell are shown in appendix.

9.3.3 Experimental procedure

The cell was cleaned and vacuumed before the initial filling of gas and solvent. The initial filling procedure was: First, the cell was filled completely full (450 cm^3) with H_2S gas at the pressure in the H_2S-bottle. Then, around 150 cm^3 of solvent was pumped into the cell from the storage vessel. After waiting for some hours, more H_2S gas was filled into the cell in order to reach high H_2S loadings in the solvent. This was sometimes repeated several times to reach H_2S loadings in the order of 1 mole/mole MDEA. Finally, methane was filled. The solvent was an aqueous solution with 50 wt% MDEA made from degassed ion exchanged water. The system was left to equilibrate at specified pressure and temperature. Equilibrium was most often reached over night, but the system was always left for at least two whole days to make sure equilibrium had been reached. Gas samples (5-10 tests) were routed directly to a gas chromatograph for analysis. One liquid sample was taken for each experiment. The liquid sampling line was first flushed with some sample, before 15 to 20 cm^3 of solvent was taken directly into a glass bottle which was preloaded with 150 to 200

cm^3 1M[38] NaOH. Accurate weights of caustic and stabilized sample (caustic plus sample) were noted in order to know the degree of dilution of the sample. The sampling line is 1/16 inch Hastelloy C276 tubing with no heat tracing, so the sample was cooled through the sampling line. The outlet of the sampling line was at the bottom of the sampling bottle. During sampling, methane escaped out of the bottle, and some H_2S followed the methane. In order to ensure that loss of H_2S was negligible, the sampling was done very slowly. The pistons inside the cell ensured that the pressure did not decrease during this operation. The stabilized sample was stored in a closed bottle. After sampling, more solvent was pumped into the cell and the system was left for another equilibration. In this way, a series of experiments was done for each initial filling of the cell. The H_2S loading in the solvent and partial pressure of H_2S decreased through the series since only solvent was added between each experiment. The length of a series was limited either by low liquid level inside the cell, or the need to do maintenance on the stirrer. At the end of each series, the cell was emptied, cleaned, opened for maintenance and vacuumed before the next initial filling.

9.3.4 Analytical Details

Gas samples were analyzed thanks to a gas chromatograph[39] equipped with a poraplot column and a thermal conductivity detector (TCD). The sampling lines and valves are made of Hastelloy C276. Some adsorption of H_2S in the sampling lines was observed, but calibration with external standards showed that the calibration curve was linear in the H_2S concentration range of interest (0.5-20 mole %) and in the volume range of calibration. For each experiment between 5 and 10 tests were done and the GC results stabilized after 2-4 injections on the GC. The liquid sample was analyzed by titration on anautotitrator (Metrohm 809 Titrando). Two titration methods were used. The total concentration of dissolved H_2S was determined by titration with 0.1 M AgNO3 using a sulfide selective titrode. Silver and sulfide ions will not coexist in a solution because silver sulfide is sparingly soluble and will precipitate. The sulfide selective titrode has Ag/Ag_2S coated electrode which detects the shift from a finite sulfide concentration (up to the equivalence point) to the extremely low concentration present when there is a surplus of silver ions in the solution (beyond the equivalence point). The sum of the MDEA and the H_2S concentrations was determined by pH-titration with 0.1 M HCl. For both analyses, 1-2 gram of stabilized sample was used, and it was

[38] M: Molar is defined as mole numbers of the constituent per one liter of the solution.

[39] GC Details: SRI 8610C. Column: 6 feet Haysep D. Detector: TCD, temp=156 °C. Carrier gas: He, 10 psi. Injector: 10 port gas sampling valve, 250 µl loop, temp = 100 °C. Oven temp=100 °C.

diluted to approximately 100 cm^3 with water. Two estimates of the H_2S loading were obtained from the titration data. The first value was calculated from the total H_2S concentration, the MDEA-concentration of the makeup solvent and the degree of dilution when liquid sample was stabilized in 1M NaOH. The other value was calculated from the titration results directly.

9.4 Results

The H_2S solubility in aqueous MDEA in presence of methane as a makeup gas was measured at total pressures of 15 (1500 kPa) and 70 bar (7000 kPa). VLE experiments for H_2S-CH_4-MDEA-H_2O system were carried out for aqueous solutions of 50 mass% MDEA at total pressure of 70 bar and temperatures of 50 and 70 °C and at total pressure of 15 bar and temperature of 50 °C. This section describes results of VLE measurements. Table 9-2 reports H_2S solubility measurements at 70 bar.

Table 9-2. Measured VLE data for H_2S-CH_4-MDEA-H_2O system at total pressure = 70 bar and MDEA mass% = 50

T, °C	Loading, moleH_2S/mole MDEA	P_{H_2S} , kPa	P, kPa
49.8	0.29	31.03	6970
49.8	0.35	42.10	6980
49.8	0.38	50.36	6990
49.8	0.54	94.77	6960
49.8	0.64	136.38	6990
49.8	0.71	192.19	6980
49.8	0.80	269.00	6990
49.8	0.86	383.39	7060
49.8	0.88	398.39	6970
49.8	0.89	431.30	6910
49.8	0.97	626.75	6930
49.7	0.97	683.65	7090
49.8	1.01	790.34	6930
49.7	1.03	973.84	7070
49.8	1.04	911.24	6990
49.8	1.04	880.41	7020
69.9	0.27	65.76	6990
69.9	0.39	114.66	6970
69.9	0.51	175.86	6940
69.9	0.65	302.97	6950
69.9	0.70	365.02	6990
69.9	0.78	506.91	6950
69.9	0.85	711.61	7020
69.9	0.86	717.87	7050
69.9	0.92	890.68	6970

Table 9-3 presented measured values at total pressures of 15 bar.

Table 9-3. Measured VLE data for H_2S-CH_4-MDEA-H_2O system at total pressure = 15 bar and MDEA mass% = 50

T, °C	Loading, mole H_2S/mole MDEA	P_{H_2S} , kPa	P, kPa
49.8	0.44	52.67	1520
49.8	0.45	54.42	1550
49.8	0.52	70.90	1570
49.8	0.52	72.28	1530
49.8	0.55	82.54	1520
49.8	0.60	95.36	1540
49.8	0.69	141.44	1530
49.8	0.70	132.69	1500
49.8	0.73	161.34	1610
49.8	0.73	163.98	1480
49.8	0.76	182.48	1520
49.8	0.79	210.73	1530
49.8	0.83	244.78	1530
49.8	0.92	386.37	1570

Figure 9-2 plotted H_2S partial pressure as a function of loading at total pressure of 70 bar. Error bars are added to each measured point on the figure. Figure 9-3 depicts the measured data graphically at total pressure of 15 bar, the same as Figure 9-2, error bars are shown on the figure, however they are not visible for all points because the markers hide them.

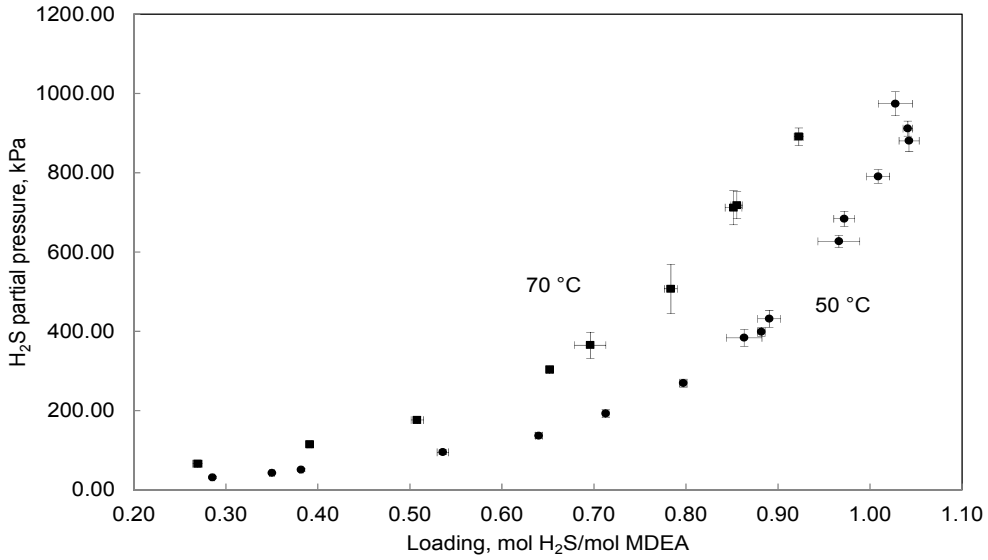

Figure 9-2. Measured solubility data of H_2S in 50 mass% MDEA aqueous solutions at 70 bar total pressure and temperatures of 50 and 70 °C. ●, experimental data at 50 °C; ■, experimental data at 70 °C. Error bars are shown in the figure.

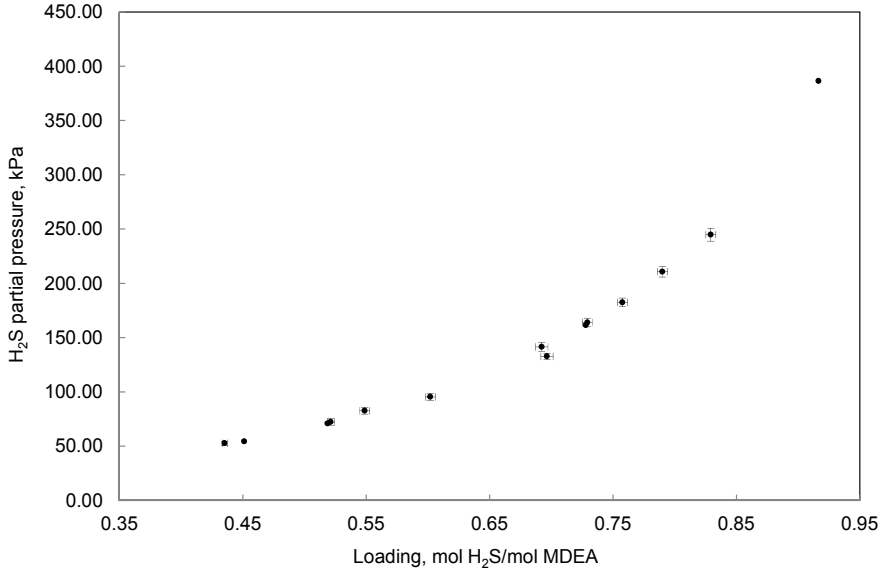

Figure 9-3. Measured solubility data of H_2S in 50 mass% MDEA aqueous solutions at 15 bar total pressure and at 50°C. ●, experimental data. Error bars are shown in the figure.

As it can be seen from Figure 9-2 and Figure 9-3, the uncertainty goes down with a decrease in loading and partial pressure. Unlike absolute uncertainty, the relative uncertainty increase when loading and partial pressure decrease.

9.5 Comparison between measurements of this study and literature data

In this study solubility of H_2S in 50 wt% MDEA aqueous solution at temperatures of 50 and 70 °C is measured at total pressure of 15 and 70 bar (in presence of methane). It is noted that the measured data are only comparable with experimental data from literature which are also carried out in presence of methane. H_2S solubility data of (Dicko et al. 2010) in 50 wt% aqueous MDEA solution at 50 °C can be compared to the measured data of this study, see Figure 9-4 (noted that the total pressures are not the same).

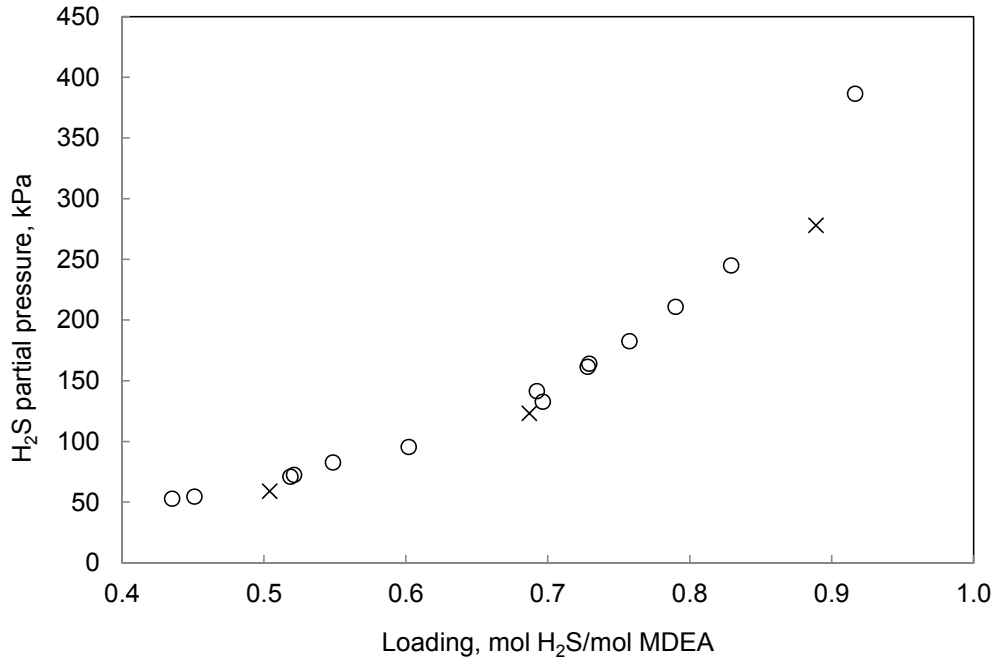

Figure 9-4. Comparison between measured and literature data for H_2S solubility data in 50 mass% MDEA aqueous solutions at 50°C. ○, measured data in this study at total pressure of 1500 kPa ; ×, Measured data by (Dicko et al. 2010) at total pressure of 500 to 700 kPa

Even though the total pressure of this study is more than twice of the total pressure reported by (Dicko et al. 2010), there is only slight difference between the measured values. It shows that in the mentioned experimental conditions, the effect of total pressure on H_2S partial pressure is negligible. It is reminded from 6.5 that approximately 6 MPa (6000 kPa) increase in total pressure leads to 30% increase in H_2S partial pressure.

9.6 Results and Discussion

This section explains the effect of the total pressure on H_2S partial pressure. Figure 9-5 compares the measured data of this study at 50 °C and for 50 mass% MDEA aqueous solutions at two different total pressures of 15 and 70 bar.

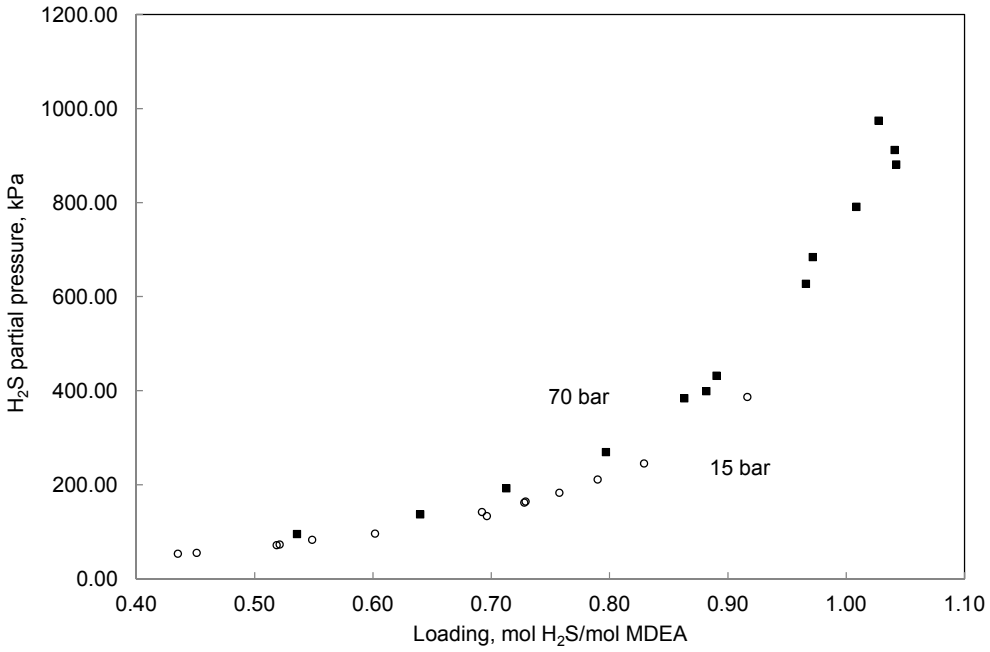

Figure 9-5. Measured H_2S partial pressure in 50 mass% MDEA aqueous solutions in presence of methane at 50 °C and total pressure of 15 and 70 bar. ○, Experimentally measured data at 15 bar; ■, Experimentally measured data at 70 bar

As it can be observed from the Figure 9-5, increasing total pressure leads to increase in H_2S partial pressure. Quantitative analysis over the measured data shows that, in the studied conditions (50 °C and 50 mass% MDEA) an increase of 55 bar (5.5 MPa) in total pressure leads to about 28 % increase in H_2S partial pressure over aqueous MDEA. This conclusion is in accordance to the observations explained in section 6.5 of chapter 6.

9.7 Model Validation

The results of H_2S solubility experiments of this work were compared to the optimized Extended UNIQUAC model in chapter 6. Note that parameters of the developed model have not been fitted to the new data; data of this work were utilized to validate the developed model as a predictive tool.

Table 9-4 and Table 9-5 summarized predicted and measured values at each studied temperature. Average absolute relative deviations between models and measured values are shown in bold in tables. Calculated and measured results are also depicted graphically in Figure 9-6 and Figure 9-7.

Table 9-4. Measured and predicted H_2S partial pressure for mixtures of H_2S-CH_4-MDEA-H_2O at total pressure = 70 bar and MDEA mass% = 50

T, °C	Loading, mole H_2S/mole MDEA	Exp P_{H_2S} , kPa	Calc P_{H_2S} , kPa (Optmized Extended UNIQUAC model)	Bias Deviation*, kPa
49.8	0.29	31.03	28.34	-2.69
49.8	0.35	42.10	40.34	-1.76
49.8	0.38	50.36	47.31	-3.05
49.8	0.54	94.77	95.68	0.92
49.8	0.64	136.38	151.08	14.70
49.8	0.71	192.19	209.15	16.96
49.8	0.80	269.00	311.20	42.20
49.8	0.86	383.39	432.01	48.61
49.8	0.88	398.39	475.06	76.67
49.8	0.89	431.30	494.18	62.88
49.8	0.97	626.75	729.16	102.41
49.8	0.97	683.65	753.04	69.40
49.8	1.01	790.34	899.41	109.07
49.8	1.03	973.84	985.95	12.11
49.8	1.04	911.24	1049.74	138.51
49.8	1.04	880.41	1056.22	175.82
70.0	0.27	65.76	53.21	-12.55
70.0	0.39	114.66	99.76	-14.91
70.0	0.51	175.86	168.33	-7.54
70.0	0.65	302.97	310.83	7.86
69.9	0.70	365.02	374.88	9.86
69.9	0.78	506.91	542.73	35.81
69.9	0.85	711.61	726.24	14.63
69.9	0.86	717.87	739.35	21.48
69.9	0.92	890.68	973.73	83.04
AARD** **%**	**9.65**			

*$AARD = \frac{1}{n}\sum_{i=1}^{n}\frac{\left|P_{H_2S,exp}-P_{H_2S,calc}\right|}{P_{H_2S,exp}}$

*$Bias\ Deviation = P_{H_2S,calc} - P_{H_2S,exp}$

Table 9-5. Measured and predicted H_2S partial pressure for mixtures of H_2S-CH_4-MDEA-H_2O at total pressure = 15 bar and MDEA mass% = 50

T, °C	Loading, mole H_2S/mole MDEA	Exp P_{H_2S} , kPa	Calc P_{H_2S} , kPa (Optmized Extended UNIQUAC model)	Bias Deviation, kPa
49.8	0.44	52.67	47.18	-5.49
49.8	0.45	54.42	50.74	-3.68
49.8	0.52	70.90	68.70	-2.20
49.8	0.52	72.28	69.37	-2.91
49.8	0.55	82.54	78.18	-4.37
49.8	0.60	95.36	98.65	3.29
49.8	0.69	141.44	146.68	5.24
49.8	0.70	132.69	149.29	16.60
49.8	0.73	161.34	172.90	11.56
49.8	0.73	163.98	172.87	8.88
49.8	0.76	182.48	197.44	14.97
49.8	0.79	210.73	230.26	19.53
49.8	0.83	244.78	278.35	33.57
49.8	0.92	386.37	431.94	45.58
AARD%	**7.48**			

As it can be seen in the above tables the developed model could very well predict high pressure H_2S solubility data which is highly requested by industry. Figure 9-6 compares model predictions with experimental data graphically.

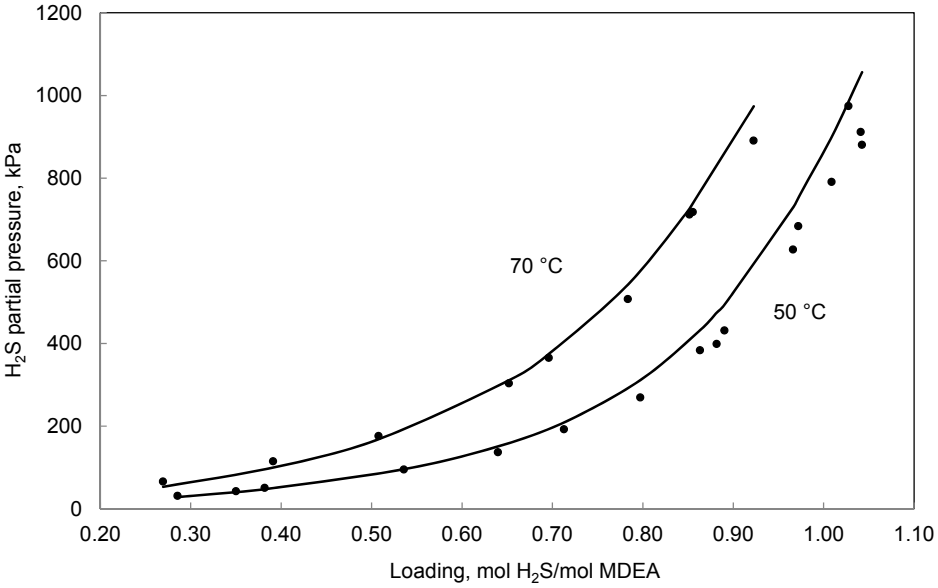

Figure 9-6. H_2S partial pressure for H_2S-CH_4-MDEA-H_2O mixture at total pressure = 70 bar, MDEA mass% = 50 and at 50 and 70 °C. ●, Experimentally measured data; Solid line, Optimized Extended UNIQUAC model

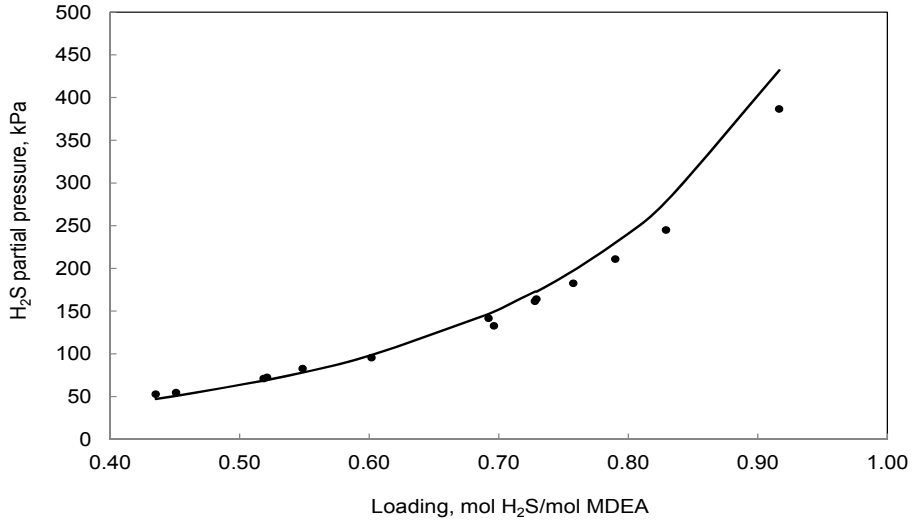

Figure 9-7. H_2S partial pressure for H_2S-CH_4-MDEA-H_2O mixture at total pressure = 15 bar, MDEA mass% = 50 and at 50 °C. ●, Experimentally measured data; Solid line, Developed Extended UNIQUAC

9.8 Conclusions

This chapter presents new vapor-liquid equilibrium data for mixtures of H_2S-CH_4-MDEA-H_2O. H_2S solubility in aqueous MDEA was measured in presence of methane as a makeup gas and at conditions encountered in industrial conditions. Data were presented for 50 mass% MDEA, at 50 and 70 °C and at total pressures of 15 and 70 bar. The influence of high pressure on H_2S partial pressure was examined by utilizing the obtained data and it was concluded that in the studied conditions an increase of 5.5 MPa in total pressure results in 28 % increase in H_2S partial pressure over aqueous MDEA. The developed thermodynamic model in chapter 6 is validated against the measured data. Model prediction results were very promising specifically at 70 °C and approved model capability for predicting high pressure solubility data. However comparison between experimental and modeling results at 50 °C and at loadings greater than 0.80 shows that adjusting model parameters to the new obtained data can improve model performance at these conditions.

Chapter 10

Summary, Conclusions and Recommendations

Chapter 10

Summary, Conclusions and Recommendations

10 Summary, Conclusions and Recommendations

At the end of each chapter detailed conclusions on each covered topic were presented. This chapter provides a summary based on previous chapters and suggests recommendations for the future work.

10.1 Summary

The aim of this work was to model thermodynamic behavior of acid gas-aqueous alkanolamine systems, to measure required acid gas solubility data and to examine the effect of high pressure on acid gas partial pressure (acid gas solubility).

In the modeling part of the project, Extended UNIQUAC model parameters were optimized for MDEA-H_2O, MEA-H_2O, MDEA-MEA-H_2O, CO_2-MDEA-H_2O, CO_2-MEA-H_2O, CO_2-MDEA-MEA-H_2O, H_2S-MDEA-H_2O, CH_4-H_2O, H_2S-CH_4-MDEA-H_2O and CO_2-CH_4-MDEA-H_2O systems. Vapor-liquid equilibria, solid-liquid equilibria, speciation and thermal properties (heat of absorption, excess enthalpy and heat capacity) were shown to be accurately predicted by the developed models. The developed models match experimental data, in addition confidently predict conditions where experimental data is non-existent or inaccurate. The developed models confidently predict VLE data at conditions encountered in industrial natural gas treating plants. Model predictions have been validated using VLE and SLE data and thermodynamically related data like speciation and heat of absorption. The obtained results revealed that the developed thermodynamic models accurately present both thermodynamic and thermal properties of acid gas-alkanolamine-water systems over an extensive range of pressure, temperature and amine concentration. The range of validity of model parameters for the investigated system is:

- H_2S-MDEA-H_2O system :
  - Temperature: 25 to 140 ℃
  - H_2S partial pressure: 0 to 4900 kPa
  - MDEA mass% : 11 to 50

- CO_2-MDEA-H_2O
  - Temperature: 20 to 200 ℃
  - CO_2 partial pressure: 0 to 7565 kPa
  - MDEA mass%: 5 to 90
- CO_2-MEA-H_2O system:
  - Temperature range: -16 to 140℃
  - CO_2 partial pressure range: 0 to 6086 kPa
  - MEA mass%: 10 to 40

The effect of high pressure on acid gas partial pressure (acid gas solubility) was quantitatively investigated by (i) experimental and (ii) modeling approaches.

In the experimental part of the project a unique set of data for CO_2 solubility in aqueous MDEA at constant total pressure of 110 kPa (1.10 bar), temperatures between 40 to 80 °C and for MDEA concentration varies in the range of 10 to 100 mass% were obtained. Density data of MDEA-H_2O solutions for MDEA wt% of 10 to 100 at temperatures between 40 to 80 °C were also acquired. Furthermore, the effect of PZ additive was investigated on increasing absorption capacity of solvent. CO_2 solubility were measured in blends of MDEA-PZ at total pressure of 110 kPa (1.10 bar), temperatures between 40 to 70 °C and for MDEA concentration varies from 25 to 75 mass% while PZ concentration was kept constant at 5 and 10 mass%. Density data of MDEA-PZ-H_2O solutions for 25 to 75 mass% MDEA mixed with 5 and 10 mass% PZ at temperatures between 40 to 80 °C were also measured.

Another part of the experimental study related to the high VLE pressure measurements. In this part of the study H_2S solubility in aqueous MDEA and in presence of methane as a makeup gas at temperatures of 50 and 70 °C, for MDEA concentration of 50 mass% and at two different total pressures, 15 and 70 bar was measured.

During this study, out of the scope of preliminary plan, an effort was made to measure the solubility of piperazine in aqueous MDEA, however due to time limitation the measurements remained incomplete. The obtained results provide an approximate estimate of the solubility of piperazine in aqueous MDEA; however more investigations are required in order to obtain the exact limit of solubility.

The main contributions of this study lie in: **1st)** Developed thermodynamic models that are aimed to accurately predict thermodynamic and thermal properties of the acid gas-alkanolamine-water systems. **2nd)** High pressure VLE measurements for H_2S-MDEA-H_2O system **3nd)** Quantification of high pressure effect on acid gas partial pressure (acid gas solubility) **4th)** VLE measurements for CO_2-MDEA-H_2O and CO_2-MDEA-PZ-H_2O covering wide amine concentration range.

10.2 Conclusions

It is found out that at constant acid gas loading, increasing system total pressure results in an incarese in acid gas partial pressure while acid gas solubility remains constant. Therefore increase of acid gas partial pressure because of increase in methane partial pressure is because of non-ideality of gas phase and not because of dissolution of small amounts of methane in the liquid phase. This behavior is due a decrease in the acid gas fugacity coefficient (in the gas phase) with increasing methane partial pressure.

It was shown that for a certain temperature and total pressure, the highest absorption capacity of CO_2 in aqueous MDEA was observed for MDEA mass% of 40 to 60.

It has been shown that adding certain amount of piperazine to aqueous MDEA, increase CO_2 absorption capacity of solvent. The enhancing effect of PZ on CO_2 absorption capacity is more pronounced at higher temperatures.

It is found out that in the studied conditions increase of 5.5 MPa in total pressure results in an increase of 28 % in H_2S partial pressure.

The experimental data obtained in this study are used to validate the optimized thermodynamic models and prediction results proved that the devolved models satisfactorily predict the measured solubility data.

10.3 Recommendations

This study could be continued in many aspects. In the following, some remarks are recommended for future research wok.

- The optimized models are rigorous enough for CO_2 and H_2S removal using aqueous MDEA and MEA and blend of both. The following remarks appeared worth to be investigated:

- In this study equilibrium constants for reactions of MEA protonation, MDEA protonation and formation of MEA carbamate were determined by fitting the standard state properties (at 25 °C) of MDEA, $MDEAH^+$, MEA, $MEAH^+$ and $MEACOO^-$ to all kinds of experimental data available in the developed regression data base. The regressed dissociation constant for MDEA in aqueous solution was compared to the measured value by (Kamps and Maurer 1996). At the time of this work, very limited data were available for the mentioned dissociation constants. It is worthwhile to accurately measure the equilibrium constants at different temperatures. Then to ensure that the calculations of the model are accurate it is recommended to compare equilibrium constants used in the model to (upcoming) experimental values at different temperatures. In case of availability of accurate dissociation constant for the required species, it is recommended to use the measured values in the program. In that case the number of adjustable parameters will reduce and the uncertainty of the calculations will be eliminated.
- In this study standard state heat capacity parameters for MEA (aq), $MEAH^+$ (aq) and $MEACOO^-$ (aq) were adjusted to all kinds of experimental data available in regression data base. The experimental values for heat capacities of MEA (aq), $MEAH^+$ (aq) and $MEACOO^-$ (aq) were not available at the time of this work. It will be useful to accurately measure heat capacities of the required species at different temperatures. In this case heat capacity parameters can determine more confidently.
- Retune parameters of the developed model for CO_2-MDEA-H_2O to the new data measured in this work. VLE data measured in this study for CO_2-MDEA-H_2O system covered a broad range of amine concentration from 10 wt% to 100 wt% MDEA. Adjusting model parameters to these data could improve model performance at high amine concentrations. It is reminded that in this study, it was aimed to use the measured data in order to validate the developed model as a predictive tool.

- Further developed thermodynamic models for additional species like PZ or Sulfolane. Aqueous blends of MDEA with PZ or Sulfolane[40] have been widely used in acid gas treating

[40] Sulfolane: Sulfolane ,

process. In acid gas purification process, PZ and sulfolane are commonly used as additives that mixed with aqueous MDEA to enhance the efficiency of the process for certain applications. PZ largely increase solubility of CO_2 into aqueous MDEA. In contrast to PZ, TMS decreases the solubility of CO_2 into aqueous MDEA. However the Sulfolane mixed with aqueous MDEA, unlike aqueous MDEA, can remove carbonyl sulfide (COS) and organic sulfur compounds (Jenab et al. 2005), (Qian et al. 1995).

- Modeling Mixed acid gas systems. Develop Extended UNIQUAC model for CO_2-H_2S-MDEA-H_2O system based on the combination of developed models in this study for CO_2-MDEA-H_2O and H_2S-MDEA-H_2O systems and from adjusting additional binary interaction parameters associated with mixed acid gas system.
- Modeling other amine systems. Develop Extended UNIQUAC model for acid gas purification using other industrially amines, like DEA.
- Integrate the developed models in commercial simulators packages like ASPEN PLUS and simulate the acid gas treating process.
- Use of an electrolyte equation of state and an empirical correlation to model thermodynamics of acid gas-alkanolamines-water mixtures (investigated systems in this study). Compare the modeling results with the developed Extended UNIQUAC models. The comparison between modeling results leads to a conclusion about the performance of three different types of models (G^E, EoS and empirical correlations) in representing thermodynamics of alkanolamine based acid gas treating process.

- In this study it was tried to measure PZ solubility in aqueous MDEA at 5, 25, 35 and 45 °C, however due to lack of time the measurements remained incomplete. It is highly recommended to complete the experiments and repeat the measurements for the scattered points.
- Investigate the effect of adding higher concentrations of PZ to MDEA, on acid gas solubility. Keep in mind that solubility of PZ in aqueous MDEA is limited. Measurements of PZ solubility into aqueous MDEA which was initiated in this study would determine extent of solubility of PZ into aqueous MDEA.

tetramethylene sulfone, abbreviated as TMS, is a compound with the formula $(CH_2)_4SO_2$.

- Perform H_2S solubility measurement in aqueous blends of MDEA-PZ at high pressures. In this study H_2S solubility into aqueous MDEA was measured at pressure of 70 bar and 15 bar. It is recommended to perform the same measurements for activated MDEA.
- Measure CO_2 solubility in aqueous MDEA and aqueous activated MDEA at high pressures.
- Measure heat capacity of aqueous blends of MDEA-PZ. At the time of this study the only source that was found for such kind of data was article by (Chen et al. 2010).
- Measure densities of mixtures of CO_2-MDEA-H_2O. In case of density measurements for the loaded solutions, in order to avoid creating bubbles at high temperatures (CO_2 bubbles may release as bubble), it is recommended to perform the measurements under pressure.
- Acquisition of further accurate VLE data for acid gas (CO_2/H_2S)-alkanolamine (MDEA/MEA)-water systems especially at high temperatures (above 120°C), low temperatures (below 40°C) and high pressures where experimental data are less abundant. Although there are lots of data available in open literature for these systems, an inconsistency between many of them has been observed. There is a demand for high pressure VLE data for (CO_2/H_2S)-Alkanolamine (MDEA/MEA)-H_2O systems, these kind of data are very rare in open literature. VLE data for mixtures of CO_2 and H_2S are required since the published data are very limited for mixed acid gas systems. Binary VLE data (partial pressure data) of alkanolamine-water systems, specifically for MEA which is relatively volatile, are required for prediction of amine loss due to vaporization. This kind of data is also useful for determining parameters of thermodynamic models such as Extended UNIQUAC. It is also recommended to measure relative volatile amine partial pressures (like MEA) above the loaded solution since these data are also useful for calculation of amine loss due to vaporization.
- There is a need for more speciation, heat of absorption, heat capacity (especially heat capacity of loaded solutions) and freezing point data (for loaded solutions).
- Measuring physical properties of loaded alkanolamine solutions in the temperature range of industrial applications are highly required. Few studies have been made on physical properties of solvents used in amine-based acid gas removal process. Physical properties of the solvents used in amine based acid gas purification process provide better understanding of thermodynamics, hydrodynamics and optimum operating conditions of the process.

References

Abrams D, Prausnitz J (1975) Statistical Thermodynamics of Liquid-Mixtures - New Expression for Excess Gibbs Energy of Partly Or Completely Miscible Systems. AIChE J 21:116-128.

Addicks J (2002) Solubility of carbon dioxide and methane in aqueous N-Methyldiethanolamine solutions at pressures between 100 and 200 bar. PhD Disseration.

Addicks J, Owren GA, Fredheim AO, Tangvik K (2002) Solubility of carbon dioxide and methane in aqueous methyldiethanolamine solutions. J Chem Eng Data 47:855-860.

Alghawas HA, Hagewiesche DP, Ruizibanez G, Sandall OC (1989) Physicochemical properties important for carbon-dioxide absorption in aqueous methyldiethanolamine. J Chem Eng Data 34:385-391.

Ali B, Aroua M (2004) Effect of piperazine on CO_2 loading in aqueous solutions of MDEA at low pressure. Int J Thermophys 25:1863-1870.

Anufrikov YA, Kuranov GL, Smirnova NA (2007) Solubility of CO_2 and H_2S in alkanolamine-containing aqueous solutions. Russian Journal of Applied Chemistry 80:515-527.

Arcis H, Rodier L, Ballerat-Busserolles K, Coxam J (2009) Enthalpy of solution of CO_2 in aqueous solutions of methyldiethanolamine at T=372.9 K and pressures up to 5 MPa. Journal of Chemical Thermodynamics 41:836-841.

Arcis H, Rodier L, Ballerat-Busserolles K, Coxam J (2008) Enthalpy of solution of CO_2 in aqueous solutions of methyldiethanolamine at T=322.5 K and pressure up to 5 MPa. J Chem Thermodyn 40:1022-1029.

Austgen DM, Rochelle GT, Chen CC (1991) Model of vapor-liquid-equilibria for aqueous acid gas-alkanolamine systems .2. Representation of H_2S and CO_2 solubility in aqueous MDEA and CO_2 solubility in aqueous mixtures of MDEA with MEA Or DEA. Ind Eng Chem Res 30:543-555.

Austgen DM (1989) A model of vapor-liquid equilibria for acid gas-alkanolamine-water systems. PhD Disseration.

Awan JA, Thomsen K, Coquelet C, Fosbol PL, Richon D (2010) Vapor-Liquid Equilibrium Measurements and Modeling of the Propyl Mercaptan plus Methane plus Water System. J Chem Eng Data 55:842-846.

Baek JI, Yoon JH (1998) Solubility of carbon dioxide in aqueous solutions of 2-amino-2-methyl-1,3-propanediol. J Chem Eng Data 43:635-637.

Barker J (1953) Determination of Activity Coefficients from Total Pressure Measurements. Aust J Chem 6:207-210.

Barreau A, le Bouhelec EB, Tounsi KNH, Mougin P, Lecomte F (2006) Absorption of H2S and CO_2 in alkanolamine aqueous solution: Experimental data and modelling with the electrolyte-NRTL model. Oil & Gas Science and Technology 61:345-361.

Bernal-García JM, Ramos-Estrada M, Iglesias-Silva G, Hall KR (2003) Densities and excess molar volumes of aqueous solutions of n-Methyldiethanolamine (MDEA) at Temperatures from (283.15 to 363.15) K. J Chem Eng Data 48:1442-1445.

Bishnoi S, Rochelle G (2002) Absorption of carbon dioxide in aqueous piperazine/methyldiethanolamine. AIChE J 48:2788-2799.

Bishnoi S (2000) Carbon Dioxide Absorption and Solution Equilibrium in Piperazine Activated Methyldiethanolamine. PhD Disseration.

Boettinger W, Maiwald M, Hasse H (2008) Online NMR spectroscopic study of species distribution in MEA-H_2O-CO_2 and DEA-H_2O-CO_2. Fluid Phase Equilib 263:131-143.

Böttger A, Ermatchkov V, Maurer G (2009) Solubility of carbon dioxide in aqueous solutions of N-methyldiethanolamine and piperazine in the high gas loading region. J Chem Eng Data 54:1905-1909.

Button JK, Gubbins KE (1999) SAFT prediction of vapour-liquid equilibria of mixtures containing carbon dioxide and aqueous monoethanolamine or diethanolamine. Fluid Phase Equilib 158:175-181.

Cadours R, Roquet D, Perdu G (2007) Competitive absorption-desorption of acid gas into water-DEA solutions. Ind Eng Chem Res 46:233-241.

Cai ZY, Xie RJ, Wu ZL (1996) Binary isobaric vapor-liquid equilibria of ethanolamines plus water. J Chem Eng Data 41:1101-1103.

Cardoso E (1921) The vapor tension of hydrogen sulfide. Gazzetta Chimica Italiana 51:153-164.

Carson JK, Marsh KN, Mather AE (2000) Enthalpy of solution of carbon dioxide in (water plus monoethanolamine, or diethanolamine, or N-methyldiethanolamine) and (water plus monoethanolamine plus N-methyldiethanolamine) at T=298.15 K. J Chem Thermodyn 32:1285-1296.

Chakma A, Meisen A (1987) Solubility of CO_2 in Aqueous Methyldiethanolamine and N,n-Bis(hydroxyethyl)piperazine Solutions. Ind Eng Chem Res 26:2461-2466.

Chang HT, Posey M, Rochelle GT (1993) Thermodynamics of Alkanolamine Water Solutions from Freezing-Point Measurements. Ind Eng Chem Res 32:2324-2335.

Chapoy A, Mohammadi A, Tohidi B, Valtz A, Richon D (2005) Experimental measurement and phase behavior modeling of hydrogen sulfide-water binary system. Ind Eng Chem Res 44:7567-7574.

Chen CC, Britt HI, Boston JF, Evans LB (1982) Local Composition Model for Excess Gibbs Energy of Electrolyte Systems .1. Single Solvent, Single Completely Dissociated Electrolyte Systems. AIChE J 28:588-596.

Chen Y, Shih T, Li M (2001) Heat Capacity of Aqueous Mixtures of Monoethanolamine with N-Methyldiethanolamine. J Chem Eng Data 46:51-55.

Chen Y, Caparanga AR, Soriano AN, Li M (2010) Liquid heat capacity of the solvent system (piperazine plus n-methyldiethanolamine plus water). J Chem Thermodyn 42:54-59.

Chiu L, Li M (1999) Heat Capacity of Alkanolamine Aqueous Solutions. J Chem Eng Data 44:1396-1401.

Clarke ECW, Glew DN (1971) Aqueous Nonelectrolyte Solutions. Deuterium and Hydrogen Sulfides Solubilities in Deuterium Oxide and Water. Can J Chem 49:691.

Clarke ECW, Glew DN (1970) Deuterium and Hydrogen Sulfides - Vapor Pressures, Molar Volumes, and Thermodynamic Properties. Can J Chem 48:764.

Crovetto R, Fernández-Prini R, Japas ML (1982) Solubilities of inert gases and methane in H_2O and in D_2O in the temperature range of 300 to 600 K. J Chem Phys 76:1077-1086.

Danckwer P, McNeil K (1967) Absorption of Carbon Dioxide into Aqueous Amine Solutions and Effects of Catalysis. Trans Inst Chem Eng, 45:T32-&.

Daneshvar N, Moattar MTZ, Abdi MA, Aber S (2004) Carbon dioxide equilibrium absorption in the multi-component systems Of CO_2+TIPA+MEA+H_2O, CO_2+TIPA+PZ+H_2O and CO_2+TIPA+H_2O at low CO_2 partial pressures: experimental solubility data, corrosion study and modeling with artificial neural network 37:135-147.

Dawodu O, Meisen A (1994) Solubility of Carbon-Dioxide in Aqueous Mixtures of Alkanolamines. J Chem Eng Data 39:548-552.

Derks PWJ, Hogendoorn JA, Versteeg GF (2010) Experimental and theoretical study of the solubility of carbon dioxide in aqueous blends of piperazine and N-methyldiethanolamine. J Chem Thermodyn 42:151-163.

Derks PWJ, Hamborg ES, Hogendoorn JA, Niederer JPM, Versteeg GF (2008) Densities, viscosities, and liquid diffusivities in aqueous piperazine and aqueous (piperazine plus N-methyldiethanolamine) solutions. J Chem Eng Data 53:1179-1185.

Deshmukh RD, Mather AE (1981) A Mathematical-Model for Equilibrium Solubility of Hydrogen-Sulfide and Carbon-Dioxide in Aqueous Alkanolamine Solutions. Chemical Engineering Science 36:355-362.

Dicko M, Coquelet C, Jarne C, Northrop S, Richon D (2010) Acid gases partial pressures above a 50 wt% aqueous methyldiethanolamine solution: Experimental work and modeling. Fluid Phase Equilib 289:99-109.

DIPPR (Design Inistitute for Physical Property Research), 2011, Predicted by Project Staff at the Pennsylvania State University using either published or internal methods.

Edwards TJ, Maurer G, Newman J, Prausnitz JM (1978) Vapor-Liquid-Equilibria in Multicomponent Aqueous-Solutions of Volatile Weak Electrolytes. AIChE J 24:966-976.

Edwards TJ, Newman J, Prausnitz JM (1975) Thermodynamics of Aqueous-Solutions Containing Volatile Weak Electrolytes. AIChE J 21:248-259.

Ermatchkov V, Perez-Salado Kamps A, Maurer G (2006) Solubility of carbon dioxide in aqueous solutions of N-methyldiethanolamine in the low gas loading region. Ind Eng Chem Res 45:6081-6091.

Faramarzi L, Kontogeorgis GM, Thomsen K, Stenby EH (2009) Extended UNIQUAC model for thermodynamic modeling of CO_2 absorption in aqueous alkanolamine solutions. Fluid Phase Equilib 282:121-132.

Fletcher R (1971) A modified Marquardt subroutine for non-linear least squares, Harwell report (1971).
http://www.hsl.rl.ac.uk/ Accessed March 2010.

Fosbol PL, Pedersen MG, Thomsen K (2011) Freezing Point Depressions of Aqueous MEA, MDEA, and MEA-MDEA Measured with a New Apparatus. J Chem Eng Data 56:995-1000.

Furst W, Renon H (1993) Representation of Excess Properties of Electrolyte-Solutions using a New Equation of State. AIChE J 39:335-343.

Gabrielsen J, Michelsen ML, Stenby EH, Kontogeorgis GM (2005) A model for estimating CO_2 solubility in aqueous alkanolamines. Ind Eng Chem Res 44:3348-3354.

Garcia AV, Thomsen K, Stenby EH (2006) Prediction of mineral scale formation in geothermal and oilfield operations using the Extended UNIQUAC model - Part II. Carbonate-scaling minerals. Geothermics 35:239-284.

Garcia A, Thomsen K, Stenby E (2005) Prediction of mineral scale formation in geothermal and oilfield operations using the extended UNIQUAC model Part I. Sulfate scaling minerals. Geothermics 34:61-97.

Gillespie PC, Wilson GM (1982) Vapor·Liquid and Uquid·Liquid Equilibria:Water-Methane, Water-Carbon Dioxide, water·Hydrogen Sulfide, Water·nPentane, Water-Methane-nPentane. GPA RR 48.

Goppert U, Maurer G (1988) Vapor Liquid Equilibria in Aqueous-Solutions of Ammonia and Carbon-Dioxide at Temperatures between 333-K and 393-K and Pressures Up to 7 Mpa. Fluid Phase Equilib 41:153-185.

Guggenheim EA, Turgeon JC (1955) Specific interaction of ions. Trans Faraday Soc 51:747-761.

Hawrylak B, Palepu R, Tremaine PR (2006) Thermodynamics of aqueous methyldiethanolamine (MDEA) and methyldiethanolammonium chloride (MDEAH($^{+}$)Cl($^{-}$)) over a wide range of temperature and pressure: Apparent molar volumes, heat capacities, and isothermal compressibilities. J Chem Thermodyn 38:988-1007.

Hawrylak B, Burke SE, Palepu R (2000) Partial Molar and Excess Volumes and Adiabatic Compressibilities of Binary Mixtures of Ethanolamines with Water. J Sol Chem 29:575-594.

Hayden TA, Smith TGA, Mather AE (1983) Heat-Capacity of Aqueous Methyldiethanolamine Solutions. J Chem Eng Data 28:196-197.

Hessen ET, Haug-Warberg T, Svendsen HF (2010) The refined e-NRTL model applied to CO_2-H2O-alkanolamine systems. Chemical Engineering Science 65:3638-3648.

Hilliard MD (2008) Predictive Thermodynamic Model for an Aqueous Blend of Potassium Carbonate, Piperazine, and Monoethanolamine for Carbon Dioxide Capture from Flue Gas. PhD Disseration.

Huang SH, Ng HJ (1998) Solubility of H_2S and CO_2 in Alkanolamines GPA Research Report- RR-155.

Huttenhuis PJG, Agrawal NJ, Versteeg GF (2009) Solubility of Carbon Dioxide and Hydrogen Sulfide in Aqueous N-Methyldiethanolamine Solutions. Ind Eng Chem Res 48:4051-4059.

Huttenhuis PJG, Agrawal NJ, Solbraa E, Versteeg GF (2008) The solubility of carbon dioxide in aqueous N-methyldiethanolamine solutions. Fluid Phase Equilib 264:99-112.

Huttenhuis PJG, Agrawal NJ, Hogendoorn JA, Versteeg GF (2007) Gas solubility of H_2S and CO_2 in aqueous solutions of N-methyldiethanolamine. Journal of Petroleum Science and Engineering 55:122-134.

Isaacs E, Otto F, Mather A (1980) Solubility of Mixtures of H_2S and CO_2 in a Monoethanolamine Solution at Low Partial Pressures. J Chem Eng Data 25:118-120.

Jakobsen JP, Krane J, Svendsen HF (2005) Liquid-phase composition determination in CO_2-H_2O-alkanolamine systems: An NMR study. Ind Eng Chem Res 44:9894-9903.

Jenab MH, Abdi MA, Najibi SH, Vahidi M, Matin NS (2005) Solubility of carbon dioxide in aqueous mixtures of N-methyldiethanolamine plus piperazine plus sulfolane. J Chem Eng Data 50:583-586.

Jepsen MS, Petersen LH (2011) Model Analyses and experiments concerning solvents for CO_2 capture.

Jones JH, Froning HR, Claytor Jr. EE (1959) Solubility of acidic gases in aqueous monoethanolamine. J Chem Eng Data 4:85-92.

Jou FY, Otto FD, Mather AE (1994) Vapor-Liquid-Equilibrium of Carbon-Dioxide in Aqueous Mixtures of Monoethanolamine and Methyldiethanolamine. Ind Eng Chem Res 33:2002-2005.

Jou FY, Carroll JJ, Mather AE, Otto FD (1993) The Solubility of Carbon-Dioxide and Hydrogen-Sulfide in a 35 Wt-Percent Aqueous-Solution of Methyldiethanolamine. Can J Chem Eng 71:264-268.

Jou F, Carroll J, Mather A, Otto F (1998) Solubility of methane and ethane in aqueous solutions of methyldiethanolamine. J Chem Eng Data 43:781-784.

Jou F, Mather A, Otto F (1995) The Solubility of CO_2 in a 30-Mass-Percent Monoethanolamine Solution. Can J Chem Eng 73:140-147.

Jou F, Mather A, Otto F (1982) Solubility of H_2S and CO_2 in Aqueous Methyldiethanolamine Solutions. Ind Eng Chem Pro Des Dev 21:539-544.

Kamps APS, Xia JZ, Maurer G (2003) Solubility of CO_2 in (H_2O+piperazine) and in (H_2O+MDEA+piperazine). AICHE J 49:2662-2670.

Kamps APS, Rumpf B, Maurer G, Anoufrikov Y, Kuranov G, Smirnova NA (2002) Solubility of CO_2 in H_2O plus N-methyldiethanolamine plus (H_2SO4 or Na_2SO4). AIChE J 48:168-177.

Kamps APS, Balaban A, Jodecke M, Kuranov G, Smirnova NA, Maurer G (2001) Solubility of single gases carbon dioxide and hydrogen sulfide in aqueous solutions of N-methyldiethanolamine at temperatures from 313 to 393 K and pressures up to 7.6 MPa: New experimental data and model extension. Ind Eng Chem Res 40:696-706.

Kamps A, Maurer G (1996) Dissociation constant of N-methyldiethanolamine in aqueous solution at temperatures from 278 K to 368 K. J Chem Eng Data 41:1505-1513.

Kent RL, Eisenberg B (1976) Better Data for Amine Treating. Hydrocarbon Process 55:87-90.

Kicrzkowska-Pawlak H (2007) Enthalpies of Absorption and Solubility of CO_2 in Aqueous Solutions of Methyldiethanolamine. Separation Science and Technology, 42:2723-2737.

Kim I, Svendsen HF, Borresen E (2008) Ebulliometric Determination of Vapor-Liquid Equilibria for Pure Water, Monoethanolamine, N-Methyldiethanolamine, 3-(Methylamino)-propylamine, and Their Binary and Ternary Solutions. J Chem Eng Data 53:2521-2531.

Kim I, Svendsen HF (2007) Heat of absorption of carbon dioxide (CO_2) in monoethanolamine (MEA) and 2-(Aminoethyl)ethanolamine (AEEA) solutions. Ind Eng Chem Res 46:5803-5809.

Kling G, Maurer G (1991) Solubility of Hydrogen in Aqueous Ethanolamine Solutions at Temperatures between 323-K and 423-K. J Chem Eng Data 36:390-394.

Kritchevsky I, Iliinskaya A (1945) Partial molal volumes of gases dissolved in liquids (a contribution to the thermodynamics of dilute solutions of non-electrolytes). Acta Physico-chim URSS 20:327-348.

Kundu M, Bandyopadhyay SS (2005) Modelling vapour - Liquid equilibrium of CO_2 in aqueous N-methyldiethanolamine through the simulate annealing algorithm. Can J Chem Eng 83:344-353.

Kuranov G, Rumpf B, Smirnova N, Maurer G (1996) Solubility of single gases carbon dioxide and hydrogen sulfide in aqueous solutions of N-methyldiethanolamine in the temperature range 313-413 K at pressures up to 5 MPa. Ind Eng Chem Res 35:1959-1966.

Lawson JD, Garst AW (1976) Gas Sweetening Data - Equilibrium Solubility of Hydrogen-Sulfide and Carbon-Dioxide in Aqueous Monoethanolamine and Aqueous Diethanolamine Solutions. J Chem Eng Data 21:20-30.

le Bouhelec EB, Mougin P, Barreau A, Solimando R (2007) Rigorous modeling of the acid gas heat of absorption in alkanolamine solutions. Energy Fuels 21:2044-2055.

Lecomte F, Broutin P, Lebas E (2009) CO_2 capture technologies to reduce greenhouse gas emissions. IFP publications.

Lee JI, Mather AE (1977) Solubility of Hydrogen-Sulfide in Water. Berichte der Bunsen-Gesellschaft 81:1020-1023.

Lee J, Otto F, Mather A (1976) Equilibrium between Carbon-Dioxide and Aqueous Monoethanolamine Solutions. J App Chem Bio 26:541-549.

Lemoine B, Li YG, Cadours R, Bouallou C, Richon D (2000) Partial vapor pressure of CO_2 and H2S over aqueous methyldiethanolamine solutions. Fluid Phase Equilib 172:261-277.

Li CX, Furst W (2000) Representation of CO_2 and H_2S solubility in aqueous MDEA solutions using an electrolyte equation of state. Chem Eng Sci 55:2975-2988.

Li MH, Lie YC (1994) Densities and Viscosities of Solutions of Monoethanolamine Plus N-Methyldiethanolamine Plus Water and Monoethanolamine Plus 2-Amino-2-Methyl-1-Propanol Plus Water. J Chem Eng Data 39:444-447.

Li M, Shen K (1993) Solubility of Hydrogen-Sulfide in Aqueous Mixtures of Monoethanolamine with N-Methyldiethanolamine. J Chem Eng Data 38:105-108.

Li YG, Mather AE (1994) Correlation and Prediction of the Solubility of Carbon-Dioxide in a Mixed Alkanolamine Solution. Ind Eng Chem Res 33:2006-2015.

Lindholdt A (2008) Thermodynamic Modeling of Hydrogen Sulfide Solubility in Weak Electrolyte Solutions. Master Thesis.

Liu HB, Zhang CF, Xu GW (1999) A study on equilibrium solubility for carbon dioxide in methyldiethanolamine-piperazine-water solution. Ind Eng Chem Res 38:4032-4036.

Macgregor RJ, Mather AE (1991) Equilibrium Solubility of H_2S and CO_2 and their Mixtures in a Mixed-Solvent. Can J Chem Eng 69:1357-1366.

Maddox RN, Bhairi AH, Diers JR (1987) Equilibrium Solubility of Carbon Dioxide or Hydrogen Sulfide in Aqueous Solutions of Monoethanolamine, Diglycolamine, Diethanoiamine and Methyldiethanolamine GPA Research Report, PR-104.

Maham Y, Mather AE, Mathonat C (2000) Excess properties of (alkyldiethanolamine plus H_2O) mixtures at temperatures from (298.15 to 338.15) K. J Chem Thermodyn 32:229-236.

Maham Y, Mather AE, Hepler LG (1997) Excess molar enthalpies of (water plus alkanolamine) systems and some thermodynamic calculations. J Chem Eng Data 42:988-992.

Ma'mun S, Nilsen R, Svendsen HF, Juliussen O (2005) Solubility of carbon dioxide in 30 mass % monoethanolamine and 50 mass % methyldiethanolamine solutions. J Chem Eng Data 50:630-634.

Mandal BP, Kundu M, Bandyopadhyay SS (2003) Density and Viscosity of Aqueous Solutions of (N-Methyldiethanolamine + Monoethanolamine), (N-Methyldiethanolamine + Diethanolamine), (2-Amino-2-methyl-1-propanol + Monoethanolamine), and (2-Amino-2-methyl-1-propanol + Diethanolamine). J Chem Eng Data 48:703-707.

Marcus Y (1997) Ion Properties. MARCEL DEKKER, INC., U.S.A.

Mathonat C, Majer V, Mather A, Grolier J (1997) Enthalpies of absorption and solubility of CO_2 in aqueous solutions of methyldiethanolamine. Fluid Phase Equilib 140:171-182.

Maurer G, Prausnitz J (1978) Derivation and Extension of Uniquac Equation. Fluid Phase Equilib 2:91-99.

Nath A, Bender E (1983) Isothermal Vapor Liquid Equilibria of Binary and Ternary Mixtures Containing Alcohol, Alkanolamine, and Water with a New Static Device. J Chem Eng Data 28:370-375.

Nielsen JC (2011) CO_2 capture, measurements and thermodynamic models.

NIST Chemical Thermodynamics Database Vesion 1.1, 1990. U.S. Department of Commerce, National Inistitute of Standards and Technology. Gaithesburg Maryland 20899.

NREL L (2009) Survey and Down-Selection of Acid Gas Removal Systems for the Thermochemical Conversion of Biomass to Ethanol with a Detailed Analysis of an MDEA System, Task 1: Acid Gas Removal Technology Survey and Screening for Thermochemical Ethanol Synthesis.

Oscarson JL, lzatt RM (1990) Enthalpies of Solution of H_2S in Aqueous Methyldiethanolamine Solutions GPA-RR-127.

Oscarson JL, Chen X, Izatt RM (August, 1995) A Thermodynamically Consistent Model for the Prediction of Solubilities and Enthalpies of Solution of Acid Gases in Aqueous Alkanolamine Solutions GPA-PR-130.

Othmer K (2005) Kirk-Othmer Encyclopedia of Chemical Technology.

Park MK, Sandall OC (2001) Solubility of carbon dioxide and nitrous oxide in 50 mass % methyldiethanolamine. J Chem Eng Data 46:166-168.

Paul S, Mandal B (2006) Density and viscosity of aqueous solutions of (N-methyldiethanolamine plus piperazine) and (2-amino-2-methyl-1-propanol plus piperazine) from (288 to 333) K. J Chem Eng Data 51:1808-1810.

Pitzer KS, Simonson JM (1986) Thermodynamics of Multicomponent, Miscible, Ionic Systems - Theory and Equations. J Phys Chem 90:3005-3009.

Posey M, L. (1997) Thermodynamic Model for Acid Gas Loaded Aqueous Alkanolamine Solutions. PhD Disseration.

Posey M, Rochelle G (1997) A thermodynamic model of methyldiethanolamine-CO_2-H_2S-water. Ind Eng Chem Res 36:3944-3953.

Prausnitz JM, Lichtenthaler RN, Azevedo EG (1999) Molecular thermodynamics of fluid-phase equilibria. Prentice Hall, Upper Saddle River.

Qian WM, Li YG, Mather AE (1995) Correlation and Prediction of the Solubility of CO_2 and H_2S in an Aqueous-Solution of Methyldiethanolamine and Sulfolane. Ind Eng Chem Res 34:2545-2550.

Reamer HH, Sage BH, Lacey WN (1950) Volumetric Behavior of Hydrogen Sulfide. Industrial and Engineering Chemistry 42:140-143.

Rho S, Yoo K, Lee J, Nam S, Son J, Min B (1997) Solubility of CO_2 in aqueous methyldiethanolamine solutions. J Chem Eng Data 42:1161-1164.

Rinker EB, Oelschlager DW, Colussi AT, Henry KR, Sandall OC (1994) Viscosity, density, and surface tension of binary mixtures of water and N-methyldiethanolamine and water and diethanolamine and tertiary mixtures of these amines with water over the temperature range 20-100 C. J Chem Eng Data 39:392-395.

Rochelle GT (1991) Research needs for acid gas kinetics and equilibria in alkanolamine systems. Gas Processors Association:66-82.

Rogers WJ, Bullin JA, Davison RR (1998) FTIR measurements of acid-gas-methyldiethanolamine systems. AICHE J 44:2423-2430.

Rumpf B, Nicolaisen H, Ocal C, Maurer G (1994) Solubility of Carbon-Dioxide in Aqueous-Solutions of Sodium-Chloride - Experimental Results and Correlation. Journal of Solution Chemistry 23:431-448.

Rumpf B, Maurer G (1993) An Experimental and Theoretical Investigation on the Solubility of Carbon-Dioxide in Aqueous-Solutions of Strong Electrolytes. Berichte Der Bunsen-Gesellschaft 97:85-97.

Sander B, Rasmussen P, Fredenslund A (1986) Calculation of Solid Liquid Equilibria in Aqueous-Solutions of Nitrate Salts using an Extended Uniquac Equation. Chem Eng Sci 41:1197-1202.

Selleck FT, Carmichael LT, Sage BH (1952) Phase Behavior in the Hydrogen Sulfide Water System. Ind Eng Chem Res 44:2219-2226.

Shen KP, Li MH (1992) Solubility of Carbon-Dioxide in Aqueous Mixtures of Monoethanolamine with Methyldiethanolamine. J Chem Eng Data 37:96-100.

Sidi-Boumedine R, Horstmann S, Fischer K, Provost E, Furst W, Gmehling J (2004) Experimental determination of carbon dioxide solubility data in aqueous alkanolamine solutions. Fluid Phase Equilib 218:85-94, a.

Sidi-Boumedine R, Horstmann S, Fischer K, Provost E, Furst W, Gmehling J (2004) Experimental determination of hydrogen sulfide solubility data in aqueous alkanolamine solutions. Fluid Phase Equilib 218:149-155, b.

Silkenbaumer D, Rumpf B, Lichtenthaler RN (1998) Solubility of carbon dioxide in aqueous solutions of 2-amino-2-methyl-1-propanol and N-methyldiethanolamine and their mixtures in the temperature range from 313 to 353 K and pressures up to 2.7 MPa. Ind Eng Chem Res 37:3133-3141.

Smith JM, Van Ness HC, Abbott MM (2005) Introduction to Chemical Engineering Thermodynamics.

Soave G (1972) Equilibrium Constants from a Modified Redlich-Kwong Equation of State. Chem Eng Sci 27:1197.

Solbraa E (2002) PhD Thesis, Measurement and Modelling of Absorption of Carbon Dioxide into Methyldiethanolamine Solutions at High Pressures.

Speyer D, Ermatchkov V, Maurer G (2010) Solubility of Carbon Dioxide in Aqueous Solutions of N-Methyldiethanolamine and Piperazine in the Low Gas Loading Region. J Chem Eng Data 55:283-290.

StatLib N Applied Statistics Algorithms, Nelder-Mead routine. http://lib.stat.cmu.edu/apstat/.

Stewart EJ, Lanning RA (May 1994) Reduce amine plant sovent losses. Hydrocarbon Processing:67-68.

Ter Maat H, Praveen S, IJben P, Arslan D, Wouters HF, Huttenhuis JG, Hogendoorn JA, Versteeg GF (2004) The Determination of VLE Data on CO_2 and H_2S in MDEA and its Blends with other Amines GPA-RR-186.

Thomsen K (1997) Aqueous electrolytes: model parameters and process simulation (PhD Disseration).

Thomsen K, Rasmussen P (1999) Modeling of vapor-liquid-solid equilibrium in gas-aqueous electrolyte systems. Chemical Engineering Science 54:1787-1802.

Thomsen K, Rasmussen P, Gani R (1996) Correlation and prediction of thermal properties and phase behaviour for a class of aqueous electrolyte systems RID A-4865-2011. Chemical Engineering Science 51:3675-3683.

Tochigi K, Akimoto K, Ochi K, Liu F, Kawase Y (1999) Isothermal vapor-liquid equilibria for water+2-aminoethanol plus dimethyl sulfoxide and its constituent three binary systems. J Chem Eng Data 44:588-590.

Vallee G, Mougin P, Jullian S, Furst W (1999) Representation of CO_2 and H_2S absorption by aqueous solutions of diethanolamine using an electrolyte equation of state. Ind Eng Chem Res 38:3473-3480.

Van Krevelen DW, Hoftijzer PJ, Huntjens FJ (1949) Composition and vapour pressures of aqueous solutions of ammmonia, carbon dioxide and hydrogen sulphide. Recueil des travaux chimiques des Pays-Bas 68:191-216.

VonNiederhausern DM, Wilson GM, Giles NF (2006b) Critical point and vapor pressure measurements for seven compounds by a low residence time flow method. J Chem Eng Data 51:1982-1985.

Voutsas E, Vrachnos A, Magoulas K (2004) Measurement and thermodynamic modeling of the phase equilibrium of aqueous N-methyldiethanolamine solutions. Fluid Phase Equilib 224:193-197.

Wang LK, Chen GJ, Han GH, Guo XQ, Guo TM (2003) Experimental study on the solubility of natural gas components in water with or without hydrate inhibitor. Fluid Phase Equilib 207:143-154.

Weiland RH, Chakravarty T, Mather AE (1993) Solubility of Carbon-Dioxide and Hydrogen-Sulfide in Aqueous Alkanolamines. Ind Eng Chem Res 32:1419-1430.

Weiland RH, Dingman JC, Cronin DB (1997) Heat Capacity of Aqueous Monoethanolamine, Diethanolamine, N-Methyldiethanolamine, and N-Methyldiethanolamine-Based Blends with Carbon Dioxide. J Chem Eng Data 42:1004-1006.

West JR (1948) Thermodynamic Properties of Hydrogen Sulfide. Chem Eng Prog 44:287-292.

Wright. RH, Maass O (1932) The Solubility of Hydrogen Sulphide in Water from the Vapor Pressures of the Solutions. Canadian Journal of Research 6:94-101.

Xu GW, Zhang CF, Qin SJ, Gao WH, Liu HB (1998) Gas-liquid equilibrium in a CO_2-MDEA-H_2O system and the effect of piperazine on it. Ind Eng Chem Res 37:1473-1477.

Xu S, Qing S, Zhen Z, Zhang C, Carroll JJ (1991) Vapor pressure measurements of aqueous N-methyldiethanolamine solutions. Fluid Phase Equilib 67:197-201.

Yokoyama C, Wakana S, Kaminishi G, Takahashi S (1988) Vapor Liquid Equilibria in the Methane Diethylene Glycol Water-System at 298.15 and 323.15-K. J Chem Eng Data 33:274-276.

Zhang K, Hawrylak B, Palepu R, Tremaine PR (2002) Thermodynamics of aqueous amines: Excess molar heat capacities, volumes, and expansibilities of {water + methyldiethanolamine (MDEA)} and {water + 2-amino-2-methyl-1-propanol (AMP)}. J Chem Thermodyn 34:679-710.

Zhang Y, Chen C (2011) Thermodynamic Modeling for CO_2 Absorption in Aqueous MDEA Solution with Electrolyte NRTL Model RID C-3054-2008. Ind Eng Chem Res 50:163-175.

Appendix

Low pressure cell Pictures

The picture of "low pressure cell" and the chemicals used in low pressure experiments are provided. This set up was used to perform CO_2 solubility experiments in aqueous MDEA and aqueous activated MDEA (MDEA-PZ) solutions.

Figure A-1: Picture of the low pressure cell set up.

Figure A-2: MDEA and PZ used in low pressure experiments.

Equilibrium Cell Set up

The provided pictures shows from the equilibrium cell set up. The set up was used to measure H_2S solubility in aqueous MDEA solutions at high pressures and in presence of methane.

Figure A-3: Picture from the equilibrium cell set up

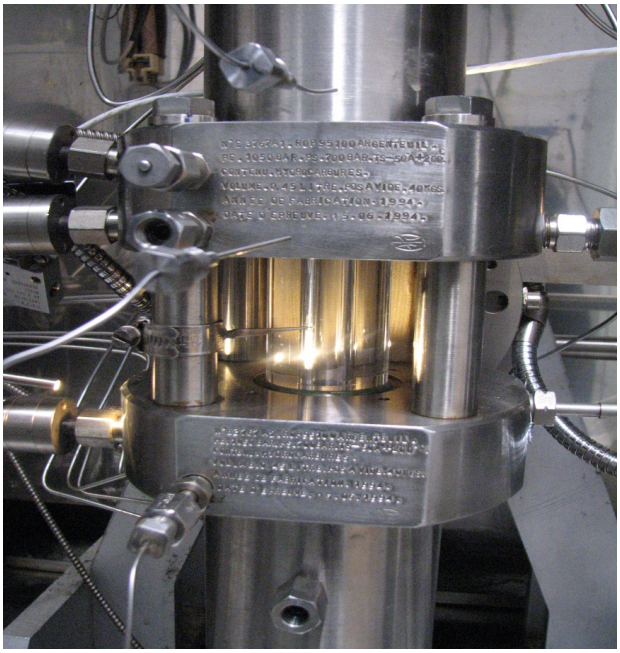

Figure A-4: Picture of the cylinder where gas and liquid phase are contacted to reach equilibrium.

Figure A-5: Picture of the stirrer.

Piperazine Solubility Measurements

This section shows the preliminary results that obtained in this study for measuring piperazine solubility in aqueous MDEA. Note that these measurements were not in the preliminary plan of the project, however because of the industrial demand they were considered in this work. Measurements were performed in Statoil laboratories. The lack of time did not allow repeating the measurements and performing them more accurately.

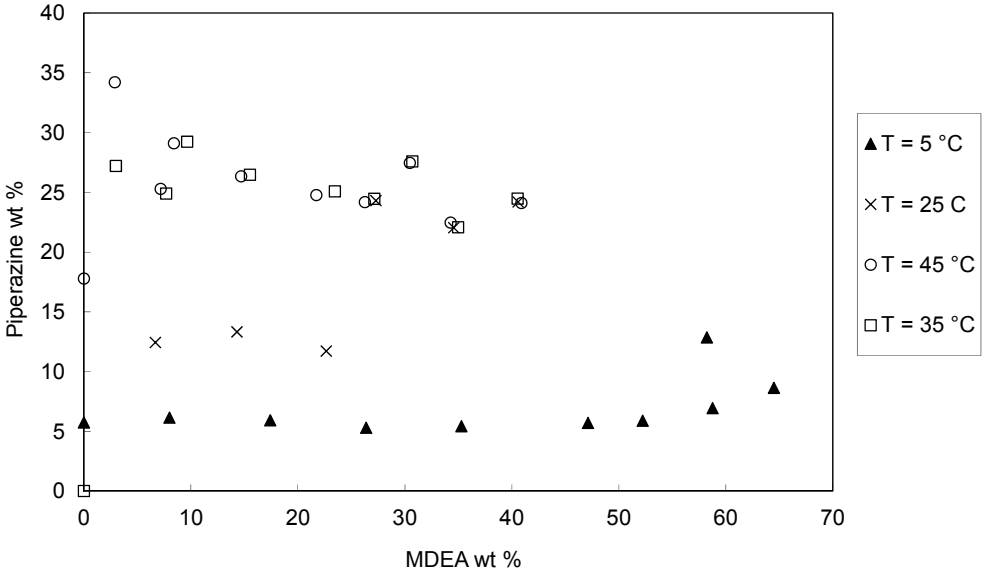

Figure A-6: PZ solubility measurements in aqueous MDEA.

List of Publications

This section shows the list of publications derived from this Ph.D. study.

The first part of the study (thermodynamic modeling of CO_2 system) was finished at almost middle of PhD. The author planned to wrote the related article before moving to Statoil in Norway but unfortunately starting the modeling of H_2S system and lots of practical works regarding moving to Norway did not allow fulfilling the task. Norway stay was intended for experimental part of the project, working hard during the week days and even most of the weekends barely left free time to write the delayed article. After coming back from Norway, author focused on calculations of high pressure effect on low pressure solubility data and H_2S modeling. The last months of PhD was spent on writhing PhD dissertation. It has been tried to write the dissertation chapters in forms of articles. The author intends to submit the articles soon after the PhD defense. Fortunately a big oil company is going to start a new project based on this PhD study. This is an opportunity for the author to submit PhD derived articles meanwhile.

List of Presentations at International Conferences

- Full conference paper and oral presentation, Proceedings of 9th AIChE Annual Meeting, Nashville, USA, November 2009.
- Oral presentation at ICCT-2010, Ibaraki, Japan, August 2010.
- Invited speaker at STC-2010 (Student SPE conference), Germany, October 2010.
- Oral presentation at ESAT-2011, Russia, June 2011.

List of Upcoming Journal Publications

- **Sadegh, N.**, Stenby, E. H., Thomsen, K. "Thermodynamic modeling of CO_2 absorption process by aqueous MDEA using Extended UNIQUAC model", under preparation.
- **Sadegh, N.**, Stenby, E. H., Thomsen, K. "Thermodynamic modeling of CO_2 absorption process by aqueous MEA and blends of MEA and MDEA using Extended UNIQUAC model", under preparation.
- **Sadegh, N.**, Stenby, E. H., Thomsen, K. "Thermodynamic modeling of hydrogen sulfide absorption by aqueous N-Methyldiethanolamine using the Extended UNIQUAC model", under preparation.
- **Sadegh, N.**,Thomsen, Stenby, E. H., "Thermodynamic modeling of H_2S-CH_4-MDEA-H_2O and CO_2-CH_4-MDEA-H_2O systems using Extended UNIQUAC model", under preparation.

- **Sadegh, N.**, Thomsen, K., Solbraa, E., Johannessen, E., Rudolfsen, G.I., Berg, O.J, "Solubility of hydrogen sulfide in aqueous solutions of N-methyldiethanolamine at high pressures", under preparation.
- **Sadegh, N.**, Thomsen, K., Solbraa, E., Johannessen, E., "Solubility of carbon dioxide in aqueous solutions of N-methyldiethanolamine, covering broad MDEA concentration range (10-100 wt%) - Part I", under preparation.
- **Sadegh, N.**, Thomsen, K., Solbraa, E., Johannessen, E., "Solubility of carbon dioxide in aqueous solutions of N-methyldiethanolamine activated with piperazine - Part II", under preparation.

Center for Energy Resources Engineering
Department of Chemical and
Biochemical Engineering
Technical University of Denmark
Søltofts Plads, Building 229
DK-2800 Kgs. Lyngby
Denmark

Phone: +45 4525 2800
Fax: +45 4525 4588
Web: www.cere.dtu.dk

ISBN : 978-87-93054-13-4